

# BM18, THE NEW ESRF-EBS BEAMLINE FOR HIERARCHICAL PHASE-CONTRAST TOMOGRAPHY

F. Cianciosi†, A.L. Buisson, P. Tafforeau, P. Van Vaerenbergh  
European Synchrotron Radiation Facility (ESRF), Grenoble, France

## Abstract

BM18 is an ESRF-EBS beamline for hierarchical tomography, it will combine sub-micron precision and the possibility to scan very large samples. The applications will include biomedical imaging, material sciences and cultural heritage. It will allow the complete scanning of a post-mortem human body at 25  $\mu\text{m}$ , with the ability to zoom-in in any location to 0.7  $\mu\text{m}$ .

BM18 is exploiting the high-energy-coherence beam of the new EBS storage ring. The X-ray source is a short tri-pole wiggler that gives a 300mm-wide beam at the sample position placed 172m away from the source. Due to this beam size, nearly all of the instruments are developed in-house. A new building was constructed to accommodate the largest synchrotron white-beam Experimental Hutch worldwide (42x5-6m). The main optical components are refractive lenses, slits, filters and a chopper. There is no crystal monochromator present but the combination of the optical elements will provide high quality filtered white beams, as well as an inline monochromator system. The energy will span from 25 to 350 keV.

The Experimental Hutch is connected by a 120m long UHV pipe with a large window at the end, followed by a last set of slits. The sample stage can position, rotate and monitor with sub-micron precision samples up to 2,5x0.6m (H x Diam.) and 300kg. The resulting machine is 4x3x5m and weighs 50 tons. The girder for detectors carries up to 9 detectors on individual 2-axis stages. It moves on air-pads on a precision marble floor up to 38m behind the sample stage to perform phase contrast imaging at a very high energy on large objects.

The commissioning is scheduled for the beginning of 2022; the first “friendly users” are expected in March 2022 and the full operation will start in September 2022.

## BM18, HIERARCHICAL PHASE-CONTRAST TOMOGRAPHY

### General Concept

BM18 is a project that developed within the ESRF-EBS project. It aims at benefiting from the new capabilities of the “bending magnet (BM)” X-ray sources from the new lattice. Indeed, the ESRF-EBS is reaching a new level in terms of X-ray coherence in a storage ring. The progress is impressive for undulators in the straight sections of the machine, but in fact, the smallest possible X-ray sources (and then the highest spatial coherence) are obtained using short

wigglers installed on the BM ports of the previous machine. As coherence depends on the X-ray source size and of the distance between the sample and the source, the BM18 concept has been developed to combine the smallest possible X-ray source with the longest possible beamline at the ESRF (220m in total).

The ESRF has a long tradition of X-ray full-field imaging at high energy, especially using propagation phase contrast. During the past two decades, important efforts have been made in order to increase the maximum size of the sample from a few mm up to about 20 cm in diameter and 50 cm vertically.

### X-ray Source

This new beamline will allow a dramatic increase of sample sizes (up to 0.7m in diameter, 2.5m vertically and a total weight of 300 kg), while also increasing the sensitivity, especially at high energy. The source was then selected as a tri-pole wiggler with the central pole at 1.56T (the two lateral poles being at 0.85T) in order to produce a continuous X-ray spectrum optimized for very hard X-rays.

### Optical Scheme

The beamline has been designed to be operated only in polychromatic mode in order to maximize the average usable energy, as well as to preserve the coherence as much as possible. The optical scheme is then based on mirror polished filters with different materials (C, SiO<sub>2</sub>, Al<sub>2</sub>O<sub>3</sub>, Al, Ti, Cu, Mo, Ag, W, Au), with different thicknesses and shapes allowing the energy to be tuned from 25 keV to 350 keV. In addition, several systems of inline monochromators have been implemented using refractive lenses and high precision slits to be able to tune the bandwidth and beam geometry when needed. A chopper is integrated in order to fine tune the beam power without changing its spectrum. All in all, these optical combinations bring most of the functionalities from a classical insertion device beamline with a moveable gap, even if BM18 will be on a fixed gap system.

### Experimental Hutch

Considering the large energy range and foreseen applications, the experimental hutch has been designed to be as long as possible (45m). This allows a propagation distance up to 38m between the centre of the sample and the most distant position of the detectors. The extremely small size of the X-ray source on this beamline makes it possible to exploit this long propagation distance for pixel size down to 13  $\mu\text{m}$ . For smaller pixel sizes, the propagation distance can be reduced as required.

† ciancios@esrf.fr

# OVERCOMING CHALLENGES DURING THE INSERTION DEVICE STRAIGHT SECTION COMPONENT PRODUCTION AND TUNING PHASE OF THE ADVANCED PHOTON SOURCE UPGRADE\*

J. Lerch<sup>†</sup>, Argonne National Laboratory-Advanced Photon Source (APS), Lemont, IL 60439, USA

## Abstract

The Advanced Photon Source Upgrade (APS-U) scope for insertion devices (IDs) and ID vacuum systems is extensive. Thirty-five of the 40 straight sections in the storage ring will be retrofitted with new 4.8-meter-long Superconducting Undulators (SCUs) or a mix of new and reused Hybrid-Permanent Magnet Undulators (HPMUs). All 35 ID straight sections will require new vacuum systems and new HPMU control systems. Production is well underway at multiple manufacturing sites around the world for these components. Simultaneously, ID assembly and HPMU tuning is occurring onsite at Argonne National Laboratory (ANL). In addition to component production and assembly/tuning activities, our team also started the ID swap out program at the Advanced Photon Source (APS) in late 2020. This program allows us to remove HPMUs intended for reuse from the APS storage ring and retune them to meet the APS-U magnetic specifications to reduce the tuning workload during the dark year. These activities have presented technical and logistical challenges that are as unique as the components themselves. Additionally, the ongoing Covid-19 pandemic presented unforeseen challenges that required new work processes to be created to sustain pace and quality of work while maintaining the high workplace safety standards required at Argonne. This paper will summarize the many challenges encountered during the project and how they were overcome.

## INTRODUCTION

The APS-U Upgrade (APS-U) project plan calls for the current APS 40-sector storage ring (SR) to be retrofitted with a new 6 GeV, 200 mA storage ring optimized for brightness above 4 keV. 35 of the 40 sector straight sections will be dedicated to insertion devices (ID) which will produce photons at various energies to ID beamline users based on their needs. The APS-U ID group is responsible for upgrading equipment within the straight sections for the upgrade. The group's extensive scope can be broken up into three main technical areas: Hybrid Permanent Magnet Undulators (HPMUs), Superconducting Undulators (SCUs), and ID Vacuum systems (IDVS). The following sections will detail each areas scope, major challenges encountered during production, and solutions to those challenges.

\*This research used resources of the Advanced Photon Source, a U.S. Department of Energy (DOE) Office of Science User Facility at Argonne National Laboratory and is based on research supported by the U.S. DOE Office of Science-Basic Energy Sciences, under Contract No. DE-AC02-06CH11357.

<sup>†</sup> jlerch@anl.gov

## HPMU

### Scope

HPMUs are the main type of ID utilized in the APS-U. 30 out of 35 straight sections will be equipped with at least one HPMU. This requires our group to deliver 55 HPMUs for which 12 are the revolving type. Of the 55 HPMUs required for the APS-U, 32 will be new period devices and 23 will be made from existing period magnet structures harvested from devices currently in use. The harvested devices will require retuning to meet APS-U magnetic specifications. All HPMUs require new motors and control system due to the obsolescence of the current motors and controls currently in use at the APS.

### Challenges and Solutions

There have been many major challenges associated with the HPMU scope. Our group is required to deliver 55 HPMUs for installation to the Removal and Installation group (R&I) prior to the start of commissioning. We have also encountered issues during assembly of the HPMUs that occurred prior to sending the devices for tuning. Finally, our tuning facility has limited space for device tuning given the aggressive timetable required to meet our delivery schedule.

**Schedule** The APS-U ID group project schedule is one of our largest challenges. We are required to deliver all 55 HPMUs, canting and phase shifter magnets, and ID control system to the R&I group prior to the start of commissioning. We implemented two strategies to meet our schedule: pre-tune new period devices and swap out reused periods during maintenance periods.

Pre-tuning new period devices will allow our team to tune all new period magnet structure sets to the APS-U magnet requirements. New period devices represent the largest subset of HPMUs that need to be delivered. To accomplish this, our group has procured 6 additional gap separation mechanisms (GSM) from our central shops. After the magnetic structure set (MSS) is assembled onto one of the spare GSM, our tuning group tunes the MSS to meet APS-U magnetic requirements. The MSS is then removed from the GSM and stored until the start of dark time when it can be assembled onto the GSM that will be installed into the storage ring. The MSS cannot be considered "final tuned" until it has been installed onto the GSM it will be installed with due to minor variations in deflection that occur between different GSM. The exception to this is the revolver HPMUs, which our group redesigned the GSM as part of the design phase of the APS-U. This allows us to assemble the MSS onto the unique revolver GSM, which

# EXPERIENCE WITH THE VACUUM SYSTEM FOR THE FIRST FOURTH GENERATION LIGHT SOURCE: MAX IV

E. AL-Dmour<sup>†</sup>, M. Grabski, K. Åhnberg, MAX IV Laboratory, Lund, Sweden

## Abstract

The 3 GeV electron storage ring of the MAX IV laboratory is the first storage-ring-based synchrotron radiation facility with the vacuum system having small aperture and with the inner surface of almost all the vacuum chambers along its circumference coated with non-evaporable getter (NEG) thin film. This concept implies challenges during the whole project from design into operation.

The fast conditioning of the vacuum system and over five years of reliable accelerator operation have demonstrated that the chosen design proved to be good and does not impose limits on the operation. A summary of the vacuum system design, production, installation and performance is presented.

## INTRODUCTION

The MAX IV facility in Lund-Sweden is composed of two storage rings with electron energies of 1.5 GeV and 3 GeV. A linear accelerator (LINAC) serves as the full energy injector to the two storage rings as well as a driver for a short pulse facility [1]. The MAX IV 3 GeV ring started delivering light to the users in April 2017.

## 3 GEV STORAGE RING

The 3 GeV storage ring is the world's first multibend achromat, ultra-low emittance light source. To achieve the low horizontal emittance, a 7 bend achromat lattice was chosen. The storage ring has a 20-fold symmetry and is 528 m in circumference [2].

Each achromat contains seven magnet blocks of two types: five unit cells (U) (with 3° bending magnets) and two matching cells (M) (with 1.5° bending magnets). Each achromat contains two short straight sections (S1 and S2). In addition 19 long straight sections (L) of 4.6 m length are used for the insertion devices (ID) and one long straight section is used as an injection straight. Figure 1 shows one standard 3 GeV ring achromat, including magnet blocks and the vacuum chambers of one achromat.

## 3 GEV STORAGE RING VACUUM SYSTEM DESIGN AND MANUFACTURING

The vacuum system of the 3 GeV ring is based on chambers which are made of copper and the chamber body is used as distributed absorbers. The inner surface of the vacuum chambers is NEG coated. Four ion pumps per achromat are installed in areas with high outgassing and provide pumping for noble gases (see Fig. 1).

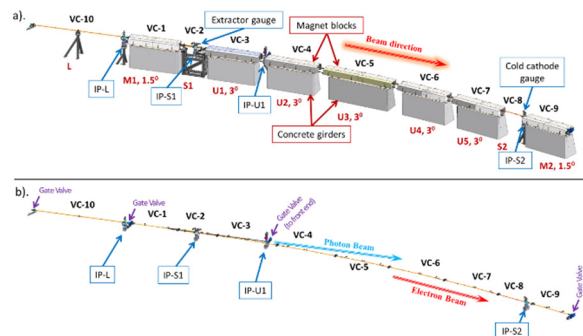


Figure 1: One standard 3 GeV storage ring achromat, a), with the magnet blocks and girders b), the vacuum chambers without the magnet blocks [3].

## Vacuum Chamber Design

The vacuum chambers are made of oxygen-free silver-bearing (Ag 0.085%) copper (OFS-C10700). The internal diameter of the vacuum chambers inside the magnet blocks is 22 mm and the chambers have 1 mm wall thickness. The vast majority of the chambers have electron welded water cooling channels on one side.

Ten beam-position monitors (BPMs) per achromat are installed and mounted directly to the magnet blocks. Bellows with internal RF fingers are located at the extremities of the vacuum chambers, the main purpose of the bellows is to shield the BPM block from any deformation occurring in the vacuum chambers due to heating up from the synchrotron radiation.

Several design challenges were faced, some of which are listed below:

- Effectively extract the photon beam to the front end.
- Avoid interferences with the magnets.
- Provide cooling for the chambers in places with limited access and space.
- Guarantee the mechanical and thermal stability of the BPMs while vacuum chambers are allowed to expand.
- Provide a design that will allow successful implementation of NEG coating on the chamber's inner surface.
- Provide a design that allows easy installation.
- Keep standardization.

To assure the mechanical stability of the BPMs, the bellows' spacers were made from epoxy glass G10, with low thermal conductivity and high radiation resistance (see Fig. 2). The BPM blocks are shadowed by small absorbers at the end of each chamber body, just before the flange.

Finite element analysis (FEA) was performed during the design stage, to study several mechanical and thermal issues related to the vacuum chamber design, such as the deformation, stress and strain of the vacuum chambers, the deformation of the BPM during operation, the design of the

<sup>†</sup> eshraq.al-dmour@maxiv.lu.se

## ALBA BL20 NEW MONOCHROMATOR DESIGN

A. Crisol\*, F. Bisti, C. Colldelram, M. Llonch, B. Molas, R. Monge, J. Nicolàs, L. Nikitina,  
 M. Quispe, L. Ribó, M. Tallarida, ALBA Synchrotron Light Source, Cerdanyola del Vallès, Spain

### Abstract

LOREA Beamline (BL20) at ALBA Synchrotron is a new soft X-Ray Beamline dedicated to investigate electronic structure of solids by means ARPES technique. Optical design has been developed in-house so as most of beamline core opto-mechanics like monochromator. The design made for LOREA is based on a Hettrick-Underwood grating type that operates without entrance slit. Experience cumulated over years allowed to face the challenge of designing and building UHV Monochromator. The large energy range of LOREA (10-1000 eV) requires a device with 3 mirrors and 4 gratings with variable line spacing to reduce aberrations. Monochromator most important part, gratings system, has been carefully designed to be isolated from external disturbances as cooling water, and at the same time having high performances. Deep analytical calculations and FEA simulations have been carried out, as well as testing prototypes. The most innovative part of Monochromator is gratings cooling with no vacuum guards or double piping that are well-known source of troubles. Heat load is removed by cooper straps in contact with a temperature controller device connected to fixed water lines. In addition, motion mechanics and services (cabling, cooling) are independent systems. Designs involved give high stability (resonance modes over 60 Hz) and angular resolution below 0,1  $\mu$ Rad over 11 deg range. On mirrors side, it has been used gonio mechanics from MIRAS [1] plus an eutectic InGa interface between cooling and optics to decouple them. Grating and mirror holders are fully removable from main mechanics to be able to assembled at lab measuring to achieve the best fit. Instrument has been already assembled and motions characterization or stability measurements are giving expected results matching with specifications.

### GENERAL DESCRIPTION

LOREA is a 10-1000 eV soft X-Ray beamline to study the electronic structure of solids by Angle Resolved Photo-Emission Spectroscopy (ARPES). Core level photoemission, resonant photoemission and X-Ray absorption spectroscopies are accessible in the entire energy range.

The whole design of the monochromator, which includes a novel cooling design of the gratings, has been fully developed at ALBA. The BL20 Monochromator is based on a Hettrick-Underwood geometry with 3 spherical mirrors (SM) and 4 plane varied line-spaced (VLS) gratings to cover the entire energy range of LOREA.

Optics and mechanics work at ultra-high vacuum (UHV) regime. It is considered a big circular vacuum chamber for gratings plus one of the mirrors and two additional

chambers for remaining two mirrors. An extra chamber contains part of the gratings pitch mechanism, Fig. 1.

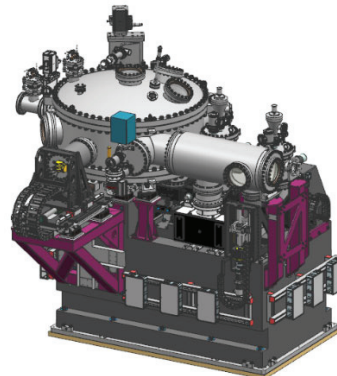


Figure 1: External view of BL20 Monochromator.

### GRATINGS MECHANISM

The gratings mechanics, which can locate up to five gratings, consists on a frame that can be moved transversally to the beam to select the suitable grating. This frame is mounted on an oscillating second frame that produces gratings pitch and it is commanded by a sine arm of 1 m long.

The entire mechanism is placed in vacuum, except the actuator of the sine arm. Two welded bellows, one of them connected to the support and thus standing all the force, compensate the vacuum force on the actuator. The vertical actuator, guided by cross roller linear guides consist on a preloaded satellite roller screw with roller recycling spindle that provides high stiffness and small pitch. Between the sine arm that describes an angular trajectory and the actuator that is lineal, there is a connecting rod with two doubled-ended flexural pivot bearings to reduce as much as possible rolling elements. Figure 2 shows full system.

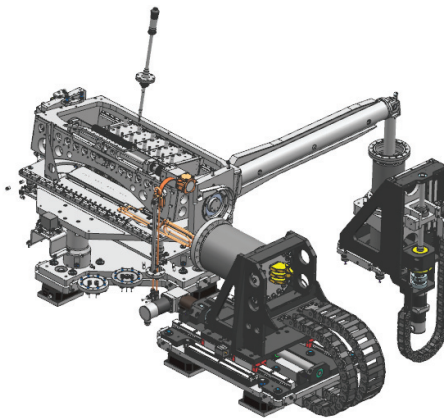


Figure 2: Gratings system design.

Regarding transversal motion, an UHV motor, vacuum adapted guides and spindle are installed, mounted directly on the pitch frame. As grating cooling lines are not linked

\* acrisol@cells.es

## BENDABLE KB TYPE FOCUSING MIRRORS DESIGNED FOR TPS IR BEAMLINE

T.C. Tseng<sup>†</sup>, H.S. Fung, H.C. Ho, K.H. Hsu, C.S. Huang, D.G. Huang, C.K. Kuan, W.Y. Lai,  
 C.J. Lin, S.Y. Perng, H.S. Wang, National Synchrotron Radiation Research Center, Hsinchu, Taiwan

### Abstract

A new IR beamline has been scheduled at TPS beam-line construction Phase III. The new beamline optical design is following the structure of the existed TLS IR beamline. However, the focusing mirrors has to be re-deign according to different situation. These KB type mirrors (HFM and VFM) are same thickness flat stainless plates assembled with bending arms and bended with single motor each to fit quintic polynomial surface profiles for focusing and also modifying arc source effect of bending section. For a same thickness plate in addition with the bending arms effect to form a desired polynomial surface profile, it demands specific width distribution. With the drawing method and FEM iteration simulation, the optimized surface polynomial equation and width distribution design of the mirror plates were defined. The detailed design sequences will be described in this paper.

### INTRODUCTION

There is an IR microscopy beamline located at 14A branch in TLS NSRRC [1, 2]. However, the TLS is scheduled to be shut down after TPS phase III due to the budget consideration. A new IR beamline is therefore scheduled at phase III construction plane. With different conditions from TLS, The TPS IR beamline has to be re-design. The TPS IR beamline adopts the similar design as TLS by using K-B type focusing mirrors in the pre-focusing period. Two Stainless flat mirror plates are to be bended to the desired surface profile. In experience, a 5<sup>th</sup> order polynomial surface profile is enough and also for the manufacturing consideration [3].

With the frontend space consideration, HFM is located 2350mm from the light source point and 4150mm from the focus point. VFM is located 3900mm from the source point and 2600mm from the focus point respectively as in Fig. 1. The beam divergence angles of horizontal and vertical are 50mrad and 25mrad from the source point, respectively. The light-reflecting areas of HFM and VFM are about 166mm x 66mm (maximum) and 77mmx138mm respectively.

For an ideal point light source, by using an elliptical mirror, the light from one focus will be reflected and concentrated in another focus. This phenomenon is well adopted in VFM because it can be regard as from a point source without considering the electron beam size.

For HFM, the light source is an arc section from bending magnet, the light will not concentrate in another focus as in the Fig. 2 drawing and the profile should be modified.

In TLS HFM design, a fourth order RungeKutta numerical method was used to find out the coefficients of the

modified polynomial equation. This method is somewhat complicated to implement. A drawing method was adopted any try to easily find out the profile polynomial.

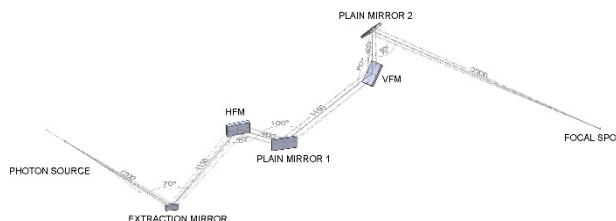


Figure 1: TPS IR beamline pre-focusing period mirror location scheme.

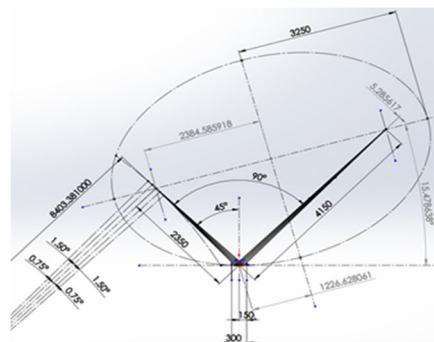


Figure 2: Drawing of light line from arc light source reflecting span on the focus point.

### IDEAL KB TYPE MIRROR SURFACE PROFILE EQUATIONS DERIVED WITH DRAWING METHOD

Let the required 5<sup>th</sup> order profile polynomials equation is (HFM & VFM both):

$$y(x) = c_2x^2 + c_3x^3 + c_4x^4 + c_5x^5 \quad (1)$$

For HFM, at first, 5 ellipses were setup according to the arc divergence angle. The crossed sections were jointed to form a new profile and fitting to get a new polynomial as in Fig. 3.

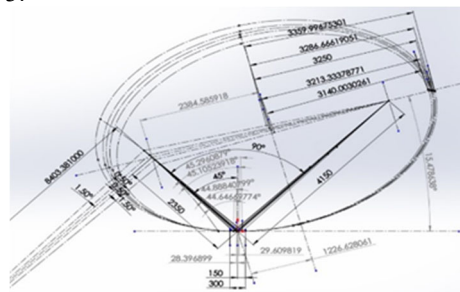


Figure 3: 5 ellipses setup according to the arc divergence angle.

<sup>†</sup> email address: tctsen@nsrrc.org.tw

# CRYOGENIC SYSTEMS FOR OPTICAL ELEMENTS COOLING AT SIRIUS/LNLS

M. Saveri Silva<sup>†</sup>, M. P. Calcanha, G.V. Claudiano, A. F. M. Fontoura, B. A. Francisco, L. M. Kofukuda, F. R. Lena, F. E. P. Meneau, G. B. Z. L. Moreno, J. H. Rezende, G. L. M. P. Rodrigues, L. Sanfelici, H. C. N. Tolentino, L. M. Volpe, LNLS, Campinas, Brazil

## Abstract

This work presents the in-house solution for cryogenic cooling of beamline optics subject to low to moderate thermal loads at Sirius at the Brazilian Synchrotron Light Laboratory (LNLS). The main requirements regarding extracted power and coolant consumption are detailed. We also discuss discoveries and improvements deployed during the commissioning of the CATERETÊ and the CARNAÚBA beamlines, such as the prevention of ice formation, stabilization of both thermal load and flow-rate, and auto-filling parameters, among others.

## INTRODUCTION

Sirius, the Brazilian 4th-generation light source at the Brazilian Synchrotron Light Laboratory (LNLS), presents high-performance requirements in terms of preserving photon-beam quality, particularly regarding wavefront integrity and position stability. In this context, it is imperative that many silicon optical elements are effectively cooled, so that temperatures and their control-related parameters can be precisely handled to the point in which thermal effects are acceptable concerning figure distortions and drifts at different timescales. Keeping in mind the class of precision equipment, the required performance can only be achieved with robust thermal modelling [1-3]. For this, relevant aspects related to the implementation of liquid nitrogen cooling systems need to be emphasized. Currently, two solutions are present in the first-phase beamlines, according to the component thermal load: (1) a commercial cryocooler for high-heat-load applications (50 – 3000 W), such as the double-crystal monochromators; and (2) an in-house low-cost system for components under moderate loads such as the mirror systems and the four-bounce monochromators (4CM). This work describes the in-house solution, with examples from the CARNAÚBA (CNB) and CATERETÊ (CAT) beamlines.

## OPEN LN2 CRYOSTAT SYSTEMS

Figure 1 illustrates the cooling circuit of a 4CM at CNB. Inside the vacuum chamber (a), the crystals are connected through thermal braids [4] to a commercial cryostat (b), which is fed with liquid nitrogen (LN2) by an instrumented cylinder (c). Level and pressure are controlled by standard beamline automation system that automatically feed it from a dedicated transfer line (d) connected to a secondary service unit external to the hutch (e) or to the LN2 line of the building. Gaseous nitrogen leaves the first vessel by an

exhaust line (f) during filling, whereas the gas in the cryostat outlet is released inside the hutch at a significantly lower rate at normal operation. The LN2 flow in the cryostats is adjustable by regulating its flow regulating valve and the pressure of the liquid cylinder.

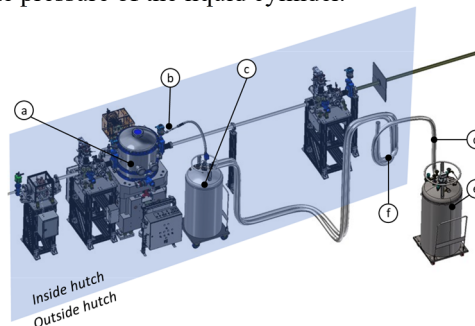


Figure 1: Third optical hutch of the CARNAÚBA beamline, highlighting the liquid nitrogen supply system of the 4CM, which comprises the vacuum chamber (a), the cryostat (b), the primary (c) and secondary (e) LN2 cylinders, the transfer line (d) and the exhaust line (f).

Figure 2 shows the top view of a primary vessel. Besides the standard items, custom stems were added to supply extra handles and solenoid valves for liquid and gas and to monitor pressure and level data.

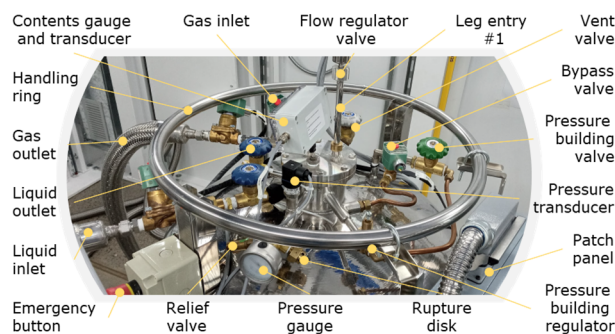


Figure 2: Top of primary LN2 cylinder and description of the connected elements.

The vessel inside the first optical hutch of CNB is connected to two cryostats, which cool the first mirror (M1) and an internal diagnostics (XDU), present in the same vacuum chamber. The same structure appears in its second optical hutch for the chamber enclosing the second mirror (M2) and the secondary source aperture (SSA). For all other optics, only one cryostat is assembled at each vessel.

<sup>†</sup> marlon.saveri@lnls.br

# COMMISSIONING AND PROSPECTS OF THE HIGH-DYNAMIC DCMs AT SIRIUS/LNLS

R. R. Geraldes<sup>†1</sup>, J. L. Brito Neto, R. M. Caliari, G. S. de Albuquerque, M. A. S. Eleotério,  
S. A. L. Luiz, M. A. L. Moraes, A. V. Perna, M. Saveri Silva  
Brazilian Synchrotron Light Laboratory (LNLS), 13083-970, Campinas, São Paulo, Brazil  
<sup>1</sup>also at the Eindhoven University of Technology (TUE), 5612AZ Eindhoven, The Netherlands

## Abstract

The High-Dynamic Double-Crystal Monochromator (HD-DCM) is an opto-mechatronic system with unique architecture, and deep paradigm changes as compared to traditional beamline monochromators. Aiming at unmatched scanning possibilities and positioning stability in vertical-bounce DCMs, it has been developed since 2015 for hard X-ray beamlines of Sirius Light Source at the Brazilian Synchrotron Light Laboratory (LNLS). Two units are currently operational at the MANACÁ (macromolecular crystallography) and EMA (extreme conditions) undulator beamlines, whereas a model for extended scanning capabilities, the so-called HD-DCM-Lite, is in advanced development stage for forthcoming bending magnet and undulator beamlines. This work presents commissioning data related to the two HD-DCM units, together with the developed operation strategies and the overall control architecture, with emphasis on the 10 nrad RMS (1 Hz to 2.5 kHz) pitch parallelism performance, the calibration procedures and flyscan-related discussions.

## INTRODUCTION

The High-Dynamic Double-Crystal Monochromator (HD-DCM) [1] has been developed by the Brazilian Synchrotron (LNLS) for Sirius [2] and the demanding new generation of X-ray beamlines. With a predictive design methodology [3] and original concepts for a DCM that are based on precision mechatronics [4], it has proven to meet the mark of 10 nrad RMS pitch parallelism performance, both in fixed-energy and scanning operation modes, over the broad frequency range from 1 Hz to 2.5 kHz, which is sui generis in vertical-bounce DCMs.

The system has already been described to the community in different aspects: the conceptual design, the mechatronic principles and thermal management solutions were presented in MEDSI 2016 [5–8]; results of in-air validation of the core, together with system identification and control techniques in the prototyping hardware, were shown in ICALEPCS 2017 [9, 10]; the offline performance of the full in-vacuum cryocooled system, including scans solutions were presented in MEDSI 2018 [11]; and the dynamic modelling work, together with updated control design and the FPGA implementation in the final NI CompactRIO (cRIO) hardware were discussed in the ASPE Topical Meeting 2020 [12–14]. Here, commissioning results of the two operational units at MANACÁ and EMA undulator

beamlines at Sirius are presented, together with procedures, strategies, and the related beamline architecture.

## COMMISSIONING PROCEDURE

The commissioning procedure that has been developed for the HD-DCM follows the steps presented in Fig. 1 and described below:

1. *Beam through* consists of passing the first monochromatic beam of a given energy to downstream sensors or visualization elements after short scans in the Bragg angle, in the pitch angle of the 2<sup>nd</sup> crystal of the DCM and/or the undulator phase, which is a quick job if off-line fiducialization and laser-tracker-based alignment procedures at the beamline are properly realized.
2. *Preliminary DCM-undulator tuning* is meant as a coarse mapping between the Bragg angle and undulator phase for different harmonics, which relies on beam simulation and can be done in terms of output flux or image processing.
3. *Preliminary Rocking Curve analysis* is related to optimizing the roll parallelism and scanning the pitch of the 2<sup>nd</sup> crystal in the DCM for a few energy values of interest. Thus, the quality of the crystalline lattice –which depends on manufacturing, mounting and the cryogenic thermal management – can be verified, while the internal metrology feedback to keep the parallelism according to maximum flux is evaluated.
4. *Preliminary energy calibration* is dedicated to calibrating the Bragg angle encoder homing offset according to one or more absolute energy values provided absorption standards in spectroscopy measurements.
5. *Fine DCM-undulator tuning* is the refinement of the undulator energy-phase calibration with the calibrated Bragg angles over the whole operational energy range.
6. *Fine energy calibration* consists in optionally exploring multiple absorption edges over the full energy range to calibrate occasional repeatable non-linearities in the encoder of the Bragg angle.
7. *Fine parallelism calibration* is an optional flux-based step for repeatable non-linearities in pitch (in the piston-tip-tilt internal metrology of the crystal cage, as described in [5]) as the gap between crystals varies over the full energy range.
8. *Fixed-exit calibration* is the final step in which angular or translational deviations of the monochromatic beam are mapped over the complete energy range by image processing, quadrant sensors or knife-edge measurements, and compensated by the internal degrees-of-freedom in the crystal cage.

<sup>†</sup> renan.geraldes@lnls.br

# FOUR-BOUNCE CRYSTAL MONOCHROMATORS FOR THE SIRIUS/LNLS BEAMLINES

M. Saveri Silva<sup>†</sup>, J. H. Rezende, L. M. Dos Santos, L. M. Kofukuda, A. P. S. Sotero  
L. M. Volpe, G. S. de Albuquerque, S. A. L. Luiz, H. C. N. Tolentino  
LNLS, Campinas, Brazil

## Abstract

Beamlines of new 4th-generation machines present high-performance requirements in terms of preserving beam quality, in particular wavefront integrity and position stability at micro and nanoprobe stations. It brings about numerous efforts to cope with engineering challenges comprehending high thermal load, cooling strategy, crystal manufacturing, vibration sources, alignment and coupled motion control. This contribution presents the design and performance of four-bounce silicon-crystal monochromators for the Sirius beamlines at the Brazilian Synchrotron Light Laboratory (LNLS), which is basically composed of two channel-cut crystals mounted on two goniometers that counter-rotate synchronously. The mechanical design ascertained the demands for the nanoprobe and coherent scattering beamlines - namely, CARNAÚBA and CATERETÊ - focusing on solutions to minimize misalignments among the parts, to grant high stiffness and to ensure that the thermal performance would not impair beam characteristics. Hence, all parts were carefully simulated, machined, and measured before being assembled. The present work introduces mechanical, thermal, diagnostics, and dynamic aspects of the instruments, from the design phase to their installation and initial commissioning at the beamlines.

## INTRODUCTION

Carnaúba (CNB) and Cateretê (CAT) are the longest Sirius beamlines. Their scientific programs bring several cutting edge contrasts and imaging techniques for research in numerous science fields. Carnaúba has a sub-microprobe (600-150 nm) and nanoprobe (120-40 nm) experimental stations and covers the energy range from 2.05 to 15 keV. Cateretê's experimental station is followed by a 30 m flight path in-vacuum detector and receives a 30  $\mu\text{m}^2$  beam in the energy range from 4 to 21 keV. In order to achieve such goals, the beamline instrumentation needs to present exceptional performance [1, 2]. Notably, such beamlines will use a four-bounce crystal monochromator (4CM) to select and scan X-rays with resolution of  $\Delta E/E=10^{-4}$ .

The main attributes of a 4CM are the high energy resolution and its independency from the beam divergence [3]. The first Sirius' 4CMs are based on cryogenically cooled Si crystals and it introduces a simple concept that prioritizes high mechanical stiffness associated to robust control.

<sup>†</sup> marlon.saveri@lnls.br

## MECHANICAL DESIGN

The equipment comprises a pair of channel-cut silicon crystals in a horizontal +--+ configuration so that the parallelism between diffraction surfaces is inherently ensured, the downstream beam keeps the same direction of the upstream beam regardless of Bragg's angle, and higher resolution in the selection of X-ray energy is achieved when compared to double crystal monochromators [4]. Table 1 shows the 4CM specifications.

Table 1: Specifications of Carnaúba and Cateretê 4CMs

Parameter	CNB	CAT
Crystal Set	Si (111)	
Angular Range (°)	7-75	4.5-50
Encoder Resolution (urad)	<< 1	
Axes synchronization (urad)	< 10% D.W.	
Crystal Size (mm <sup>3</sup> )	62x90x50	50x98x62
Channel-Cut gap (mm)	8.0	6.2
Crystal Temperature	125 K	
Beam Size (mm <sup>2</sup> )	1.5x2.6	0.99 x 0.51
Heat Load from Beam (W)	7	17.4
Base Pressure	<5E-8 mbar	

The rotation of the crystals around Bragg angle is driven by a pair of high-resolution goniometers Aerotech APR-200. Naturally, both axes must rotate in opposite directions. Hard stops and limit switches confine the ranges to avoid damage.

The cooling source is a commercial ST-400 UHV cryostat (Janis) supplied by an open cycle liquid nitrogen flow, capable of dissipating 70 W and linked to the crystals by copper thermal straps (TS), which allows the rotations. Additional copper parts are used to fit the different geometries and follow the crystal rotation movement. The straps are also useful to attenuate vibrations from the cooling system, whereas the goniometers are rigidly fixed on a granite bench, which aims to minimize the amplification of vibrations from the ground, Figure 1.

Each channel-cut crystal is clamped to a titanium frame at three contact zones with flexible links designed to minimize deformation and maximize stiffness. The frame is kept in an intermediary temperature, while the rotary stage below it is kept at environmental temperature, Figure 2 zooms the previous figure, highlighting the crystal frame.

# INSTALLATION AND COMMISSIONING OF THE EXACTLY-CONSTRAINED X-RAY MIRROR SYSTEMS FOR SIRIUS/LNLS

V.B. Zilli†, C.S.N.C. Bueno, G.V. Claudiano, R.R. Geraldés, G.N. Kontogiorgos, F.R. Lena, S.A.L. Luiz, G.B.Z.L. Moreno, A.C. Pinto, G.L.M.P. Rodrigues, M.S. Souza, L.M. Volpe  
Brazilian Synchrotron Light Laboratory (LNLS), Brazilian Center for Research in Energy and Materials (CNPEM), 13083-970, Campinas, Sao Paulo, Brazil

## Abstract

Innovative exactly-constrained thermo-mechanical designs for beamline X-ray mirrors have been developed since 2017 at the 4th-generation Sirius Light Source at the Brazilian Synchrotron Light Laboratory (LNLS). Due to the specific optical layouts of the beamlines, multiple systems cover a broad range of characteristics, including: power management from a few tens of mW to tens of W, via passive room-temperature operation, water cooling or indirect cryocooling using copper braids; mirror sizes ranging from 50 mm to more than 500 mm; mirrors with single or multiple optical stripes, with and without coatings; and internal mechanics with one or two degrees of freedom for optimized compromise between alignment features, with sub-100-nrad resolution, and high dynamic performance, with first resonances typically above 150 Hz. Currently, nearly a dozen of these in-house mirror systems is operational or in commissioning at 5 beamlines at Sirius: MANACÁ, CATERETÊ, CARNAÚBA, EMA and IPÊ, whereas a few more are expected by the end of 2021 with the next set of the forthcoming beamlines. This work highlights some of the design variations and describes in detail the workflow and the lessons learned in the installation of these systems, including: modal and motion validations, as well as cleaning, assembling, transportation, metrology, fiducialization, alignment, baking and cooling. Finally, commissioning results are shown for dynamic and thermal stabilities, and for optical performances.

## INTRODUCTION

For the past couple of years many beamlines have passed from the design stage to assembly, installation, and commissioning at the 4th-generation Sirius Light Source at the Brazilian Synchrotron Light Laboratory (LNLS) [1]. Regarding the novel exactly-constrained X-ray mirrors for Sirius [2], during the design phase extra care was taken to ensure beam characteristics – i.e., acceptable nanometric deformation into the mirror’s optical faces –, and alignment capabilities at the beamline, with new procedures, tools, and manuals being developed to certify installations.

Five beamlines at Sirius, namely, MANACÁ (MAN), CATERETÊ (CAT), CARNAÚBA (CNB), EMA and IPÊ, summarized in Table 1, currently rely on these in-house solutions, and a few more are expected by 2021. Through the commissioning phase on the first three of them, some important results have been found regarding fine and coarse alignment, leading to some significant beam results. Ther-

mal management and cryogenics, modal and bench stability results are briefly presented. Some potential future improvements were found and are briefly discussed.

Table 1: First Beamlines Summary

Beam-line	Energy Range	Source	Status
CNB	2.05–15 keV	ID	Commissioning
MAN	5–20 keV	ID	Commissioning
CAT	5–20 keV	ID	Commissioning
IPÊ	100–2000 eV	ID	Installation
EMA	2.7-30 keV	ID	Assembling

## ASSEMBLY AND INSTALLATION

Following standardized step-by-step guidelines, internal mechanisms pre-assembly, characterization and fiducialization ensures high-quality and repeatability to the assembly and installation processes. The main procedures steps are presented and discussed.

### Assembly

A well-done cleaning certifies the removal of any contaminants into the ultra-high vacuum (UHV), to which most of the mirror systems are submitted. The main contaminants identified are machine oil used for lubrication, human skin oil, dust, and metal particles from machining which are mainly encountered on surface roughness and holes.

The first cleaning process is mechanically pre-cleaning the parts using the alkaline detergent IC115 which is followed by common water and demineralized water rinsing. To guarantee the part cleanliness, when necessary, an ultrasonic bath with the part submerged into a IC115 (10%) and water solution at ambient temperature is made for variable times, depending on the part size, geometrical complexity, and material.

A comprehensive and intuitive pre-assembly workflow has been developed ensuring quality and repeatability. The internal mechanism assembly method can be subcategorized into some main stages and were executed inside a controlled clean room [3]. Firstly, the mirror support is fixated, securing position, and favoring the precision mechanism fixation. Then, dowel pins and folded leaf-springs (FLS) fixation can be done (see [2]). The pins guarantee positions according to design. All FLS need to be screwed by hand before tightening, to prevent pre-tensioning, which might induce asymmetric stiffness into the system. Numer-

† vinicius.zilli@lnls.br

## VIBRATION ASSESSMENT AT THE CARNAUBA BEAMLINE AT THE SIRIUS/LNLS

C. S. N. C. Bueno†, F. A. Borges, G. S. de Albuquerque, G. R. B. Ferreira, R. R. Geraldés, L. M. Kofukuda, M. A. L. Moraes, G. B. Z. L. Moreno, D. V. Rocha e Silva, M. H. S. Silva, H. Tolentino, L.M. Volpe, V. B. Zilli, Brazilian Synchrotron Light Laboratory (LNLS), Brazilian Center for Research in Energy and Materials (CNPEM), 13083-970, Campinas, Sao Paulo, Brazil

### Abstract

CARNAÚBA (Coherent X-Ray Nanoprobe Beam-line) is the longest beamline at Sirius Light Source at the Brazilian Synchrotron Light Laboratory (LNLS), working in the energy range between 2.05 and 15 keV and hosting two stations: the sub-microprobe TARUMÃ and the nanoprobe SAPOTI, with coherent beam size varying from 500 to 30 nm. Due to the long distances from the insertion device to the stations (135 and 143 m) and the extremely small beam sizes, the mechanical stability of all opto-mechanical systems along the facility is of paramount importance. In this work we present a comprehensive set of measurements of both floor stability and modal analyses for the main components, including: two side-bounce mirror systems; the four-crystal monochromator; the Kirkpatrick-Baez (KB) focalizing optics; and the station bench and the sample stage at TARUMÃ. To complement the components analyses, we also present synchronized long-distance floor acceleration measurements that make it possible to evaluate the relative stability through different floor slabs: the accelerator slab; experimental hall slab; and the slabs in the satellite building, consisting of three inertial blocks lying over a common roller-compacted concrete foundation, the first with the monochromator and the remaining ones with one station each. In addition to assessing the stability across this beamline, this study benchmarks the in-house design of the recently installed mirrors, monochromators, and end-station.

### INTRODUCTION

CARNAÚBA's (Coherent X-Ray Nanoprobe Beamline) [1] sub-micron station TARUMÃ and nanoprobe SAPOTI are the two experimental station at Sirius Light Source with the largest distances to the source, namely, at 135 meters and 143 meters from the insertion device, respectively. Then, due to the long optical lever-arms, beam sizes at the sample between 30 and 500 nm, and strict stability requirements for coherent imaging techniques, all opto-mechanical systems in CARNAÚBA must be carefully designed [2], assembled, installed, and validated.

As shown in the simplified diagram of Fig. 1, CARNAÚBA relies on an undulator source, which is located inside the storage ring tunnel, lies on the storage ring especial floor [3], and serves as the origin for the CARNAÚBA coordinate system. At 27.4m, already outside the tunnel, but still on the storage ring special floor, the first main opto-mechanical system is the side-bounce elliptical mirror

(M1) [4], that focalizes the beam in the secondary source. Next, in the experimental hall, at about 54.3m from the source, the second main opto-mechanical system is composed of the secondary source mechanism and the planar mirror (M2), which finally directs the beam to the satellite building, where the monochromator (4CM) [5] and the experimental stations, TARUMÃ (TAR) [6] and SAPOTI (SAP), are found on special inertial blocks at 130m, 135m and 143m, respectively.

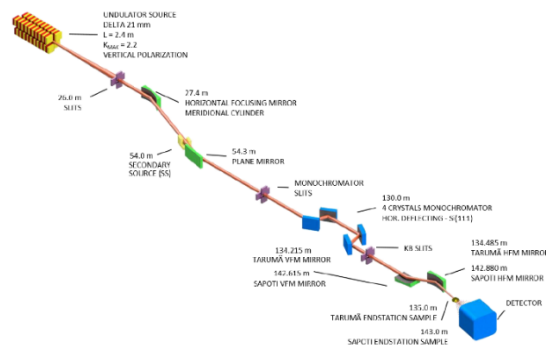


Figure 1: Simplified diagram of the CARNAUBA beamline.

### METHODOLOGY

The different types of measurements relied on specific setups, hardware, and software. In the modal analyses, a triaxial modal accelerometer Kistler 8762A5, an instrumented impact hammer PCB Instruments 086C03, and a NI USB-4431 DAQ acquisition board with 24-bit resolution running with NI Signal Express at 10kHz, were used for the frequency response function characterizations. In a sequence of measurements for each component, by attaching the accelerometer to different points of the structure, while keeping the excitation with the impact hammer in a convenient point, animated mode shapes can be created using a software toolbox developed in-house. For each measurement point, a series of four impacts was repeated to maximize statistics for coherence and data quality. For each impact, the time signal was recorded for 2s, with a pre-trigger margin of 10% of this.

In the floor and component stability analyses two seismic accelerometers Wilcoxon 731 together with two power amplifiers P31 were used with the same acquisition board and rate mentioned above, but for a total of 60s. For the power spectrum density (PSD) calculations, it was used a window of 10s and 50% overlap. Then, for cumulative power spectrum (CPS) and cumulative amplitude spectrum (CAS) data, integration is made up to 450Hz, that is the maximum frequency for this seismic accelerometer.

† cassiano.bueno@lnls.br

# THE DESIGN AND MANUFACTURING OF SUPERCONDUCTING UNDULATOR MAGNETS FOR THE ADVANCED PHOTON SOURCE UPGRADE\*

E. Anliker†, Q. Hasse, Y. Ivanyushenkov, M. Kasa, Y. Shiroyanagi  
Argonne National Laboratory, Lemont, Illinois, United States of America

## Abstract

The Advanced Photon Source Upgrade (APS-U) will include 4 full length Superconducting Undulators (SCU). These SCUs require new undulator magnets to achieve the required performance of the new machine. The magnets are fabricated from low carbon steel and wound with NbTi superconductor. To meet the needs of the users, the magnets will be manufactured in different lengths and magnetic periods to accommodate SCUs in both inline and canted configurations. Because their operational conditions do not allow for shimming or other tuning adjustment, the magnets used in the APS-U SCUs require very tight tolerances for the poles and winding grooves that push the extents of their manufacturability. This paper will cover the design of the 1.9m long magnets for the inline SCUs, their measurement data, lessons learned from manufacturing, and an overview of design changes that were made for the magnets to be used in the canted SCU configurations.

## INTRODUCTION

The Advanced Photon Source (APS) located at Argonne National Laboratory (ANL) is currently undergoing an upgrade (APS-U) including a new storage ring and new insertion devices (IDs). Among the new IDs are four new Superconducting Undulators (SCUs) that will occupy the entire space provided in a straight section (~5.3 m) of the new storage ring. The SCUs required new magnets to be designed and manufactured to fit inside the new devices while achieving the magnetic performance required by the new accelerator. The new magnet designs aim to preserve desired features and functionality from past magnet designs, while also integrating new features to make the design more universal and easier to manufacture.

## INITIAL DESIGN

The APS-U SCU magnet designs are an evolution of previous magnet designs used in past SCUs [1]. The previous designs (Fig. 1) consisted of a low-carbon steel core with G-10 spacers on top that were held in place with spring pins and low carbon steel poles on the bottom held in place with screws. These spacers and poles created grooves that would be used to wind the conductor around the magnet. The magnets also included holes drilled into the top of the magnet core so turn-around pins could be inserted during the winding process.

\* This research used resources of the Advanced Photon Source, a U.S. Department of Energy (DOE) Office of Science User Facility at Argonne National Laboratory and is based on research supported by the U.S. DOE Office of Science-Basic Energy Sciences, under Contract No. DE-AC02-06CH11357.

† eanliker@anl.gov

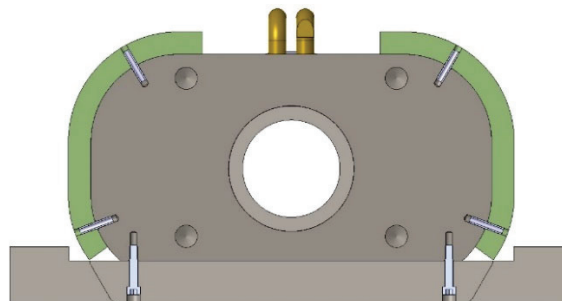


Figure 1: Previous SCU magnet core design that encompassed G-10 spacers and individual pole inserts.

The new SCU magnet designs for APS-U vary in length from 1.3 m - 1.9 m and have magnetic periods of 16.5 mm and 18.5 mm. This is the longest magnet that has been manufactured and wound by the SCU team at the APS. Features retained from previous designs include holes on top of the magnet core for the turn-around pins, helium channels that pass through the magnet, and a modified footed pole to be used during the resin impregnation (potting) process that extends out of the sides near the bottom of the magnet.

The magnets were modified from previous designs by changing the overall height and width of the magnet to have a better fit inside of the new cryostat [2]. Another benefit of a wider magnet is that the region of the magnet influencing the electron beam would be expanded and allow for a looser alignment tolerance of the magnets.

Other modifications include the removal of the G-10 spacers and individual poles on the magnet. The magnets now consist of a single piece with the grooves machined directly into the core, replacing the individual poles and spacers. This new magnet design can be seen in Fig. 2. This dramatically reduced the number of holes being drilled and tapped into the magnet core and reduced the overall number of pieces in the magnet assembly. The magnets still need to incorporate an extended pole insert at specific locations along the length of the core to be used in the potting process. Instead of using individual inserts like previous designs the inserts were changed to a single machined piece that included three poles and two grooves fastened by two 4-40 screws.

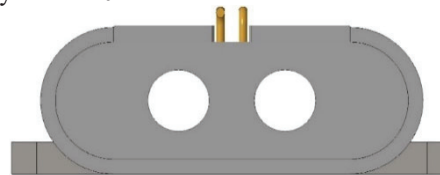


Figure 2: Magnet design used on the APS-U 1.9 m SCUs showing single piece core and footed poles.

# THE ADVANCED PHOTON SOURCE UPGRADE (APSU) SUPERCONDUCTING UNDULATOR (SCU) COMPONENT DATABASE (CDB) UTILIZATION

G. Avellar<sup>†</sup>, E. Anliker, J. Lerch, J. Saliba, M. Szubert  
 Argonne National Laboratory, Advanced Photon Source-Upgrade, Lemont, USA

## Abstract

The Component Database (CDB) is a document management platform created for the use of the Advanced Photon Source Upgrade (APSU) Project. It serves two major functions: (1) a centralized location to link all data relating to field-replaceable upgrade components, and (2) a way to track the components throughout the machine's 25-year lifetime. There are four (4) Superconducting Undulators (SCUs): two (2) Inline 16.5mm period devices, one (1) Canted 16.5mm period device, and one (1) Canted 18.5mm period device. Throughout the production process for these devices, tracking components between the different designs of SCU's has proven to be a logistical issue, as there are uniform components among all 4 devices, but many unique components as well. As the scope evolved from a Research and Development (R&D) activity to a production scope, the CDB has been critical in communicating with a growing team, allowing anyone to identify a part or assembly and access all its design and manufacturing data. The 4.8-meter long SCUs are the first of their kind, requiring thorough onsite inspections, intricate assembly procedural, and approved safety protocols. This is ideal information to document in an electronic traveler (e-traveler), which can then be attached to an item within the CDB. By providing a straightforward process for technicians to follow, the risk of miscommunication and unsafe practices are minimized. The CDB plays a vital role in simplifying and optimizing the transition of the SCU from an R&D unit to a production scope, from procurement to inspection, assembly and installation, and throughout the lifespan of machine maintenance.

## INTRODUCTION

The Advanced Photon Source Upgrade (APSU) Project will replace the current storage ring with a combination of new and refurbished components. The result will be a new machine producing X-rays up to 500 times brighter than the current device. The design phase is complete, procurements are well underway, and the year-long shut down for installation is set to start in April 2023 [1]. Four of the Insertion Device (ID) straight sections will be equipped with new 4.8-meter long Superconducting Undulators (SCUs) of various magnetic periods, which accommodate canted and inline configurations. These complex devices produce photons at different energies to be used by the ID beamline users. A single cryostat and base assembly can house two undulator magnet pairs, the cryogenic cooling system, and vacuum chamber (Fig. 1) [2]. With the various designs for

the inline 16.5mm period device, canted 16.5mm period device, and canted 18.5mm period device, the need for a streamlined database to organize procurements and procedures, and to effectively communicate this information, was evident. The Component Database (CDB) has proven to be vital in the transition of SCUs from a Research and Development (R&D) scope to a production process. The defining feature of the CDB is that it is an integrated system that links many other databases and can pull data seamlessly from many sources.

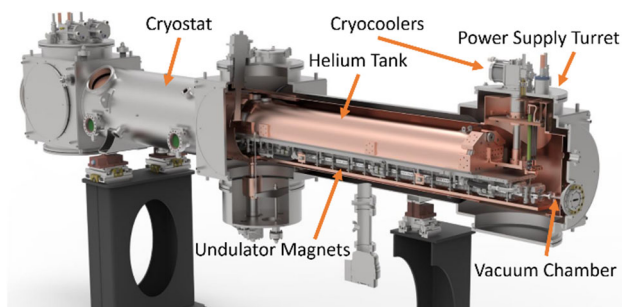


Figure 1: Cross-section rendering of the inline 16.5mm Superconducting Undulator, showing the cooling system, magnets, power supply turrets, and vacuum chamber.

## OVERVIEW

The CDB is used Project wide and became increasingly more important as APSU procurements ramped up and the project transitioned into the production phase. The CDB is organized into two layers, the *Catalog* level and *Inventory* level. At the *Catalog* level, components are organized by Technical System and then by Function. Specifically, for SCU's, this path is *Insertion Devices* and then *Undulator-Superconducting*. Once here, a list of all components relating to the device are listed along with important information, such as model number, images, a description, and inventory information. There is also a search bar at the top of the CDB page allowing for ease of access if the model number or a key word is known. This allows anyone, project-wide, to quickly access information, even if they are not intimately familiar with the assembly and subassembly breakdown of an SCU. Selecting a part will redirect the page to that part's *Catalog* level where all general information on it can be found. Here, the *Inventory* sub-section is listed as one *Instance* entry for each item ordered, and if selected will display all the information collected for that item. This includes location, status, date received, the purchase requisition, links to vendor documentation and drawings, and an electronic traveler (e-traveler) that is filled out by the technicians and engineers after the part is inspected.

<sup>†</sup> Email: gavellar@anl.gov

# THE ADVANCED PHOTON SOURCE UPGRADE (APSU) STRAIGHT SECTION VACUUM SYSTEMS FIRST ARTICLE FABRICATION\*

M. Szubert<sup>†</sup>, E. Anliker, G. Avellar, J. Lerch

Argonne National Laboratory (ANL), Advanced Photon Source-Upgrade, Lemont, IL, USA

## Abstract

The Advanced Photon Source Upgrade (APSU) includes 40 straight sections, 35 of which will be outfitted with Superconducting Undulators (SCUs) or Hybrid-Permanent Magnetic Undulators (HPMUs). The vacuum systems for these devices are primarily fabricated from aluminum extrusions and are required to provide Ultra-High Vacuum continuity between storage ring (SR) sectors for a nominal distance of ~5.4 meters. Each vacuum system has unique fabrication challenges, but all first article (FA) components have been produced successfully. The FAs arrived onsite at ANL installation-ready but have undergone functional testing activities to verify the production and vacuum certifications. The Insertion Device Vacuum Chamber (IDVC), used in HPMU sectors, is produced by SAES Rial Vacuum (Parma, Italy). The SCU vacuum system components are produced by two vendors, Cinel Instruments (Venice, Italy) and Anderson Dahlen (Ramsey, MN, USA). Based on the reliable outcomes and lessons learned from the FAs, production of the straight section vacuum systems is underway.

## INTRODUCTION

The Advanced Photon Source Upgrade (APSU) project plan calls for the current APS 40 sector storage ring (SR) to be retrofitted with a new 6 GeV, 200 mA storage ring optimized for brightness above 4 keV [1]. Thirty-five straight sections produce photons at various energies to the Insertion Device (ID) beamline users, with 31 straight sections equipped with Hybrid Permanent Magnet Undulators (HPMUs) and 4 straight sections equipped with Superconducting Undulators (SCUs).

Each of these ID straight sections require a vacuum system to ensure Ultra-High Vacuum continuity between SR sector arcs. They both interface with the P0 Beam Position Monitor Bellows assembly at the upstream (US) and downstream (DS) locations. At these locations, the vacuum systems match the Ø22 mm SR aperture, but transition to various shapes at their thin-wall locations. In addition, both vacuum systems accommodate two configurations, i.e. canted and inline. While the HPMU ID Vacuum Chamber (IDVC) and SCU Vacuum System designs differ based on their operational and interface requirements, each vacuum system has been independently optimized to achieve a uniform design for both the canted and inline variants in their respective sectors [2, 3].

\* This research used resources of the Advanced Photon Source, a U.S. Department of Energy (DOE) Office of Science User Facility at Argonne National Laboratory and is based on research supported by the U.S. DOE Office of Science-Basic Energy Sciences, under Contract No. DE-AC02-06CH11357.

<sup>†</sup> Corresponding Author's Email: mszubert@anl.gov

## OVERVIEW

Procuring the ID straight section components included long lead items, sole-source awards, and best-value vendor evaluation. Each purchase order introduced its own unique challenges, both due to technical capabilities and aggressive scheduling. The first articles (FAs) are necessary to prove the design concept and uncover issues that would avoid future production complications that may incur a cost increase or add schedule delays.

The designs require the use of complex manufacturing processes, modified vacuum procedures, complicated weld joints, and off-site testing by the vendors. The FAs for the straight section vacuum system are critical hold points in the production process for these new vacuum designs.

## ID VACUUM SYSTEM

The fabrication of the ID Vacuum System consists of 3 aluminum extrusions, each modified to create a vacuum chamber (VC) with an integrated aperture transition, a strongback (SB) spanning the length of the straight section (~5.4 meters), and an additional support bracket to satisfy the aperture alignment requirements. After competitively bidding the fabrication of the IDVC and supports, the scope was awarded to SAES Rial Vacuum (SRV) in Parma, Italy. The aluminum components, extrusions and flanges, were supplied to SRV at the beginning of the project, with the remaining material, components, and equipment acquired by the vendor.

Fabrication of the FA included procuring the aluminum extrusions and aluminum flanges early in the design process as they were long lead items. Fig. 1 shows the extrusions at various stages of manufacturing: preliminary material removal of the VC (Fig. 1a), the trapezoidal SB with a mounting plate prepared for shipping (Fig. 1b), and the l-brackets that support the chamber 5 places along its length, allowing for alignment (Fig. 1c).

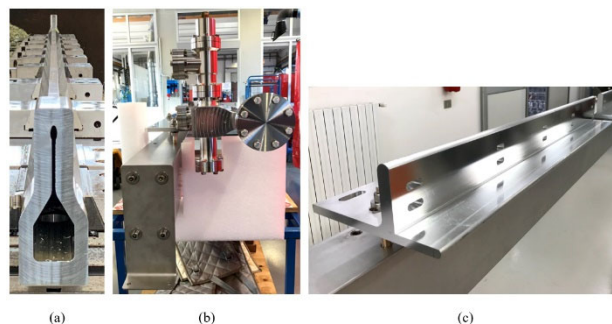


Figure 1: IDVC extrusion profiles throughout the fabrication process, 1a shows the VC, 1b shows a side view of the SB profile, and 1c shows the modified l-bracket profile.

# AUTOMATED MECHANICAL INSPECTION AND CALIBRATION OF INSERTION DEVICES IN APS STORAGE RING\*

N. Weir<sup>†</sup>, E. Gubbels, Advanced Photon Source, Argonne National Laboratory, Lemont, IL, USA

## Abstract

A novel technique has been developed to automatically inspect and calibrate the 53 permanent magnet insertion devices in the Advanced Photon Source (APS) storage ring. This technique employs standard frequency domain analysis to create easily identifiable signatures in an actionable format. We will discuss the mechanisms and actions taken behind various observed trends and its application for continuous monitoring and predictive maintenance of these devices. This technique has enabled predictive maintenance and provided new insights into optimizing device performance.

## INTRODUCTION

Hybrid permanent magnet undulator (HPMU) insertion devices require reliable micron level accuracy and precision during operation [1]. Many of the devices have been in service for more than 25 years. Each of these devices have four or more drivetrains totalling to over 212 in operation. The continuous operation and radiation environment of the APS storage ring presents unique challenges for maintenance. To ensure the reliability of devices, manual measurements at common points of operation and regular preventative maintenance are performed during the available triannual “shutdowns”. While this provides a sanity check and adheres to manufacturers’ recommended maintenance schedule, it does not effectively prevent or provide insight to commonly occurring issues during operation. To enable a more efficient, comprehensive, and data-driven solution, a program to perform automated inspections was written.

Positioning of the upper and lower magnetic support structures (strongbacks) are each controlled by two individual drivetrains. Though they are controlled and operated individually, each of these two drivetrains are coupled through their shared connections with the upper or lower strongback. This coupling action can lead to a constructive amplification of errors in each drivetrain. Additionally, the drivetrain and feedback systems are inset from the end of the strongback. Small angular changes in the orientation of the strongback due to small errors in the drivetrain system will be magnified over the length of the strongback, leading to larger uncertainty in the exact position of the ends of the magnetic structures. These magnification effects make it crucial to identify and eliminate preventable errors in the drivetrain.

The most common faults during operations in order of occurrence is overtravel limit trip, extreme limit trip, motor stall, linear encoder failure, and rotary encoder failure. The overtravel switches are often set within 100  $\mu\text{m}$  of the usable gap to balance machine safety and user reliability. Given that these switches are located at the ends of the strongback, the mechanical inaccuracies present are significantly amplified. Without quantitative characterization, reasons for the fault are difficult to troubleshoot due to the initial switch setting, start of travel position, and travel end positions all being factors in the diagnosis. The other faults can be equally difficult to diagnose due to the mechanical, electrical, and software components involved.

## METHOD

Each HPMU contains a redundant set of feedback devices meant to maintain operation in case one fails; a rotary encoder directly coupled to the motor and a linear encoder directly coupled between the static frame and strongback. The rotary encoder uses a hard coded relationship between turns of the motor and physical position of the strongback to extrapolate its position. The linear encoder directly measures the position of the strongback. Errors in the drivetrain system (Fig. 1) that controls the strongback will therefore present themselves as an accumulated discrepancy between the rotary feedback and linear feedback. By analysing the discrepancy as a function of actual gap, a complete characterization of the drivetrain and crosschecking between the encoders can occur.

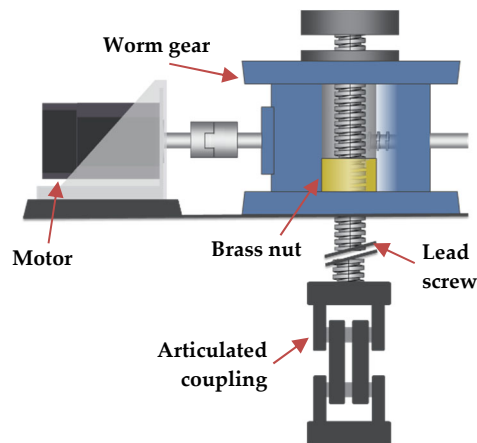


Figure 1: The drivetrain of an APS undulator device consists of a motor coupled to a 60:1 worm gear assembly. Motion is transferred to a lead screw, which is threaded through a bronze nut and connected directly to the strongback via an articulating coupling.

A python script sequentially commands each of the 53 insertion devices installed in the APS storage ring to move at a slow speed while oversampling the position readback

\* This research used resources of the Advanced Photon Source, a U.S. Department of Energy (DOE) Office of Science User Facility at Argonne National Laboratory and is based on research supported by the U.S. DOE Office of Science-Basic Energy Sciences, under Contract No. DE-AC02-06CH11357.

<sup>†</sup> nweir@anl.gov

# A COMPARISON OF FRONT-END DESIGN REQUIREMENTS

S. Sharma†, NSLS-II, Brookhaven National Laboratory, Upton, NY, USA

## Abstract

Front ends of the NSLS-II storage ring have numerous design requirements to ensure equipment and personal safety aspects of their designs. These design requirements, especially many pertaining to raytracings, have gradually become overly stringent and a review is underway to simplify them for building future front ends. As a part of this effort, we have assembled the front-end design requirements used in several other light sources. In this paper the assembled design requirements are discussed in comparison with those currently in use at NSLS-II.

## INTRODUCTION

Front ends are used to control the size of photon and gas bremsstrahlung beams traversing from the storage ring to the users' beamlines. At NSLS-II there are presently 17 front ends for insertion device (ID) beamlines and 6 front ends for BM (bending magnet or 3-pole wiggler) beamlines. A typical ID front end [1] is shown in Fig. 1. Its main components are, (1) XBPM, (2) fixed aperture mask (FM), (3) lead collimators (LCO), (4) a pair of XY slits, (5) photon shutter (PS), (6) safety shutters (SS), and (7) ratchet wall collimator (RCO). The components that trim or stop the bremsstrahlung beam, namely, LCO, SS and RCO, are classified as PSS (personnel safety system) components and the remaining as EPS (equipment protection system) components.

The design of NSLS-II front ends is deemed to be too conservative, in part due to a very stringent approach to raytracings involving PSS components, and to the requirement of minimizing the size of bremsstrahlung beam. For the new front ends, presently in the planning stage, some simplified design criteria are being evaluated. As a part of this evaluation, front end design criteria collected from several light source facilities (APS-U, ALS-U, CLS, DLS, ESRF(EBS), HEPS, SOLEIL, SSRF and TPS) are compared with those used at NSLS-II. The focus of this

comparison is on source definitions of photon and bremsstrahlung beams, and thermal fatigue design criteria.

## FRONT END CONFIGURATIONS

Front-end configurations of different facilities mentioned above are quite similar except that XBPMs, XY slits and LCOs are not considered to be required components. XBPMs are not installed in ALS-U and most of the NSLS-II ID front ends to save space and/or cost. XY slits are not available in APS-U, ESRF(EBS) and SSRF front ends. In general, LCOs (to trim the bremsstrahlung beam) are not installed in the front ends of DLS, ESRF and TPS. A second SS for redundancy is used only at NSLS-II, APS-U, CLS and DLS. Vacuum pressure gages in the front ends of all facilities are interlocked to dump the stored beam. Thermal sensors are also used at ALS-U, HEPS, SSRF, Soleil, and DLS, although they are not interlocked in some cases. Trimming of un-interlocked photon beams by burn-through devices (explained below) is done only at NSLS-II and APS-U front ends. Only one of the facilities, (ALS-U), employs a sweeper magnet as safety against accidental entry of the injected e-beam into the front end.

## RAYTRACINGS

Raytracings for both the photon and bremsstrahlung beams are critical part of the front-end design process at NSLS-II and a considerable design effort is devoted to generating formal raytracing drawings. The drawings are usually revised iteratively in order to optimize the apertures, lengths, and locations of the various front-end components.

## Photon Beam Sources

Source definitions for raytracings consist of 3 parts, namely, (1) e-beam deviations, (2) location of the source in Z (along the beam) direction, and (3) fan angles of the device (defined by  $K$  and  $\gamma$  parameters) at the source point.

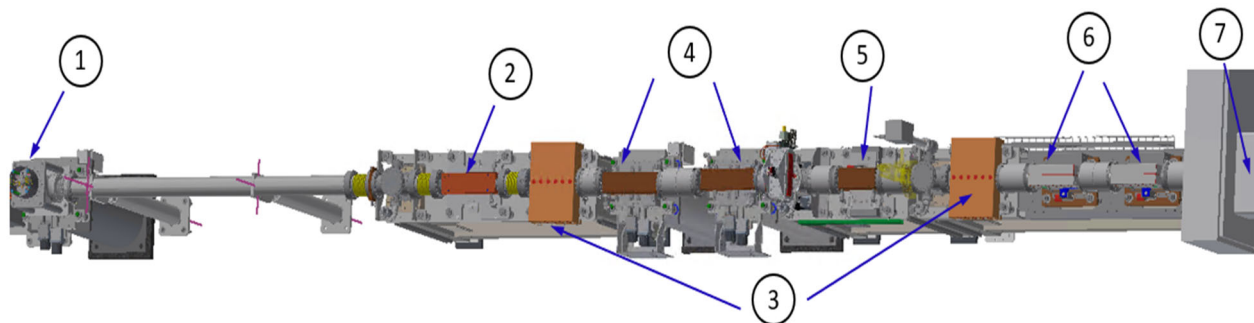


Figure 1: A typical NSLS-II ID front end; (1) XBPM, (2) fixed aperture mask (FM), (3) lead collimators (LCO), (4) XY slits, (5) photon shutter (PS), (6) safety shutters (SS), and (7) ratchet wall collimator (RCO).

† sharma@bnl.gov

# MECHANICAL DESIGN OF A SOFT X-RAY BEAM POSITION MONITOR FOR THE COHERENT SOFT X-RAY SCATTERING BEAMLINE

C. Eng, D. Donetski<sup>1</sup>, J. Liu<sup>1</sup>, S. Hulbert, C. Mazzoli, B. Podobedov  
 Brookhaven National Laboratory (BNL), <sup>1</sup>Stony Brook University (SBU)

## Abstract

Achieving photon beam stability, a critical property of modern synchrotron beamlines, requires a means of high resolution, non-invasive photon beam position measurement. While such measurement techniques exist for hard x-ray beamlines, they have yet to be achieved for soft x-ray beamlines. A new soft X-ray beam position monitor (SXBPM) design based on GaAs detector arrays is being developed and will be installed in the first optical enclosure of the Coherent Soft X-ray Scattering (CSX) beamline at the National Synchrotron Light Source II (NSLS-II).

The SXBPM assembly contains four water-cooled blade assemblies, each of which will have a GaAs detector assembly mounted within it, that can be inserted into the outer edges of the CSX undulator beam with sub-micron accuracy and resolution. The primary challenges in design of the SXBPM include: 1) mechanical stability of the assembly, 2) management of the heat load from the undulator x-ray beam to protect GaAs detector assemblies from unwanted illumination, 3) assembly compactness to fit within the first optical enclosure (FOE) of the CSX beamline, and 4) accessibility for modifications. Balancing the unique design requirements of the SXBPM along with their associated constraints has resulted in the design of a non-invasive beam position monitor which will be installed in the CSX FOE as a prototype for testing and iterative improvement. The ultimate goal is development of a widely useful SXBPM instrument for soft X-ray beamlines at high brightness synchrotron storage ring facilities worldwide.

## INTRODUCTION

Quality of data produced by the beamline is highly dependent on their soft x-ray beam control: both high positional beam stability and wavefront control are required at the sample position. In this respect, diagnostics such as Beam Position Monitors (BPMs) are a critical tool for evaluating and controlling photon beam delivered by modern highly coherent sources. Photoemission blade based BPMs work well for white beams of considerable power, while diamond x-ray BMS in transmissive geometry have proved effective for hard x-ray monochromatic beams. However, none of the above are ideal for soft coherent undulator sources, where a non-invasive device with high spatial resolution is needed. Stringent limitations come from intrinsic characteristics of the soft sources (halo extent, coherence of soft cone in the center of the undulator emission) and from the limited transmissive power of soft x-rays in materials.

Additionally, an optimal BPM design should permit positioning of the blades as far possible from the undulator central cone to preserve the wavefront coherence of the usable fraction of the beam. The BPM design described herein uses arrays of 1D strips of pixelated GaAs detectors mounted on adjustable blades that are inserted partially into the beam to intercept only the outer edge of the beam [1]. The SXBPM will be installed inside the FOE of the CSX beamline (Fig. 1) for ease of access to facilitate testing and development. Following commissioning and testing of this prototype, a subsequent “production” version is envisioned to be developed for placement in beamline front ends.

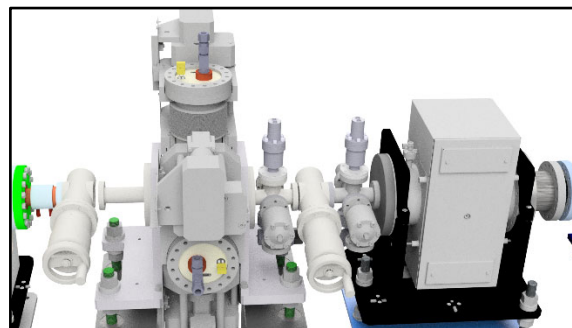


Figure 1: Rendering of the SXBPM installed in the CSX FOE as a separate section to facilitate replacement and reconfiguration of the detector assemblies.

## DESIGN REQUIREMENTS

The SXBPM’s primary function is to non-invasively monitor the position of the soft x-ray beam upstream of the first optics element using novel GaAs detector arrays. As a beam position monitor, the device must be stable and support sub-micron scale resolution positioning of the detector arrays, while providing a stroke/travel range sufficient to remove the detector arrays completely from the photon beam. Additionally, the SXBPM requires accessibility in order to facilitate reconfiguration or replacement of the detector arrays for testing (Fig. 2). The selected location for the SXBPM is upstream of the first optics element of the CSX (23-ID) beamline, necessitating careful consideration for handling the heat load.

## DESIGN OVERVIEW

The GaAs detector arrays will be mounted on the ends of 4 water-cooled blades consisting of OFHC copper. To protect the vulnerable parts of the detector arrays from excessive heating, a tungsten plate is mounted in front of each assembly. On the beam-facing edge of the tungsten plate, an array of laser-drilled 30 micron diameter holes

# DIAMOND REFRACTIVE OPTICS FABRICATION BY LASER ABLATION AND AT-WAVELENGTH TESTING

S. Antipov†, E. Gomez, Euclid Techlabs LLC, Bolingbrook, IL, USA  
R. Celestre, T. Roth, European Synchrotron Radiation Facility, Grenoble, France

## Abstract

The next generation light sources will require x-ray optical components capable of handling large instantaneous and average power densities while tailoring the properties of the x-ray beams for a variety of scientific experiments. Diamond being radiation hard, low Z material with outstanding thermal properties is proposed for front-end pre-focusing optics applications. Euclid Techlabs had been developing x-ray refractive diamond lens to meet this need. Standard deviation of lens shape error figure gradually was decreased to sub-micron values. Post-ablation polishing procedure yields  $\sim 10\text{nm}$  surface roughness. In this paper we will report on recent developments towards beamline-ready lens including packaging and compound refractive lens stacking. Diamond lens fabrication is done by femto-second laser micromachining. We had been using this technology for customization of other beamline components.

## INTRODUCTION

Significant increase in average synchrotron beam brightness is projected for numerous facilities as they upgrade to diffraction limited storage rings. For ultrafast experiments, x-ray free electron lasers produce 10 orders of magnitude larger peak brightness than storage rings. It is therefore extremely important to develop next generation x-ray optics for these new light sources. Diamond is a "go to" material for high heat load applications. Single crystal diamond is an excellent material for x-ray optics due to its high x-ray transmissivity and uniform index of refraction [1]. For compound refractive lens (CRL) application there is an additional benefit from the single crystal material of choice for the lens because small angle reflections on defects and voids, typical for polycrystalline materials, are minimized and the x-ray beam quality is preserved [2, 3].

It is, however, a challenging task to manufacture complex shapes out of diamond. We use femtosecond laser cutting technology to manufacture a compound refractive lens, the most popular x-ray optics element, from a single crystal diamond. A femtosecond laser pulse duration is extremely short: material is ablated while pulse heating effects are minimized. In the past 3 years we have developed a fs-laser ablation procedure that yields diamond refractive parabolic lenses with shape error of  $0.8\ \mu\text{m}$  r.m.s. with surface roughness on the order of 200-300 nm Ra and polishing procedure that brings surface roughness into 10-20 nm Ra region but increases the figure error to  $1.4\ \mu\text{m}$  r.m.s.

## DIAMOND LENS FABRICATION

For diamond lens production we developed a femto-second laser ablation system. It consists of a fs-laser operating at the second harmonic (515 nm), a motorized lens that allows moving the position of the focal spot  $\pm 2\ \text{mm}$  and a set of computer-controlled mirrors paired with a large aperture final-focus lens. Using this setup a laser beam can be steered at large speeds in the focal plane of the lens. The work surface is mounted on a linear stage for sample examination under a microscope for an in-line metrology.

We developed ablation scripting to minimize surface roughness and achieve high degree of shape fidelity. A typical lens parameters that we ablate is  $450\ \mu\text{m}$  aperture with radius of curvature  $100\ \mu\text{m}$ . Given the difference in refractive decrement such lens is roughly equivalent to an industry standard beryllium lens of the same aperture and  $R=50\ \mu\text{m}$ .

As-ablated lenses have roughness on the order of 200-300 nm. For x-ray applications we are developing post-ablation chemical – mechanical polishing procedure. In this procedure a conformal bit is lowered into the diamond lens along with fine sub-micron diamond slurry and spun inside for anywhere from 4 to 8 hours. Large number of factors make this procedure quite complicated: uneven pressure distribution, not equal linear velocity at different parts of the polishing bit, different diamond crystal orientation along the paraboloid surface and some others. We are able to polish full lens surface to 10-20 nm Ra roughness. Figure 1 shows a comparison of polished and un-polished lens along with the residual plots of the paraboloid fit.

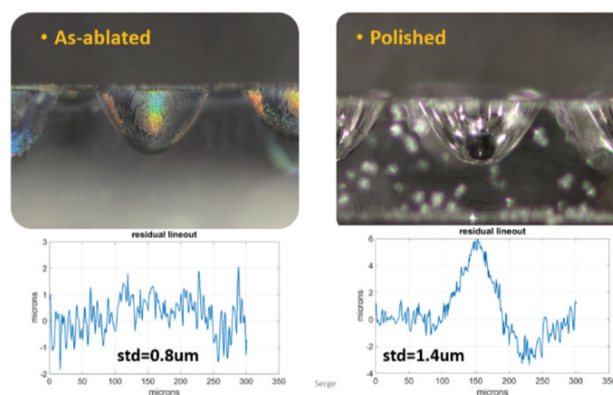


Figure 1: Top: Optical image through a polished side of the diamond plate. Left: as-ablated lens. Right: Polished lens. Bottom: corresponding lineouts of paraboloid fit residuals.

† s.antipov@euclidtechlabs.com

# BEAMLINE ALIGNMENT AND CHARACTERIZATION WITH AN AUTOCOLLIMATOR\*

M. V. Fisher†, A. Khan, J. Knopp

Advanced Photon Source, Argonne National Laboratory, Argonne, IL, USA

## Abstract

An electronic autocollimator is a valuable tool that can assist in the alignment of optical beamline components such as mirrors and monochromators. It is also a powerful tool for *in situ* diagnoses of the mechanical behavior of such components. This can include the repeatability of crystals, gratings, and mirrors as they are rotated; the parasitic errors of these same optical elements as they are rotated and/or translated; and the repeatability and parasitic errors as bendable mirrors are actuated. The autocollimator can even be used to establish a secondary reference if such components require servicing. This paper will provide examples of such alignments, diagnoses, and references that have been made with an autocollimator on existing and recently commissioned beamlines at the Advanced Photon Source (APS). In addition, this paper will discuss how this experience influenced the specifications and subsequent designs of the new primary high-heat-load mirror systems (PHHLMs) that are currently under fabrication for six of the APS Upgrade (APS-U) feature beamlines. Each mirror was specified to provide *in situ* line-of-sight access for an autocollimator to either the center of the mirror's optical surface or to a smaller polished surface centered on the backside of each mirror substrate. This line of sight will be used for initial alignment of the mirror and will be available for *in situ* diagnoses if required in the future.

## INTRODUCTION

Many strategies can be employed in the alignment of optical beamline components such as mirrors and monochromators. One can reference the actual optical surfaces with classical optical tooling (white face scale, jig transit, etc.) or get more sophisticated and use a portable coordinating measuring machine that relates the measured position of the optical surface to an external reference. A mirror or monochromator can then be installed onto a beamline using these predetermined external references and these techniques have been employed at the Advanced Photon Source (APS). An electronic autocollimator offers an additional means of establishing such alignments as it can measure the pitch and roll of the optical surface assuming an appropriate line of sight is available. A vertical leveling mirror (VLM) [1] is useful optical tool that can be used in concert with an autocollimator to establish an absolute angular reference relative to gravity. This is especially helpful in setting the roll of horizontally defecting mirrors and

horizontally diffracting gratings and crystals. This paper begins with a discussion of how this technique was successfully used to align such a mirror system at the APS. This is followed by discussions of how an autocollimator was used to diagnose *in situ* the mechanical behavior of the motion systems on a couple of mirrors and one monochromator.

## DUAL MIRROR SYSTEM AT 2-ID

The 2-ID beamline was converted from a colinear to a canted configuration [2] in late 2019. Part of that conversion involved installing two primary high-heat-load mirrors that share a common vacuum chamber into the upstream end of the first optical enclosure (FOE). The two mirrors increase the separation between the canted beams and focus these beams at slits located near the downstream end of the FOE. The upstream/inboard (us/in) mirror horizontally deflects the inboard canted beam outward. The downstream/outboard (ds/out) mirror horizontally deflects the outboard canted beam inward. The beams cross over each other about halfway along their path to their respective slits. The roll of these two mirrors was initially set using a jig transit lined up on the downstream end of each mirror. Each mirror was adjusted such that the top and bottom edges of each optical surface were aligned vertically. The holder and mechanism made it difficult to get a good line of sight to the mirror edges. Fortunately, the overall assembly was designed with an unobstructed line of sight to each optical surface. The process of setting up a VLM and auto-collimator was straightforward for the us/in mirror, which faces outward, but not as easy to implement for the ds/out mirror that faces inward. The setup for the ds/out mirror is complicated by its proximity to the inboard wall of the FOE. One can establish a line of sight to the mirror's optical surface using a VLM oriented at 45° to the mirror, but it is a two-stage process where the autocollimator is first leveled in roll by viewing the VLM straight on before rotating by 45°. The autocollimator indicated that the initial roll alignment on each mirror was in error by more than 1.0 mrad. The roll was eventually set to better than 100  $\mu$ rad and could have been set more accurately if needed.

Work continued into early 2020 on converting the 2-ID beamline to a canted configuration. That work came to a halt when the APS went into minimum safe operations during the early stages of the COVID pandemic. During that time a water leak developed on the us/in mirror. The leak was confined to a single air guard bellows that surrounded the leaking cooling line and the leak did not compromise the vacuum integrity of the mirror system. Fortunately, the leak was discovered, and the water turned off in a timely fashion, but the repair did not start until a few months later once COVID protocols were put in place. The repair

\* This research used resources of the Advanced Photon Source, a U.S. Department of Energy (DOE) Office of Science User Facility at Argonne National Laboratory and is based on research supported by the U.S. DOE Office of Science-Basic Energy Sciences, under Contract No. DE-AC02-06CH11357.

† mfisher@anl.gov

# WELDABLE COPPER CHROMIUM ZIRCONIUM MASK

T. J. Bender†, O. A. Schmidt, W. F. Toter, Argonne National Laboratory, Lemont, IL, USA

## Abstract

A novel design for a weldable copper chromium zirconium (CuCrZr) mask is being developed for use in the Advanced Photon Source Upgrade (APSU) beamlines at the Argonne National Laboratory (ANL). This alternative attempts to drastically reduce cost and lead time over traditional brazed Glidcop® mask designs. Thermal analysis simulations of the mask have predicted that it will meet mechanical and thermal requirements, even when subjected to the intense white beam of the new superconducting undulators (SCU) of the APSU. As of the writing of this paper, a prototype is being fabricated for testing and eventual installation on the 28-ID Coherent High Energy X-ray (CHEX) beamline.

## INTRODUCTION

Photon masks are radiation safety components meant to limit missteering of synchrotron radiation and protect downstream components in beamlines. They are also often used as in-vacuum beamstops and secondary apertures for controlling the size of the beam. Without photon masks, heat-sensitive radiation safety components like collimators would be exposed to the heat carried by the unattenuated beam.

The 28-ID CHEX beamline relies on two separate X-ray beams from the storage ring using a canted SCU configuration. One beam is multiplexed three times creating fixed discrete energy beamlines and one beamline is left fully tunable. This configuration will exploit the coherent flux enabled by APSU to advance the frontier for *in situ*, real-time studies of materials synthesis and chemical transformations in natural operating environments.

The proposed welded mask design will reside on the 5-60 keV tunable branch line, roughly 44 meters from the source in a lead-shielded mini-enclosure (Fig. 1). Its purpose is to protect downstream components from missteered synchrotron beam, define the size of the outboard canted beam, and prevent passage of the inboard canted beam to the 28-ID-B enclosure located downstream of the mini-enclosure.

CuCrZr masks are becoming widely used since it is affordable and simple to fabricate from a single piece of material, however more complicated absorber designs with overlapping internal features are difficult or impossible to machine [1, 2]. Also, brazing CuCrZr will anneal and negate useful properties of the beam intercepting surface and the hardened knife edge. Tests done by Bill Toter, ANL welding engineer show that gas tungsten arc welding (GTAW) is a viable strategy for joining CuCrZr bodies. The heat effective zone should be localized enough to not effect the knife edge and material properties.

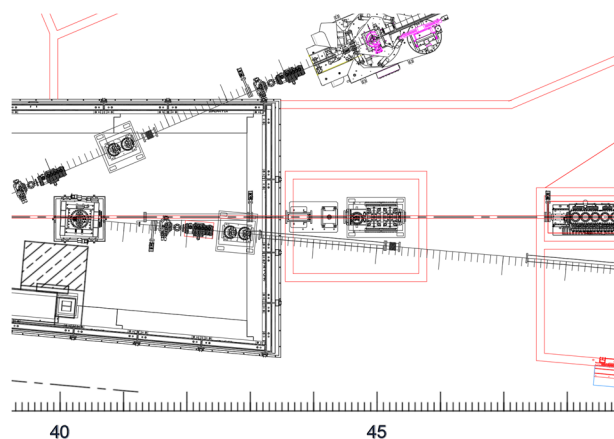


Figure 1: Location of mask in CHEX beamline.

## MECHANICAL DESIGN

### Absorbing Body

The main absorbing body of the mask consists of two CuCrZr top and bottom halves (Fig. 2). Both halves each contain five .375 in diameter water cooling channels with .25 in NPT threaded holes on either side to accept stainless steel compression fittings and return loops. The channels are drilled perpendicular to the beam direction to maximize the number of cooling channels present.

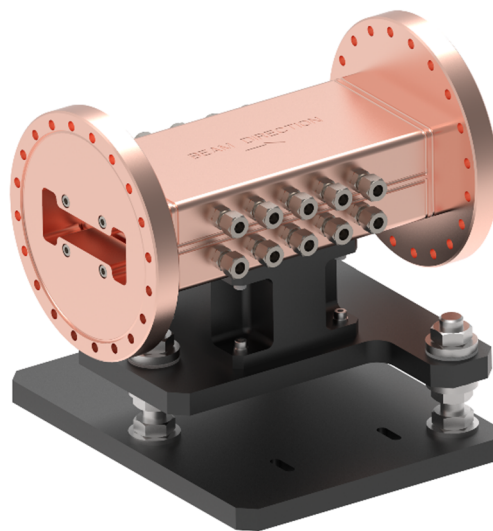


Figure 2: Welded mask assembly.

The top half contains the 2 mm horizontal x 10 mm vertical exit aperture meant to slit the outboard canted beam. The bottom half of the body contains the incident surface meant to absorb the extremal synchrotron rays as well as four M4 tapped holes for securing the assembly to an adjustable-height support table. Both halves also have inside surfaces angled in such a way as to block passage of the inboard canted beam. The inner angled surfaces on both halves are to be cut via wire EDM.

† tbender@anl.gov

# COMPACT X-RAY AND BREMSSTRAHLUNG COLLIMATOR FOR LCLS-II

N. A. Boiadjieva<sup>†</sup> D. Fritz, T. Rabedeau  
 SLAC National Accelerator Laboratory, Menlo Park, CA, USA

## Abstract

Beam collimation is crucial to maintaining machine and personal safety during LCLS-II operation. This paper discusses a compact collimator consisting of an X-ray beam power collimator, a burn through monitor (BTM) designed to detect failure of the X-ray beam collimator, and a Bremsstrahlung collimator. The x-ray collimator body is a monolithic machined from CuCrZr that eliminates costly braze operations and reduces assembly time and complexity. Sintered high thermal conductivity SiC is employed as the X-ray absorber. The allowed beam power is limited to 100W and 50W/mm<sup>2</sup>. Finite element analyses (FEA) ensure that the power absorber remains in safe temperature and stress regimes under the maximum power loading and smallest expected beam dimensions. Beam containment requirements stipulate the inclusion of a monitor to detect burn through events owing to absorber failure. The BTM is a gas-filled, thin wall vessel which, if illuminated by the beam, will burn through and release the contained gas and trip pressure switches that initiate beam shutdown. The beam absorber and BTM shadow the Bremsstrahlung collimator shielding after appropriate propagation of manufacturing, assembly, and installation tolerances. Tooling is developed to minimize assembly complexity and ensure minimal alignment errors.

## INTRODUCTION

This presentation discusses a package consisting of photon collimator that intercepts and collimates the x-ray beam, Burn Through Monitor (BTM) that monitor for beam excursion from the design path, and Bremsstrahlung collimator which collimates high energy photons associated with electron beam interaction with residual gas and physical aperture. In general those three components are situated in sequence along a given beam line though in some cases not all three elements are required.

The key requirement for this design were:

- Design a compact and modular x-ray power and Bremsstrahlung collimators.
- X-ray collimator to handle allowed power of 100W.
- Come up with fixtures and locating features to minimize the relative alignment error on assembly and hence maximize allowed beam aperture while providing downstream beam containment.

## DESIGN

### *X-ray Collimator*

Previously designed collimator bodies have employed a vacuum nipple with welded flanges and braised copper elements that provide cooling for the beam intercepting disk. For this design the body is a monolithic machined Copper alloy CuCrZr (18150) that allows compact design with integrated conflat seal knife edges and eliminates the need for flanges welding [1]. See Fig. 1. In addition, the cooling channels are machined in the body which eliminates the brazing of an additional cooling block. The resulting mask body extends 72mm along the beam direction.

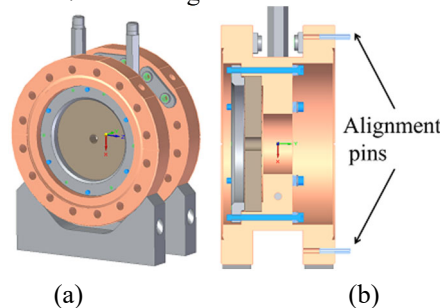


Figure 1: X-ray collimator. (a) CAD model, (b) cross section.

X-ray collimators are illuminated by x-ray beam power composed of high intensity, high frequency, short duration pulses. The collimator must not be damaged by the average beam power nor ablated through pulse by pulse energy deposition. Sintered high thermal conductivity SiC is employed as the x-ray absorber with design provisions incorporated to permit the inclusion of additional absorbers (e.g. diamond). The allowed beam power is limited to 100W.

The first beam intercepting element is cooled indirectly via indium mediated conduction cooling by the water-cooled collimator body. Figure 2 shows that the indium is positioned in the shadow of the beam intercepting element and maintained safely under the indium melting temperature at maximum power loading and maximum beam missteering.

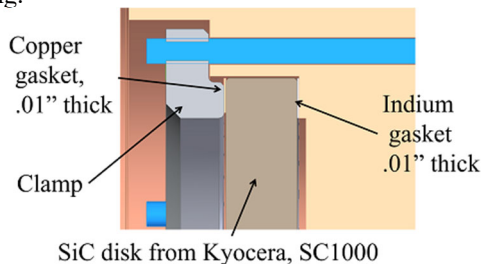


Figure 2: Design interface around SiC disk.

<sup>†</sup> ninab@slac.stanford.edu

# MECHANICAL DESIGN PROGRESS OF THE IN SITU NANOPROBE INSTRUMENT FOR APS-U\*

Steven P. Kearney†, Deming Shu, Tim Mooney, Barry Lai, Si Chen, and Jörg Maser  
Advanced Photon Source, Argonne National Laboratory, Lemont, IL 60439, U.S.A.

## Abstract

The In Situ Nanoprobe (ISN, 19-ID) beamline will be a new best-in-class long beamline to be constructed as part of the Advanced Photon Source Upgrade (APS-U) project [1, 2]. To achieve long working distance at high spatial resolution, the ISN instrument will be positioned 210 m downstream of the x-ray source, in a dedicated satellite building, currently under construction [3]. The ISN instrument will use a nano-focusing Kirkpatrick-Baez (K-B) mirror system, which will focus hard x-rays to a focal spot as small as 20 nm, with a large working distance of 61 mm. The large working distance provides space for various *in situ* sample cells for x-ray fluorescence tomography and ptychographic 3D imaging, allows the use of a separate, independent vacuum chambers for the optics and sample, and provides the flexibility to run experiments in vacuum or at ambient pressure. A consequence of the small spot size and large working distance are stringent requirements for high angular stability of the K-B mirrors (5 nrad V-mirror and 16 nrad H-mirror) and high relative stability between focus spot and sample (4 nm<sub>RMS</sub>). Additional features include fly-scanning up to 2 kg mass, sample plus *in situ* cell, at 1 mm/s in vertical and/or horizontal directions over an area of 10 mm x 10 mm. Environmental capabilities will include heating and cooling, flow of fluids and applied fields, as required for electrochemistry and flow of gases at high temperature for catalysis. To achieve these capabilities and precise requirements we have used precision engineering fundamentals to guide the design process.

## INTRODUCTION

The advanced photon source (APS) at Argonne National Laboratory (ANL) is being upgraded with a new multi-bend achromat storage ring lattice and insertion devices that will provide increased brightness and coherence through reduced emittance of the stored electron beam [4]. To take full advantage of the new beam specifications, a new best-in-class In Situ Nanoprobe (ISN) instrument is being developed for the 19-ID beamline.

The ISN instrument will use a nano-focusing Kirkpatrick-Baez (K-B) mirror system to focus hard x-rays to a focal spot as small as 20 nm, with a large working distance of 61 mm. The large working distance provides space for various *in situ* sample cells for x-ray fluorescence tomography and ptychographic 3D imaging, allows the use of separate, independent vacuum chambers for the optics and

sample, and provides the flexibility to run experiments in vacuum or at ambient pressure.

Requirements of the ISN instrument that make it unique and a technically challenging design and allow it to support a broad range of *in situ* conditions are: high angular stability of the K-B mirrors (5 nrad V-mirror and 16 nrad H-mirror) and high relative stability between focus spot and sample (4 nm<sub>RMS</sub>), fly-scanning a maximum of a 2 kg *in situ* cell at 1 mm/s in vertical and/or horizontal directions over an area of 10 mm x 10 mm, and separate vacuum chambers result in a metrology frame that needs to be transferred between two environments.

Achieving the requirements of ISN has required precision engineering of the entire instrument system from the soil up. All the components of the system need to work together, and any one component could push the instrument out of specification. In this paper we will discuss the design and state of the soil and foundation, enclosure environment, nanopositioning systems, and stable metrology frames. For details on the instrument support, which is a modification of granite stages developed by APS, see Preissner *et al.* [5].

## INSTRUMENT DESIGN

### Location

The ISN instrument will be positioned 210 m downstream of the x-ray source, in a dedicated satellite building, currently under construction. A sketch of the location of the new satellite building with respect to the main APS building and building schematic of the instrument control room and enclosure floor is shown in Fig. 1.

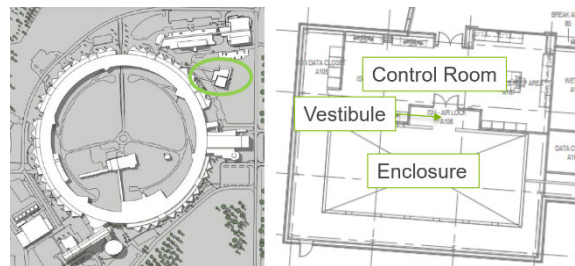


Figure 1: Left, circle is satellite building for ISN and High-Energy X-ray Microscope instruments. Right, floor plan of ISN showing control room, vestibule, and enclosure.

### Foundation

We started the design process of the ISN with details of the foundation, which eventually included the soil underneath. To achieve a highly stable floor we measured the vibrations of other similar instrument foundations [3], and found a common successful strategy using slab isolation and 1 m thickness. With an isolated slab, there is a risk of

\* This research used resources of the Advanced Photon Source, a U.S. Department of Energy (DOE) Office of Science User Facility at Argonne National Laboratory and is based on research supported by the U.S. DOE Office of Science-Basic Energy Sciences, under Contract No. DE-AC02-06CH11357.

†skearney@anl.gov

# DISCRETE PHOTON ABSORBERS FOR THE APS-UPGRADE STORAGE RING VACUUM SYSTEM\*

O. K. Mulvany†, B. Billett, B. Brajuskovic, J. A. Carter, A. McElderry, R. Swanson  
Advanced Photon Source, Argonne National Laboratory, Lemont, IL, USA

## Abstract

The Advanced Photon Source Upgrade storage ring arc vacuum system features a diverse set of photon beam-intercepting components, including five discrete photon absorbers and a series of small-aperture vacuum chambers that shadow downstream components. The discrete photon absorbers—typically fabricated from electron beam-welded GlidCop® AL-15—are subject to heat loads ranging from approximately 170 to 3400 watts, with a peak power density up to approximately 610 W/mm<sup>2</sup> at normal incidence. Four of the five photon absorber designs are housed in vacuum chambers, including three that are mounted to the antechambers of curved aluminum extrusion-based L-bend vacuum chambers and one that is mounted to a stainless steel vacuum-pumping cross. Furthermore, two of the photon absorbers that are mounted to L-bend vacuum chambers are equipped with position-adjustment mechanisms, which are necessitated by the challenging design and fabrication of the curved vacuum chambers. The fifth photon absorber, unlike the rest, is a brazed design that is integral in sealing the vacuum system and intercepts approximately 170 watts. Each photon absorber design was optimized with thermal-structural finite element analyses while ensuring functional and spatial requirements were met. Some of these requirements include meeting internal high-heat-load component design criteria, respecting challenging component interfaces and alignment requirements, and minimizing impedance effects. Furthermore, photon beam scattering effects called for the use of scattering shields on three designs to minimize potential heating of vacuum chambers. This paper details the careful balance of functionality and manufacturability, and the overall design process followed to achieve the final designs.

## INTRODUCTION

The Advanced Photon Source Upgrade (APS-U) project is building a storage ring upgrade that will be retrofitted to the current 1.1-km circumference APS storage ring. By utilizing narrow aperture magnets and thus a small-aperture vacuum system in a multi-bend achromat (MBA) lattice, the upgrade will produce a 6-GeV, 200-mA beam that is optimized for brightness above 4 keV [1].

Five GlidCop® AL-15 discrete photon absorbers (in addition to water-cooled, small-aperture vacuum chambers)

\* This research used resources of the Advanced Photon Source, a U.S. Department of Energy (DOE) Office of Science User Facility at Argonne National Laboratory and is based on research supported by the U.S. DOE Office of Science-Basic Energy Sciences, under Contract No. DE-AC02-06CH11357.

† omulvany@anl.gov

were designed to shadow, or protect, neighboring electron and photon beam vacuum components in the APS-U MBA lattice. The final photon absorber designs were driven by several requirements, most notably including: protecting neighboring components in the storage ring vacuum system while safely handling the heat loads produced by the MBA lattice; achieving minimum vertical and horizontal apertures for the photon beams produced by the upstream straight sections and bending magnets; and finally, a need for seamless integration into the storage ring vacuum system.

Three of the five photon absorbers—A:CA1, A:CA2, and B:CA1—are considered “crotch” absorbers and thus permit photon extraction to the front ends while typically intercepting higher heat loads (Fig. 1a-1c). The final two photon absorbers include an “end” absorber, B:EA1 (Fig. 1d), and an “inline” absorber, B:FA1 (Fig. 1e), both of which strictly shadow uncooled downstream components from synchrotron radiation. The B:FA1 inline photon absorber, which is 60 mm in length, serves a dual purpose in that it is a vacuum chamber and also shadows downstream components. Each of the five photon absorber designs are required in the 40 repeating sector arcs of the APS-U storage ring vacuum system.

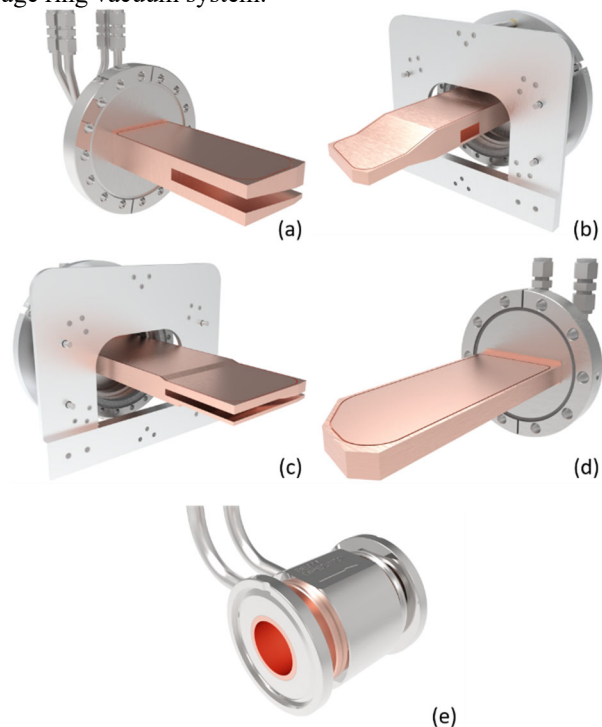


Figure 1: Discrete photon absorber designs, including crotch absorbers (a) A:CA1, (b) A:CA2, and (c) B:CA1, an end absorber (d) B:EA1, and an inline absorber (e) B:FA1.

# A NEW MAGNETIC MEASUREMENT SYSTEM FOR THE FUTURE LOW EMITTANCE NSLS-II STORAGE RING\*

M. Musardo†, T. Corwin, F. DePaola, L. Doom, R. Faussete, D. Harder, S. Sharma, T. Tanabe  
 Brookhaven National Laboratory, Upton, New York, USA  
 C. L. Doose, A. K. Jain, Argonne National Laboratory, Lemont, Illinois, USA  
 D. Assell, J. DiMarco, Fermilab, Batavia, Illinois, USA

## Abstract

A new magnetic measurement system is under construction at BNL for accurate field harmonic measurements and fiducialization of magnets for a future upgrade of the NSLS-II storage ring. The entire storage ring is envisioned to be replaced with a new lattice concept, known as Complex Bend, which superimposes dipole and high-gradient quadrupole fields. The magnetic measurement system will use rotating wire and a PCB rotating coil specifically designed for small-aperture (< 15 mm) high gradient magnets. In this paper we describe in detail the mechanical design and the data acquisition hardware and software.

## INTRODUCTION

Achieving a low-emittance ring design with high brightness is one of the most challenging aspects of advanced synchrotron light source projects. The major planned future improvement and upgrade of the National Synchrotron Light Source II (NSLS-IIU) at Brookhaven National Laboratory (BNL) is to replace the existing Double Bend Achromat lattice (DBA) with a new lattice element called “Complex Bend” [1-3], which consists of a combination of dipoles and high-gradient quadrupoles with superposing fields [4]. This approach provides reduction of the electron beam emittance to about 20 pm. Accurate and precise higher-order field harmonic measurements are essential to guarantee that the field performance of future magnets fulfills the demanding specifications.

## MAGNETIC MEASUREMENT EQUIPMENT

The magnetic measurement system configured at NSLS-II is based on the measuring bench developed at Argonne National Lab (ANL) for the Advanced Photon Source (APS) upgrade project [5].

The new measuring bench consists of a Printed Circuit Board (PCB) rotating coil, designed for measuring field strength and field quality to a level of 0.1 units up to the 15<sup>th</sup> harmonic and a rotating wire system for determining the magnetic center and for fiducializing multipole magnets with an accuracy better than 10 μm using a Laser Tracker.

### Rotating Wire System

Field integral measurement with continuously rotating wire loop was first tried at SPring-8 for the magnetic

measurement of an undulator with 3 mm gap [6]. Unlike a flip coil bench with finite rotation angle, continuously rotating system can use various techniques to improve a S/N ratio.

The measurement bench is assembled on a 2.75 m long granite block supported on 3 leveling jacks. The leveling jacks are JOYCE WJ123 with a 3 Ton capacity, 1 inch of screw travel and 12:1 ratio gearset. The granite block has machined T-slots and Survey & Alignment holes. Both the magnets and the stages are supported on three anodized aluminum plates affixed to the granite surface. Stop blocks on the center plate provide banking surfaces to align the magnet to the rotating wire. Other banking alignment features, such as magnet pushers and support assemblies, help to align the rotating wire and rotating coil to any type of magnet. Aluminum shims between the stop-blocks and the magnet reference surfaces are used depending on the geometry and dimensions of the magnet to be measured. The two outer aluminum plates are populated with Newport X,Y, Z and R stage assemblies as shown in Fig. 1. Thus there is independent X, Y, Z and R positioning at each end of the bench which can operate in tandem.

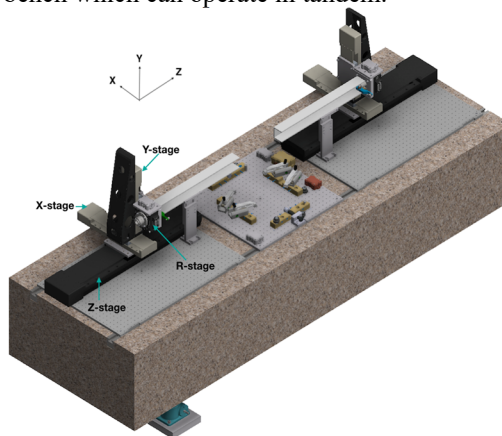


Figure 1: 3D rendering of the NSLS-II magnetic measurement system.

The longitudinal stages have a 600 mm travel range and a DC motor with a rotary encoder on the drive screw that provides 1.25 μm resolution and 2.5 μm bi-directional repeatability. The horizontal and vertical DC servo linear stages have a 200 mm and 100 mm travel range respectively. Both stages have a minimum incremental motion of 1 μm and a bi-directional repeatability of about ± 0.4 μm. A 4000 pts/rev. encoder is mounted directly on the screw in order to prevent screw/motor coupling errors consequently boosting stage motion accuracy. A compact rotation stage equipped with brushless direct drive technology

\* Work supported by DOE under contract DE-SC0012704

† Email address musardo@bnl.gov

# RECENT STUDIES ON THE VIBRATION RESPONSE OF NSLS-II GIRDER SUPPORT SYSTEM

S. Sharma<sup>†</sup> and C. Spataro, NSLS-II, Brookhaven National Laboratory, Upton, NY, USA

## Abstract

The designs of various girder support systems were reviewed recently in a MEDSI School tutorial [1]. A comparison of their horizontal transmissibility values in (2-100 Hz) band showed that the NSLS-II girder support system had a lower transmissibility despite its first natural frequency being the lowest (~30 Hz). Detailed vibration tests and finite element (FE) analyses have been performed to understand this anomaly and to assess the role of viscoelastic damping pads underneath the NSLS-II girders. The analyses were extended to include harmonic response analysis to model viscoelastic properties, and to random vibration analysis to obtain uncorrelated motions between the magnets. The results of these new tests and FE analyses are discussed in this paper.

## INTRODUCTION

Ambient floor motion is one of the major sources of beam stability perturbations in the storage rings. The floor motion is magnified by high transmissibility ratios of the girder-magnet assemblies at their natural frequencies. At higher frequencies, the floor motion reduces exponentially [2] as  $1/f^n$  with exponent  $n = 4$ . Therefore, the girder support systems are usually designed with the requirement of high natural frequencies, specifically the 1<sup>st</sup> natural frequency of > 30 Hz. Girder support systems with higher 1<sup>st</sup> natural frequencies (see Table 1) are expected to have lower broadband (2 – 100 Hz) transmissibility ratios.

Table 1: Comparison of 1<sup>st</sup> Natural Frequencies and Transmissibility Ratios in (2 – 100 Hz) Band

Facility	1 <sup>st</sup> Nat. Freq.	Trans. (H)	Trans. (V)
NSLS-II	30 Hz	1.03*	1.01
APSU <sup>†</sup>	42 Hz	1.30	1.01
ESRF	42 Hz	1.24	1.21
TPS	44 Hz	1.20	1.01
SIRIUS	133 Hz	1.39	1.07

\* Corrected to 1.07 <sup>†</sup> Estimated from FE Model

A low transmissivity ratio of 1.03 for NSLS-II girders in the horizontal direction appeared to be inconsistent with a lower 1<sup>st</sup> natural frequency,  $f_{n,1}$ , of 30 Hz. Additional vibrations tests were performed at NSLS-II in December 2019 and March 2020. The transmissibility ratio was corrected to 1.07 to account for a calibration difference between the seismometers in the very low frequency range of (2 – 4 Hz), but the apparent discrepancy was still significant.

The design of NSLS-II girder support system is unique in its use of viscoelastic pads for thermal stability. For any fluctuation in the tunnel-air temperature, or the floor

temperature, the viscoelastic pads allow the girders to expand or contract without bending, thereby minimizing magnet-to-magnet misalignment [3, 4]. Although not intended for vibration damping, they are expected to have some effect on reducing the transmissibility ratios. This was investigated by vibration tests and FE models as described in the following sections.

## NSLS-II GIRDER-MAGNET ASSEMBLY

A typical NSLS-II multipole girder-magnet assembly is shown in Fig. 1(top). The girder is supported on 2-inch diameter threaded rods at 4 locations approximately 1.2 m apart. Multiple support points increase the stiffness of the girder and raise its natural frequencies. At the bottom, the threaded rods are bolted to a solid 2.5-inch steel plate at the 2<sup>nd</sup> location from the upstream end, and to viscoelastic pads (Fig. 1(bottom)) at the other locations.

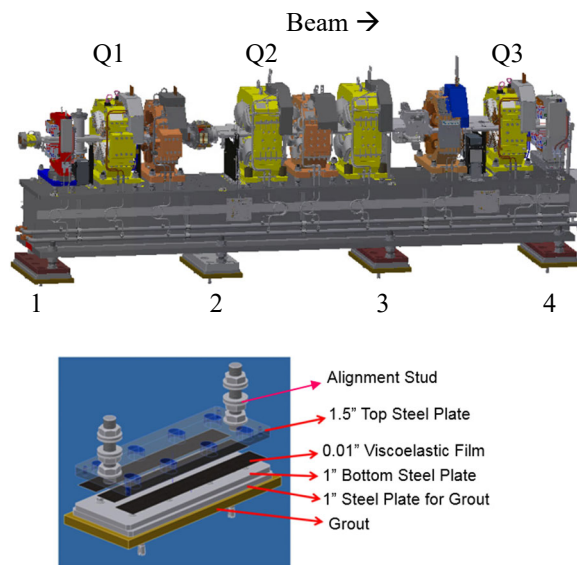


Figure 1: A typical NSLS-II girder (top) is supported at 4 locations. Viscoelastic pads (bottom) are used at locations 1, 3 and 4.

Viscoelastic pads consist of two steel plates, 1.5-inch thick (top) and 1.0-inch thick (bottom), joined by 0.01-inch thick viscoelastic films, brand-name VHB F9469PC, made by 3M<sup>®</sup>. Experimental data for the storage and loss moduli [5] for this film are plotted in Fig. 2.

## FE MODELING OF VISCOELASTIC FILM

In Ansys FE models, viscoelastic properties can be expressed as shear and bulk relaxation moduli ( $G(t)$  and  $K(t)$ ) in Prony series:

$$G(t) = G_{\infty} + \sum_{i=1}^n G_i \exp\left(-\frac{t}{\tau_i^G}\right) \quad (1)$$

$$K(t) = K_{\infty} + \sum_{i=1}^n K_i \exp\left(-\frac{t}{\tau_i^K}\right) \quad (2)$$

<sup>†</sup> sharma@bnl.gov

# VACUUM PUMPING CROSSES AND KEYHOLE VACUUM CHAMBERS FOR THE APS-UPGRADE STORAGE RING VACUUM SYSTEM\*

A. McElderry<sup>†</sup>, B. Billett, J. Carter, O. Mulvany  
Argonne National Laboratory, Lemont, Illinois, 60439 USA

## Abstract

The Advanced Photon Source Upgrade (APS-U) storage ring arc consists of a diverse system of narrow-aperture chambers in compact magnet assemblies with gaps often less than 1 mm. The vacuum system contains two stainless steel pumping crosses and two keyhole-shaped vacuum chambers, as well as eight non-evaporative getter (NEG) coated aluminum chambers and crosses per sector (40 total sectors). Each chamber contains a 22 mm diameter electron beam aperture and the keyhole components also feature a photon extraction antechamber. Each design balances functionality, manufacturability, and installation needs.

The design process was aided by a flexible CAD skeleton model which allowed for easier adjustments. Synchrotron radiation heat loads applied to inline chamber photon absorbers and photon extraction beam envelopes were determined via a 3D ray tracing CAD model. The inline photon absorber and the keyhole shapes were optimized using iterative thermal-structural FEA. Focus was put on mesh quality to model the <0.5 mm tall synchrotron radiation heat load absorbed across the length of the chamber to verify cooling parameters. The design process also required careful routing of the water system and vacuum pumps. The designs incorporate beam physics constraints of the inline absorbers, cross-housed discrete absorbers, and pumping slots.

The group of chambers require complex manufacturing processes including explosion bonding, EDM, NEG and copper coating, extruded and drawn tubing, e-beam welding, challenging TIG welding, UHV cleaning, and critical dimensional measurements. The 528 chambers entered the production phase starting in 2019 with some design evolution reflecting the vendors' capabilities. This paper details the design, analysis, and manufacturing of these chambers.

## INTRODUCTION

The APS-Upgrade (APS-U), when completed, will have a 6 GeV, 200 mA 1.1 km storage ring with a brightness greater than 4 keV. The storage ring consists of a diverse set of vacuum chambers including, but not limited to two stainless steel (SST) keyhole chambers, two specialty SST pumping crosses, and eight non-evaporative getter (NEG) coated aluminum vacuum chambers and crosses per sector (40 total sectors). The vacuum system also features NEG-coated copper and Inconel chambers, aluminum L-bend chambers, discrete photon absorbers, and beam position

monitors with RF-lined welded-on bellows [1, 2]. Generally, all chambers house the electron beam within a Ø22 mm aperture, often with a minimum ~1 mm wall thickness and magnet gap <1 mm. An example of an aluminum cross is shown in Fig. 1.



Figure 1: Rendering of the NEG-coated aluminum pumping cross; chamber lengths range from 289 mm to 792 mm.

The SST keyhole chambers feature an extended outboard aperture to serve in the photon extraction scheme as shown in Fig. 2.



Figure 2: Rendering of a SST keyhole vacuum chamber; chambers lengths range from 305 mm to 350 mm.

The specialty SST crosses (Fig. 3) adapt similar concepts from the keyhole and aluminum chambers. The more complex A:VC6 cross houses a discrete crotch photon absorber and branches the photon extraction away from the electron beam.

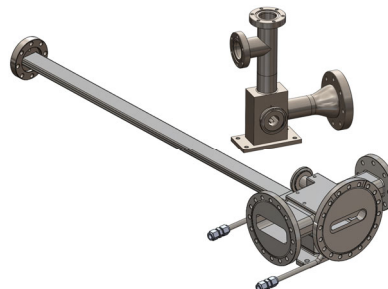


Figure 3: Rendering of the two specialty SST crosses (A:VC15 on top and A:VC6 on the bottom).

## INTERFACES

All chambers interface with the following systems: magnets, water circuits, electrical bakeout system, and other vacuum components. The primary design constraint is the narrow space envelope allowed within the quadrupoles and sextupole magnet bores. Figure 4 and Fig. 5 highlight the common constraints.

\* This research used resources of the Advanced Photon Source, a U.S. Department of Energy (DOE) Office of Science User Facility at Argonne National Laboratory and is based on research supported by the U.S. DOE Office of Science-Basic Energy Sciences, under Contract No. DE-AC02-06CH11357.

<sup>†</sup> amcelderry@anl.gov

# VALIDATION OF APS-U MAGNET SUPPORT DESIGN ANALYSIS AND PREDICTION\*

Z. Liu<sup>†</sup>, W.G. Jansma, J. Nudell, C.A. Preissner  
 Advanced Photon Source, Argonne National Laboratory, Lemont, IL 60439, USA

## Abstract

The Advanced Photon Source Upgrade (APS-U) accelerator magnets have stringent stability requirements [1]. The project schedule and budget did not allow for full prototyping of the final design. Therefore, the engineers relied on accurate simulation to ensure that the design would meet the specifications. Recently, assembly and free-boundary vibration tests have been done on the first article of the upstream quadrupole Doublet, Longitudinal gradient dipole and Multipole module (DLM-A). The top surface flatness of the girder and the magnet alignment measurement results demonstrate the static positioning requirement of magnet-to-magnet is met. The free-boundary condition modal test results were used to validate dynamic performance of the FEA analysis used in the DLM-A design. These validations then confirm the predicted performance of the magnet support system design. Mode shapes and corresponding frequencies from the FEA modal analysis agree with the experimental modal analysis within an acceptable tolerance. The validation approves not only the procedure for accurate modelling of magnet support system that APS-U has developed, but also provides confidence in predicting the accelerator performance.

## INTRODUCTION

The Advanced Photon Source Upgrade (APS-U) accelerator magnets have stringent stability requirement [1]. Some of the requirements are listed in Tables 1 and 2, which service as a guideline through all design phases.

Table 1: Positioning Tolerances

Elements within a girder		
Magnet to magnet (2 sigma cutoff)	30	$\mu\text{m rms}$
Dipole roll	0.4	mrad
Quadrupole roll	0.4	mrad
Sextupole roll	0.4	mrad

Table 2: Vibrational Tolerances

(1-100 Hz)	X (rms)	Y (rms)
Girder vibration	20 nm	20 nm
Quadrupole vibration	10 nm	10 nm
Dipole roll vibration	--	0.2 $\mu\text{rad}$

\* This research used resources of the Advanced Photon Source, a U.S. Department of Energy (DOE) Office of Science User Facility at Argonne National Laboratory and is based on research supported by the U.S. DOE Office of Science-Basic Energy Sciences, under Contract No. DE-AC02-06CH11357.

<sup>†</sup> zpliu@anl.gov

The APS-U magnet support design has gone through phases of conceptual, preliminary, and final design. In preliminary design a prototype of FODO module assembly was reported [2-5]. The magnet grouping has been changed through the design phases [6]. Figure 1 shows APS-U magnet grouping of final design. The “QMQ” places a dipole magnet with its adjacent two quadrupoles on a common support (girder), while “A” and “B” imply upstream and downstream positions. Three plinths provide support to corresponding girders above each, while a QMQ girder is supported on adjacent plinths at each end.



Figure 1: APS-U magnet grouping of final design.

A testing and modelling process has been developed and established to close the loop on the design-analysis-testing workflow [4, 7]. This process provides confidence in simulation results and enables the exploration of many different design iterations using the same components.

These design iterations reflect updates of constraints, such as more stringent space limitations from interfacing systems. The support components between girder and plinth are also updated. Some constraints remained the same throughout the process, such as maximizing eigenvalues of low vibration modes of the system, whose mode shapes would cause dynamic deformation in a direction transverse to the beam path. For static deformation, minimizing the girder deformation improves alignment between magnets within a girder. One must also ensure that thermal fluctuations within the storage ring tunnel will not cause unacceptable changes in magnet alignment. Fabrication and material selection also constraint the design. All these constraints play roles in optimizing the design at each iteration.

Recently, the first article of the DLM-A module magnet support system arrived. Girder flatness was measured, both with and without magnets installed. Then, assembly of the DLM-A module without the APS-U vacuum system was completed. A free-boundary condition experimental modal analysis (EMA) was conducted using a Data Physics Abacus DAQ system [8] and Vibrant Technology MEScope [9] for modal property estimation. These results were used to validate the finite element (FE) analysis used in the DLM-A design.

This design-analysis-measurement chain for the DLM-A module validates the FEA prediction and modelling process. This validation provides confidence in predicting the accelerator performance.

# MECHATRONICS APPROACH FOR THE DEVELOPMENT OF A NANO-ACTIVE-STABILIZATION-SYSTEM

T. Dehaeze<sup>1,†</sup>, J. Bonnefoy, ESRF, Grenoble, France

C. Collette<sup>1</sup>, Université Libre de Bruxelles, BEAMS department, Brussels, Belgium

<sup>1</sup>also at Precision Mechatronics Laboratory, University of Liege, Belgium

## Abstract

With the growing number of fourth generation light sources, there is an increased need of fast positioning end-stations with nanometric precision. Such systems are usually including dedicated control strategies, and many factors may limit their performances. In order to design such complex systems in a predictive way, a mechatronics design approach also known as “model based design”, may be utilized. In this paper, we present how this mechatronics design approach was used for the development of a nano-hexapod for the ESRF ID31 beamline. The chosen design approach consists of using models of the mechatronics system (including sensors, actuators and control strategies) to predict its behavior. Based on this behavior and closed-loop simulations, the elements that are limiting the performances can be identified and re-designed accordingly. This allows to make adequate choices regarding the design of the nano-hexapod and the overall mechatronics architecture early in the project and therefore save precious time and resources. Several test benches were used to validate the models and to gain confidence on the predictability of the final system’s performances. Measured nano-hexapod’s dynamics was shown to be in very good agreement with the models. Further tests should be done in order to confirm that the performances of the system match the predicted one. The presented development approach is foreseen to be applied more frequently to future mechatronics system design at the ESRF.

## INTRODUCTION

With the new 4<sup>th</sup> generation machines, there is an increasing need of fast and accurate positioning systems [1]. These systems are usually including feedback control loops and therefore their performances are not only depending on the quality of the mechanical design, but also on its correct integration with the actuators, sensors and control system.

In order to optimize the performances of such system, it is essential to consider a design approach in which the structural design and the control design are integrated. This approach, also called the “mechatronics approach”, was shown to be very effective for the design many complex systems [2, 3]. Such design methodology was recently used for the development of several systems used by the synchrotron community [4–6].

The present paper presents how the “mechatronic approach” was used for the design of a Nano Active Stabilization System (NASS) for the ESRF ID31 beamline.

<sup>†</sup> thomas.dehaeze@esrf.fr

## NASS - MECHATRONICS APPROACH

### The ID31 Micro-Station

The ID31 micro-station is used to position samples along complex trajectories [7]. It is composed of several stacked stages (represented in yellow in Fig. 1) which allows an high mobility. This however limits the position accuracy to tens of micrometers.

### The Nano Active Stabilization System

The NASS is a system whose goal is to improve the positioning accuracy of the micro-station. It is represented in Fig. 1 and consists of three main elements:

- A nano-hexapod located between the sample to be positioned and the micro-station
- An interferometric metrology system measuring the sample’s position with respect to the focusing optics
- A control system (not represented), which based on the measured position, properly actuates the nano-hexapod in order to stabilize the sample’s position.

This system should be able to actively stabilize the sample position down to tens of nanometers while the micro-station is performing complex trajectories.

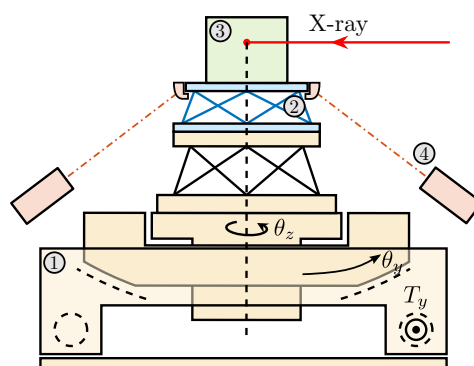


Figure 1: NASS - Schematic representation. 1) Micro-station, 2) Nano-hexapod, 3) Sample, 4) Metrology system.

### Mechatronics Approach - Overview

In order to design the NASS in a predictive way, a mechatronics approach, schematically represented in Fig. 2, was used. It consists of three main phases:

1. *Conceptual phase*: Simple models of both the micro-station and the nano-hexapod are used to first evaluate the performances of several concepts. During this

# SURFACE TWIST CHARACTERIZATION AND COMPENSATION OF AN ELLIPTICALLY BENT HARD X-RAY MIRROR\*

Z. Qiao<sup>†</sup>, J. Anton, L. Assoufid, S. Kearney, S. Mashrafi, J. Qian, X. Shi, D. Shu  
Advanced Photon Source, Argonne National Laboratory, Lemont, IL, USA

## Abstract

Adaptive optics, including bendable and bimorph mirrors, have been widely used for hard X-ray dynamical focusing and wavefront correction. A recently developed elliptically bent mirror based on a laminar flexure bending mechanism has shown excellent performance. In this work, the mirror surface twist of the bent mirror was characterized using a Fizeau interferometer under different bending conditions. By applying a shimming correction, the surface twist was successfully reduced from 5.3  $\mu\text{rad}/\text{cm}$  to 0.09  $\mu\text{rad}/\text{cm}$ . The twist angle variation from no bending to the maximum bending is about 0.05  $\mu\text{rad}/\text{cm}$ . Simulation results show that these numbers are significantly lower than the required values to ensure optimum optical performance. The study helps confirm the bender design and guides the twist compensation procedures.

## INTRODUCTION

The Advanced Photon Source (APS) at the Argonne National Laboratory (ANL) is under a major upgrade with more than two orders of magnitude increase in brightness [1]. The low emittance of the APS upgrade (APS-U) source will enable nanometer focused beam with high coherent flux, which requires optics with ultra-high quality. Many APS-U beamlines also demand variable focal spot sizes to adapt to different sample feature sizes. Such a zoomable beam can only be achieved by combining multiple optics [2] and using deformable optics, e.g., bendable mirrors and bimorph mirrors [3].

A high-precision compact flexure bending mechanism has been recently designed in-house at APS to provide elliptical (or hyperbolic) shaped mirror surfaces [4, 5]. A prototype bender mirror was fabricated and has demonstrated excellent performance in achieving variable shapes and focal spot sizes [3, 6]. In this paper, the surface twist of such a bender mirror is characterized using optical metrology. Then a practical twist compensation procedure is introduced and demonstrated.

## BENDER MIRROR PROTOTYPE

A photograph of the bender mirror prototype is shown in Fig. 1. The mirror has a trapezoidal shape with a length of 300 mm, a narrow-end width of 19.32 mm, a wide-end width of 36.28 mm, and a thickness of 12 mm. It is a single-crystal silicon substrate coated with Pt on the optical surface. The bending moment is applied on each end of the

mirror by the flexure mechanism driven by a piezo linear actuator pushing a 65 mm long bending arm, the position of which is monitored by a capacitive sensor. There is also an array of capacitive sensors mounted underneath the mirror to record the surface profile of the bottom surface.

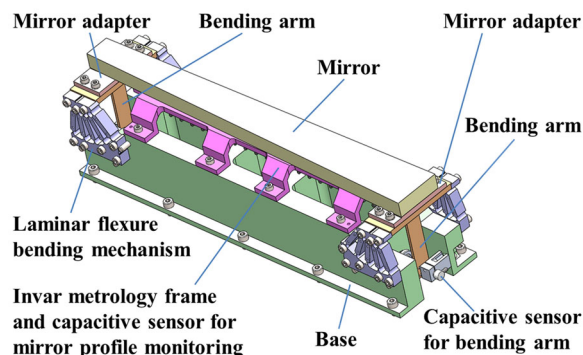


Figure 1: Photograph of the bender mirror prototype.

Although the mechanical design has shown excellent bending performance, a possible surface twist can exist due to the manufacture tolerance and the uniformity of the epoxy bonding the mirror to the adapter plates. There is no motorized or manual twist adjustment in the prototype design.

## SURFACE TWIST TOLERANCE

Surface twist tolerance was studied for a typical bender mirror designed for focusing APS-U source as an example. The mirror can provide a minimum focal spot size of 200 nm. The effect of surface twist was simulated using ray-tracing software ShadowOui [7] and shown in Fig. 2.

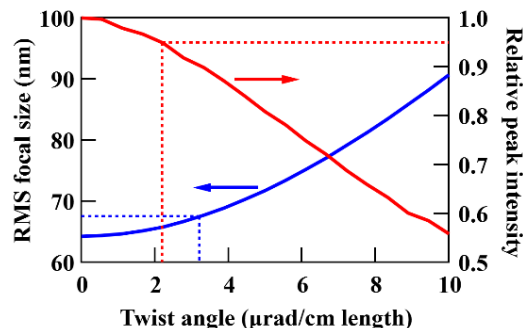


Figure 2: Simulated effects of mirror surface twist on the focal spot size and peak intensity.

As the twist angle increases, the focal spot size increases, while the relative peak intensity decrease. We specify the tolerance of the twist angle to ensure that both the focal size broadening and peak intensity reduction are less than 5%. Figure 2 shows that the twist angle needs to be smaller than 2  $\mu\text{rad}/\text{cm}$ .

\*This research used resources of the Advanced Photon Source, a U.S. Department of Energy (DOE) Office of Science User Facility at Argonne National Laboratory and is based on research supported by the U.S. DOE Office of Science-Basic Energy Sciences, under Contract No. DE-AC02-06CH11357.

<sup>†</sup> zqiao@anl.gov



# ZERO-LENGTH CONFLAT FIN-TYPE NONEVAPORABLE GETTER PUMP COATED WITH OXYGEN-FREE PALLADIUM/TITANIUM

K. Mase<sup>†,1</sup>, T. Kikuchi, Institute of Materials Structure Science, KEK, 1-1 Oho, Tsukuba 305-0801, Japan

Y. Sato, S. Ohno, Graduate School of Engineering Science, Yokohama National University, 79-5 Tokiwadai, Hodogaya-ku, Yokohama 240-8501, Japan

A. Hashimoto<sup>2</sup>, M. Yamanaka, National Institute for Materials Science, Tsukuba 305-0047, Japan  
T. Miyazawa, Department of Materials Structure Science, SOKENDAI (The Graduate University for Advanced Studies), 1-1 Oho, Tsukuba 305-0801, Japan

<sup>1</sup>also at Department of Materials Structure Science, SOKENDAI (The Graduate University for Advanced Studies), 1-1 Oho, Tsukuba 305-0801, Japan

<sup>2</sup>also at University of Tsukuba, Tsukuba 305-0047, Japan

## Abstract

Nonevaporable getter (NEG) pumps are widely used in synchrotron radiation facilities because they are oil-free, vibration-free, space-saving, lightweight, and energy-saving. However, conventional NEG pumps have the following disadvantages: (1) a relatively high activation temperature (typically 300–450 °C for ZrVFe alloy); (2) the requirement for a dedicated power supply and electric feedthroughs; and (3) decreased pumping speeds after repeated cycles of activation and exposure to air. To overcome these disadvantages, we have developed a new zero-length conflat (CF) fin-type NEG pump with a DN 160 CF that uses oxygen-free Pd/Ti thin films as a new NEG material for evacuating residual H<sub>2</sub> and CO. The advantages of the new NEG pump are as follows: (1) it can be activated by baking at 150 °C; (2) no dedicated power supply or electric feedthrough is required; (3) pumping speeds do not degrade even after repeated cycles of activation and exposure to air; and (4) the unit is space-saving and lightweight.

## INTRODUCTION

A nonevaporable getter (NEG) pump evacuates residual reactive gases at room temperature after it has been activated under clean ultrahigh vacuum (UHV) conditions [1-3]. However, the activation temperature of conventional NEG pumps is relatively high (typically 300-450 °C for ZrVFe alloy). In 1997, Benvenuti *et al.* proposed the idea of depositing a NEG thin film on the inner walls of a vacuum chamber to achieve a UHV after baking [4-6]. They named this method ‘NEG coating’. A thin film of TiZr, deposited by direct-current (DC) magnetron sputtering, with an activation temperature of 250 °C, was proposed for use as the NEG coating [4-6]. Shortly thereafter, it was reported that TiZrV thin films deposited by DC magnetron sputtering could be activated by baking at 180 °C for 24 hours [7, 8]. This TiZrV coating were used with great success at CERN and has now been adopted in accelerator facilities around the world [9].

Another disadvantage of a conventional NEG is that repeated activation and exposure to air results in oxidation of the surface, degrading its pumping performance. To overcome this disadvantage, a method was developed involving the sequential deposition of TiZr or TiZrV and Pd by DC magnetron sputtering (Pd/TiZr or Pd/TiZrV) [10-13]. Pd surface is capable of dissociating H<sub>2</sub> molecules into their constituent H atoms at room temperature, and the resulting H atoms diffuse into the bulk of the Pd [14]. Pd surface is also capable of chemisorbing CO at room temperature [15]. Consequently, Pd/TiZr and Pd/TiZrV can evacuate H<sub>2</sub> and CO at room temperature after activation. Because Pd surface does not readily oxidize, its pumping performance should not deteriorate after repeated activation and exposure to air. In fact, Mura, and Paolini reported that Pd/TiZrV is activated by baking at 150 °C and that it pumps H<sub>2</sub> and CO at room temperature; moreover, the pumping speed for H<sub>2</sub> does not decrease even after 30 cycles of activation and exposure to air [12].

Recently Mase *et al.* developed a new method for depositing a Pd-overcoated NEG thin film without using sputtering [16, 17]. Their NEG was fabricated by sequential sublimation of Ti and Pd under UHV at 10<sup>-7</sup> to 10<sup>-8</sup> Pa. This new NEG was named ‘oxygen-free Pd/Ti’ because its oxygen content was estimated to be less than 0.05% [17]. Kikuchi *et al.* developed a prototype of a NEG pump with a DN 160 conflat (CF) flange that used oxygen-free Pd/Ti (Fig. 1) [18]. Here, we report the development of a zero-length CF fin-type NEG pump [19]. This NEG pump can be easily fabricated by using a ring to which fins are attached. The pumping speeds of the NEG pump for H<sub>2</sub> and CO were measured by the orifice method [20].



Figure 1: Schematic showing the activation and pumping mechanisms of oxygen-free Pd/Ti deposited on stainless-steel SS304L. Reproduced from Ref. [18].

<sup>†</sup> mase@post.kek.jp

# EXACTLY-CONSTRAINED KB MIRRORS FOR SIRIUS/LNLS BEAMLINES: DESIGN AND COMMISSIONING OF THE TARUMÁ STATION NANOFOCUSING OPTICS AT CARNAÚBA BEAMLINE

G. B. Z. L. Moreno<sup>†</sup>, R. R. Geraldés, C. S. N. C. Bueno, F. R. Lena, S. A. L. Luiz, Y. R. Tonin, E. O. Pereira, W. H. Wilendorf, H. C. N. Tolentino, Brazilian Synchrotron Light Laboratory (LNLS), Brazilian Centre for Research in Energy and Materials (CNPEM), Campinas, SP, Brazil

## Abstract

Next-generation nanoprobe, empowered by diffraction-limited storage rings, as Sirius at the Brazilian Synchrotron Light Source (LNLS), present high-performance requirements aiming at high spatial resolution and throughput. For the focusing optics, this means assuring a small and non-astigmatic probe, high flux density, and remarkably high position stability, while simultaneously preserving beam wavefront. At stations further dedicated to spectromicroscopy and *in-situ* experiments, these requirements add up to having achromatic design and suitable working distance, respectively. In this way, Kirkpatrick-Baez (KB) mirrors have been chosen as an appropriate solution for many of Sirius focusing optics. Yet, the consequent requirements on mirror angular stability in less than 10 nrad RMS, surface quality in single-digit nanometers, and alignment tolerances in the range of hundreds of nanoradians, are particularly challenging regarding clamping, vibration, and thermal expansion budgets, even exceeding optical metrology limits. This work discusses the specifications, design concept, and assembly aspects of the new KB systems for Sirius, taking the TARUMÁ station from CARNAÚBA beamline as a case study with its early commissioning results.

## INTRODUCTION

The design of efficient X-ray nanofocusing systems, with high mechanical stability and optimized compatibility with progressively ambitious experimental setups, is an investment of significant potential in spatial and temporal resolution, especially when fully utilizing the brightness and coherence of 4th-generation light sources [1]. Achromaticity, large working distances, and higher acceptance guided the choice for Kirkpatrick-Baez (KB) mirrors as the nanofocusing optics for many stations at Sirius [2].

TARUMÁ [3] is a sub-microprobe dedicated to multi-technique microscopy and spectroscopy experiments in the energy range of 2.05 to 15 keV in *in-situ* and *in-operando* conditions at CARNAÚBA (Coherent X-Ray Nanoprobe Beamline) [4, 5]. Starting commissioning in December 2020, it is the first nanoprobe at Sirius, where a KB focuses x-rays to 120 nm spot sizes (>8 keV) with 450 mm working distance and up to 1e11 ph/s/100mA on the sample.

Although very promising for scientific opportunities, this optical design brings remarkably strict requirements in manufacturing, installation, and positioning. This is clear from the short summary in Table 1, which includes the forthcoming station at MOGNO and the SAPOTI station at CARNAÚBA, with even tighter specifications. Hence, a high-stability KB system, built on precision engineering

Precision mechanics

Stability Issues & Vibration

concepts and following a predictive design approach, has been developed in-house. The first system, built for TARUMÁ, is also as a proof of concept for the next KB sets.

Table 1: Short Specifications for the First Sirius KB Sets

KB set	TARUMÁ	MOGNO	SAPOTI
Focus size	120 nm	100 nm	35 nm
Dep. of Focus	80 $\mu$ m	20 $\mu$ m	5 $\mu$ m
Max. Mir. Len.	210 mm	450 mm	390 mm
Work. Distance	450 mm	175 mm	55 mm
Grazing Angle	3.9 mrad	4.0 mrad	3.9 mrad
Pitch stability	<10 nrad	< 10 nrad	< 4 nrad
Surface Error	< 1 nm	< 1 nm	< 1 nm

## CONCEPT AND DESIGN

As compared with other X-ray focalizing elements, such as zone plates and refractive lenses, KB systems can be used in achromatic optical designs, reach larger working distances, and eventually allow for higher acceptance [6]. On the other hand, when also bounded to high numerical apertures and small grazing angles, mirrors are longer and heavier components, which are more difficult to handle and position, often resulting in limited dynamics. Moreover, apart from small focalizing elements, relative metrology over the extense mirror substrates and/or between the optics and the sample gets complicated. At TARUMÁ, for instance, where the KB set is in Ultra-High-Vacuum and the sample is in open-atmosphere, metrology with sufficient accuracy would be hardly even possible (see [7]).

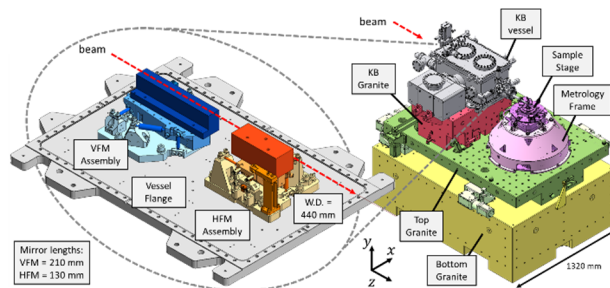


Figure 1: Reduced drawings of experimental bench and KB set with VFM and HFM assemblies in the vacuum vessel.

Building up from previous KB system and mirror base designs [8-12], and recent developments in primary optics for Sirius mirror systems [13], a deterministic design for passive high-stability performance was implemented for KB systems. The concept relies in maximizing the suspension frequency of both mirrors with respect to a single

TUOB01

111

# DEVELOPMENT OF A PASSIVE TUNED MASS DAMPER FOR ULTRA-HIGH VACUUM BEAMLINE OPTICS

F. Khan, D. Crivelli, J. Kelly, A. Male, Diamond Light Source Ltd., Didcot, England

## Abstract

Vibration in beamline optics can degrade the quality of experiments: the resulting movement of a mirror increases the X-ray beam position uncertainty and introduces flux variations at the sample. This is normally dealt with by averaging data collection over longer periods of time, by slowing down the data acquisition rates, or by accepting low-quality blurred images. With the development of faster camera technology and smaller beam sizes in next generation synchrotron upgrades, older optics designs can become less suitable, but still very expensive to redesign.

Mechanically, mirror actuation systems require a balance between repeatability of motion and stability. This leads to designs that are “soft” with resonant modes at a relatively low frequency, which can be easily excited by external disturbances such as ground vibration and local noise. In ultra-high vacuum applications, the damping is inherently low, and the vibration amplification at resonance tends to be very high.

At Diamond we designed a process for passively damping beamline mirror optics. First, we experimentally analyse the mirror’s vibration modes; we then determine the tuned mass damper (TMD) parameters using mathematical and dynamic models. Finally, we design a flexure-based metal TMD which relies on eddy current damping through magnets and a conductor plate. The TMD can be retrofitted using a clamping system that requires no modification to the existing optic. In this conference paper we show a case study on a mirror system on Diamond Light Source’s Small Molecule Single Crystal Diffraction Beamline, I19.

## INTRODUCTION

The vibrational behaviour of the Horizontally Focusing Mirror (HFM) at I19 (Fig. 1) was evaluated upon witnessing low resonant signatures in the Fast Fourier Transform (FFT) of the X-ray beam positioning data. Figure 2 shows

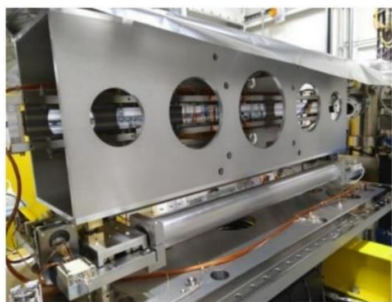


Figure 1: The HFM sitting on actuators is placed at the Small Molecule Single Crystal Diffraction Beamline, I19, at Diamond Light Source.

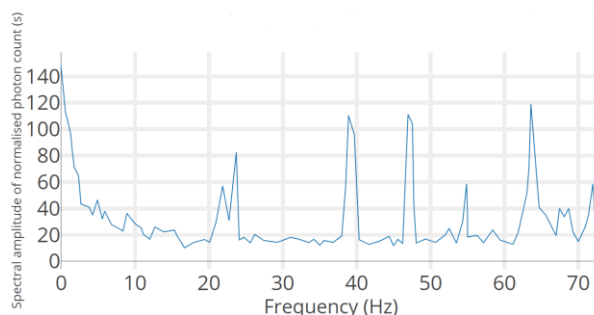


Figure 2: FFT plot of the HFM X-ray beam stability.

distinct peaks at 23, 40 and 47 Hz respectively. An experimental modal analysis characterised these natural frequencies with rocking and pitching modes in the actuators, which would magnify with distance from the centre of the mirror and affect beam positioning if left untreated.

A proposition was developed to house four retrofitted tuned mass dampers (TMDs) to effectively dampen the specific resonances. The TMDs would be installed and secured using slide-in trays and clamps, virtually leaving the expensive mirror system unchanged.

## 3D PRINTED TMD

An initial 3D printed TMD prototype was tuned to target the 23 Hz mode, as shown in Fig. 3. The monolithic design used calibrated double-hinged PLA flexures [1] (shown in purple) as a means of lateral motion and dissipation of energy through eddy current damping (ECD) (permanent magnets shown in yellow). The derived theory behind the flexure geometry is discussed under Design Process.

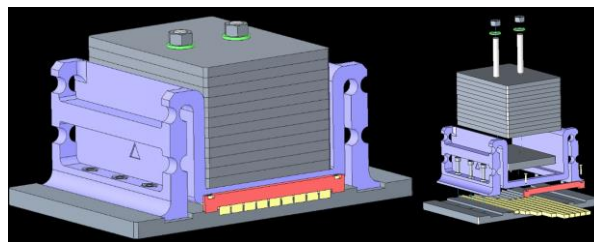


Figure 3: A representation of the 3D printed monolithic TMD prototype in a CAD assembly.

The passive vibration of the HFM was experimentally measured once more with the mounted TMD prototype. In the FFT plot (Fig. 4), the amplitude of the 23 Hz resonance visibly decreased with no additional parasitic motion introduced to the system. The 15 Hz peak, found to be a translation mode, was present during vibrational testing but was not registered by the beam positioning data seen in Fig. 2, hence it was disregarded.

# OXYGEN-FREE TITANIUM THIN FILM AS A NEW NONEVAPORABLE GETTER WITH AN ACTIVATION TEMPERATURE AS LOW AS 185 °C

Kazuhiko Mase<sup>†,1</sup>, Takashi Kikuchi, Institute of Materials Structure Science, KEK, 1-1 Oho, Tsukuba 305-0801, Japan

Masato Ono, Kazuo Yoshioka, Ichiro Yoshikawa, Department of Complexity Science and Engineering, University of Tokyo, 5-1-5 Kashiwanoha, Kashiwa 277-0882, Japan

Kenichi Ozawa<sup>2</sup>, Department of Chemistry, Tokyo Institute of Technology, Meguro, Tokyo 152-8551, Japan

Yusuke Masuda, Yasuo Nakayama, Department of Pure and Applied Chemistry, Tokyo University of Science, 2641 Yamazaki, Noda, Chiba 278-8510, Japan

Yuta Sato, Shinya Ohno, Graduate School of Engineering Science, Yokohama National University, 79-5 Tokiwadai, Hodogaya-ku, Yokohama 240-8501, Japan

<sup>1</sup>also at Department of Materials Structure Science, SOKENDAI (The Graduate University for Advanced Studies), 1-1 Oho, Tsukuba 305-0801, Japan

<sup>2</sup>also at Institute of Materials Structure Science, KEK, 1-1 Oho, Tsukuba 305-0801, Japan

## Abstract

Although nonevaporable getter (NEG) pumps are widely used in synchrotron-radiation facilities, unalloyed titanium (Ti) has rarely been used as a NEG. It has been previously shown that high-purity Ti deposited under an ultrahigh vacuum, followed by introduction of N<sub>2</sub>, operated as a NEG with an activation temperature of 185 °C. This Ti thin film contained a concentration of oxygen and related impurities of 0.05% or less. In the present study, we used synchrotron-radiation X-ray photoelectron spectroscopy to analyze the oxygen-free Ti thin films after the introduction of high-purity N<sub>2</sub> or air. After the deposition of oxygen-free Ti, more surface TiN was formed by the introduction of high-purity N<sub>2</sub> than by introduction of air. We also evaluated the pumping properties of the oxygen-free Ti thin films treated with high-purity N<sub>2</sub> by means of total and partial pressure measurements. A vacuum vessel with oxygen-free Ti deposited on its inner walls was found to pump H<sub>2</sub>, H<sub>2</sub>O, O<sub>2</sub>, and CO even after 30 cycles of pumping, baking at 185 °C for 6 hours, cooling to room temperature, introduction of high-purity N<sub>2</sub>, and exposure to air. The high purity of the Ti thin film and the formation of TiN on its surface appear to be responsible for the reduced activation temperature of 185 °C.

## INTRODUCTION

A nonevaporable getter (NEG) is a material that evacuates residual reactive gases at room temperature after it has been activated under clean ultrahigh-vacuum (UHV) conditions (Fig. 1) [1–3]. In 1997, Benvenuti *et al.* proposed the idea of depositing NEG thin films on the inner walls of vacuum chambers to achieve an UHV after baking [4–6]. They named this method ‘NEG coating’. Soon afterward, they reported that thin films of TiZrV deposited by direct-current magnetron sputtering can be activated by baking at 180–250 °C for 24 hours [7, 8]. This TiZrV coating was used with great success at the European

Organization for Nuclear Research (CERN) and has now been adopted in accelerator facilities around the world [9, 10].

Although a single-metal Ti deposition is widely used in Ti sublimation pumps [11], it has rarely been used as a NEG coating because its activation temperature has been reported to be as high as 350–400 °C [4–6]. However, Miyazawa *et al.* found that a thin film of high-purity Ti deposited by sublimation of Ti metal under UHV followed by introduction of N<sub>2</sub> can work as a NEG with an activation temperature of 185 °C [12, 13]. Because the concentration of oxygen and related impurities in the Ti thin film was 0.05% or less, we refer to it as ‘oxygen-free Ti’ hereafter. Here, we present the results of our study by synchrotron-radiation X-ray photoelectron spectroscopy (SR-XPS) of oxygen-free Ti thin films treated with high-purity N<sub>2</sub>, together with measurements of total and partial pressures to verify their NEG properties [14].

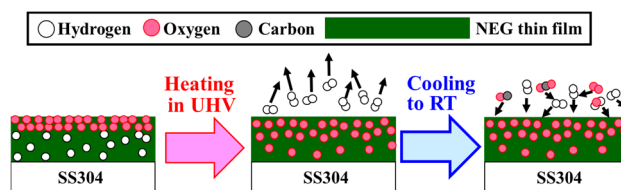


Figure 1: Schematic showing the activation and pumping mechanisms of a NEG thin film deposited on an SS304 stainless-steel substrate.

## EXPERIMENTS

Thin films of oxygen-free Ti were deposited on silicon wafers or the inner surfaces of a vacuum vessel by means of Ti sublimation under UHV in the range 10<sup>-7</sup> to 10<sup>-8</sup> Pa. N<sub>2</sub> with a purity of more than 99.9% was then introduced (Figs. 2-4). The purity of the oxygen-free Ti thin films was estimated to be more than 99.995% from the pressure and the Ti deposition rate. The oxygen-free Ti thin films were analyzed by SR-XPS at BL-13B of the Photon Factory

<sup>†</sup> mase@post.kek.jp

# DESIGN OF REMOTE HELIUM MASS SPECTROMETER LEAK DETECTOR\*

H. Y. He<sup>†</sup>, J.M. Liu, R.H. Liu, H. Song, G.Y. Wang, Spallation Neutron Source Science Centre,  
Dongguan, China

## Abstract

Leak detection is the key to get a good vacuum system. For the dangerous areas, or facility with complicit structure required to be detect online, it is a hard mask to seek for the suspected leaks one after another. After studying the basic principle of helium mass leak detection, design a remote leak detector based on the PLC, as well as multi monitoring cameras, which can achieve successfully injection and sniffer probe leak detection during the range of 270 degree. Compared with the manual operation, this device aims at accurately and reliably detecting leak rate, which can greatly provide technique support of online leak detection. And it can bring the value of reducing the labour intensity and ensuring personal safety.

## INTRODUCTION

Vacuum With the continuous development of science and technology and industrial production, the requirements of vacuum equipment are higher and higher, and vacuum leak detection technology is also playing a more and more important role. The injection method and the inhalation method can be used to determine the location of the leak, and the helium mass spectrometry method is the most commonly used. In the process of leak detection, controlling the leak detector and auxiliary spray gun at the same time, observing the change of leak rate, data analysis and feedback operation in time, often requires multiple operators to work together, which greatly reduces the efficiency and accuracy of measurement. The development of computer technology leads the development of measuring instruments to automation and intelligence. At present, the helium mass spectrometer leak detector is controlled by microcomputer, but the intelligent leak detection and defect diagnosis still have a long way to go.

Based on PLC (programmable logic controller) and camera monitoring, helium injection method and positive pressure suction gun leak detection are carried out to realize remote online intelligent detection of vacuum system in high-risk environment

## BASIC PRINCIPLES AND METHOD FOR HELIUM MASS SPECTROMETRY LEAK DETECTION

With vacuum leak detection technology is a technology to determine whether there is air leakage in the vacuum system and to determine the location and size of the leakage. Helium mass spectrometer leak detection is to add helium to one side of the workpiece to be tested by certain

means, and then use helium mass spectrometer leak detector to detect the helium overflowing through the leak hole by appropriate methods on the other side to achieve the purpose of detection. Helium injection method and positive pressure method are two basic methods of helium mass spectrometry leak detection [1].

Helium injection leak detection is to vacuum the inner cavity of the tested part, and use the gun to inject helium with a certain pressure on the surface of the tested part, to detect the helium leakage into the tested part. Helium injection method takes a lot of time, but it can determine the location of the leak, and has the advantages of high sensitivity and low cost. It is a common qualitative leak detection method.

## OVERALL DESIGN OF THE DEVICE

The remote vacuum leak detector consists of two main modules: the control and adjustment module of the probe and helium mass spectrometer leak detector, and the identification and monitoring module of the camera. The core function is to realize the remote control of the helium mass spectrometer leak detector and its accessory spray gun based on the auxiliary identification and real-time monitoring of the camera to complete the leak detection operation of the vacuum specimen [2]. The overall block diagram of the remote helium mass spectrometer leak detector is shown in Fig. 1 [3].



Figure 1: Structure of mobile prob for remote helium mass leak detector.

### *Helium injection leak test and result analysis*

With The test is divided into two parts: helium injection method and positive pressure suction gun. During the test, the ambient temperature is about 24 °C. Firstly, the leakage rate of different positions is detected by the conventional manual method as the benchmark, and then the leakage rate data of each position is detected by the remote controlling mobile probe. To eliminate the accidental error, repeated tests were carried out and the average value was taken as the last result [4].

\* Work supported by Institute of High Energy Physics

<sup>†</sup> hehy@ihep.ac.cn.

# INVESTIGATIONS ON STABILITY PERFORMANCE OF BEAMLINE OPTICS SUPPORTS AT BSRF

W.F. Sheng<sup>1</sup> H. Liang<sup>†,1</sup> Y.S. Lu, Z. Zhang

Institute of High Energy Physics, [100049] Beijing, P. R. China

<sup>1</sup>also at University of Chinese Academy of Sciences, School of Physics, [100049] Beijing, China

## Abstract

The stability of beamline optics directly affects the beamline's performances, such as coherence, focal size, position stability of the beam and so on, it has become a serious issue for a low emittance 4th generation light source. The vibration transmitting function of supports plays a big role in the stability performance of the optics. In order to design better supporting structure, several types of support structures were tested, and the transfer ratio were studied. The result shows that wedge structures generally have a lower transfer ratio, and point contact support structures should be avoided.

## INTRODUCTION

HEPS is a new generation light source which aims to reach emittance as low as 60 pmrad with a circumference of about 1360 m. [1] It started construction in 2019 and will be finished in 2025. With the new light source there will be very small sized source, vibration will be a big challenge for HEPS. The beam position, intensity and focal size are often affected by stability of beamline optics such as monochromators, mirrors, sample stages, optical tables, etc. Those instruments are usually very sensitive to ground vibration, the vibration transfer ratio, or transfer function of their supporting structure, plays a big role in the performance of optics under ground motion and vibration. In order to build better optics for the HEPS project, also to get a better understanding of the issue of stability, investigations were carried out to find out what the common performances are, and provide some basic guidelines regarding design of stable supports.

The following sections will introduce the test conditions, and some results of different optics support.

## TEST CONDITIONS AND METHODS

Most of the tests were carried out at BSRF, a first generation light source with about 3 months of dedicated synchrotron mode every year. The ground vibration level is about 18 nm RMS in the range of 1 Hz to 100Hz.

The vibration data was acquired by a DEWESOFT SIRIUSi 8xACC ADC [2], with DYTRAN 3192A and 3191A1 accelerometers [3]. The accelerometers were attached to different layers of optics support and on the ground. Sampling rate is usually set at 2000 Hz or 3000 Hz. The acceleration data then was integrated into RMS displacement. Then by comparing the RMS displacement of upper layer to lower layer, or to the ground, the transfer ratio, or transfer function of the RMS vibration displacement can be obtained. The eigenfrequencies are deduced

by the peaks of amplification curve. Due to the noise of the accelerometers at low frequency ( $<5\text{Hz}$ ), the analysis frequency range is defined between 5 Hz to 1000 Hz.

## TEST RESULTS

### DCM Support

A DCM prototype shown in Fig. 1 was designed to verify technologies to be used for HEPS [4]. When it was designed, not much consideration in support stability was taken other than a granite table. The support of this DCM granite table are 6 wedges. A steel frame sits on those wedges, supporting a granite table with 6 screw levellers, which has ball bearings to make the adjustment easier. It is not good for high stability, because the ball bearings provide small area of contact, also screw levellers are not strong enough.

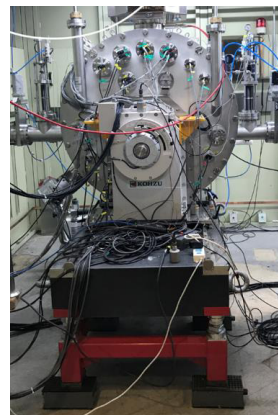


Figure 1: DCM under test.

The integrated RMS vibration of different layers are shown in Fig. 2. It shows that vibration level increase at 8 Hz and 31 Hz for the granite table (line 3, line 4 in the graph). With an eigenfrequency of 8 and 31 Hz, it has an overall transfer ratio of 3 from granite table to ground.

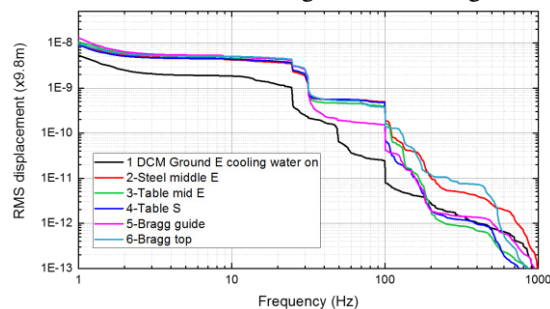


Figure 2: Integrated RMS vibration of DCM.

<sup>†</sup> Email address: lianghao@ihep.ac.cn

# RESEARCH ON VIBRATION STABILITY OF SAPS FOUNDATION

G. Y. Wang<sup>†</sup>, J. X. Chen, H. Y. He, L. Kang, L. Liu, R. H. Liu, X. J. Nie, C. J. Ning,  
 A. X. Wang, J. B. Yu, Y. J. Yu, J. S. Zhang, L.Q. Zhao, D. H. Zhu  
 Institute of High Energy Physics, Chinese Academy of Sciences, Beijing, China  
 Spallation Neutron Source Science Center, Dongguan, China

## Abstract

With the development of science and technology, the technology of synchrotron radiation light source is further developed. As the fourth generation synchrotron radiation light source, Southern advanced photon source forward more stringent requirements on the beam stability. The foundation vibration is the main factor affecting the beam stability. In this paper, the foundation vibration characteristics of the proposed site of Southern advanced photon source are studied, and the foundation vibration test is carried out. The data analysis is carried out from the aspects of different locations, day - night vibration variation characteristics, vibration source frequency, vibration attenuation, and the influence of Expressway on the foundation vibration. This paper provides guidance for the follow-up construction and anti micro vibration foundation vibration treatment of Southern advanced photon source

## PREFACE

With the improvement of science and technology, the performance of large scientific devices is constantly developing towards higher requirements. Southern advanced photon source (SAPS) is the fourth generation synchrotron radiation light source to meet the new development requirements. As the fourth generation synchrotron radiation source, South light source needs higher performance, and beam stability is a very important index. Beam stability needs a stable and non-interference equipment environment. The settlement of the ground, the movement of the surrounding ground, the vibration caused by the fluid and the change of the ambient temperature will affect the mechanical stability of the equipment itself. The foundation vibration is transmitted to the magnet, BPM and other beam equipment through the equipment girder, which eventually leads to the degradation of beam stability. In order to meet the requirements of beam stability, it is necessary to carry out a detailed study on the foundation vibration of the proposed site of the South light source, and clarify the characteristics of the foundation vibration, so as to lay the foundation for the subsequent construction of the light source.

## MEASUREMENT CONTENT AND ANALYSIS METHOD

Southern advanced photon source is located on the west side of China spallation neutron source. The experimental measurement system uses 3ESPCDE seismograph to obtain the velocity signal of foundation vibration. In order to

<sup>†</sup> gywang@ihep.ac.cn.

grasp the overall foundation vibration situation of Southern advanced photon source, the vibration measurement is divided into six areas, each area is arranged with 5 measuring points, and the 24-hour vibration measurement is carried out in three directions of east-west, north-south and elevation. The layout of each point is shown in Fig. 1. Because the survey area is mountain forest area, the surface layer is soft soil, and the bottom layer is hard rock. In order to get the ground vibration results more accurately, each measuring point is dug to remove the loose soil on the surface, and the concrete with the thickness of 100 mm is poured to make the measured value of the seismograph closer to the real situation of the foundation, as shown in Fig. 2.



Figure 1: Distribution points of vibration measurement.

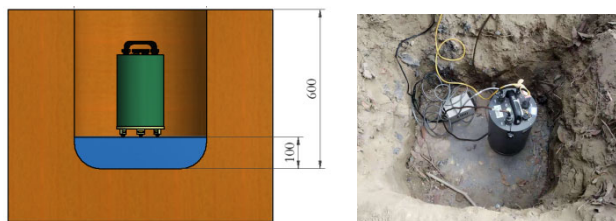


Figure 2: Installation method of seismograph.

Time domain analysis, frequency domain analysis and wavelet analysis are often used in vibration data analysis [1]. In this study, the vibration data are analyzed and evaluated by root mean square (RMS) and power spectral density (PSD), and the time domain RMS value is used to evaluate the energy of foundation vibration signal. The calculation formula of RMS value is shown in Formula 1, In frequency domain, the power spectral density is taken as the evaluation standard, and the calculation formula is formula 2. Considering the measurement accuracy of the seismograph, and the artificial vibration interference in the environment is mainly within 1-100hz. For the evaluation of foundation vibration, the RMS value of 1-100hz is taken as the evaluation standard, and formula 3 is used for calculation [2].

# STUDY THE ACTIVE VIBRATION CONTROL SYSTEM OF THE PARALLEL 6-DOF PLATFORM\*

R.H. Liu<sup>†</sup>, H.Y. He, L. Kang, Z. Y. Ke, L. Liu, X.J. Nie, C.J. Ning, A.X. Wang, G.Y. Wang, Y.J. Yu, J.S. Zhang, D.H. Zhu, CSNS/IHEP, CAS, Dongguan, 523803, China

## Abstract

With the development of high-energy synchrotron radiation light source with high energy, high brightness, low emittance and nano-scale light spot, accelerators and beamline stations have higher requirements for the stability of the system, and active vibration isolation technology has been paid more and more attention. It has become the key technology for the development of major scientific devices (such as high-energy synchrotron radiation light source, free electron laser, etc.) in the future. In this paper, an active vibration control system driven by piezoelectric ceramic actuator with strong adaptability is designed. NI CompactRIO real-time control system and Fx-LMS adaptive filter control algorithm are used for the active vibration control system. The identification method of input and output channels and the active control module are simulated by MATLAB. And an active vibration control system based on a parallel 6-DOF platform was built for experimental verification. The experimental results show that the designed active vibration control system has a good control effect for low-frequency micro-vibration.

## INTRODUCTION

The micro-vibration of synchrotron radiation light sources such as ESRF, APS and SSRF etc. shows that the low-frequency micro-vibration below 20Hz contributes significantly to the overall vibration in the frequency domain, which will cause micro-displacement and micro-deformation between pose-sensitive equipment and various parts of the optical system, thus affecting the performance of various precision components. Therefore, the control of low-frequency micro-vibration interference has become one of the factors that cannot be ignored in the development of advanced light source technology [1]. Low-frequency micro-vibration has the characteristics of miniature, inherent and difficult to control, which makes the micro-vibration dynamic environment become extremely complex and special, and the analysis and vibration control are very difficult, so it is urgent to restrain and control the micro-vibration [2]. Active vibration control has the advantages of good low frequency damping performance, high reliability, easy expansion and easy to realize multi-machine distributed parallel processing due to the existence of actuators [3]. It has been more and more widely used in large scientific devices such as synchrotron radiation light source, aerospace, industrial control, communication and scientific research.

## THE ACTIVE CONTROL PRINCIPLE OF MICRO-VIBRATION

In the actual control engineering, the mathematical models of the actual controlled systems are difficult to be identified in advance through mechanism modeling or off-line system identification, or some parameters or structures of their mathematical models are in change. In the face of the situation that the characteristics of these systems are unknown or often changing and can't be completely determined in advance, how to design a satisfactory control system that can actively adapt to the unknown or changing characteristics is the problem to be solved by the adaptive control algorithm.

### Principles of the FX-LMS Active Control

In practical application, the error signal (vibration response signal)  $e(n)$  is not a simple superposition of the filter output  $y(n)$  and the desired signal  $d(n)$ . There is a transfer function of a secondary channel between  $y(n)$  and  $e(n)$ .  $S(z)$  is the transfer function from the control input of the actuator to the load response, which represents the dynamic characteristic of the actuator, as shown in Fig. 1. Morgan proposed Fx-LMS algorithm to eliminate the influence of secondary channel [4]. The identification process of secondary channels can be carried out by online or offline. The implementation of online identification is relatively complex, so the  $S(z)$  is usually identified by offline [5]. According to the derivation process of the standard LMS algorithm, a similar result can be obtained. The whole filtered Fx-LMS algorithm can be simply summarized as follows:

$$\left\{ \begin{array}{l} y(n) = \sum_{l=0}^{L-1} w_l x(n-l) \\ e(n) = d(n) - S^T Y(n) \\ w(n+1) = w(n) + \frac{\tilde{\mu} e(n) X'(n)}{\gamma + X'^T(n) X'(n)} \\ X'(n) = [x'(n) \quad x'(n-1) \quad \dots \quad x'(n-L+1)] \\ x'(n) = \sum_{h=0}^{H-1} s_h x(n-h) \end{array} \right. \quad (1)$$

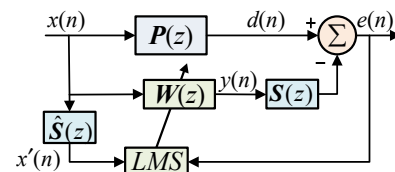


Figure 1: The principle of FX-LMS algorithm.

\* Work supported by NNSF of China: N0. 11905231

<sup>†</sup> liurh@ihep.ac.cn

# PERFORMANCE OF A DOUBLE CRYSTAL MONOCHROMATOR PROTOTYPE FOR HEPS UNDER WATER COOLING CONDITION AT A WIGGLER BEAMLINE OF BSRF

Hao Liang<sup>†,1</sup>, Weifan Sheng<sup>1</sup>, Hong Shi, Yiming Yang, Lirong Zheng<sup>1</sup>  
 Institute of High Energy Physics, 100049 Beijing, P. R. China

<sup>1</sup>also at University of Chinese Academy of Sciences, School of Physics, 100049 Beijing, China

## Abstract

The performance of monochromator is crucial to the performance of a beamline, especially for a 4th generation synchrotron light source. To find out the performance of the monochromator prototype built for the HEPS project, it was tested at a wiggler beamline of BSRF with water cooling. The cooling of the crystals was measured by rocking curve broadening at different energy and cooling seems to be not enough due to indium foils. The repeatability in 1 hour was about 0.1 eV. The energy drift in 9 hours after the beam hit the beamline was 0.4 eV at the Cu K edge. The short-term stability was tested with synchrotron beam under various cooling condition, and results between 4.4 nrad to around 400 nrad were observed. In conclusion, some performances are satisfying, but further improvements should be carried out in the future.

## INTRODUCTION

HEPS is a new generation light source which employs multi-bend achromat lattices and aims to reach emittance as low as 60 pm·rad with a circumference of about 1360 m [1]. A double crystal monochromator prototype was built for the HEPS project, as shown in Fig 1. It went through a series of offline and online test with LN2 cooling during 2016~2019, some key performances were tested. The prototype has a stability of 40 nrad RMS with a LN2 flow rate of about 4.5 L/min. The LN2 cooling works fine under 800 watts of heat load provided by a heater. Other performances such as mechanical resolution, repeatability, vacuum, motion functions are all up to design requirements. Details can be found in [2].

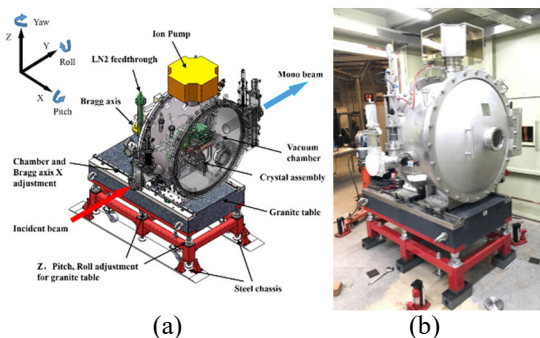


Figure 1: DCM design model (a) and prototype (b).

However, it's still not guaranteed that it will really work for demanding experiments such as XAFS. In order to find out its reliability, it was installed in 3W1 of BSRF, a

wiggler beamline. It was tested only under water cooling condition, since BSRF does not have dedicated LN2 distribution lines. XAFS experiments requires good repeatability of the energy, and good energy stability. Test methods were also developed for such kinds of requirements.

The following sections will share the test conditions, methods and results.

## TEST CONDITIONS

The new 3W1 test beamline layout is shown in Fig. 2. The original 3W1 was dismantled for optics testing. The DCM is 20.8 meters from the source, before the DCM is a collimating mirror, which will reduce the heat load irradiated to the monochromator. By measurement of cooling water temperature rise, the heat load is about 35W. After the DCM is a toroidal mirror at 23 meter. The focal point is 32 meter from the source. The monochromator was cooled by a water chiller made in China, LX series from Coolium Instruments [3], which has a cooling capability of 1000 watts.

Most of the tests and experiments were done under XAFS mode, as shown in Fig. 3. Two Ion Chambers and diamond XBPM were used to measure intensity before and after sample. An ADC [4] were used to take data at high speed in order to measure vibration level.

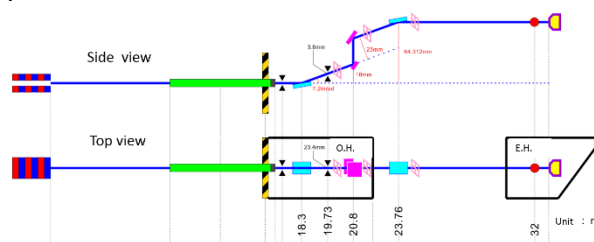


Figure 2: Test beamline layout.

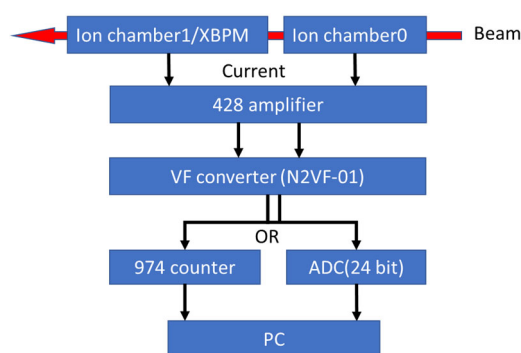


Figure 3: Data acquisition equipment.

<sup>†</sup>lianghao@ihep.ac.cn

# DESIGN OF MAGNET GIRDER SYSTEM FOR SIAM PHOTON SOURCE II

O. Utke<sup>†</sup>, S. Chaichuay, S. Klinkhieo, S. Pongampai, K. Sittisard, S. Srichan  
Synchrotron Light Research Institute, Nakhon Ratchasima, Thailand

## Abstract

The new Siam Photon Source II (SPS-II) storage ring is designed with a circumference of 327.502 m. It consists of 14 DTBA cells, where each cell requires six magnet girders. For the storage ring of SPS-II we developed a magnet girder system which uses wedgemounts for the precision alignment. The girder alignment is based on a 3-2-1 alignment method and requires three wedgemounts to control Z direction, two wedgemounts to control Y-direction and one wedgemount for the X-direction. The magnet alignment is based on mechanical tolerances. Therefore, the girders top plate is designed with precision surfaces with a flatness tolerance of 30  $\mu\text{m}$ . Regarding low girder deformation (from magnet load) and gaining a high mechanical natural frequency to reduce the amplitude of vibrations, FEM simulations were carried out. In this paper simulation results are presented as well as the design of the girder, pedestal and its wedgemount based alignment system.

## INTRODUCTION

The existing storage ring of Siam Photon Source (SPS) has 1.2 GeV beam energy and  $\sim 41$  nm·rad beam emittance. The new Siam Photon Source II (SPS-II) has to provide better parameters to stay competitive for the user community in the South-East Asian region. Therefore, a new machine is being designed with a storage ring circumference of 327.502 meters, a beam energy of 3 GeV and a beam current of 300 mA. The beam emittance should be lower than 1.0 nm·rad. For the lattice design a Double Triple Bend Achromat (DTBA) lattice was chosen. The storage ring consists of 14 DTBA cells where each cell requires six girders to provide a stable platform for the magnets of the storage ring.

Since the DTBA cell consists of two mirrored halves only three different girders have to be designed (Fig. 1). The girders are 2240 mm, 2750 mm and 2870 mm long. All of them have a width of 750 mm. The beam height was set to 1.2 meters. For all three girders a 3-2-1 alignment system was developed where wedgemounts are being used.

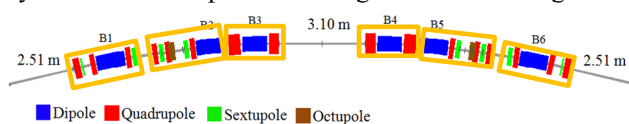


Figure 1: DTBA cell divided into girder sections.

The girder structure was developed focusing on low deformation and high vibration stability. Simulation software was used to design girders with less than 20  $\mu\text{m}$  deformation under full magnet load. Also, modal simulation

software was used to optimize the girder structure in terms of pushing the natural frequency as high as possible.

## GIRDER DESIGN

The designed girder structure is a box-type structure with a thick top plate and seven internal enforcement ribs (Fig. 2). The steel plates thicknesses are between 30 to 70 mm. There are three 80 mm thick support beams welded transversal to the top plate and they provide a basis for three vertical girder support points.

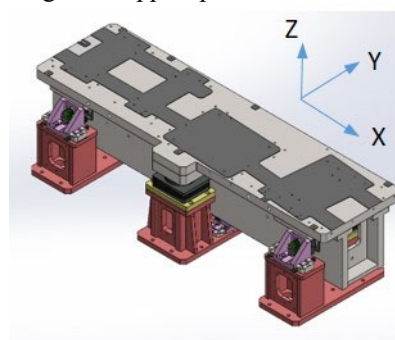


Figure 2: Girder system with three vertical support points.

The top plate of the girder requires high precision surfaces for the magnets. These surfaces as well as surfaces for fiducial marks will be machined with a flatness of 30  $\mu\text{m}$ .

The pedestals are the connection between girder and the ground/concrete floor. The pedestals carry the weight of the girder and magnets. They transfer vibration into the girder which is caused by the ground itself (low frequencies) or from machines such as water-/vacuum pumps, air conditions, etc. installed nearby. Therefore, it is planned to install a damping layer (e.g. epoxy concrete) between concrete floor and pedestal base plate to improve the vibration stability.

The pedestals carry not only the weight of the girder and magnets but also they accommodate the adjustment components for horizontal girder alignment. The material for the pedestals is the same as for the girder structure which is a structural steel S355JR (or A572 Grade 50). This steel shows a good strength, durability and weld ability. The pedestals as well as the girder structure are put together by full penetration welding (wherever its possible). The pedestal deformation was decreased by increasing the steel plate thickness at high load areas. Also, an exchangeable “height compensation plate” was added between pedestal and each vertical wedgemount in case of large floor settlement.

<sup>†</sup>utke@slri.or.th

# THE DESIGN AND PROTOTYPE TEST FOR THE TUNNEL FOUNDATION OF HIGH ENERGY PHOTON SOURCE

F. Yan<sup>1</sup>, G. Xu<sup>1†</sup>, G.P. Lin<sup>1</sup>, N.C. Zhou<sup>1</sup>, X.P. Jing<sup>1</sup>, J. Qiu<sup>1</sup>  
Y.L. Xing<sup>2</sup>, Z.G. Xu<sup>2</sup>, A.Z. Lu<sup>2</sup>, Y.S. Zhang<sup>2</sup>

<sup>1</sup>Key Laboratory of Particle Acceleration Physics and Technology, Institute of High Energy Physics (IHEP), Chinese Academy of Sciences 100049, Beijing, China

<sup>2</sup>China Electronic Engineering Design Institute (CEEDI), Beijing 100142, China

## Abstract

High Energy Photon Source (HEPS) is being built in China with challenging beam stability requirements. To fulfil the 25 nm ground motion restriction on the storage ring tunnel slab, two prototype slabs with different design schemes were constructed on the HEPS site. The first scheme adopted a 1 m reinforced concrete with replacement layer of a 1 m sand & stone underneath. The second scheme employed an extra 5 m grouting layer below the previously mentioned two layers. A series of tests had been carried out. The prototype slab with grouting layer is testified to have comparable vibration level with the bare ground, which is under 25 nm without traffic inside the HEPS campus, while the vibration level is amplified a lot on the other prototype slab. However, it is hard to make the grouting layer homogeneously under the kilometre-scale tunnel and besides the cost is unacceptable for 5 m grouting with such a large scale. The finalized design is fixed to be a 1 m reinforced concrete slab and 3 m replacement layer underneath using plain concrete. In this paper, the details of the prototype slab test results will be presented.

## INTRODUCTION

Currently, the low emittance storage ring has considered being future development direction of the photo sources. However, with the decreasing of the designed emittance of the ring, the problems caused by the ambient ground motion have been increasingly highlighted. High Energy Photon Source (HEPS) is a 6 GeV, 1.3 km, ultralow-emittance storage ring light source to be built in Beijing, China [1]. The designed natural emittance is about 35 pm [2]. To ensure the stability of the beam on experimental station, the RMS displacement integration of vibrations on the slab has to be kept smaller than 25 nm over frequency range of 1 Hz up to 100 Hz [3]. In order to fulfil this requirement, three more specifications are set up according to the ground motion level of HEPS site:

- 1) Ambient motions on the slab caused by internal and external vibration sources have to be smaller than 1 nm in all three directions;
- 2) No vibration amplification by the slab of the storage ring (RMS integral over frequency of 1-100Hz);
- 3) No vibration amplification by the pedestal-girder-magnet assembling.

The first one will be realized by setting regulation plan to the transportation inside the HEPS campus and taking damping measures for the vibration utilities. And the Egan

frequency of the pedestal-girder-magnet assembling is specified to be not smaller than 54 Hz for achieving amplification factor closing to one [3]. A well designed and made slab has no vibration magnification to the ground motions [4]. To construct such a slab and finalize the slab design, two prototype slabs with different design schemes were constructed on the HEPS site. The test results will be introduced in this paper.

## PROTOTYPE SLABS

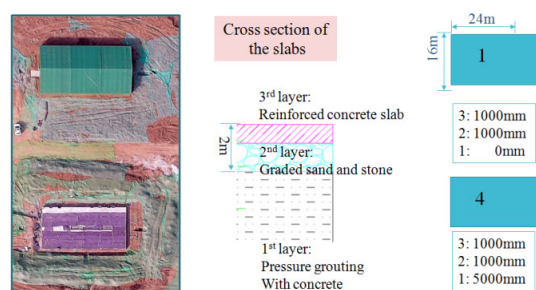


Figure 1: The schematic design of the two prototype slabs.



Figure 2: The prototype #4 slab: after grouting.

As shown in Fig. 1, the dimension of the prototype slab is 16×24 m. To construct slab #1, the soil from 2 m underground to the top were taken out and backfilled with one meter of "graded sand and stone" and one meter of "reinforced concrete slab". For the 2<sup>th</sup> slab (slab #4), there is an extra grouting layer from -2 m (underground) to -7m.

For constructing the grouting layer, as shown in Fig. 2, steel pipes (about 8 m long) were inserted in the ground using boring machine. The pipes are placed at the intervals of 1 m (0.8 m for the outermost two rows). There are some small holes regularly distributed on the pipe from depth of -2 m to -7 m. Mixture of cement and water were grouted through the pipe for reinforcement of the underground layer (-2 m to -7 m). The maintenance time for the grouting layer is ~28 days, all the other steps are the same with slab #1 hereafter.

† email address: xug@ihep.ac.cn

# RESEARCH OF BELLOW SHIELD STRUCTURE APPLIED TO BPM

X.J. Nie\*, L. Kang, R. Liu, S.K. Tian

Institute of High Energy Physics (IHEP) Accelerator Center, Dongguan, China

J.X. Chen, H.Y. He, L. Liu, C.J. Ning, A.X. Wang,

G.Y. Wang, J.B. Yu, Y.J. Yu, J.S. Zhang, D.H. Zhu

Institute of High Energy Physics (IHEP CSNS) China Spallation Neutron Source, Dongguan, China

## Abstract

The design of shield structure for bellow is an important content for the research of beam position monitor (BPM). The bellow shield structure consists of contact fingers and spring fingers. Several alternative schemes for bellow shield were achieved based on BPM detailed structure. The optimal scheme was achieved by the impedance simulation analysis with CST. The dimension of the contact finger was decided based on the length of BPM with the stress condition. The C-type string was manufactured, and the spring force was measured as well.

## INSTRUCTIONS

Beam position monitor (BPM) is an important diagnostic equipment of beam position. It is widely applied on accelerator. Normally, four electrodes are applied to get the beam signal and the beam position is calculated by the signal contrast. To decrease the effect of near equipment to BPM, the bellows are applied to the two ends of BPM [1, 2]. But they will lead to a discontinuous surface inside the vacuum chamber and thus the impedance will increase accordingly. So, it is necessary to design the shield structure to reduce the impedance of the bellows.

## DESIGN OF BELLOW SHIELD STRUCTURE FOR BPM

The shielding principle is stated as the following. Some mental wires or strips are used to contact the two ends of the bellows to form a smooth transition. This can eliminate the cavity structure inside the vacuum chamber, decrease the impedance and the HOM leakage [3, 4].

### Design of Shield Plan

According to some related references and the overall structure of BPM, several alternative shielding structures were achieved as Fig. 1. Model 1 was the C type shielding structure in which the C type string was used to press the contact fingers. Model 2 was the double fingers in which the contact fingers touch the vacuum chamber and spring fingers pressed on them. Model 3 had a simple structure which just had contact fingers to touch a cone-shaped sleeve. An insert block was used in model 4 to touch the spring finger, which could get a small step with big gaps. Model 5 had a net type shield structure to touch the vacuum chamber.

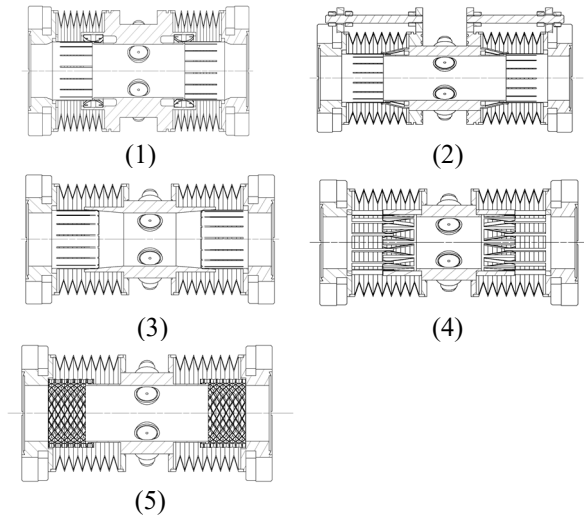


Figure 1: Shield plans of BPM bellow.

To understand the impedance characteristic for above shield structures, the simulation of impedance was done for them. The result showed as Figs. 2 and 3.

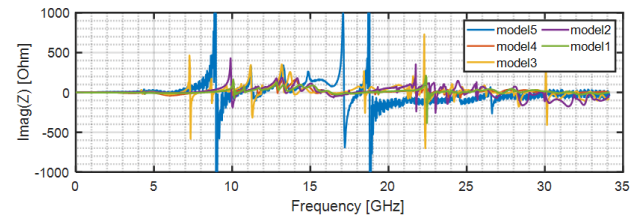


Figure 2: Imaginary part of impedance for the shield structures.

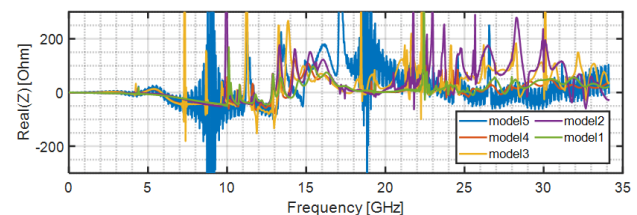


Figure 3: Real part of impedance for the shield structures.

It seemed that model 1 had the best impedance characteristic. So, the further study was focused on it. The main structure of the final shield plan showed as Fig. 4.

\* niexj@ihep.ac.cn

# PROCESSING OF HEPS LOW ENERGY TRANSPORT LINE COLLIMATOR\*

J. B. Yu<sup>1†</sup>, J. X. Chen<sup>1</sup>, H.Y. He<sup>1</sup>, L. Kang<sup>1</sup>, L. Liu<sup>1</sup>, R. H. Liu<sup>1</sup>, X. J. Nie<sup>1</sup>, C. J. Ning<sup>1</sup>, A. X. Wang<sup>1</sup>,  
G. Y. Wang<sup>1</sup>, Y. J. Yu<sup>1</sup>, J. S. Zhang<sup>1</sup>, D. H. Zhu<sup>1</sup>

Institute of High Energy Physics, Chinese Academy of Sciences, Beijing, China  
<sup>1</sup>also at Spallation Neutron Source Science Center, Dongguan, China

## Abstract

In order to protect the equipment such as BPM at low energy transport line (LB), a momentum collimator is designed with one movable absorber. This paper will show the mechanical design and manufacturing of the collimator.

## DESIGN OF THE LB MOMENTUM COLLIMATOR

HEPS is an ultra-low emittance synchrotron light source will be constructed in Beijing. Its injector consists of a 500MeV linac with a thermionic gun, a 500MeV low energy transport line, a full energy booster which ramping the beam energy from 500MeV to 6 GeV and two high energy transport lines [1]. LB is a transport line connecting the linac and the booster [2].

With the distance of 700mm away from the LBQ4, a momentum collimator with one movable absorber is designed to protect the downstream equipment, the layout is shown in Fig. 1.

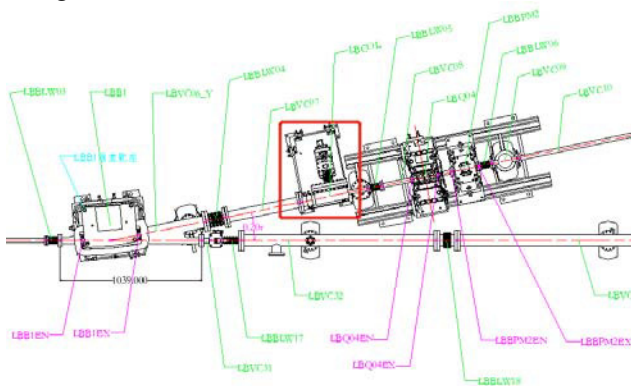


Figure 1: Position of the collimator at the LB layout.

According to the physical requirements, the absorber should be designed with the material of copper, and the profile is shown in Fig. 2, the maximum energy deposited on it is 20J. In order to make sure the thermal structure of the absorber, thermal analysis with different power deposition have been done, and the analysis results are shown in Fig. 3, the maximum temperature on the absorber is 134.5°C with the load of 20W, and the maximum temperature is 30.5°C when the load is 1W. Figure 4 shows the stress distribution of the absorber.

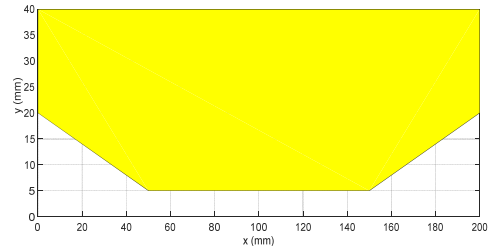
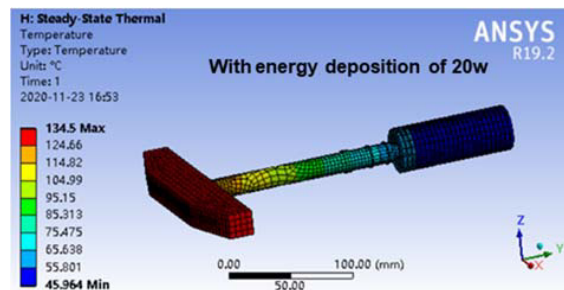
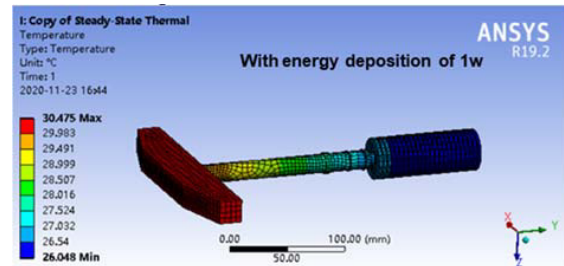


Figure 2: Profile of the absorber.



(a) Temperature distribution with 20W load



(b) Temperature distribution with 1W load

Figure 3: Temperature distribution of absorber component with different energy deposition.

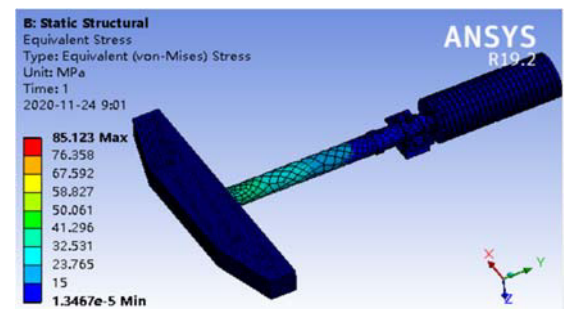


Figure 4: Stress distribution of absorber component with load of 20W.

The support structure of the absorber is designed far from the absorber and it is similar to cantilever structure, in order to ensure the straightness of the trajectory while

\*Work supported by Natural Science Foundation of Guangdong Province (No. 2018A030313959)

†email address yuib@ihep.ac.cn.

Content from this work may be used under the terms of the CC BY 3.0 licence (© 2021). Any distribution of this work must maintain attribution to the author(s), title of the work, publisher, and DOI

# DESIGN AND DEVELOPMENT OF THE ADVANCED DIFFRACTION AND SCATTERING BEAMLINES AT THE AUSTRALIAN SYNCHROTRON

B.J. McMahon<sup>†</sup>, J. Auckett, M. Fenwick, R. Hogan, J.A Kimpton, R. Lippi, S. Porsa  
 ANSTO, Australian Synchrotron, Melbourne, Australia

## Abstract

The Advanced Diffraction and Scattering (ADS) beamlines will provide high energy synchrotron X-rays for a variety of different diffraction- and imaging-based experiments at the Australian Synchrotron. A 4.5 T superconducting multipole wiggler will be used to provide X-rays in the range 50-150 keV, to two experimental endstations. The high power density of the beam requires significant thermal management through the whole beamline from the front end to the endstation. Flexible endstation designs have been developed to facilitate X-ray diffraction experiments on a range of sample types and environments (up to 300 kg). Detector positioning systems have been developed from industrial CNC robots to provide high speed, precise motion over large spatial envelopes.

## SOURCE & BEAM CONDITIONING

The SCMPW source for the beamline produces a beam with a central power density of 33 kW/mrad<sup>2</sup>, a total power of 45 kW and divergence of  $7 \times 1$  mrad<sup>2</sup>. The final beam size required in the beamline is  $0.3 \times 0.3$  mrad<sup>2</sup>. The heat load from reducing the beam size this amount was difficult to achieve in the storage ring for the compact front ends at the Australia Synchrotron.

Due to space constraints in the storage ring the beam conditioning was split between the front end and the beamline. Inside the front end a crotch absorber, mask and a diamond filter reduce the beam to  $0.85 \times 0.75$  mrad<sup>2</sup> and absorb 40 kW, as shown Fig. 1. Inside the beamline a secondary mask trims the beam to the final size of  $0.3 \times 0.3$  mrad<sup>2</sup> and a SiC filter absorbs another 0.8 kW of low energy photons. A summary of the beam conditioning is shown Table 1.

The front end mask was designed to absorb only the horizontal fan, to decrease the thermal strain and thereby increase the power absorption capability of the front end mask. A design consisting of  $2 \times 800$  mm flat cooled plates eliminates the need for an aperture throat and reduces the peak strain on the absorber. The mask absorbs a total power of 35 kW with a central power density up to 460 W/mm<sup>2</sup>. Figure 2 shows the layout of the mask and the thermal stress under a missteer event.



Figure 1: Front end and source in ADS beamlines.

<sup>†</sup> mcmahonb@ansto.gov.au

Table 1: Beam Conditioning in ADS Beamlines

Element	Divergence		Power	
	Vert. (mrad)	Horiz. (mrad)	Absorbed (kW)	Transmitted (kW)
Source	1	7	–	45
CA	0.85	6	2.5	42.5
FE Mask	0.85	0.75	35.4	7.1
Diamond Filter (1.2mm)	0.85	0.75	2.0	5.1
PDS Mask	0.3	0.3	3.5	1.6
SiC Filter (2mm)	0.3	0.3	0.8	0.8

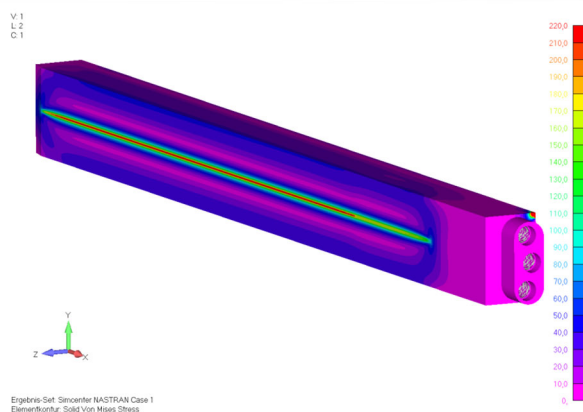


Figure 2: Front end mask (top showing assembly design, lower showing FEA of stress in beam missteer loading (22kW on one half of mask). Images courtesy of FMB-Berlin.

## ADS-1 BEAMLINE

The primary beamline, ADS-1, will provide white, pink and monochromatic beam (50-150 keV) to a large end-station located outside the main synchrotron building.

# INVESTIGATION OF THERMAL INSTABILITIES IN THE ALBA COOLING SYSTEM, BASED ON NUMERICAL SIMULATIONS AND EXPERIMENTAL MEASUREMENTS

F. Hernández<sup>†</sup>, Universitat Politècnica de Catalunya, Barcelona, Spain  
M. Quispe\*, E. Ayas, J.J. Casas, C. Colldelram, M.Ll. Fuentes, J. Iglesias  
ALBA – CELLS Synchrotron, Cerdanyola del Vallès, Spain

## Abstract

This paper presents an investigation into the thermal instability problems that currently affect the ALBA Cooling System. During these periods of instabilities, which occur for a few hours every week of operation, there are deviations up to +1.5 °C, concerning the nominal temperature of  $23 \pm 0.2$  °C in the four rings of ALBA: Service Area, Booster, Storage and Experimental Hall. This problem has a direct impact on the quality of the beam of the Accelerator. Previous studies have preliminarily concluded that the causes of this problem are due to (1) thermohydraulic anomalies in the operation of the external cogeneration plant, which supplies cold water to ALBA, and (2) cavitation problems in the pumping system (the water mass flow has been reduced to 67% of its nominal value to temporarily mitigate the cavitation). In order to confirm these hypotheses and propose solutions to the problem, an investigation has been developed making use of one-dimensional thermo-hydraulic simulations, performing Computational Fluid Dynamic (CFD) studies, statistical evaluations of data taken from our control system, and systematic flow measurements in critical areas, with ultrasonic flowmeters. As a result of this research, a set of solutions and recommendations are finally proposed to solve this problem.

## BACKGROUND

ALBA is a third-generation synchrotron light source facility located in Cerdanyola del Vallès, Spain, with more than eleven years of operation and eight operating beamlines. Over the last years, the water-cooling system of ALBA has been under thermal instability problems, which affect the control of the inlet temperature in its four main rings: Service Area (SA), Booster (BO), Storage (SR) and Experimental Hall (EH).

These anomalies appear during changes in the operating modes of the external cogeneration plant, called ST4, which supplies cold water to ALBA. An increment of the ST4 water temperature rises the in-tank temperature of D02, which is a high-capacity tank of 40 m<sup>3</sup> [1].

Otherwise, the volumetric flow circulating through the ALBA's circuit, where heat is exchanged with ST4, is reduced from the design value of 645 m<sup>3</sup>/h to 430 m<sup>3</sup>/h, to mitigate unexpected cavitation problems that affect the performance of the principal recirculation pump in ALBA, called P11. One possible cause of this cavitation

problem is an inappropriate sizing of the manifold located in the suction zone of the P11 pumps.

This is an utmost magnitude issue, insofar there is a direct linkage between the electron beam stability and the thermal stability of the water-cooling circuit. Moreover, this behaviour restricts ALBA's expansion capability in terms of machine current: whereas its design current is 400 mA, ALBA operates at 250 mA. Furthermore, this would affect the growth plan of ALBA II [2].

## ALBA'S THERMOHYDRAULIC CIRCUIT

The ALBA's thermohydraulic cooling system in nominal conditions is described in a simplified scheme in Fig. 1. The circuit begins with the hot deionized water returning from the machine headed to the P11 pump, which should move 645 m<sup>3</sup>/h at 26.8 °C after a filtering process. The water circulates through E01 heat exchangers, where heat is partially exchanged with the Cooling Towers. In real operation, all the flow circulates through E01B and steers to heat exchangers E07, where each exchanger takes 156 m<sup>3</sup>/h and transfers 1815 kW of heat to ST4 water, aiming to decrease the water temperature to 22 °C. After that, the water is stored in tank D02.

The circuit ends with the 3-way valve and the P7-P10 pumps, which allow the impulsion of the water from D02 to the machine. The function of the bidirectional tube is to maintain the hydraulic balance in the system.

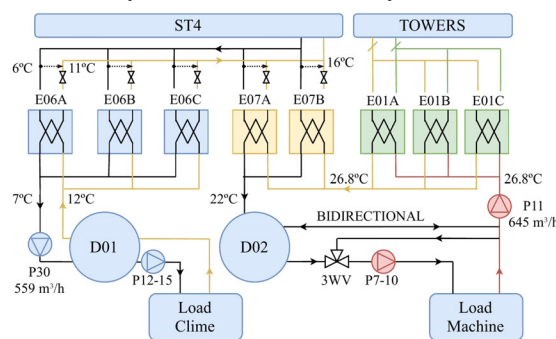


Figure 1: Simplified scheme of the ALBA's thermohydraulic cooling system.

The HVAC applications use water from the D01 tank employing P12-P15 pumps. The water from D01 is cooled with the E06 heat exchangers, each one taking 187 m<sup>3</sup>/h and transferring 1080 kW of heat to ST4 water. Once cooled, the flow returns to D01 circulating through the P30 pumps, which move 559 m<sup>3</sup>/h. Two-way mixing valves and differential pressure valves regulate the flow that circulates through E06 and E07 exchangers.

<sup>†</sup> fran.14hg@gmail.com  
\* mquispe@cells.es

# DESIGN OF MINIATURE WAVEGUIDES AND DIAMOND WINDOW ASSEMBLY FOR RF EXTRACTION AND VACUUM ISOLATION FOR THE CWA \*

B. Popovic<sup>†</sup>, S. Lee, E. Trakhtenberg, K. Suthar, A. Siy<sup>1</sup>,  
 G. J. Waldschmidt, S. Sorsher, A. Zholents, Argonne National Laboratory, Lemont, IL, USA  
<sup>1</sup>also at University of Wisconsin, Madison, WI, USA

## Abstract

This paper outlines the design of a diamond vacuum window and a millimeter wavelength (mmWave) waveguide assembly that will hold vacuum but still allow the mmWaves to propagate out of the structure for diagnosis and thermal management purposes. Currently under development at Argonne is a corrugated wakefield accelerator (CWA) that will operate at mmWave frequencies, with its fundamental mode of operation at 180 GHz and relatively high power levels up to 600 W. The fundamental mode needs to be extracted from the accelerator at approximately every 0.5 m to prevent the unwanted heating of the accelerator structure. Therefore, the structure is intentionally designed so this fundamental mode does not propagate further; instead it is transmitted through the waveguide assembly under vacuum and out via the vacuum window. As a result of the relatively high mmWave power densities, CVD diamond was chosen as the vacuum window material due to its low electromagnetic losses, mechanical strength, and superior thermophysical properties. Mechanically it is necessary to be able to hold the tight tolerances necessary for window performance at millimeter wavelengths. Other mechanical difficulties involve assembly of the window due to the CVD diamond material and preservation of ultra-high vacuum even if the integrity of the CVD diamond window is somehow compromised.

## INTRODUCTION

Under development at Argonne National Laboratory (ANL) is a miniature accelerator that utilizes Čerenkov radiation to generate an accelerating electromagnetic (EM) mode at 180 GHz. The structure facilitates this Čerenkov radiation due to its corrugated waveguide structure and high-charge electron bunches [1]. After the accelerating structure ends, it is necessary to extract this accelerating mode using a fundamental coupler. This coupler is designed to couple only to the accelerating mode and transport it out of the main section via four rectangular waveguides. These waveguides then transport the mode out via the vacuum windows to RF loads. The fundamental coupler is shown in Fig. 1, along with a portion of the accelerating structure.

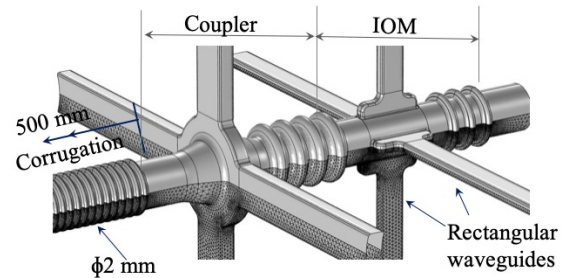


Figure 1: The corrugated waveguide and fundamental coupler followed by the IOM.

First and foremost, the vacuum window must perform adequately electromagnetically, with minimal losses and reflection of the extracted electromagnetic (EM) wave, thereby maximizing transmission out of the structure via the window. Any reflection off the window or its structure could return to the accelerator and disrupt its operation, potentially heating or, even worse, destabilizing the beam. Minimizing EM losses is vital since it is necessary to transport as much of the wave's energy as possible to a location outside of the accelerator vacuum where it can be properly cooled. The main basis of the design is the window material; specifically, chemical vapor deposition (CVD) diamond was chosen for its thermal and electrical properties. Currently CVD diamond windows are used extensively in mmWave gyrotrons operating at megawatt power levels [2, 3].

It is also necessary to keep in mind that this accelerator is operating at a much shorter wavelength than a typical accelerator, these mmWaves having a freespace wavelength of 1.7 mm at 180 GHz. Thus, all the design parameters that are on the EM side must have submillimeter tolerances to ensure EM performance. There are additional issues relating to machining finishes.

As mentioned previously, the outputs of the fundamental coupler are rectangular waveguides but for structural and vacuum reasons, windows at these frequencies are typically circular. A rectangular window is not as structurally strong and is more difficult to fabricate, more difficult to braze, and more prone to vacuum leaks in the corners. Thus, it is necessary to transition from a rectangular waveguide to a circular one, and then uptaper to a larger diameter waveguide. A larger diameter window is preferable for heating concerns along with ease of manufacturing and assembly, though it introduces more potentially disruptive resonances within the window itself.

\* This research used resources of the Advanced Photon Source, a U.S. Department of Energy (DOE) Office of Science User Facility and is based on work supported by Laboratory Directed Research and Development (LDRD) funding from Argonne National Laboratory, provided by the Director, Office of Science, of the U.S. DOE under Contract No. DE-AC02-06CH11357.

<sup>†</sup> bpopovic@anl.gov

# VACUUM ANALYSIS OF A CORRUGATED WAVEGUIDE WAKEFIELD ACCELERATOR

K. Suthar\*, E. Trakhtenberg, S. Sorsher, and A. Zholents  
 Argonne National Laboratory, Lemont, IL, USA

## Abstract

The vacuum level in a 2-mm-diameter, 0.5-m-long copper corrugated waveguide tube proposed for a compact high repetition rate wakefield accelerator has been investigated. The analytical calculations have been found to be in good agreement with the result of computer modeling using the finite element method. A representative experiment has been conducted using a smooth copper tube with the same inner diameter as the corrugated tube. The vacuum level calculated for this experiment agrees well with the measurement.

## INTRODUCTION

The sustainable operation of all accelerators requires high vacuum within the vacuum chamber [1], which is very challenging for the long tubular chamber with a small-diameter opening that is employed in a miniature collinear wakefield accelerator (CWA)—A-STAR—under development at Argonne National Laboratory. This accelerator uses a corrugated waveguide and sub-terahertz Čerenkov radiation produced by an electron bunch traveling longitudinally on the centerline of the waveguide [2].

This paper focuses on vacuum analysis of the accelerator. The 2-mm-inner-diameter, 0.517-m-long corrugated vacuum chamber of the accelerator module will be assembled from five 100-mm-long, thin-wall corrugated tubes. It will operate with 1-GeV, 10-nC electron bunches that will be coming to the accelerator with a 15-kHz repetition rate, producing Čerenkov radiation, inducing surface currents on the corrugation, and depositing about 800 W of heat distributed over the entire accelerator module [3]. As a result, the chamber will heat up from room temperature to ~50 °C [4]. The heat load increases along the length of the structure, causing a progressively higher thermal outgassing in the downstream direction. Additionally, an electroforming fabrication technique will be used to produce the corrugated waveguide [5]; therefore, due to hydrogen trapping [6], a higher outgassing rate is expected in the electroformed copper compared to the oxygen-free copper used in the accelerator applications.

While the accelerator chamber fabrication concept is still being developed [7], we performed a preliminary vacuum analysis using the chamber dimensions presented in [7] and report it here in the first section.

A major concern for the accelerator module fabrication is the integrity of the brazed joints between the adjacent corrugated waveguide sections. Therefore, we fabricated a 152-mm-long mock-up vacuum chamber containing three 2.1-mm-inner-diameter, 50-mm-long oxygen-free copper tubes without corrugation and measured vacuum in two

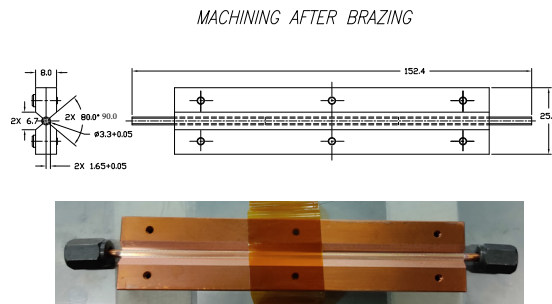


Figure 1: Test piece of the vacuum chamber showing dimensions (top) and the machined chamber (bottom).

setups: a) with these joints enclosed and brazed inside the copper block, and b) after machining the copper block to obtain a vacuum chamber profile. The machined chamber has a thin (<0.9-mm-thick) section exposed to atmospheric pressure, as seen in Fig. 1. The result of this experiment is reported in the second section.

## VACUUM CALCULATIONS

### Analytical Estimation

For vacuum calculations we modeled the corrugated waveguide as a smooth tube with an effective diameter  $d=2.26$  mm and an effective length  $\ell=0.95$  m that has the same surface area as a 2-mm-diameter, 0.517-m-long tube with corrugations. We calculated the tube's molecular flow using the engineering formula [8]

$$C(x) = 12.1 \frac{d^3}{x} \quad (1)$$

that defines the conductance  $C$  in liter/sec for a tube with an internal diameter  $d$  and length  $x$  in cm. Expecting pumping efficiency to be limited by the tube's conductance, and assuming use of pumps on both sides of the vacuum chamber, we obtained a result for the vacuum pressure as a function of the relative distance along the tube length  $\xi = x/\ell$ :

$$P(\xi) = \pi R \frac{\ell^2}{12.1 d^2} \xi(1 - \xi), \quad (2)$$

where  $R$  is the outgassing coefficient, and we ignore here a small variation of this coefficient with the temperature. Using  $R=3.6 \times 10^{-11} \frac{\text{torr L}}{\text{cm}^2 \text{ s}}$  for copper after backing [6, 9], we calculated the vacuum pressure at the center of the tube as  $P(1/2) \approx 1.5 \times 10^{-6}$  torr.

\* suthar@anl.gov

# HIGH-PRECISION SYNCHROTRON KAPPA DIFFRACTOMETER

G. Olea<sup>†</sup>, N. Huber, J. Zeeb, HUBER Diffraction GmbH & Co.KG, Rimsting, Germany

## Abstract

A new research product aiming to work in a 3rd generation synchrotron facility has been developed. Based on increased energy X-ray synchrotron radiation tool and well-known Kappa geometry, the product is expected that will investigate atomic and molecular structures of materials at nanoscale level using X-ray diffraction (XRD) technique. The Kappa Diffractometer (KDm) machine is maintaining the common structural principle of its family, but working with an extreme precision, which is far of the competition. The main body is consisting of a customized Kappa goniometer (KGm) device with vertical axis of rotation for high-precision sample (cryostat) manipulation, versatile detector arm (Da) for manipulating in horizontal plan different detectors (optics, slits, etc.) after X-ray beam is scattered and stable alignment base (Ab) for roughly adjusting the product towards the X-ray beam. In addition, a new XYZ cryo-carrier inside of the KGm is included for fine(submicron) sample adjustments. The kinematic, design and precision concepts applied, together with the obtained test results are all in detail presented.

## INTRODUCTION

Synchrotron radiation is one of the most powerful investigative tools available today for exploring internal structure of the matter. Last generation (4th) synchrotrons are being currently on the way to be built and several other (3<sup>rd</sup>generation) took a modernization process. However, advanced investigations are requiring not only new modern techniques [1], but dedicated instruments adapted to the specificity of the applications, as well.

Korean Pohang Accelerator Laboratory (PAL) research facility is managing the 3th generation accelerator, which was under an upgradation process (2009-2012). In the actual configuration (PLS II) it is including a portfolio of 40 beamlines [2] from which an appreciable number are dedicated to X-ray diffraction (XRD). 1C beam line is managed by Institute of Basic Science (IBS) being currently under the development. After its completion, it will investigate the properties of advanced functional materials lattices dynamics using time-resolved scattering technique (TR-XRS).

A growing interest is seen today to discover new materials with improved quantum features. A research centre at IBS (CALDES) is focusing on investigating such properties based on untapped potential of low-dimensional electronic materials [3]. An international request to develop a specific diffractometer has been launched [4] and attracted several proposals. In one of them [5], the intention was to use a four-circle diffractometer with Kappa geometry (horizontal), to provides a better access and large Bragg diffraction angles for preferred crystallographic orientations. However, after the proposal was accepted, based on a more detail analysis of required precision and load - sample and

specific instruments manipulation, it has been concluded that a new solution must be adopted to cope with all the specifications. The proposed diffractometer hoping to offer not only an improved manipulation capability, maintain at the same time the intrinsic advantages of the architecture, but an increased precision, as well.

The main features of the first product (prototype) are described below, including most important aspects related with kinematics, design and precision concepts.

## DIFFRACTOMETER

Generally, diffractometers have been conceived till now based on two type of architectures- Eulerian (E) and Kappa (K), respectively. These are deriving from the way a sample is manipulated; specifically, the working principle chosen for the manipulation mechanisms. There are several well-known companies producing both of such machines (HUBER, NEWPORT, KOHZU).

Euler Diffractometer (EDm) is using a combination of three orthogonal gonio (G) stages, forming Euler goniometer (EGm) device. It delivers high precision positions, able to carry instruments with appreciable weight and size because of its intrinsic high stiffness of the mechanism (closed loop). However, it is providing a limited access of X-ray (incident, scattered) to the sample, and to operator (setup, maintenance). On contrary, Kappa diffractometers (KDm) are based on an open loop angular device to manipulate the sample, called Kappa goniometer (KGm). By this, the access at the sample is almost entirely free. However, the precision of the manipulated load and size are limited, because of intrinsic flexible (open loop) working principle of the mechanism. A good overview of Kappa diffractometer capabilities is given in [6].

## Requirements

One of the express requirements for the new Kappa Diffractometer (KDm) was to manipulate a specific atmosphere & temperature-controlled instrument (cryostat) having a maximum - weight (20kg) and size (500mm) with highest possible accuracy (SoC<30 $\mu$ m). In addition, the orthogonality of the last rotation axis has to be less than a maximum value (20"). It should accommodate the use of several type of detectors - in-line and area, weighing a value of about (40kg) for related processes use. An overview of the most important motion parameters and their values for precision are included in Table 1.

Table 1: Motion Parameters (Sample)

Range (°/mm)	Acc. ("/ $\mu$ m)	Rep. ("/ $\mu$ m)	Res. ("/ $\mu$ m)
$\varphi=\kappa=\theta=\pm 180$	20	1	0.36
X,Y,Z= $\pm 5,5,3$	2,2,2	1	<1

# CRYOGENICS MONITORING AND CONTROL SYSTEM FOR EMBL FACILITIES AT PETRA III

Moises Bueno<sup>1</sup>, Liliana Kolwicz-Chodak, Jochen Meyer, Uwe Ristau and Stefan Fiedler<sup>2</sup>  
European Molecular Laboratory (EMBL), Hamburg, Germany

## Abstract

At the integrated facility for structural biology of the EMBL at PETRA III on the DESY campus in Hamburg, several devices require cryogenic cooling with liquid nitrogen (LN<sub>2</sub>). For the cryogenic devices local servers and clients have been created to monitor and operate the corresponding sensors, actuators and provide the safety logic. In addition, the local cryo-clients are integrated in a cryogenics supervision interface. The supervision client allows password protected access to three levels: monitoring, operator and expert. The monitoring level offers an overview of the status of all EMBL cryogenic sub-systems. At the higher access levels, cryogenic components can be also controlled. The application can be used from remote via a VPN connection or the TeamViewer software or a web client (in preparation). Because of the heterogeneity of the cryogenic devices different protocols for interfacing had to be applied.

## INTRODUCTION

Cryogenic installations and their controls are key components of the infrastructure for many large research facilities [1-3]. This is also valid for smaller size structural biology facilities like the EMBL beamlines at PETRA III on the DESY campus in Hamburg where EMBL is operating a small angle scattering beamline for proteins in solution and two macromolecular crystallography beamlines. Cryogenic cooling with liquid nitrogen (LN<sub>2</sub>) is needed for commercial or in-house built instruments like cryo-coolers to stabilize the temperature of the Double Crystal Monochromators (DCMs) under thermal load, cold gas stream units for cryo-protection of protein crystals during the different phases of an experiment and cryogenic sample dewars for robotic sample handling under LN<sub>2</sub>. In order to communicate with the controllers of each device, servers and clients based on the TINE control system (Three-fold Integrated Networking Environment) developed by DESY [4] and the LabVIEW software suite [5] have been created, that monitor and operate the corresponding sensors, actuators and provide the safety logic. Depending on the options offered by the different controllers, the servers had to be interfaced with several other communication protocols such as EtherCAT [6], ADS-OCX [7] and EPICS [8]. The wide variety of instruments that have to be monitored and controlled, with single clients for each element, distributed over several computers on different beamlines, called for centralizing

the cryogenic information. For every beamline and/or laboratory, a central client has been written and an overarching cryo-client in which all cryogenic devices are combined that are operated at the EMBL PETRA III facilities.

## MATERIAL AND METHODS

### Hardware Components

LN<sub>2</sub> is supplied by central storage tanks managed by DESY to all consumers in the Max-von-Laue Hall where also the EMBL beamlines are situated. The EMBL installations comprise (see Fig. 1):

- three cryo-coolers for the DCMs (from FMB Oxford) [9] of the P12, P13 (type D cryo-coolers) and P14 beamlines (type XV cryo-cooler);
- four cold gas stream units for cryo-crystallography, ('cryostream 800' series by Oxford Cryosystems [10]);
- three LN<sub>2</sub> sample storage dewars for robotic protein crystal mounting, the in-house built MARVIN systems [11] at the P13 and P14 beamlines respectively and for the automatic Crystal Direct Harvester (CDH) system [12].

Hardware:

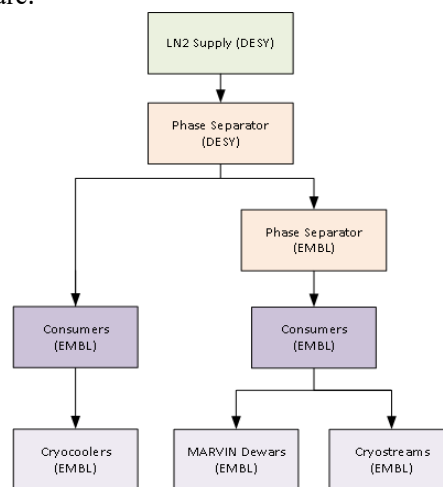


Figure 1: Cryogenics system: layered structure of hardware.

An additional 100 liter (Cryotherm [13]) phase separator has been installed on top of the macromolecular crystallography beamlines in sector-9 of the Max-von-Laue hall in order to achieve an efficient filling of the different LN<sub>2</sub> reservoirs (with exception of the ones for the DCM cryo-coolers).

The LN<sub>2</sub> consumers are connected by super insulated LN<sub>2</sub> transfer lines equipped with remotely controllable

<sup>1</sup>m.bueno@embl-hamburg.de

<sup>2</sup>stefan.fiedler@embl-hamburg.de

# ASSESSMENT OF THE CORROSION OF COPPER COMPONENTS IN THE WATER COOLING SYSTEM OF ALBA SYNCHROTRON LIGHT SOURCE; PRESENTATION OF A PROPOSAL TO MITTIGATE THE CORROSION RATE OF COPPER

M. Quispe<sup>†</sup>, E. Ayas, J.J. Casas, C. Colldelram, M.Ll. Fuentes, J.C. Giraldo, J. Iglesias, M. Pont  
ALBA – CELLS Synchrotron, Cerdanyola del Vallès, Spain  
J. Buxadera, M. Punset, Universitat Politècnica de Catalunya, Barcelona, Spain

## Abstract

This paper presents the most recent results on the corrosion of copper components in ALBA water cooling system. The studies have been carried out using a variety of techniques: Scanning Electron Microscopy (SEM), Energy-Dispersive X-Ray Spectroscopy (EDS) and X-Ray Diffraction (XRD).

Representative samples of the Accelerator Facility were examined: Storage Ring Absorbers, Front End Masks, Radio Frequency Cavity Pipes, Experimental Line Mask, Radio Frequency Plant Pipes at Service Area and Booster Quadrupole.

The studies show the presence of intergranular, pitting and generalized corrosion. The presence of Copper Oxide is confirmed, as well as other elements such as Aluminum, Carbon, Sulfur, Silver, Calcium, Silicon, Titanium and Iron in some regions of the samples. Likewise, other elements from circulating water such as Potassium and Chlorine have also been detected. The depth of pitting corrosion is less than 119.4  $\mu\text{m}$  for the samples studied, after 10 years of operation.

To minimize the corrosion problem, an upgrade of the ALBA cooling system is under study. The objective is to reduce the current corrosion rate by a conservative factor of 5. This change is possible by modifying the characteristics of the cooling water, reducing the dissolved oxygen content to values below 10 ppb and increasing the pH above 7.5. Technical aspects of this upgrade are discussed in this paper.

## BACKGROUND

The phenomenon of copper corrosion has been studied with special interest in the field of accelerators, due to its impact on the equipment life of the installation, and on the efficient and continuous operation of the deionized water cooling system. Specifically, corrosion can cause an increase in the pressure drop of the components and hydraulic interfaces, loss of thermal dissipation capacity, clogging in water cooling circuit resulting from the deposition of corrosion products, and in a worst scenario crack of the absorbers located inside the vacuum chambers.

At ALBA, after 10 years in operation, there are some indications may be attributed to corrosion, such as: (i) agglomeration of oxide particles in some small cavities of regulation valves that cause a localized decrease in water

flow and (ii) malfunction of flow switches due to accumulation of oxide particles in its orifice plate geometry. In order to understand and mitigate these effects, we are investigating the state of corrosion of copper components and planning preventive actions.

## THE ALBA WATER COOLING SYSTEM

By design, the ALBA cooling system is a hydraulic closed loop [1]. It consists of four main rings which feed the local consumption of the Service Area (SA), Booster (BO), Storage Ring (SR) and Experimental Area (EA) (see Fig. 1). The water is heated through all the rings and it is collected in a common return. The total water flow for the accelerator is approximately 525  $\text{m}^3/\text{h}$ .

By means of a reverse osmosis plant, the conductivity of water is controlled at 0.2  $\mu\text{S}/\text{cm}$ . The average values of pH and dissolved oxygen (DO) content are 7 and 6500 ppb, respectively, both properties are not actively controlled.

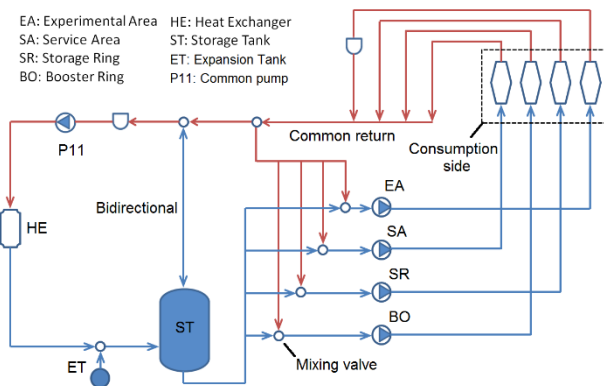


Figure 1: ALBA cooling system scheme.

## Antecedent: Irregular pH Evolution

The pH is one of the main parameters involved in copper corrosion. As a practical number, it is recommended to have the water with a pH above 7.5. In Fig. 2 the evolution of the pH in ALBA is represented for the last 9 years. According to this result, most of the time the average pH value has been 7, but irregular values of 5.5 to 6.5 are reported for the years 2013 and 2014. Very high pH values (between 8 and 8.5) have also been found during the year 2012. It is assumed as a hypothesis that the pH data in the first years have been affected by problems in the instrumentation.

<sup>†</sup>mquispe@cells.es

# FABRICATION OF THE TRANSITION SECTION OF A CORRUGATED WAKEFIELD ACCELERATOR VIA LASER MICROMACHINING\*

P. Bado†, M. A. Dugan, and A. A. Said, Translume, Inc., Ann Arbor, MI, 48108, USA  
S. Siy, K. Suthar, A. Zholents, Argonne National Laboratory, Lemont, IL, 60439, USA

## Abstract

A wakefield accelerating structure is being designed to facilitate sub-terahertz Čerenkov radiation. This accelerating structure consists of several sections of internally corrugated tubes, that are coupled together using transition sections. The fabrication of these transition sections is presented. Modelling of various fabrication errors was undertaken to understand their effect and to determine fabrication tolerances. Source of machining imperfections are reviewed and their impact compared to the modelling results.

## INTRODUCTION

A cylindrical, corrugated wakefield accelerating (CWA) structure [1] is being developed to create sub-terahertz Čerenkov radiation produced by an electron bunch. The accelerating structure consists of several copper-based, 50-cm long, sections of internally corrugated tubes with a 1-mm inner-radius. These elements are coupled together using ultra-compact transition sections, as shown in Fig. 1, which are also copper-based.

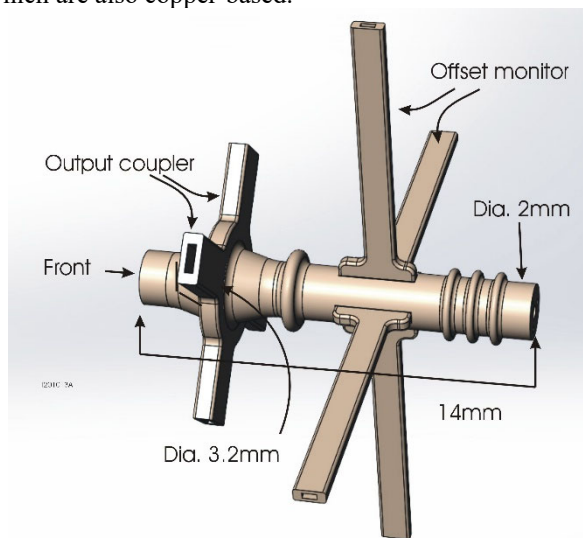


Figure 1: Model of the inner volume of a transition section, with main dimensions.

Beside their mechanical and vacuum coupling functions, these transition sections provide a means to monitor the centering of the electron bunch, and to couple out unused energy in the TM01 accelerating mode from the corrugated

waveguide while allowing the TE11 transverse mode to pass through. The output coupler is expected to extract on the order of a kilowatt of power.

## FABRICATION APPROACH

The fabrication is divided into four main steps: First, a fused silica glass mandrel is fabricated. Its external shape corresponds to the internal volume of the transition section. Second, a thin layer of Gold is sputtered onto the surface of this glass mandrel, and subsequently a thick copper layer is electro-deposited on top of the gold. Third, the glass mandrel that is at the core of this assembly is etched away, leaving a hollowed copper shell with the desired internal geometry; and finally secondary machining operations, such as milling and drilling, generate the external end faces and other reference surfaces required for the integration of the transition section into the general CWA structure.

The first step – the fabrication of the sacrificial fused silica glass mandrel- is based on a sequential combination of laser irradiation and chemical etching [2], as illustrated in Fig. 2. Shape-contouring is introduced by illuminating a defined pattern with a laser generating ultrashort pulses. The pulse energy is set sufficiently low to avoid ablation, yet high enough to locally modify the short-range ordered fused silica molecular matrix.

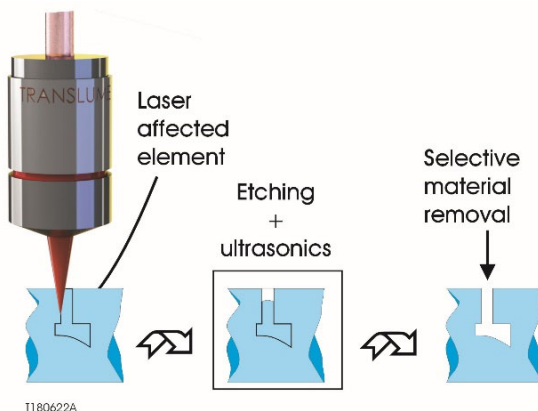


Figure 2: The two-step glass shaping process - Laser direct write, followed by selective etching.

With the proper processing parameters, the laser-exposed volume elements (*i.e.* voxels) etching susceptibility is greatly increased. This localized enhanced etching is used to shape the desired glass part geometry. One of the key metrics associated with this part of the fabrication process is the ratio of the etching rate of the laser-exposed voxels versus the etching rate of the virgin fused silica glass. Under optimized conditions this etching ratio can exceed 100:1, but it degrades rapidly with the depth of the laser processing.

\* This manuscript is based upon work supported by the Director, Office of Science, Office of Basic Energy Sciences, of the U.S. Department of Energy under Contract No. DE-AC02-06CH11357; and by the Office of Science, SC-1, U.S. Department of Energy under Award No. DE-SC0019677.

† pbado@translume.com

# STUDY OF COPPER MICROSTRUCTURE PRODUCED BY ELECTROFORMING FOR THE 180-GHz FREQUENCY CORRUGATED WAVEGUIDE\*

K. Suthar<sup>†</sup>, G. Navrotski, P. Carriere<sup>1</sup>, and A. Zholents  
Argonne National Laboratory, Lemont, IL, USA  
<sup>1</sup>RadiaBeam Inc., Santa Monica, CA, USA

## Abstract

Fabrication of the corrugated structure that generates a field gradient of  $100 \text{ MV m}^{-1}$  at 180 GHz is a challenge, requiring unconventional manufacturing methods. The corrugated waveguide with 2-mm-inner-diameter will be produced by electroplating copper on the aluminum mandrel as proposed in [1]. A thin seed layer is usually applied to achieve uniform wetting of the plated copper on the aluminum mandrel. The copper waveguide is retrieved by removing the mandrel. Uniform copper plating and etching of the aluminum are crucial steps to keep the surface uniformly smooth and free of impurities that are especially necessary for the vacuum RF application. Previous studies suggest that electroplated copper has variations in both electrical and mechanical properties compared with those of bulk copper from batch production. In this paper we discuss the copper microstructure produced by the electroforming method and a literature study on variations, which can be attributed to disparity in the crystalline grain structure of the plated material.

## INTRODUCTION

A 0.5-m-long, 1 mm internal radius, miniature cylindrical corrugated waveguide accelerator (CWA) is being proposed [2] and designed to create sub-terahertz Čerenkov radiation produced by an electron bunch traveling longitudinally on the centerline of the corrugated waveguide [1]. The dimensions of the corrugated structure are shown in Fig. 1. While the RF design [3] and prototype fabrication efforts are under development [4], we are investigating the limits of operating conditions based on the heat transfer and mechanical robustness of the structure during operation via fully coupled multiphysics finite element analyses.

The corrugated structure operates at 180 GHz with a transformer ratio of 5 that can deposit about 600 W of heat load at 10 kHz repetition rate on the inner surface of the corrugation and the transition section. The RF-heat-load deposition increases along the length of the structure producing a temperature gradient that can generate progressively higher thermal expansion in the downstream direction. Estima-

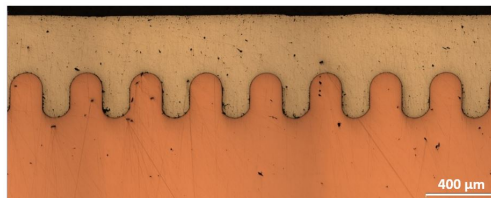


Figure 1: A micrograph of a section of the copper corrugated waveguide on an aluminum forming mandrel.

tion of unavoidable fabrication errors and the differential dimensional changes due to thermal expansion are crucial for achieving the required performance from the corrugated waveguide. The resulting thermal stress from the differential thermal expansion can lead to tensile-yield failure. Such failure can generate arcing due to surface cracking that ultimately causes loss of the beam. Operating parameters, such as energy and repetition rate, are the deciding factors for how much energy and how fast heat will be deposited on the structure. Therefore, fabrication acceptance criteria are also critical in reducing the beam instabilities that are potentially caused by fabrication errors. To quantify such behavior and to evaluate the mitigation scheme in the high-frequency structure, we are investigating the thermal budget for the structure via careful and detailed finite element analyses [1].

## ANALYSIS

### The Geometry

The corrugated waveguide geometry is shown in Fig. 1, and further details can be found in [4]. The CWA length with the corrugated waveguide is 0.5 m.

Table 1: Dimensions of Corrugation

Dimension	Value
$a$ - Waveguide inner radius)	1 mm
$d$ - Corrugation depth	263 $\mu\text{m}$
$t$ - Corrugation tooth width	160 $\mu\text{m}$
$v$ - Corrugation spacing	340 $\mu\text{m}$
$r$ - Corrugation corner radius	80 $\mu\text{m}$

### Fabrication Considerations

The corrugated waveguide is produced by electroplating copper on an aluminum mandrel. A thin seed layer of copper, measuring  $2.0 \pm 0.5 \mu\text{m}$  in thickness is usually applied

\* This research used resources of the Advanced Photon Source, a U.S. Department of Energy (DOE) Office of Science User Facility and is based on work supported by Laboratory Directed Research and Development (LDRD) funding from Argonne National Laboratory, provided by the Director, Office of Science, of the U.S. DOE under Contract No. DE-AC02-06CH11357.

<sup>†</sup> suthar@anl.gov

# BRINGING THE GROUND UP (WHEN IS TWO LESS THAN ONE?)

A. A. Khan, C. A. Preissner, Argonne National Laboratory, Lemont, Illinois, USA

## Abstract

The Advanced Photon Source Upgrade (APSU) project has employed the use of high-heat-load dual-mirror systems in the new feature beamlines being built. Due to the shallow operating angles of the mirrors at a particular beamline, XPCS, the two mirrors needed to be approximately 2.5 m apart to create a distinct offset. Two separate mirror tanks are used for this system. However, it is unclear if the vibrational performance of these tanks would be better if they were both mounted on one large plinth or each mounted on a small plinth. Using accelerometers at the installation location, the floor vibrations were measured. The resulting frequency response function was then imported into a finite element analysis software to generate a harmonic response analysis. The two different plinth schemes were modeled, and the floor vibration was introduced as an excitation to the analysis. The relative pitch angle ( $\theta_Y$ ) between the mirrors was evaluated as well as the relative gap between the mirrors ( $X_{MAG}$ ). Results showed that a single plinth reduces the relative  $X_{MAG}$  (RMS) compared to two plinths by approximately 25%. However, the relative  $\theta_Y$  (RMS), which is arguably more critical, is significantly lower by approximately 99.7% in two plinths when compared to a single plinth. Therefore, it is more effective to use two separate plinths over a longer distance as opposed to a single longer granite plinth.

## INTRODUCTION

Floor and support vibrations can introduce unwanted motion in a beamline. Optics, such as mirrors, are especially sensitive to these vibrations as they operate at small angles. Small variations in the angle can propagate into large errors over a distance of several meters. Therefore, it is important to design support structures that minimize these vibrations.

In the case of the XPCS beamline at APSU, the high-heat-load dual-mirror system operates at a shallow angle, and to create a distinct offset, the mirrors must be separated by 2.5 m along the beam direction. The question arose whether having the mirror tanks share one large granite plinth as a base would be better to minimize vibrations or would it be better to use two smaller granite plinths, one for each mirror tank.

### Definition of Parameters

Two important parameters affect the beam position and energy range. To better illustrate, a top-down view of the mirrors is shown in Fig. 1.



Figure 1: Top-down view of mirrors showing  $0^\circ$  angle with respect to the beam (dotted line). Beam travels left to right. The first mirror is called M1 and the second mirror is M2.

The first parameter of interest is the relative gap between the mirrors ( $X_{MAG}$ ).  $X_{MAG}$  can affect the offset beam position downstream of the mirror system as it may cause the beam to wander along the X direction. Ideally the  $X_{MAG}$  should be zero.

Using the absolute motion of each mirror as shown in Fig. 2, the relative gap can be calculated:

$$X_{MAG} = X_1 - X_2 .$$



Figure 2: Top-down view of the mirror system showing absolute motion of each mirror with respect to the beam in the X direction.

The second parameter of interest is the relative pitch angle between the mirrors ( $\theta_Y$ ). The relative pitch angle is more critical as it can affect the energy range of the beam passing through the mirror system as well as reduce its effectiveness at absorbing high heat load from the white beam. Ideally  $\theta_Y$  should be zero.

Using the absolute pitch angle of each mirror as shown in Fig. 3, the relative pitch angle can be calculated:

$$\theta_Y = \theta_1 - \theta_2 .$$

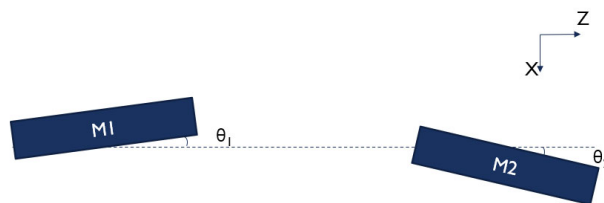


Figure 3: Top-down view of the mirror system showing the absolute pitch angle of each mirror with respect to the beam. Pitch angle is considered rotation about the Y axis coming out of the page.

# A REVIEW OF ULTRASONIC ADDITIVE MANUFACTURING FOR PARTICLE ACCELERATOR APPLICATIONS

J. Brandt\*, Enrico Fermi Institute - University of Chicago, Chicago, IL 60637, USA

## Abstract

Additive manufacturing (AM) technologies have been used for prototyping and production parts in many industries. However, due to process limitations and the unknown material properties of AM parts, there has been limited adoption of the technology in accelerator and light-source facilities.

Ultrasonic Additive Manufacturing (UAM) is a hybrid additive-subtractive manufacturing process that uses a solid-state ultrasonic bonding mechanism attached to a CNC mill to join and machine metal parts in a layer-by-layer manner. The solid-state and hybrid nature of UAM ensures base material properties are retained and mitigates process limitations which traditionally inhibit integration of parts produced by other AM processes.

This paper presents a review of the UAM process and its potential application to accelerator and beamline needs. Several specific areas are discussed including: replacement of traditional manufacturing approaches, such as explosion bonding to join dissimilar metals; improved internal cooling channel fabrication for thermal management; and imbedding of electronics and materials for more accurate remote sensing and radiation shielding.

## INTRODUCTION

Components used in accelerators and beamlines operate in demanding environments which often require specialized and difficult fabrication processes to manufacture. Ultra-high vacuum (UHV) chambers may require explosion welding and beam stops and collimators utilize electrical discharge machining (EDM), both of which can be time consuming, costly, and are limited in their application.

As a hybrid, additive-subtractive manufacturing process, ultrasonic additive manufacturing (UAM) possesses unique capabilities which could make explosion welding or EDM options instead of necessities. The solid-state additive welding stage operates well below the melting temperature of the substrate materials, which ensures bulk material properties are largely retained.

Subtractive machining is completed by a computerized numerical control (CNC) mill to which the ultrasonic transducer and sonotrode are also mounted. This allows for both three and five-axis milling operations of complex geometries and retains the tolerances, surface finish, stability, and repeatability inherent to milling processes. In turn, parts printed using UAM can be more rapidly integrated without the need for time-consuming and costly post-processing operations that can include finish machining and surface finishing. A schematic depiction of both additive and subtractive stages of UAM is shown in Fig. 1.

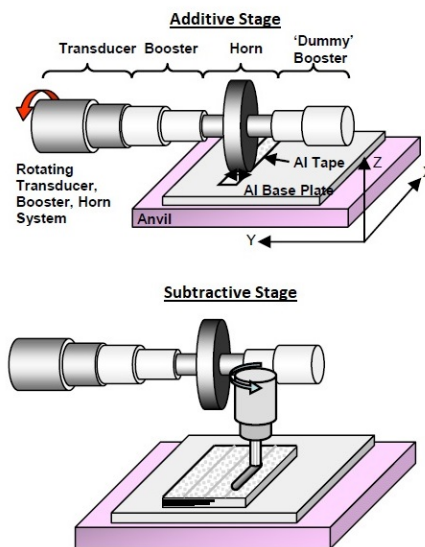


Figure 1: UAM process schematic showing additive and subtractive stages [1].

## APPLICATIONS FOR ACCELERATORS

Accelerator facility adoption of parts printed with other metal additive manufacturing (AM) processes like selective laser melting (SLM), or electron beam melting (EBM) has been slow in part due to the uncertainty of printed parts' material properties. However, with the advantages of UAM, more rapid adoption of metal AM parts could occur for certain application areas.

### Dissimilar Metal Welding

Bi-metallic joints are widely used for accelerator vacuum systems, thermal management components, and instrument feedthroughs with explosion welding serving as a common method of fabrication. Explosion welded joints are formed when a controlled explosion shockwave accelerates one material of the joint into the other [2]. The process is limited to simplistic geometries, which in turn limits the parts that can be fabricated.

The mechanisms for successful bonding during the UAM process are similar and generally believed to be shear deformation, inter-diffusion, and sometimes mechanical interlocking. The applied normal force from the sonotrode head compresses the foils ensuring good contact of the asperities which are subsequently sheared by the ultrasonic oscillations. Both the down force and ultrasonic oscillations also contribute to plastic flow of the material and breakdown and redistribution of surface oxide layers and impurities to promote a clean mating surface for solid joints [3]. Figure 2 shows several UAM welded dissimilar metal interfaces with varying bond topographies.

\*brandtj@uchicago.edu

# UTILIZING ADDITIVE MANUFACTURING TO CREATE PROTOTYPE AND FUNCTIONAL BEAMLINE INSTRUMENTATION AND SUPPORT COMPONENTS

D. Jensen<sup>†</sup>, Argonne National Laboratory, Lemont, Illinois, USA

## Abstract

The world of beamline science is often fast-paced and dynamic. One of the major challenges in this environment is to be able to design, manufacture and then implement new items for use on the beamlines in a fast and accurate manner. Many times, this involves iterating the design to address unknown or new variables which were not present at the beginning of the project planning task. Through the use of additive manufacturing, I have been able to support the user programs of various (APS) Advanced Photon Source beamlines\* across multiple scientific disciplines. I will provide a few detailed examples of Items that were created for specific beamline applications and discuss what benefits they provided to the pertinent project. I will also talk about why choosing consumer-level printer options to produce the parts has been the direction I went and the pros and cons of this decision. Primarily, this choice allowed for quicker turnaround times and the ability to make more frequent changes in an efficient manner. Currently, we are utilizing only the fused deposition modelling (FDM) type printers but I am exploring the addition of UV-activated resin printing, exotic materials that can be utilized using the current toolset, and the possibility of commercial metal printing systems. This technology has been a game-changer for the implementation of new support items and instrumentation over the last couple of years for the different disciplines I am supporting. I will discuss how the roadmap ahead and what the evolving technologies could potentially allow us to do.

## INTRODUCTION

The Advanced Photon Source (APS) located at Argonne National Laboratory (ANL) has many user programs. In my daily function I am supporting a variety of these groups. Time is something that is very limited and budgetary constraints are always in the backs of our minds. With the adoption of Additive manufacturing (AM) I have been able to provide a cost effective and timely way in which to produce instrumentation and beamline support components. The approach I have taken is to utilize a consumer-grade machine, which allows me to support the devices, and run it at very low cost without the need for lengthy licensing agreements.

## EXAMPLES OF USE CASES

Use case example one, as shown in Fig. 1, is a collimator holder for use on the 11-ID-D beam line at the APS. This is a Time Resolved Research (TRR) Group [1] Project. The scientist approached me as the existing holder was not

functioning in a manner that was still optimal. The experiment was going to be happening in the following week. The task was design and print a holder for the collimator. Using Fused deposition modelling (FDM) I was able to produce the part from a 3d CAD model to finished fixture in about 3 days. Average turn around for an item such as this is around 2 to 4 weeks utilizing a traditional manufacturing route. There was also issues as the current collimator had taken on a non-cylindrical shape on the outer surface from the normal use by the staff over the years. The benefit of a printed part was I could then install the collimator in a semi clamped manner and hone it into a good fit using the rough surface of the outer diameter of the collimator. The fact that I could turn this around in about 3 days with a material cost of around ten Us Dollars (USD) was a huge benefit. It was also found that the stability was good enough that we did not see the immediate need to move forward with a traditionally manufactured setup.

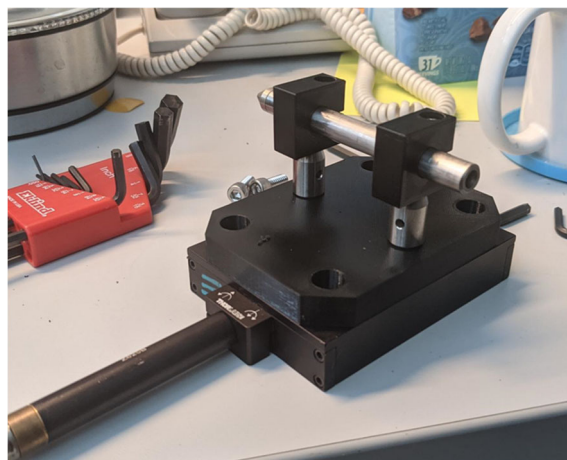


Figure 1: Collimator Mounting setup 11-ID-D.

Use case example two, as shown in Fig. 2, is a flight path to keep the beam scatter coming off the sample and directed to the detector in a vacuum or gas environment. The set up was done for 6-ID-B for the Magnetic Materials (MM) Group [2], the item was originally quoted at twelve hundred USD and a 8 to 12 week lead time through a tradition manufacturing method. The Support staff at this beamline approached me and asked if it would be possible to create this using AM. We decided it was worth a try. The challenge on this is that it is about a meter long. The limitations of the tools I have at my disposal are about 9 inches of print height in the vertical. What this led me to do was to break the piece up into multiple segments and then epoxy them together. I used key features to help with alignment and the 5-minute epoxy which is readily available created the equivalent of a plastic seam weld. The total cost material wise was around fifteen to twenty dollars out

<sup>†</sup> dpjensen@anl.gov

# DESIGN AND DEVELOPMENT OF AI AUGMENTED ROBOT FOR SURVEILLANCE OF HIGH RADIATION FACILITIES

K. Suthar\*, M. White

Argonne National Laboratory, Lemont, IL, USA

A. Suthar<sup>1</sup>, S. Suthar<sup>1</sup>, G. Mistri, mySTEMbuddy Robotics, Naperville, IL, USA

<sup>1</sup>also at Neuqua Valley High School, Naperville, IL, USA

## Abstract

Scientific instruments and utility equipment at high-radiation facilities such as the Advanced Photon Source at Argonne National Laboratory are often challenging to monitor during actual operation. To help augment monitoring capabilities, we are developing an instrumented robot that uses artificial intelligence (AI) to create a thermal and spatial 3D map of its surroundings. The robot can be self-driven or controlled remotely. The robotic vehicle—whose overall dimensions are 50 cm in length, 20 cm in width, and 20 cm in height—carries a depth perception camera to guide itself on a predetermined path; an IR camera for thermal imaging; dosimeters to measure stray radiation; and a cluster of other sensors to assist in communications and navigation, as well as measuring noise, vibration, temperature, and humidity of the surrounding space. This inexpensive robot is operated and controlled by NVIDIA’s Jetson Nano™ development board, one brushless DC motor, and one servomotor that controls the movement of the robot. All control and data acquisition programs are written in Python for ease of integration with institution-specific operating systems such as EPICS. The AI robot was trained using machine learning followed by the application of a trained algorithm for navigation. This paper discusses our preliminary development of the robot.

## INTRODUCTION

Synchrotron radiation facilities such as the Advanced Photon Source, and nuclear radiation facilities—e.g., nuclear power plants, isotope fabrication plants, and nuclear material handling plants—often require continuous monitoring to ensure the safety of radiation workers, existing infrastructure, and the environment [1]. The existing practice for radiological monitoring uses static devices during operation or intervention using human operators. These methods are often costly, time-consuming, and challenging when intervention is necessary or unavoidable. In a radiation facility, the radiation decay and heat immediately after a shutdown due to routine maintenance or due to failure needs to be quantified quickly [2]. To assess the damage or contain/collect contamination is very difficult if human intervention is required [3]. In all such events, a robotic system can be beneficial to assess the condition of the instruments, collect any samples, and monitor the radiation [4]. Moreover, due to recent developments in robotics and artificial intelligence, it

is easier to develop a robotic system that can be utilized for this purpose.

The challenge of monitoring scientific instruments in radiation facilities can be solved through this self-guided robot. Equipped with various sensors and artificial intelligence, the robot can successfully and autonomously navigate through facilities while acquiring thermal environmental data and images essential to monitoring scientific instruments, equipment, and the environment. The lead case around the robot protects its various electronic components from damage while navigating through a facility.

In this paper, we discuss our preliminary design of an AI-driven autonomous robot. The robot uses a ready-made radio-controlled car chassis that is equipped with an open-source software platform called Donkey Car [5] installed on a NVIDIA Jetson Nano board [6]. The robot was manually trained on a convoluted path using machine learning [7] and used its very own AI algorithm to select parameters to control the brushless DC motor and servomotor with help from processing the images that it acquired during its travels. The FLIR Lepton camera [8] was used to identify temperature anomalies in the acquired thermal images/video. The robot was trained to identify its travel boundaries via blue tape placed on the floor.

## ROBOT DESIGN

The current design of the robot is a WiFi operated, front-wheel controlled, all-wheel-drive vehicle, as shown in Fig. 1. The textured wheels grip smooth surfaces and prove efficient traction over various other types of surfaces. The 3D-printed outer shell combined with lead plates protects the internal hardware from becoming damaged in high radiation conditions. The internal mounting structure allows for seamless cable management through routing slots between the NVIDIA Jetson Nano™ and the motor controller. The slightly raised structure provides room for the batteries needed by the NVIDIA Jetson Nano™, the FLIR Lepton camera, the Intel RealSense camera, and the motors. The Intel RealSense mount maintains a consistent view of the robot’s surroundings, while the FLIR Lepton mount is strategically raised to procure more useful thermography. The on-board NVIDIA Jetson Nano™ acquires images and sensor data to control the robot. The robot can also be remotely controlled using SSH to acquire the navigation panel and access the robot’s camera view. A brushless motor is used as a drive, while a servomotor attached to an Ackerman’s steering trapezium is used for turning the vehicle. The controlling

\* suthar@anl.gov

# PROGRESS OF NANO-POSITIONING DESIGN FOR THE COHERENT SURFACE SCATTERING IMAGING INSTRUMENT

J.W.J. Anton<sup>†</sup>, M. Chu, Z. Jiang, S. Narayanan, D. Shu, J. Strzalka, J. Wang  
 Advanced Photon Source, Argonne National Laboratory, Lemont, IL 60439, USA

## Abstract

As part of the Advanced Photon Source Upgrade (APS-U) project, the Coherent Surface Scattering Imaging (CSSI) [1] instrument is currently being developed. One of the most important components of the CSSI instrument at the 9-ID beamline of the APS-U, the Kirkpatrick-Baez (K-B) mirror system, will focus hard X-rays to a diffraction-limited size of 500 nanometers at a working distance of 550 mm. High angular stability (19 nrad for the horizontal mirror and 14 nrad for the vertical mirror) is specified not just for the focused beamsizes but, more importantly, to ensure the beam stability at the detector position that is up to 24 m from the K-B mirrors. A large sample-to-detector distance (up to 23 m), one of the beamline's unique features for achieving a sufficient coherent-imaging spatial oversampling, requires sample angular stability of 50 nrad. In CSSI scattering geometry, the vertically placed sample reflects X-rays in the horizontal direction at an extremely shallow angle. The design includes two high-precision rotary stages for sample pitch (vertical axis) and yaw (horizontal axis). The current design of instrument's nano-positioning stages [2] and metrology required to satisfy the stability and positioning requirements are discussed in this paper.

## INTRODUCTION

### Motivation

The instrument will use coherent X-ray scattering for non-destructive, in-situ structure characterization with high three-dimensional resolution and high temporal resolution. This will allow for the investigation of self-assembly of mesoscale structures at surfaces at interfaces, as well as three-dimensional surface nano-patterning and nano-fabrication.

Large Sample to detector distance (up to 23m) is needed to achieve speckle oversampling. Figure 1 shows a schematic of the instrument, K-B mirrors, and the detector. The X-ray beam is shown in red and the horizontally scattered beam as it travels to the detector is in orange.

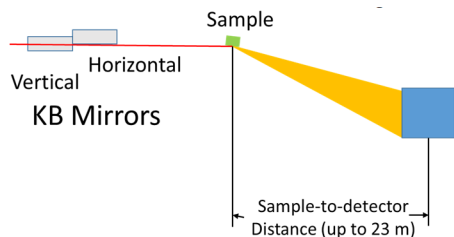


Figure 1: Instrument schematic: Not to scale.

Samples must be scanned with five (5) degrees of freedom (3 linear directions and 2 rotary directions: sample pitch and sample yaw [axis normal to sample surface]).

### Technical Approach

To meet the stability and positioning requirements the design makes use of precision commercial stages, custom weak-link laminar flexure stages, and a metrology systems.

Weak-link laminar flexures are used to overcome limitations of ball-/cross-roller bearing stages. Resulting in minimal motion error and high repeatability of motion [2].

Four (4) different metrology frames using capacitive sensors and laser interferometers to achieve positioning and stability requirements. The KB mirror nanopositioning stages measured by a metrology frame with four (4) laser interferometers. The sample nanopositioning stages have three (3) metrology frames. One (1) capacitive sensor based metrology for both rotation scanning stages. The other frame with both capacitive sensors and laser interferometers is used to measure linear scanning stage motion errors.

## INSTRUMENT LAYOUT

The CSSI Instrument consists of five (5) major components as shown in Fig. 2:

- Granite air-bearing stages for aligning K-B mirrors and sample to the Beam
- Ultra-high Vacuum Chambers for K-B mirrors
- High vacuum chamber for samples
- Kirkpatrick-Baez mirrors with alignment apparatuses and laser interferometer metrology.
- Sample nanopositioning stages and metrology frames

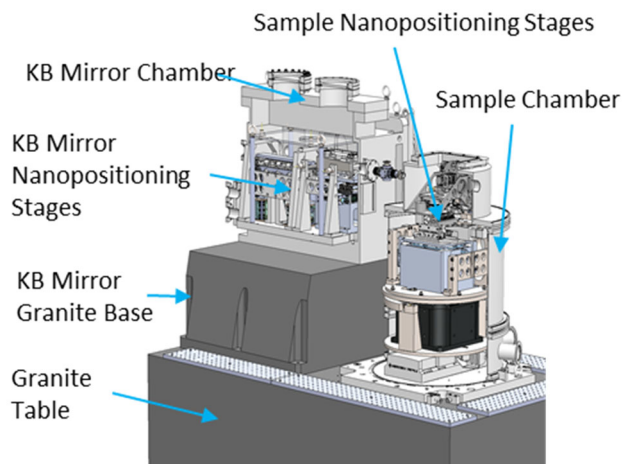


Figure 2: 3D model of the APS CSSI instrument.

<sup>†</sup>anton@anl.gov

# MODULAR NANOPositionING FLEXURE STAGES DEVELOPMENT FOR APS UPGRADE K-B MIRROR NANOFOCUSING OPTICS\*

D. Shu<sup>†</sup>, J. Anton, L. Assoufid, S. Bean, D. Capatina, V. De Andrade, E. Dufresne, T. Graber, R. Harder, D. Haskel, K. Jasionowski, S. Kearney, A. Khan, B. Lai, W. Liu, J. Maser, S. Mashrafi, G. Mistri, S. Narayanan, C. Preissner, M. Ramanathan L. Rebuffi, R. Reininger, O. Schmidt, X. Shi, J. Tischler, K. Wakefield, D. Walko, J. Wang, X. Zhang,

Advanced Photon Source, Argonne National Laboratory, Lemont, IL 60439, USA

## Abstract

Kirkpatrick and Baez (K-B) mirror-based nanofocusing optics [1] will be applied to many beamlines endstation instruments for the APS-Upgrade (APS-U) project. Precision nanopositioning stages with nanometer-scale linear positioning resolution and nanoradian-scale angular stability are needed as alignment apparatuses for the K-B mirror hard X-ray nanofocusing optics. For instance, at the APS-U 19-ID-E In Situ Nanoprobe beamline endstation [2], to maintain stability of a 20-nm focal spot on the sample, nanofocusing K-B mirror system with 5-nrad angular stability is required. Similar angular resolution and stability are also required for APS-U 9-ID CSSI, APS-U 34-ID ATOMIC and other beamline endstation instruments [3, 4]. Modular nanopositioning flexure stages have been developed for the K-B mirror nanofocusing optics, which includes: linear vertical and horizontal flexure stages, tip-tilting flexure stages, and flexure mirror benders for bendable nanofocusing K-B mirrors, to overcome the performance limitations of precision ball-bearing-based or roller-bearing-based stage systems. The mechanical design and applications are described in this paper.

## INTRODUCTION

The Advanced Photon Source (APS) at Argonne National Laboratory (ANL) is scheduled to undergo a massive upgrade that will replace the current electron storage ring with a new Multi-Bend-Achromat (MBA) reverse bent lattice model. X-rays generated by the upgraded APS will be up to 500 times brighter than those created by the current APS. Nine new feature beamlines and enhancements to many existing beamlines will be completed to enable many new exciting scientific research and development capabilities. A total of 12 pairs of K-B nanofocusing mirror systems, including 8 pairs of prefigured mirrors and 4 pairs of bendable mirrors, will be designed and constructed for the APS-U project.

To overcome the performance limitations of precision ball-bearing-based or roller-bearing-based stage systems, precision flexure nanopositioning stages with nanometer-scale linear positioning resolution and nanoradian-scale angular stability are developed at the APS to use as

alignment apparatuses for the K-B mirror hard X-ray nanofocusing optics [5]. These modular stages are designed based on the experiences gained from the flexure stages APS developed for high resolution monochromators [6-10], and especially, for the K-B mirror alignment apparatus for APS 34-ID-E sub-micron 3-D Diffraction experimental station [11, 12]. Laminar weak-link mechanisms [13-15] are applied as a motion guiding structure for the flexure stages. The planar-shape weak-link laminar structure is configured and manufactured by chemical etching and lithography techniques with high-stiffness and high-precision.

As shown in Fig. 1, a typical K-B mirror optics for hard x-ray micro- or nano- focusing is a two-mirror system. Placed orthogonal to each other, each mirror is responsible for a single direction focusing and focused to the same focal spot [5]. With assistance of manual alignment processes prior to the x-ray alignment, the motorized manipulations for the K-B mirrors alignment can be minimized for the linear motion axes  $X_h$ ,  $Y_v$ , and angular tilting motion axes  $A_{xv}$ ,  $A_{yh}$ . In many in-vacuum setup, the orthogonality and distance between the two mirrors are also need to be aligned under X-ray.

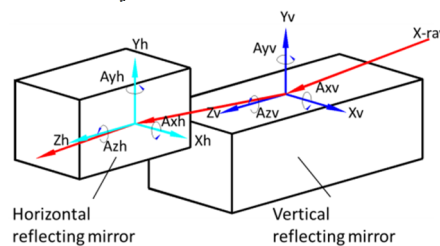


Figure 1: Schematic diagram of the K-B mirror hard X-ray nanofocusing optics.

## STAGES DESIGN ENHANCEMENT

Several design enhancements are made for the modular K-B mirror stages for the APS-Upgrade project, which include:

- Designed linear flexure stages with optional extended travel range.
- Designed flexures linkage mechanisms with two vertical or horizontal linear flexure stages to perform linear and angular adjustment for longer mirrors.
- Designed motorized flexure stages for orthogonality adjustment.
- Equipped capacitive sensor for all linear and tip-tilt flexure stages as an option.

\* This research used resources of the Advanced Photon Source, a U.S. Department of Energy (DOE) Office of Science User Facility at Argonne National Laboratory and is based on research supported by the U.S. DOE Office of Science-Basic Energy Sciences, under Contract No. DE-AC02-06CH11357.

<sup>†</sup>shud@anl.gov

# THE HD-DCM-Lite: A HIGH-DYNAMIC DCM WITH EXTENDED SCANNING CAPABILITIES FOR SIRIUS/LNLS BEAMLINES

A. V. Perna<sup>†</sup>, G. S. de Albuquerque, H. O. C. Duarte, R. R. Gerald<sup>1</sup>, M. A. L. Moraes,  
M. Saveri Silva, M. S. Souza, LNLS, Campinas, Brazil

<sup>1</sup>also at the Eindhoven University of Technology (TUE), 5612AZ Eindhoven, The Netherlands

## Abstract

After successfully designing, installing, and commissioning two units of the High-Dynamic Double-Crystal Monochromator (HD-DCM) at the Brazilian Synchrotron Light Laboratory (LNLS) - Sirius, two more units are now required. Since they demand only a smaller energy range (5 to 35 keV), the total gap stroke of the new instruments can be significantly reduced, creating an opportunity to adapt the existing design towards the so-called HD-DCM-Lite. Removing the large gap adjustment mechanism allows a reduction of the main inertia by a factor of 5, enabling the HD-DCM-Lite to deliver energy flyscans of hundreds of eV reaching 20 cycles per second while keeping fixed exit and the pitch stability in the range of 10 nrad RMS (1 Hz - 2.5 kHz). Hence, an unparallel bridge between slow step-scan DCMs and fast channel-cut monochromators is created. This work presents the in-house development of the HD-DCM-Lite, focusing on its mechanical design, discussions on the ultimate scanning constraints (rotary stage torque, voice-coil forces, interferometers, and encoders readout speed limits and subdivisional errors), and thermal management.

## INTRODUCTION

A lighter version of the High-Dynamic Double-Crystal Monochromator (HD-DCM) [1-3] has been designed for two of the new Sirius beamlines at the Brazilian Synchrotron Light Laboratory (LNLS): the QUATI (quick absorption spectroscopy) and the SAPUCAIA (small-angle scattering) beamline. Differently from the two first beamlines that required larger angular ( $3^\circ$  to  $60^\circ$ ) and energy range (2.3 to 35 keV), these two forthcoming beamlines have smaller energy range requirements – namely, 5 to 35 keV for QUATI and 5 to 18 keV for SAPUCAIA –, allowing a design with an angular range from  $5^\circ$  to  $40^\circ$ . In addition, QUATI also adds the challenge of time-resolved analysis, benefiting from quick energy scans. The new design focus on extending its scan capabilities while preserving stability creating a solution between the current HD-DCM (limited in speed but with fixed-offset and extremely stable) and fast channel-cut monochromators [4], which suffer from offset variation. This work will present the main topics considered during the design of the HD-DCM-Lite.

## MECHANICAL DESIGN

The current HD-DCM design was used as starting point for the HD-DCM-Lite because it is an extensively optimized and tested system, proven to reach 10 nrad RMS

(root mean square) of pitch parallelism performance (within 1 Hz to 2.5 kHz) [2]. Nevertheless, the design had to be adapted to become capable of meeting the fast energy scan requirements for quick-EXAFS (Extended X-ray Absorption Fine-Structure) experiments. Since only the design variations can be discussed here for conciseness, [1] may be consulted for the full set of specifications.

The total gap range between crystals could be reduced from 9 mm to 2.75 mm, such that the long-stroke (LOS) mechanism (see [1]) could be eliminated, enabling a more compact, easier to assemble and cheaper system. Consequently, the moment of inertia was reduced from 13.5 kg.m<sup>2</sup> to 2.7 kg.m<sup>2</sup>, allowing higher accelerations, an important upgrade towards fast scan capability.

Another essential step was doubling the torque capability, now reaching 58.2 N.m after substituting the passive bearing by another Aerotech's APR-260DR-180 rotary stage, thus increasing the scanning capabilities. To handle the power dissipation of the two rotary stages in demanding long-term scan trajectories, a water-cooling circuit has been implemented on the stages. The HD-DCM-Lite is shown in Fig. 1 in comparison to the original HD-DCM.

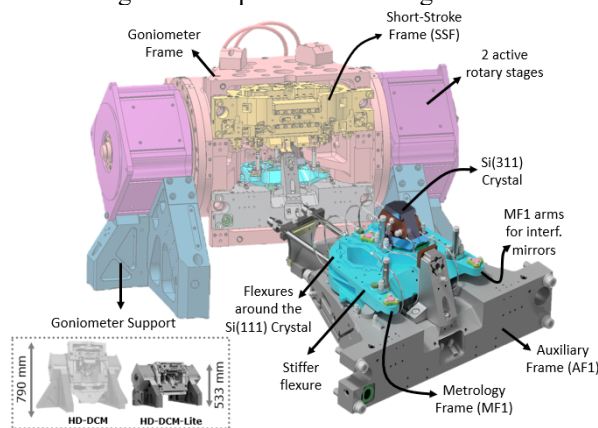


Figure 1: Highlights of the main mechanical design changes and improvements in the HD-DCM-Lite.

From lessons learned [5], this designing opportunity is also taken for improvements in the dynamics of the metrology frame (MF1) supporting the first crystals (CR1s). Increasing its mounting stiffness – by removing the zirconia spacers between MF1 and Auxiliary Frame (AF1) and stiffening the flexures between them – and shortening its “arms” for the interferometer mirrors, the first eigenfrequency should increase from 500 to 800 Hz, reducing the sensitivity to disturbances. Then, to recover the required thermal resistance between the CR1s and the AF1, a complementary set of flexures is added around the CR1s.

<sup>†</sup> alain.perna@lnls.br

# COPPER BRAID HEAT CONDUCTORS FOR SIRIUS CRYOGENIC X-RAY OPTICS

F. R. Lena<sup>†</sup>, G. V. Claudiano, J. C. Corsaletti, R. R. Geraldes, D. Y. Kakizaki, R. L. Parise,  
M. Saveri Silva, M. S. Souza, L. M. Volpe, LNLS, Campinas, Brazil

## Abstract

The low emittance and high photon flux beam present at the 4th-generation Sirius synchrotron light source beamlines result in high energy densities and high heat loads at some specific X-ray optics such as monochromators and white beam mirrors. This challenges the design of such systems since the introduction of thermal stresses may lead to optical surface deformation and beam degradation. Thus, to keep the systems within acceptable deformations some of the optical elements are cryogenically cooled. However, this poses the requirements of decoupling the thermal sinks (cryostats) from the optics and the mechanisms to maintain their desired degrees of freedom for alignment and dynamic operation. In this context we present the development of low-stiffness copper-braid-based heat conductors, summarizing the motivation and main aspects regarding their fabrication and application at the beamlines.

## INTRODUCTION

For high heat-loads monocrystalline silicon optics at Sirius beamlines, one of the standard design concepts for beam-load deformation suppression is the use of liquid nitrogen (LN<sub>2</sub>) cryostats for cooling the elements down to near 125K, where their coefficient of thermal expansion is virtually zero and deformations due to thermal gradients are minimized [1]. In this context, low-stiffness copper braids are widely used to thermally couple the optics to the cryostats while limiting the mechanical coupling between them, such that external vibration disturbances are avoided and kinematic is preserved. Even though commercial solutions for cryogenic, ultra-high vacuum (UHV) compatible copper braids exist worldwide, the high costs, long lead time and customization limitations stimulated the development of an in-house solution with local partners. For special applications, either because of complex geometry or heat extraction capacity, smaller braided modules can be soldered into larger systems using low temperature fillers.

## COPPER BRAID MANUFACTURE

The basic manufacturing process consists in cold forging (ambient temperature), or *pressing*, copper ropes inside bulky copper terminals. The copper ropes are usually made from cold-drawn thin wires stranded together to form a small braid with the diameter in the millimeter range. This results in an all-copper, weld free braid system with solid ends that can be machined for different geometries. As there is no metallurgical joint between the wires themselves and the end-blocks, the heat must be carried across multiple contact interfaces, making the correct design of these interfaces a point of attention. Furthermore, the

copper thermal conduction at low temperatures has a strong correlation with its electrical conductivity [2] and is heavily affected by impurities as oxygen and sulphur, leading to the correct material selection [3].

## Commercial and 1st-Generation In-House Braids

An initial effort of in-house development of copper braids for mirrors and monochromators was made between the years of 2017 and 2019. The first systems were designed by the LNLS team and manufactures by a local partner (Barbanera Qualità) and consisted of pressing multiple braids of 2.5mm in diameter inside electrical-discharge-machined (EDM) cavities in the electrolytic copper end-blocks. The braids were made of 588 40 AWG stranded electrolytic-tough-pitch (ETP) copper wires by the national manufacturer Indel LTDA. The pressing was performed with a 100-ton hydraulic press in an open-die fashion, i.e. without any mold. The compaction criteria were visual, with the pressing process being stopped when there were no visible gaps between the wires and the block. The large end-blocks were then machined, and the entire braid system gold plated to reduce radiation heat transfer.

Despite the good geometry and low-stiffness results, they presented much lower thermal conductivity when compared to commercial systems that were already in use. In fact, some of the braided systems had a tested performance as low as 57% of the theoretical calculated thermal conductivity (CATERETÉ beamline M2 braid). Initial investigations performed via microscopy, after cutting both a commercial braid and an in-house one (Fig. 1), highlighted the potential culprit, namely: the poor wire compaction inside the end blocks. It was found that the cross section of the first one had an average void density of 4.2%, whereas the problematic one had 24.1% (ImageJ). Also, the wires were much less deformed, leading to limited contact area between them due to insufficient pressing forces. This resulted in a poor thermal coupling among both the wires themselves and the end-blocks.

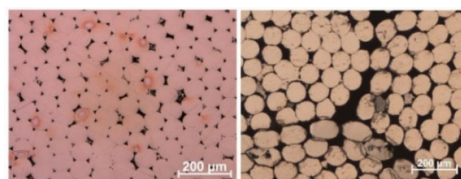


Figure 1: Microographies of the commercial (left) and the 1st-generation in-house (right) solutions from section-cut of the braids inside the end-blocks.

The hypotheses for the bad pressing consisted of a combination of insufficient hydraulic pressing forces and excessively large and stiff end-blocks, resulting in low plastic

<sup>†</sup> francesco.lena@lnls.br

# A NEW ULTRA-STABLE VARIABLE PROJECTION MICROSCOPE FOR THE APS UPGRADE OF 32-ID\*

S. Bean, V. De Andrade, A. Deriy, K. Fezzaa, T. Graber<sup>†</sup>, J. Matus, C. Preissner, D. Shu  
Advanced Photon Source, Argonne National Laboratory, Lemont, IL 60439, USA

<sup>†</sup>Deceased April 29, 2021

## Abstract

A new nano-computed tomography projection microscope (n-CT) is being designed as part the Advanced Photon Source Upgrade (APS-U) beamline enhancement at sector 32-ID. The n-CT will take advantage of the APS-U source and provide new capabilities to the imaging program at 32-ID. A Kirkpatrick and Baez (KB) mirror-based nanofocusing optics [1, 2] will be implemented in this design. To meet the n-CT imaging goals, it is the desire to have sub 10 nanometer vibrational and thermal drift stability over 10-minute measurement durations between the optic and the sample. In addition to the stability requirements, it is desired to have a variable length sample projection axis of up to 450 mm. Such stability and motion requirements are challenging to accomplish simultaneously due to performance limitations of traditional motion mechanics and present a significant engineering challenge. To overcome these limitations, the proposed n-CT design incorporates granite air bearing concepts initially used in the Velociprobe [3]. These types of granite stages have been incorporated into many designs at APS [4] and at other synchrotron facilities [5]. Utilizing the granite air bearing concept, in tandem with other design aspects in the instrument, the requirements become reachable. A novel multi-degree of freedom wedge configuration is also incorporated to overcome space limitations. The design of this instrument is described in this paper.

## INTRODUCTION

The new n-CT instrument will exploit the new APS-U source characteristics by implementing projection x-ray imaging for the high-speed imaging program at APS. A throughput gain is achieved as the temporal resolution of the nano-imaging tomography instrument goes from 500 ms to tens of  $\mu$ s. A unique advantage of the instrument geometry allows zooming capability that fills the gap in terms of resolution and field of view between the currently available  $\mu$ -computed tomography ( $\mu$ -CT) and the transmission x-ray microscopy (TXM) based nano-computed tomography (n-CT). Another unique advantage of the instrument geometry allows the multi-modality measurement capability coming from the simplicity of using the focused beam as a probe for XRF measurement.

\* This research used resources of the Advanced Photon Source, a U.S. Department of Energy (DOE) Office of Science User Facility at Argonne National Laboratory and is based on research supported by the U.S. DOE Office of Science-Basic Energy Sciences, under Contract No. DE-AC02-06CH11357.

The variable projection microscope at 32-ID will be a combination of a KB mirror system and a high precision sample rotation and nano positioning stack on a common support structure with separate granite air bearing coarse positioning axes. A separate camera and detector system will be integrated just downstream of the instrument. A visualization of the instrument is shown in Fig. 1.

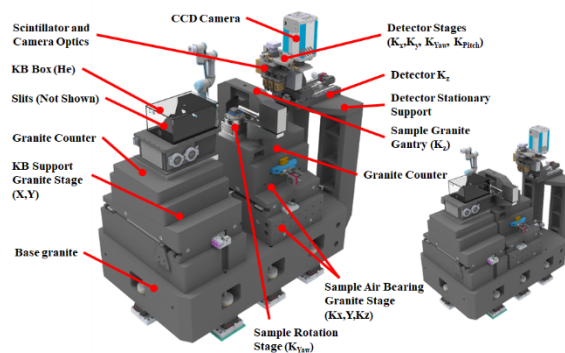


Figure 1: Rendering [6] of the n-CT instrument design, labeling major components. Largest working distance (left) and probing stage (bottom right).

It is the desire to have sub 10 nm vibration and thermal drift stability over the course of 10-minute measurements. Because of the long variable zoom axis of this instrument, it is difficult to implement relative optic to sample metrology to correct thermal drifts. It is the design of the coarse granite stage positioning system and support that enables this relative stability. The instrument design and these details are discussed in subsequent sections.

## N-CT CONFIGURATION METHODOLOGY

The following numbered items represent the most critical requirements of design and configuration for this instrument:

1. A stable, helium isolated KB optics environment is required to achieve the nanofocusing of the KB's along with extending their lifetime.
2. Optics to sample stability is required. This is both when considering contributions of vibrations and thermal drifts.
3. Variable projection zoom axis of 450 mm must be implemented in the design. Stability cannot be compromised with variable zoom.
4. Various sample environments must be accommodated with  $>360$  rotation capability. Voltage biasing and fluid feedthroughs must be integrated into the design

# CAD INTEGRATION FOR PETRA-IV

B. List\*, L. Hagge, M. Hüning, D. Miller, P.-O. Petersen  
Deutsches Elektronen-Synchrotron DESY, Hamburg, Germany

## Abstract

The PETRA-IV next-generation synchrotron radiation source at DESY is currently in preparation with a completely new accelerator and a new experimental hall, retaining as much of the existing PETRA-III buildings, tunnels and experimental beamlines as possible.

We have set up a CAD integration model for the complete accelerator and photon science complex. The model hierarchy has levels reflecting decisions on project organisation, project phases, design process, and overall product structure. Modularisation and designing in three levels of detail help to manage the complexity and keep the model performant. Placement of accelerator components is determined by the lattice through direct access to spreadsheet data, allowing fast design changes after a lattice update and ensuring consistency between mechanical and lattice design. The resulting model will support engineering processes over the complete facility lifecycle.

## INTRODUCTION

Lifecycles of accelerator facilities extend over decades, spanning a number of phases from concept over design, construction, and operation to dismantling. Computer Aided Design (CAD) is an essential tool for supporting the engineering in the various stages of the lifecycle. CAD applications include space allocation, basic and detailed engineering, matching of interfaces, clash checks, technical documentation for installation, operation, and maintenance. Figure 1 shows a simplified lifecycle of an accelerator facility and highlights phases with important CAD contributions. The CAD integration model accumulates and conserves all mechanical engineering designs, decisions, and knowledge throughout the entire lifecycle. It is implemented and maintained in the CAD software Siemens NX and the PLM system Teamcenter.

## OBJECTIVES

The integrated CAD model of PETRA-IV [1] is intended to serve as a comprehensive mechanical model of the entire system: the accelerators with all their components, photon beamlines with optics and experiments, supporting infrastructure such as water, electricity, ventilation, and buildings. It will be maintained throughout the project life span and remain usable during its whole life cycle for all stakeholders with their differing needs. The overarching objectives of the model are to establish vision sharing, support interface management, enable early detection of potential clashes, foster design collaboration, and to support better and faster decision making

\* Benno.List@desy.de

## REQUIREMENTS

Performance is a major requirement: the model has to provide the means to efficiently edit the data and provide the necessary design context. Collaboration across different trades and organisational units needs to be supported with minimal side effects from changes in one trade to other parts of the model and with data protection against unwanted changes from third-party groups.

Collaboration with external groups and suppliers, who do not have access to the integration model, demands support for work with minimal context: clearly defined interfaces and space reservations for import of the contributed data, are required.

Accelerator design starts from a mathematical model of the components governing the beam dynamics (the so-called lattice). An associative relation between the CAD model components and their lattice representations and the ability of automatic geometry updates are needed for fast design iterations.

Collaboration with civil engineering requires the import of the building and tunnel CAD models from dedicated architectural CAD systems into the integration model, with accurate placement of the buildings and an exchange of space reservations as input for the civil engineering design process. Infrastructure, such as water and electricity supplies and heating and ventilation, has interfaces to the buildings and the accelerator and experimental facilities that need to be present in the model.

## METHODS

In the following, we describe briefly some of the methods we have employed in response to the CAD model objectives and requirements.

### *Model Structure*

CAD models are typically structured according to a spatial and functional decomposition of the product. A close correspondence between CAD model structure and the product breakdown structure (PBS) supports processes that are closely linked to the PBS such as verification of requirements, validation, and testing.

The structure has a consistent set of levels corresponding to a logical hierarchy, namely program, complex, facility, area, and unit, inspired by the physical model of the ISA-106 set of standards, as illustrated in Fig. 3. Additional interim levels (not shown in the figure) implement different levels of detail, organize responsibilities and access rights of the different trades and work packages, and manage different configurations.

We find that the CAD model structure reflects, and often necessitates, project decisions on topics such as responsibil-

# DESIGN OF GIRDERS ON THE NEW UPGRADE LATTICE AT SOLEIL

J-L Giorgetta<sup>†</sup>, A. Lestrade, A. Mary, K. Tavakoli, Synchrotron SOLEIL, Paris, France

## Abstract

The current girder set of SOLEIL features 4 girder types weighing from 1.85 t to 3 t, with a respective mass payload varying from 4.1 t to 8 t and lengths from 2.4 m to 4.8 m. The smaller size of magnets used for the present version of the SOLEIL upgrade allows a dramatic size and weight reduction of the magnet-girder assemblies (Fig. 1). On the other hand, the number of magnets has increased by a factor of 3, implying longer alignment and installation operations. Several setups involving 116 to 212 girders with various magnet layouts and binding systems have been studied. Dynamic and thermal performances have been evaluated by FEA analysis. This approach gives to accelerator physicists the performance of each solution, and thus a great versatility in the choice of the best setup in terms of dynamic and thermal stability.

## DESIGN BASELINE

The design of the new magnet-girder assemblies considers experience gained from the existing installation, using concepts with proven efficiency and good performance in terms of stability. However, some other features are not optimized for the new storage ring and had to be adapted or totally redesigned. The large number of girders and magnets in the new lattice leads to a need to reduce unit cost and alignment time.

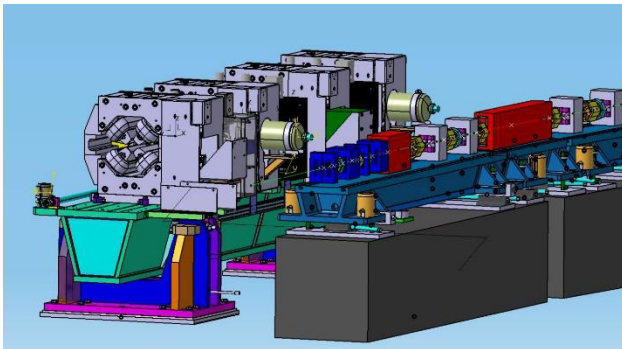


Figure 1 : SOLEIL vs Upgrade magnet girder assembly.

The small size of magnets makes possible to reduce the distance between beam axis and the upper face of girders to 240 mm, improving overall stability. However, the girder position is then higher with respect to the ground, imposing increased stability requirements on the girder support structures. Both granite and welded steel plinths have been considered as girder supports. These plinths are aligned, in all directions, with an accuracy of  $\pm 1$  mm and grouted to the ground. The new lattice features 4 or 6 fixing

point girders depending on the length. Due to the high long-term stability of the SOLEIL slab, motorization of the positioning system is not envisaged, particularly when considering its extra cost and complexity. In the same way, the current lock/release system is replaced by high stiffness wedges for vertical adjustment and push-pull screws for horizontal position. Stiffness is improved by applying a permanent vertical preload on wedges.

Girders are equipped with a HLS (Hydrostatic Leveling System) used during alignment operations. The new design implements a tooling referenced on the girder side face to set magnets on the beam axis with the requested accuracy.

## MAIN SPECIFICATIONS

- Dynamic sensitivity of beam towards magnet position: lowest frequency  $> 70$  Hz
- Sensitivity of beam towards magnet alignment:
  - girder to girder  $30 \mu\text{m}$  vertical and  $50 \mu\text{m}$  horizontal
- $100 \mu\text{m}$  RMS in both planes for all girders
- Thermal stability based upon BPM specification:
  - $50 \text{ nm}$  a couple of minutes
  - $500 \text{ nm}$  on one day
  - $\sim 1 \mu\text{m}$  on a week
- Ex-situ bake-out of vacuum chambers:
  - C-shape dipoles and transverse motion mandatory

## GENERAL LAYOUT

SOLEIL Upgrade features 2 basic cells: 7 BA\* and 4 BA\* 3 configurations have been studied:

- 212 girders with 1.80 m max length (Fig. 2).
- 116 girders with 3.60 m max length (Fig. 3).
- 176 girders with 3.20 m max length (Fig. 4).

In the 2 first layouts, long dipoles share the plinth with adjacent girders, the third layout features standalone dipole stands. Using a girder as a dipole support allows for fine setting and avoids the low resonance frequency of dipoles encountered on the present SOLEIL setup. Dipoles are fixed on an air bearing cradle which can be removed from beam axis for vacuum chamber installation (Fig. 5).

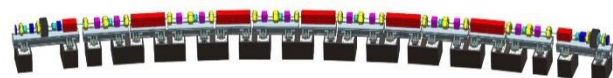


Figure 2: Configuration 1 (7BA segment).

\*BA: Bending Achromat

<sup>†</sup> jean-luc.giorgetta@synchrotron-soleil.fr.

# UPDATED HIGH HEAT LOAD FRONT-ENDS FOR SLS 2.0

D.M. Just†, C. Pradervand, Paul Scherrer Institute, 5232 Villigen, Switzerland

## Abstract

The Swiss Light Source (SLS) at the Paul Scherrer Institute (PSI) in Switzerland undergoes from 2021 to 2024 an upgrade named SLS 2.0 to increase brightness and coherence. This upgrade will have a significant impact on the existing front-ends. Due to the proven reliability and good concept, we plan a refurbishment strategy for all front-end (FE) components where possible. New source points for all beam-lines – resulting in shifts both lateral and tangential, newly developed insertion devices and bending magnets as well as spatial restrictions due to the multi bend achromat (MBA) design challenges this strategy. We demonstrate how we plan to deal with these challenges for the case of high heat load FEs. We discuss the design and thermal analysis of a novel primary aperture and high heat load slits, the adaptations that will be made to the tungsten blade x-ray beam positioning monitors (XBPM) and the modifications on the photon shutter will be discussed

## PURPOSE OF A FRONT-END

A front-end delivers a synchrotron radiation beam, through the tunnel wall, to the beamlines and end stations in order to perform experiments using said beam. Another important task of the front-end is to securely shut the radiation to allow people to work in downstream areas even if the rest of the beamlines is in operation mode.

Additionally the front-end performs some first beam conditioning. Most importantly the maximum beam size is defined by a diaphragm (or fixed aperture). This helps to reduce the heat load on all downstream elements. Additionally slits define the beam size according to the need of the beamline and downstream optical elements.

## FRONT-END STRATEGY FOR SLS 2.0

The front-ends at SLS have proven to be very reliable and low-maintenance during the last two decades. Therefore we plan to reuse some of the existing components after refurbishment for SLS 2.0. All elements will be updated to state of the art motion control and safety standards [1]. However some FE elements need to be completely redesigned. The primary reason for this is the increased heat load on the exposed elements. For hard x-ray FEs, generally associated with high power loads, the power has increased by a factor of three coming from SLS going to SLS 2.0. This is due to the increase in storage ring energy from 2.4 GeV to 2.7 GeV and more powerful insertion devices.

Due to the new lattice all beamlines shift in lateral and longitudinal direction and available FE floor space has been reduced due to the more round storage ring with MBAs (see Fig. 1).

Because of these reasons all FEs need to be completely removed from the storage ring tunnel and carefully reassembled in dedicated areas during the SLS 2.0 dark time.

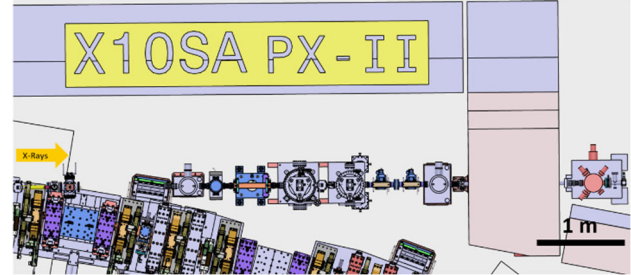


Figure 1: The PX-III front-end in its SLS 2.0 confines.

## HIGH HEAT LOAD FRONT END COMPONENTS

The most demanding FEs in terms of thermal management are the hard x-ray FEs (see Fig. 2). In the most extreme case a cryogenically cooled U16 undulator produces up to 10 kW and 56 kW/mrad<sup>2</sup>. But also some soft x-ray front ends are equipped with very powerful undulators producing comparable amounts of heat load which needs to be dealt with.

This is why our novel high heat load components are designed for versatility: by adapting only a few computer-aided design (CAD) parameters the same design can be used for different beam sizes to suit the diversity between the different FEs.

Following the most important components of a high heat load FE are outlined.

### Tungsten Balde XBPM

Tungsten blade XBPMs (Pos. 1, Fig. 2) will be used to provide a feedback of the beam position to the machine and the beamline. This feedback will be used to optimize the electron-beam stability and serves as a reference for the beamline.

For SLS 2.0 we will reuse the existing tungsten blade monitors (W-XBPM). In order to use the W-XBPMs with the new beam parameters we developed a python script to calculate the response function of tungsten i.e. the probability of a photon emitting an electron from a tungsten blade and thus generating a signal using Eq. (1).

$$Y = \int_{30 \text{ eV}}^{30 \text{ keV}} F'(E) \cdot BW \cdot \sigma_{ph}(E) dE \quad (1)$$

Where Y is the tungsten response function  $F'(E)$  is the flux density per energy [ph/s/mrad<sup>2</sup>/0.1BW], BW the band width and  $\sigma_{ph}(E)$  the photoelectric cross section.

The result is then plotted together with the power density and the blades are then manually adjusted in order to maximize the signal and minimize the heat exposure (see Fig. 3). We will then physically adapt the position of each blade for SLS 2.0 according to these findings.

† david.just@psi.ch

## ENGINEERING CHALLENGES IN BIOSAXS FOR AUSTRALIAN SYNCHROTRON

S. Venkatesan, C. Kamma-Lorger, L. Barnsley, A. Clulow, G. Conesa-Zamora, R. Grubb, B. Jensen,  
 N. Hamed, V. Samardzic-Boban, C. Roy, T. Mazonowicz  
 Australian Synchrotron, ANSTO, Melbourne, Australia

### Abstract

The Biological Small Angle X-Ray Scattering (BioSAXS) beamline is the third beamline designed, developed and soon to be installed as part of the BRIGHT Program at the Australian Synchrotron. The BioSAXS beamline will deliver a high flux beam at sample position and will be optimised for time resolved experiments and low concentration/low scattering samples. This paper presents the various engineering challenges in this high flux design, including thermal management of critical components, design developments to accommodate the various operational modes and various stages of the Photon Delivery System and Experimental Station components. The paper aims to present details of design, Finite Element Analysis results and approaches taken to solve problems.

### INTRODUCTION

The Biological Small Angle X-Ray Scattering (BioSAXS) beamline is the third beamline designed, developed and soon to be installed as part of the BRIGHT Program at the Australian Synchrotron. The BioSAXS beamline will deliver a high flux beam at sample position and will be optimised for time resolved experiments and low concentration/low scattering samples. The beamline will offer increased efficiency, and data quality, for all liquid phase scattering experiments, allowing measurement of new and novel samples, and experiments, that otherwise would not be possible. The BioSAXS beamline will accommodate a wide range of experiments by offering a q-range of  $\sim 0.001 - 4 \text{ \AA}^{-1}$  and an optical design optimized for high flux ( $\sim 5 \times 10^{14} \text{ ph/s}$ ) x-rays. At this flux rate, BioSAXS will offer users one of the highest flux beamlines in the world.

To achieve this, the beamline will use a superconducting undulator insertion device, double multilayer

monochromator, and vertical and horizontal bending mirrors, providing flexibility in optical configurations. The beamline will primarily collect data in a vertically unfocused mode. BioSAXS will also be able to achieve a fully focused and a fully unfocused beam.

The beamline is designed in 8 vacuum sections. The first contains a fixed mask, a bremsstrahlung collimator, cooled filter rack and a fluorescence screen. Vacuum section 2 is designed for the Double Multilayer Monochromator, two bremsstrahlung elements in each of the ports and a QBPM. The third vacuum section houses diagnostics and the attenuators. These are used to determine any shift in the beam location and enable correction for the beamline. The fourth vacuum section is design for the KB mirror system with horizontal and vertical focussing mirrors. This is followed by another group of diagnostics, formed by a grouping of QBPM and Fluorescence screens for real time analysis and correction, when combined with F460 electronics and in-flange slits, as well as a fast closing valve in the fifth vacuum section and the safety shutter in the sixth vacuum sections respectively. A beam conditioning table to manipulate the beam to sample is designed in vacuum section 7 and the end station as vacuum section 8. The beam conditioning table consists of a NanoBPM, two guard slits, XBPM and a Sample Camera for the visualisation of the sample at 29 m from the source and a mica exit window. The end station is formed by a sample table to carry samples in various environments, a vacuum vessel to house the in-vacuum Dectris detector, a detector actuation system for in-vacuum manipulation of detector position, the Beamstops and the vacuum vessel actuation.

The design of the beamline is shown in Fig 1.

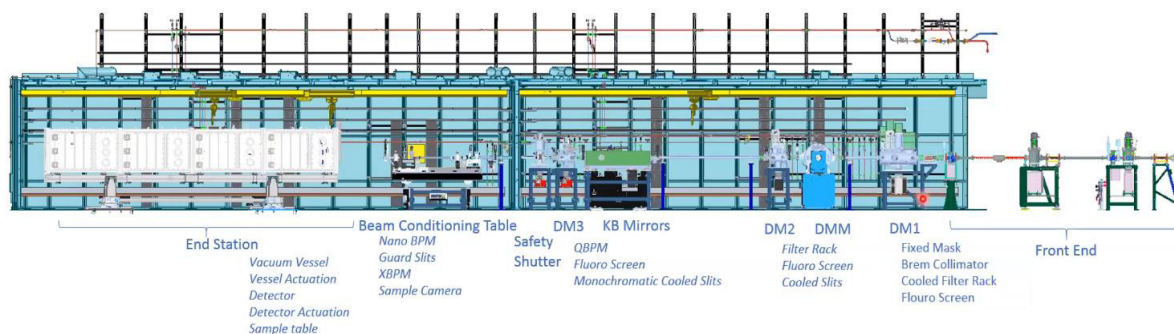


Figure 1: BioSAXS beamline schematic.

# DEVELOPMENT OF A LINEAR FAST SHUTTER FOR BM05 AT ESRF AND BEATS AT SESAME

C. Muñoz Pequeño <sup>†</sup>, J. M. Clement, P. Thevenau, P. Van Vaerenbergh  
 European Synchrotron Radiation Facility, 38043 Grenoble, France

## Abstract

A new linear fast shutter for X-ray topography and tomography is currently under development. This first prototype will be assembled and tested on the BM05 beamline at the ESRF, and another unit will be installed in the future BEATS beamline at SESAME. The new shutter aims to overcome the stability, control and thermal issues reported with previous versions. This versatile design can be used with monochromatic and white-beam, reaching minimum exposure times of 50 ms for a beam size of H 80 mm × V 20 mm.

Powered by two linear brushless DC motors, the exposure sequence is achieved through the synchronization of two tantalum blades. This concept has been tested in a dedicated bench to characterize the sequence produced by the linear motors, and exposure times of 50 ms with a maximum error of 1.5 ms have been measured. This article describes the main features of the shutter prototype design and its associated motion control system. The main results of the measurements with the test bench are discussed as well.

## INTRODUCTION

Fast shutters are widely used in synchrotron beamlines for applications in X-ray topography and tomography. Topography typically requires exposure times ranging from milliseconds to hundreds of seconds. Due to its low signal-to-noise ratio, it is essential to shield the CCD detector during readout to avoid added noise [1]. In addition, shutters are of special relevance when performing white beam tomography in delicate samples that are easily degraded when exposed to high photon flux. The use of a shutter allows for sample repositioning and prevents sample irradiation when data is not being recorded. This highlights the importance of the control in the exposure time and its uniformity to guarantee an adequate image quality.

In the context of the refurbishment of the BM05 instrumentation beamline at the ESRF, an old shutter was installed in the tunnel located before the experimental hutch EH2. In this model, the exposure sequence was achieved through the synchronization of two stainless steel blades powered by electromagnets. However, in addition to the tremendous vibrations and the limited duration of the exposure cycle due to the electromagnets overheating, their control system was obsolete. The main motivation of this project was to develop a new shutter that can overcome these issues with up-to-date controls to replace the prototype installed at BM05. Another prototype is being developed for installation in the experimental hutch of the BEATS tomography beamline currently under construction at SESAME [2].

<sup>†</sup> munozpeq@esrf.fr

## DESIGN

The main advantage of the proposed concept is its suitability for larger beams thanks to the use of linear brush-less DC motors featuring high dynamics and precision. Other technologies often employed in the synchrotron community, such as rotary and piezoelectric shutters [3], can achieve very small exposure times as well, but over much smaller beam apertures.

Table 1: Fast Shutter Specifications

Parameter	Value
Beam size [mm × mm]	80 × 20
Exposure time [ms]	< 100
Repetition rate [Hz]	> 1
Maximum beam power [W]	380
Blade material	Tantalum
Blade thickness [mm]	4

The motors have been selected to fulfil the specifications listed in Table 1. The objective is to achieve a reproducible and uniform exposure time over the beam window. The exposure cycle is achieved through the synchronization of two blades so that the exposure time depends on the delay between their opening and closing trajectories. Therefore, it is crucial that the trajectories of the blades are identical, i.e. to ensure the delay between the opening and closing of the blades,  $\Delta t_1$  and  $\Delta t_2$ , is the same for all the points of the window (see Fig. 1).

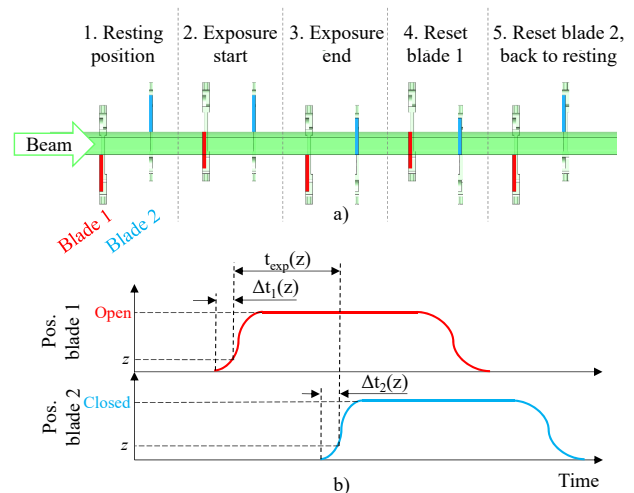


Figure 1: Exposure sequence, a) schematic of the phases of the exposure cycle b) diagram of the blades trajectories.

# THE BEAMLIN MOTOR CONTROL SYSTEM OF TAIWAN PHOTON SOURCE

C.F. Chang<sup>†</sup>, C.Y. Liu  
 National Synchrotron Radiation Research Center, Hsinchu, Taiwan

## Abstract

Different experiments have different features, so does the optical design; however, all of them are necessary to be adjusted according to mechanism. For example, adjusting mechanism of optical element is often based on stepper motor, for stepper motor possesses high resolution ability, which can adjust mechanism to precise location. This study illustrates how motor system of our Taiwan Photon Source integrates adjusting mechanisms of stepper motor on beamline. In addition, the firmware of close-loop system is cooperated to further improve veracity of location.

## INTRODUCTION

When using the beamline, in order to be able to adjust the light source to the required environment of the experiment, the optical system on the beamline is designed to be adjustable. The types of mechanisms on the beamline are divided into two categories. The first is the optical path adjustment mechanism used to adjust the position of the light source; the second is the light path diagnosis mechanism, used to check the condition of the light source when it is in use. Most of the mechanisms are designed with stepper motors. This article explains how the TPS beamline motor control system control various movable mechanisms on the beamline.

## SYSTEM STRUCTURE

The movable components on the beamline use the eight-axis motor controller as the control core and can be moved after being equipped with a suitable driver, so the user can freely match according to the needs of use, and the controller adopts an independent. In addition, the TPS beamline has improved position accuracy, so all the motor control components on the beamline are equipped with various optical scales to obtain the actual position signal, and the TPS beamline the motor controller of the beamline selection can read the encoder, allowing the control system to fine-tune the mechanism, so that the position accuracy is improved [1-2]. (See Fig. 1.)

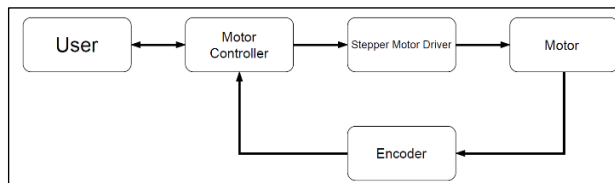


Figure 1: System architecture of Beamline Motor Control System.

<sup>†</sup> donnychang@nsrrc.org.tw

## HARDWARE DESCRIPTION

The DMC-40x0 motion controller is Galil's highest performance, stand-alone motion controller packaged with optional multi-axis drives in a compact, metal enclosure. The unit operates stand-alone or interfaces to a PC with Ethernet 10/100Base-T or RS232 [3]. (See Fig. 2.)



Figure 2: The picture of DMC-40x0 motion controller.

## CONTROL HARDWARE

TPS motor control system is based on the eight-axis motor controller DMC-4080 manufactured by GALIL, and the peripheral hardware is different due to the experimental characteristics of the beamline, and the stepping motor selected for the optical system will be different, but most of them are divided into Two types, one is a 5-phase stepper motor, the number of divisions is more than 500 (0.72°/Step), and the other is a 2-phase stepper motor, the number of divisions is more than 200 (1.8°/Step), the difference is the smallest part The difference in resolution is set by 5-phase stepper motor 1000 (0.36°/Step) and 2-phase stepper motor 400 (0.9°/Step) in TPS. As for the actual resolution, it is set by stepping motor. The ratio between the motor and the mechanical structure is determined. (See Fig. 3.)

# THE FIZEAU SYSTEM INSTRUMENT AT ALBA OPTICS LABORATORY

Llibert Ribó†, Igors Sics, Domingo Alloza, Carles Colldelram, Josep Nicolas  
ALBA Synchrotron, Carrer de la Llum 2 26, 08290 Cerdanyola del Vallès, Spain

## Abstract

The ALBA optics laboratory has recently acquired a new Zygo Verifire HD Fizeau interferometer. The instrument has been integrated into a positioning stage to allow stitching of long x-ray optical elements. The mechanical set up, with four axes, allows for automatic positioning and alignment of the interferometer aperture to the surface under test. The longitudinal movement allows for scan of X-ray mirrors up to 1500 m long. The positioning platform includes two angles, roll and yaw, and two translations, vertical and longitudinal translations. The longitudinal translation is a custom designed linear stage. The yaw rotation is based on a sine arm mechanism. The vertical and roll motions are combined in a single stage, closely integrated around the main linear stage. The system reaches repeatability better than 1  $\mu\text{m}$  or 1  $\mu\text{rad}$  for all axes. The system is mounted on top of a vibration isolated bench in the clean room of the laboratory. The control software of the instrument allows direct control of every individual axis, and allows selecting the centre of rotation for both roll and yaw. The system includes inclinometers and autocollimators to control the relative orientation between the interferometer and the mirror under test. The system is integrated to the software of the interferometer, and includes features for automatic alignment of the interferometer to the mirror, or for automatic stitching acquisition, with selectable parameters. The system allows for full three-dimensional characterization of the optical surface of mirrors and gratings, and provides height map reconstructions with accuracy in the order of 1 nm, for flat or curved surfaces with lengths up to 1500 mm.

## POSITIONING STAGE

The positioning stage consists on an integration of 5 motorized actuators for the positioning of the Fizeau interferometer. It has been designed to achieve the maximum compactness to give versatility to all possible measurements set ups. The stage has to operate on top of an antivibration system, thus the design included the weight as a requirement.

### Design Description

The specifications for the positioning of the interferometer are listed below in Table 1 and Fig. 1.

The longitudinal actuator has a range of 1500 mm. The guides are mounted on the sides of an aluminum standard profile but on precise machined intermediate plates. The carriage is positioned by a ball spindle driven by a stepper motor. In order to avoid stresses caused by guidance errors between the spindle and the guides, a flexible nut support has been included. The system has been designed to reach

a speed of 25 mm/s and a theoretical resolution of 8,3  $\mu\text{m}$  at full step. The resolution is achieved by means of micro stepping down to 1/8 of step.

Table 1: Specifications Table

Axis	Specification	Value
X	Longitudinal Stroke	1500 mm
	Resolution	5 $\mu\text{m}$
	Guidance Flatness	<50 $\mu\text{m}$
Z	Vertical stroke	$\pm 10\text{mm}$
Roll	Angular Range	20 mrad
	Resolution	1 $\mu\text{rad}$
Yaw	Angular Range	50 mrad
	Resolution	1 $\mu\text{rad}$

The vertical stage is mounted around the longitudinal one and it is based on the design of a double flexure that compacts the vertical movement and the rotation in a single following the concept *ALBA XALOC Beamline diffractometer table skin concept* [1, 2]. The angular resolution of the system is 5  $\mu\text{rad}$ /full step, while the system is operated at 1/8-step.

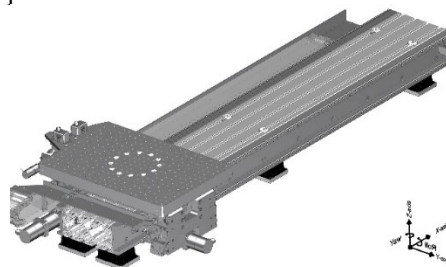


Figure 1: Representation of the axis.

The yaw actuator is the last stage mounted on the top of the vertical stage, and is the mechanical interface with the interferometer. The rotation is driven by means a sine arm. The mechanical architecture, allows for a fine yaw positioning resolution of 0,26  $\mu\text{rad}$ /full step.

All axes include absolute encoders for positioning feedback and dynamic close-loop motion.

### FEA Analysis

The design has been validated with simulation to check its stability (see Fig. 2). The lowest resonance modes, (at 49 Hz and 56 Hz) are related to the displacement of the full system due to the spindles compliance, although they but are within tolerance, particularly considering the weight of the system.

The skin concept flexures have been also calculated and optimized simulating the differential displacement between both plates for maximum Roll. The maximum stress is 198 MPa and in this case a high strength aluminium from serial 7000 has been chosen with a yield stress beyond

† lribo@cells.es

# INVESTIGATING OF EBW PROCESS WELDMENT CONNECTIONS STRESSES IN ILSF 100 MHz CAVITY BY Simufact.Welding SOFTWARE\*

V. Moradi<sup>†</sup>, Department of Mechanical Engineering, ILSF, Tehran, Iran

A. Adamian, N. B. Arab, Dept. of Mechanical Engineering, Tehran Central Azad Univ., Tehran, Iran

## Abstract

The cavity is one of the main components of all accelerators, which is used to increase the energy level of charged particles (electrons, protons, etc.). The cavities increase the energy level of the charged particle by providing a suitable electric field to accelerate the charged particle. Here, information about electron beam welding analysis in 100 MHz cavities of ILSF design will be explained. According to studies performed in most accelerators in the world, connections in cavities are made by various methods such as explosive welding, brazing, electron beam welding, etc. Many articles on large cavities state that the connection of the side doors must be done by the electron beam welding process. However, in the present paper, the three-dimensional model of the cavity is imported into Simufact.Welding software after simplification and mesh process was done, then the heat source of electron beam welding and other welding factors such as beam power, Gaussian distribution, etc. are applied in the software. The purpose of this study is the number of residual stresses during the EBW process in the 100 MHz cavity of ILSF.

## INTRODUCTION

Since the early 1970s, finite element modelling has been used to simulate mechanical problems in welding. Some popular sources up to the 1990s are the works of Ueda and Yamakawa [1], Goldak [2] and Radaj [3]. Finite element codes have been described to address these issues among numerous articles such as Dexter [4] and Karlsson [5]. In most finite element models, it is common to assume a number of simplifications. The reason for this simplification is the high computational cost of 3D models (which, of course, is not always approved). However, Duranton et al. [6] showed that when the heat flux in the welding direction is ignored, shortcomings in the two-dimensional method in longitudinal welding will occur.

According to the mechanical explanations of the problem, in some articles such as Song et al. [7] and several other articles, it is assumed that the material acts as a viscous elastoplasty pattern, and in others such as Branza et al. [8], Duranton et al. [6] The assumption of hard isotropic materials, or in other articles such as Nandan et al. [9], has considered the material as an elasto-viscoplastic material. Alberg and Berglund [10] compare the plastic and viscoelastic models used to simulate welding and recommend that a simple plastic model be used in the early stages of the study. However, the viscosity effects of materials at high temperatures cannot be ignored, as they have a

significant effect on the behaviour of metals. Also, welding generally involves cooling cycles whose effect on the mechanical behaviour of the material will only be considered if the material is in a state of kinematic hardening. Therefore, the justification for using simpler models such as plastic elastic, without considering the hardening of the material or just the isotropic hardening (which has been the most widely used to date) is only to reduce computational costs. In this paper, the analysis of welding joint calculations in ILSF 100 MHz cavity will be investigated. According to studies performed in most accelerators in the world, the welding connections of the cavities have been done by electron beam. Therefore, in the forthcoming research, the three-dimensional cavity model after simplification and meshing was entered into Simufact.Welding software and then the heat source of electron beam welding and other welding factors such as beam power, Gaussian distribution amount, and etc. Finally, in the software, the simulation of the beam welding process will be done. The purpose of this study is to determine the number of residual stresses in the cavity after the EBW process.

## NUMERICAL MODEL OF HEAT SOURCE

The heat source model in the EBW process is combined in such a way that the thermal effect of the key hole in the penetration depth is modelled with a three-dimensional conical heat source and also the molten metal vapor at the weld surface which has its own local thermodynamic equations of the surface heat source. Used by a Gaussian heat source model to simulate the effect of surface heat.

The formula for the distribution of Gaussian heat source is as follows [11]:

$$q_s(x, y) = \frac{3Q_s}{\pi R^2} \times \exp\left[-\frac{3(x^2+y^2)}{R^2}\right] \quad (1)$$

Where, ( $q_s$ ) is the heat flux in the Cartesian coordinates, ( $Q_s$ ) is the Gaussian heat source power, and ( $R$ ) is the effective radius of the electron beam. Of course, assuming that ( $r$ ) is the distance of each point from the heat source to its center, the relation  $x^2 + y^2 = r^2$  holds. Also, by moving the welding heat source, the inlet heat flux changes in different positions along the direction of the welding speed. The relationship between moving coordinates and static coordinates is defined as follows:

$$u = y + v(\tau - t) \quad (2)$$

Where, ( $t$ ) is the welding time, ( $v$ ) the welding speed and ( $\tau$ ) the time delay factor. After converting the static coordinates to motion coordinates in Eq. (1) we will have:

$$q_s(x, y) = \frac{3Q_s}{\pi R^2} \times \exp\left[-\frac{3(x^2 + y + v(\tau - t)^2)}{R^2}\right] \quad (3)$$

\* Work supported by Iranian Light Source Facility (ILSF)

<sup>†</sup> v.moradi1985@gmail.com

# A NEW THREE-SIGNAL 2D-BEAM-POSITION-MONITOR BASED ON A SEGMENTED IONIZATION CHAMBER

M. Goerlitz\*, W. A. Caliebe, DESY, Hamburg, Germany

## Abstract

At DESY in 2020 a three-signal beam position monitor (BPM) was constructed, which is based on a Ionization Chamber design with split up electrodes. It is using three signals to determinate horizontal and vertical positions of a x-ray beam. The relation between signals and position can be described by a multiple linear regression (MLR). The calibration is done by linear optimization algorithms, which are described in detail, especially to give an engineering-based resume, which can easily applied to other systems. The results of the solution will be compared and discussed.

## INTRODUCTION AND MOTIVATION

Due to the facts that synchrotron x-ray beam sizes are getting smaller and more experiments demand a focussed beam, the necessity of a controlled stable beam increases. Some demands of monitoring devices are, that they should not absorb significantly x-ray intensity, do not lead to bragg peaks on x-ray cameras, nor have a large signal to noise ratio. Most available transmissive BPMs are based on: (1) deposited segmented diamond windows [1,2] with measurement ranges in the  $\mu\text{m}$ -region and fast acquisition times. (2) two 90°-turned ionization chambers with split up electrodes [3,4], wherefore the measuring range is in the mm-range. They have in common that they need four raw signals to calculate a 2D-position  $xy$ -location. A conventional ionization chamber at a synchrotron beamline consists of two plates, which are arranged parallel to each other and give one signal. They have the advantage to measure at low as well as high energies, whereas the absorption can be adjusted by using heavier gas like Krypton for higher energies or Nitrogen for lower energies [5].

The new evaluated design of a beam position ionization chamber is based on three signals.

## MATERIAL AND METHODS

### Design and FEM

Figure 1 shows the design of the electrodes: two small electrodes on the front and back, which are connected to the same signal wire; two bigger measuring electrodes, which are each connected to a single signal wire; one large high voltage electrode. The highest density of the electric field is reached in between the parallel 6 mm gap (see Fig. 1b).

### Signal Evaluation

The three raw signals can be used to calculate the  $xy$ -coordinates. The transformation (Eq. 1) can be written within a matrix quite similar to the Clarke-transformation [6],

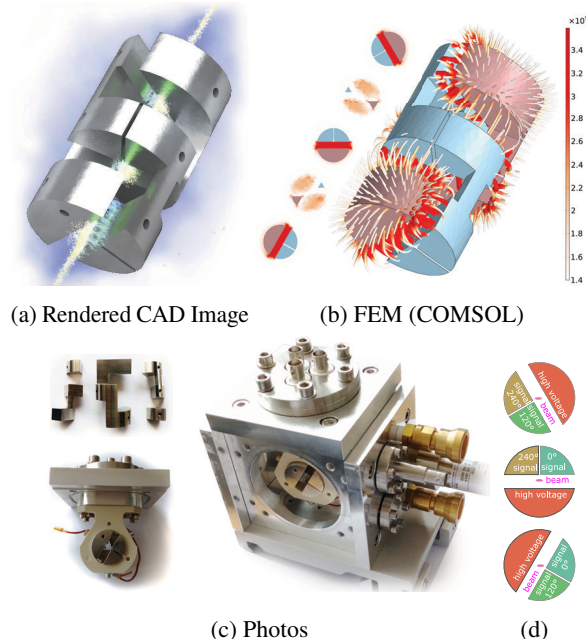


Figure 1: (a) expected location of gas-ions (*light-yellow*), trajectory of free electrons (*lightblue*) (b) electrostatic: measuring electrodes (blue), HV electrode (red), tube-thickness and color: electric field strength [ $\text{V m}^{-1}$ ] (d) signal and HV connections.

which is well-known in electromechanical theory. The values of  $u, v$  and  $w$  are normalized, taking into account the sum of all intensities. The values  $c_i$  are fixed calibration parameters. They can be obtained by linear optimization using measured data.

$$\begin{bmatrix} x \\ y \end{bmatrix} = \begin{bmatrix} c_{x0} & c_{x1} & c_{x2} & c_{x3} \\ c_{y0} & c_{y1} & c_{y2} & c_{y3} \end{bmatrix} \cdot \begin{bmatrix} 1 \\ u \\ v \\ w \end{bmatrix} \quad (1a)$$

$$u = \frac{I_A}{I_A+I_B+I_C} \quad v = \frac{I_B}{I_A+I_B+I_C} \quad w = \frac{I_C}{I_A+I_B+I_C} \quad (1b)$$

### Signal-Position Calibration

For the calibration several tuples  $\langle u_i, v_i, w_i, x_i, y_i, p_i \rangle$  are needed. They have to include the three measure signal values and the corresponding true real  $x$  and  $y$  positions. Weighting or proportional factors  $p_i(x, y)$  assure that some regions will be taken more into account than others. For both algorithms five or more linear independent point assignments are needed. More values will improve the precision of calibration.

**Calibration Method I: Simplex-algorithm including weighted residuals** To calculate the different coefficients  $c_*$ , a Simplex-algorithm was applied. All examples are shown for the  $y$ -axis.  $x$ -coordinate will be calculated similar to the procedure shown in that chapter. The expression  $x$  in

\* marcel.goerlitz@desy.de

# DESIGN AND RAY-TRACING OF THE BEATS BEAMLINE OF SESAME\*

G. Iori<sup>†</sup>, M. Al’Najdawi<sup>1</sup>, M. Al Shehab, A. Lausi, SESAME, Allan, Jordan  
 I. Cudin, M. Altissimo, Elettra-Sincrotrone Trieste, Basovizza, Trieste, Italy  
 T. Kołodziej, NSRC SOLARIS, Jagiellonian University, Krakow, Poland  
 P. Van Vaerenbergh, J. Reyes-Herrera, A. Kaprolat, ESRF, Grenoble, France  
<sup>1</sup>also at MAX IV Laboratory, Lund University, Sweden

## Abstract

The European Horizon 2020 project BEAmline for Tomography at SESAME (BEATS) has the objective to design, procure, construct and commission a beamline for hard X-ray full-field tomography at the SESAME synchrotron in Jordan. In this paper we present the raytracing simulations performed to quantify the performance and verify the optical design of the beamline. The specifications of a vertically-deflecting double multilayer monochromator are investigated comparing multilayer mirrors with different meridional slope error. The use of a pinhole in the beamline Front-End (FE) acting as a secondary source with enhanced spatial coherence is discussed for phase-contrast applications. We anticipate that the BEATS beamline will fulfill the needs of a heterogeneous community of users of X-ray tomography at SESAME.

## INTRODUCTION

The BEATS beamline will operate an X-ray micro tomography station serving a broad user community. The scientific case of the BEATS beamline is the result of close interactions with the scientific communities of current and potential synchrotron users in the SESAME region. Special emphasis is given to the regional aspect, taking stock of existing research contributions from the region. Four key areas for the scientific case for BEATS in the SESAME landscape are identified:

- Archaeology and Cultural Heritage – This includes the study of archaeological materials such as human, plant or animal remains and artefacts of animal bone, antler and teeth.
- Health, Biology and Food – Research in bone and dentistry; in vitro imaging of the brain vascular and neuronal network and of other organs such as the eye, heart, lung and liver; musculoskeletal and soft tissue imaging; bio mineralisation; entomology; food science.
- Material science and Engineering – Study and development of light and composite materials for construction and transport engineering; energy materials research
- Geology and Environment – Research in soil and rock characterization.

Applications within other domains as well as the possibility to provide services to industrial and private sector users are also envisaged.

\* BEATS project has received funding from the EU’s H2020 framework programme for research and innovation under grant agreement n°822535.

<sup>†</sup> gianluca.iori@sesame.org.jo

## BEAMLINE DESIGN

The design of the beamline allows for a variety of operation modes and ensures sufficient photon flux density in filtered white beam or monochromatic beam from 8 keV and up to 50 keV. The broad energy range and required high photon flux is achieved by a 3 T wavelength shifter insertion device (ID) installed on one of SESAME’s short straight sections. The beamline can work with either monochromatic or filtered white beam, with minimum energy tunable by absorbers in the FE. The beam size at the sample position and the propagation distance between sample and detector can be varied displacing the rotation and detector stages along the beam path. For measurements requiring high sensitivity and spatial coherence of the beam (e.g., for phase-contrast tomography), the beamline FE slits are partly closed to define a smaller, secondary source with higher spatial coherence.

### Layout

The beamline FE comprises photon absorbers and stoppers, a mask defining a useful beamline aperture of 1.8 mrad (h) by 0.36 mrad (v), a CVD diamond window separating the machine and the beamline vacuum, filters and primary slits. The main optical component is a Double Multilayer Monochromator (DMM) placed outside of the SESAME storage ring tunnel in a dedicated optics hutch. The experimental station is located approximately 45 m from the photon source and comprises secondary slits, a linear fast shutter allowing to reduce exposure of delicate samples [1], a high precision sample positioning and rotation stage, and two full-field detectors based on scintillating screens and sCMOS sensor cameras mounted on a common granite stage [2].

### Raytracing

The BEATS optical design is verified with simulation tools included in the OASYS suite [3]. Raytracing calculations are performed in ShadowOui, while power profiles are computed using XOPPY. Software and notebooks for the reproduction of this work are available on Zenodo [4].

### Heat Load

The beam power density is calculated for each beamline component sustaining the white beam during operation or possibly in direct sight of the white beam with the OASYS *Wiggler Radiation* widget [5]. The power density profile of the incoming or absorbed beam is used as input for thermal verification with commercial Finite-Element software. Due to the position of absorbers and apertures in the storage ring

# DESIGN OF MONOCHROMATIC AND WHITE BEAM FLUORESCENCE SCREEN MONITORS FOR XAIRA BEAMLINE AT THE ALBA SYNCHROTRON

J.M. Álvarez<sup>†</sup>, C. Colldelram, N. González, J. Juanhuix, J. Nicolas, I. Šics  
ALBA Synchrotron Light Source, Cerdanyola del Vallès, Spain

## Abstract

XAIRA, the hard X-ray microfocus beamline at ALBA, includes three monochromatic fluorescence screens and one water cooled white beam monitor in its layout, mounting respectively YAG:Ce and polycrystalline CVD diamond as scintillator screens. All monitors share the same design scheme, with a re-entrant viewport for the visualization system that allows reducing the working distance, as required for high magnification imaging. The scintillator screen assembly is held by the same CF63 flange, making the whole system very compact and stable. The re-entrant flange is driven by a stepper motor actuated linear stage that positions or retracts the screen with respect to the beam path.

To cope with high power density (18,6 W/m<sup>2</sup>) on the white beam monitor 100 μm-thick diamond screen, an InGa-based cooling system has been developed. The general design of the new fluorescence screens, to be used also in other ALBA's upcoming beamlines, with particular detail on the water-cooled white beam monitor, is described here.

## INTRODUCTION

This paper reviews the design of the Fluorescence Screen Monitors (FSM) of XAIRA, the microfocus Macromolecular Crystallography (MX) beamline at ALBA. Two types of FSM have been developed: the water-cooled White Beam Fluorescence Screen (FSWB) and the Monochromatic Fluorescence Screen Monitor (FSM1 and FSM2), which mount respectively as scintillator screen polycrystalline CVD and YAG:Ce.

Due to the high heat flux deposition (18,6 W/m<sup>2</sup>) on the FSWB screen, FEM analysis has been performed to optimize the cooling design, adopting InGa contact interface to enhance heat transmission.

The design has been conceived to produce a compact and stable instrument to be used as a standard FSM in future beamlines.

## TECHNICAL SPECIFICATIONS

From an optical point of view the design of the FSM must comply with the following specifications:

- Beam envelope in each FSM should represent ~25% field of view (FOV) to allow severe beam misalignment.
- Partial beam transmission through diagnostic device is not required.

- Each beam dimension should be made at least of 100-200 pixels to allow identification of beam shape pathologies.
- Two different configurations of screen-imaging system are proposed for FSWB or FSM1 and FSM2 (Fig. 1).

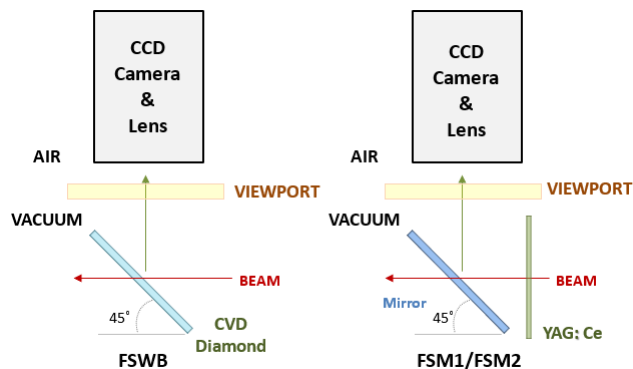


Figure 1: Geometrical configurations of the FSMs.

Both camera-lens system and fluorescence screen support should be mounted on the same moving DN63 CF flange, maximizing compactness and imaging system stability.

## SYSTEM DESCRIPTION

### General Description

The camera-lens system and the sensible scintillator screen are mounted on a common moving re-entrant flange. This flange is assembled on a DN63 CF welded bellow that is actuated by a linear moving stage consisting on a high precision ball screw, high precision linear guideways and low backlash stepper motor. Finally, the system is controlled with absolute encoder feedback. (Fig. 2).

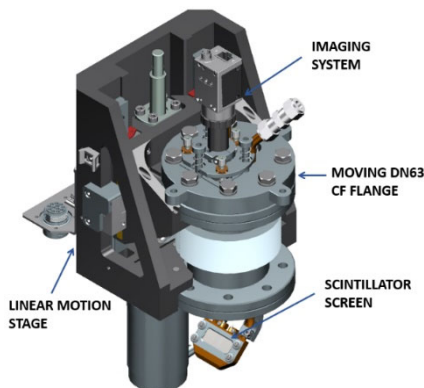


Figure 2: FSWB assembly.

<sup>†</sup> jalvarez@cells.es

# X-RAY FACILITY FOR THE CHARACTERIZATION OF THE ATHENA MIRROR MODULES AT THE ALBA SYNCHROTRON

A. Carballedo<sup>†</sup>, D. Heinis, C. Colldelram, C. Cuní, N. Valls Vidal, O. Matilla, J. Marcos, A. Sánchez, J. Casas, J. Nicolàs, ALBA Synchrotron, Cerdanyola del Vallès, Spain  
N. Barrière, M. J. Collon, G. Vacanti, Cosine Measurement Systems, Warmond, The Netherlands  
E. Handick, P. Müller, M. Krumrey  
Physikalisch-Technische Bundesanstalt (PTB), Berlin, Germany  
I. Ferreira, M. Bavdaz, European Space Agency (ESA), Noordwijk, The Netherlands

## Abstract

MINERVA is a new X-ray facility under construction at the ALBA synchrotron specially designed to support the development of the ATHENA (Advanced Telescope for High Energy Astrophysics) mission [1]. The beamline design is originally based on the monochromatic pencil beam XPBF 2.0 from the Physikalisch-Technische Bundesanstalt (PTB), at BESSY II already in use at this effect [2]. MINERVA will host the necessary metrology equipment to integrate the stacks produced by the cosine company in a mirror module (MM) and characterize their optical performances. From the opto-mechanical point of view, the beamline is made up of three main subsystems. First of all, a water-cooled multilayer toroidal mirror based on a high precision mechanical goniometer, then a sample manipulator constituted by a combination of linear stages and in-vacuum hexapod and finally an X-ray detector which trajectory follows a cylinder of about 12 m radius away from the MM. MINERVA is funded by the European Space Agency (ESA) and the Spanish Ministry of Science and Innovation. MINERVA is today under construction and will be completed to operate in 2022.

## INTRODUCTION

The ATHENA telescope is a space observatory that will address fundamental questions about energetic objects (accretion disk around black holes, large-scale structure, etc...). One of the key elements of the telescope is the innovative modular architecture of its optics subdivided by 15 concentric rings and filed by about 600 sub-systems called mirror modules (MMs). The technology used to manufacture the MM is based on the Silicon Pore Optics technology developed at cosine. At XPBF 2.0, cosine is currently optimizing the method to produce MMs at large scale [3] and today MINERVA is built to strengthen and boost their production and characterization while preserving the interoperability with XPBF 2.0. The final angular resolution of ATHENA strongly depends on the alignment accuracy between the 4 stacks constituting a singular MM. It is why stability, accuracy and repeatability are crucial parameters for the opto-mechanical components specifications.

## GENERAL BEAMLINE DESCRIPTION

MINERVA takes port 25 at the ALBA experimental hall. This port is fed by a bending magnet source and provides optimal spatial distribution to allow future upgrades of the components. The beamline will operate under Ultra High Vacuum conditions (UHV) from the source to the exit of the photon shutter, where a vacuum window (Silicon Nitride) will separate them from the rest of the beamline. Downstream the vacuum window, the beamline will operate under High Vacuum conditions (HV, 10-5 mbar). The beamline will assess the absolute distance between the end detector and the MM origin with the adequate accuracy needed by the data analysis. This measurement is performed by the combination of laser tracking technology and high positioning repeatability of the mechanics. The whole beamline will be controlled using the Tango control system, standard at ALBA. MINERVA follows the optical layout sketched in Fig. 1. In there are presented the following components:

- A bending magnet of the ALBA storage ring as the X-ray source and the front-end elements.
- A toroidal mirror (M1) with a multilayer coating. The mirror deflects the beam inboard, with a total deflection angle of 14 degrees. It collimates the beam in both the horizontal and vertical planes. Its reflective surface selects a narrow bandwidth at the nominal energy of 1.0 keV. This element is enclosed in the optics hutch.
- A filter unit consisting of one Si3N4 membrane coated with a thin Al deposition. This filter removes the visible light reflected by the M1 mirror.
- A set of pinholes ranging from 10  $\mu\text{m}$  to 500  $\mu\text{m}$  in diameter.
- A photon beam shutter which includes a fluorescent screen beam diagnostic unit.
- A Si3N4 window, which separates the upstream UHV section from the downstream HV.
- A four-blade slit system that allow for apertures from fully closed to more than 10 mm in aperture.

<sup>†</sup> acarballedo@cells.es

# DESIGN OF A HIGH-PRECISION LIFTING SYSTEM FOR THE HL-LHC HEAVY COMPONENTS IN THE INTERACTION REGION

F. Micolon, M. Sosin, CERN, 1211 Geneva 23, Switzerland

## Abstract

Given the high radiation level and the tight alignment tolerances, the HL-LHC interaction region components are designed to be realigned remotely using motorized supporting jacks, as human interventions in these zones must be limited to the strict minimum.

A position adjustment system will allow a vertical and horizontal displacement of each jack support by at least +/- 2.5 mm with a resolution of less than 10 μm. The weight of the supported elements, up to 170 kN and transverse loads reaching 30 kN, will have to be remotely moved by means of mechanical actuators. The system will be exposed to a cumulated radiation dose of up to 2 MGy during the 15 years of lifetime [1].

To comply with these requirements, an extensive design effort has been initiated at CERN to study the possible system layouts. This includes the prototyping of various solutions, studying subsystems through dedicated test setups and using simulations to obtain a clear understanding of the mechanical principles at play.

This paper reports on the work undertaken to design the high-precision lifting system, the various mechanical analysis carried out, and their main outcome. It reviews the proposed solutions and their expected alignment performance.

## SYSTEM INTEGRATION REQUIREMENT

The heavy components of the HL-LHC interaction region are designed to be supported on standardized HL-LHC jacks, closely derived from the original design of the LHC supporting jacks [2].

These jacks are based on the concept of a tilting-column with two bearings on each end (see Fig. 1). They allow the accurate positioning within a range of +/-10 mm of the top bearing in one direction of the horizontal plane, while the other horizontal position is left free to move.

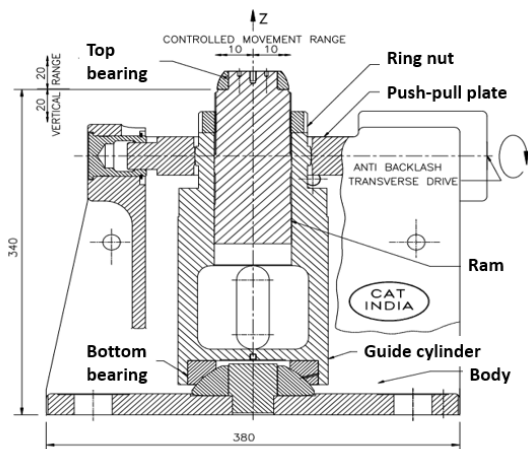


Figure 1: Transverse cross section of the LHC jack [2].

Like in the LHC, the heavy accelerator components are designed to be supported on three jacks located on two support planes on both ends of the component (see Fig. 2).

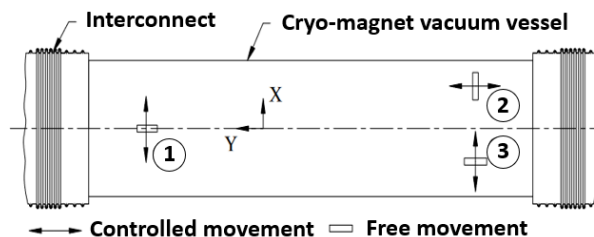


Figure 2: Top view of a cryomagnet - supporting jacks at position 1, 2 and 3 – adapted from [1].

Jacks 1 and 3 will permit the accurate positioning of the component in the radial (X) direction while jack 2 will determine the position in the longitudinal direction (Y).

The height (Z) of the component can be controlled on each jack by lifting the ram inside the guide cylinder, following which the ring nut is adjusted to retain the chosen height (see Fig. 1).

In the HL-LHC interaction region, the ram will be permanently supported by the motorized lifting system. Thanks to this, the height can be adjusted remotely without a manual intervention underground. Consequently, the lifting system must fit inside the bottom cavity of the guide cylinder to allow actuation of the ram from below.

## STICK SLIP AND SYSTEM STIFFNESS REQUIREMENTS

### The Principle of Frictional Stick-Slip

The so-called « stick-slip » describes the oscillatory motion affecting most common materials when they are sliding. For example it commonly occurs when rubbing a wet finger on the edge of a crystal glass or when dragging a chair on the floor. The amplitude of the sliding motion is directly dependent on the materials in contact and the system stiffness. With a simple demonstration, based on the conservation of energy [3], it can be shown that the stick slip amplitude for a sliding system is:

$$d = \frac{2.N.(\mu_s - \mu_d)}{k} = \frac{N.(\mu_s - \mu_{stop})}{k} \quad (1)$$

With N being the normal force at the sliding interface,  $\mu_s$ ,  $\mu_d$ ,  $\mu_{stop}$  respectively the static, dynamic and rest friction coefficient, and k the system stiffness along the sliding direction. In our case, this amplitude defines the alignment resolution of the system. This highlights the importance of good material selection for loaded sliding surfaces and the need for sufficient system stiffness along the alignment direction.

## ALL APPLICATIONS OF THE ALBA SKIN CONCEPT

Llibert Ribó†, Nahikari Gonzalez<sup>1</sup>, Joaquín González<sup>2</sup>, Alejandro Crisol<sup>1</sup>,  
Antonio Carballo<sup>1</sup>, Luke Adamson<sup>3</sup>, Elliot Reece Jane<sup>4</sup>, Claude Ruget<sup>1</sup>,  
Judith Juanhuix<sup>1</sup>, Josep Nicolas<sup>1</sup>, Carles Colldelram<sup>1</sup>,

<sup>1</sup>ALBA Synchrotron, Carrer de la Llum 2 26, 08290 Cerdanyola del Vallès, Spain

<sup>2</sup>MAX IV Laboratory, Lund University, Box 188, SE 221 00 Lund, Sweden

<sup>3</sup>Australian Synchrotron, 800 Blackburn Rd, Clayton VIC 3168, Melbourne, Australia

<sup>4</sup>FMB Oxford, Ltd. Units 1 4 Ferry Mills, Osney Mead, Oxford, OX2 0ES, United Kingdom

### Abstract

During the ALBA design phase, the protein macromolecular protein crystallography beamline, XALOC, required several in-house developments. The major part of these designs was at the end station where the necessity of customization is always much higher. The most relevant of these instruments was the beam conditioning elements table [1]. This accurate stage, which supports the diffractometer as well, includes the four movements required to align the components to the nominal beam as well as position the diffractometer. This design compacts, especially the vertical and pitch movements, both in a single stage, with a couple of stages for all four excursions. The solution maximises the stiffness and preserves at the same time the resolution close to  $0.1\mu\text{m}$  while being able to withstand a half tone of payload. Thanks this compactness and performances this design concept, the vertical and pitch combined stage, was not only applied at XALOC for its diffractometer and detector table, but it has been widely adapted at several ALBA beamlines: at NCD-SWEET [2] as a detector table, a beam conditioning elements table [3] and sample table, at MSPD beamline as the KB table, at NOTOS beamline as metrology table, and also at the new ESA MINERVA beamline [4] for their sample mirror modules positioning. Beamlines have not been the only beneficiaries of this design, also different kind of instrumentation like an hall probe measuring bench [5], and even a stitching platform for the ALBA optics laboratory [6]. Moreover, the concept has outreach ALBA and has been adopted also at other facilities worldwide, synchrotrons and also scientific instrumentation suppliers around Europe. This poster presents most of the applications of the skin concept and their variations and main measured performances.

### INTRODUCTION

The original design of the ALBA Skin Concept Design [1] was the diffractometer and beam conditioning elements table for the protein macromolecular protein crystallography beamline, BL13 XALOC [7]. The beamline has a simple optical lay-out based in three main instruments a S111 channel-cut DCM monochromator and a Kirkpatrick-Baez (KB) mirrors pair. The different beamline configurations, vertically and horizontally mirrors focus or unfocused, divert the beam at sample position. The diffractometer, the sample, has to follow the beam excursions.

† lribo@cells.es

Moreover, the previous beam conditioning elements have to be aligned jointly with the diffractometer, to the beam. All this system has to be positioned not only on position but also colinear with the beam path. These requires for this positioning system four axis (vertical, transversal, pitch and yaw), with resolutions well below  $1\mu\text{m}$  and  $1\mu\text{rad}$  for ranges up to 70 mm for the translations and 15 mrad for the rotations. In addition, these specifications have to be met still being able to withstand heavy load capacity, up to half a tone, and at the same time being accurate and stable.

### ORIGINAL DESIGN

High payload, accuracy, resolution and stability are requirements that are very difficult to achieve all together. Moreover, the diffractometer and beam conditioning elements define an elongated shape. In order to achieve proper performance for all characteristics at the same time it was proposed the skin concept [1] where vertical translation and pitch were compact in a single stage as well as for the transversal and yaw movements.

While accuracy and resolution, but also the payload, are assured by means the quality of the mechanical elements the stability is achieved by several different strategies. The quality of the mechanical elements is guaranteed selecting the proper supplier's: high precision preloaded linear guides and oversized balls grind spindles for instance. In the other hand the stability approach is based on a design architecture intrinsically stable: using a big granite reference base, compacting movements by pairs: a translation and a rotation in a single stage, placing these stages surrounding the granite base (skin concept), with approach the loads are as close as possible to the granite minimizing the mass level arms, etc... With this configuration, especially for the combined vertical and pitch movements, the stage is placed like an inverted U shape along the granite with a vertical motion at each of the longitudinal extremes of the granite, light grey at Fig. 1a. A motor synchronized motion

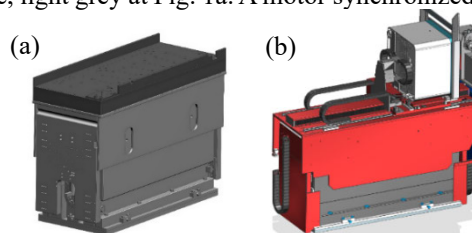


Figure 1: a) ALBA BL13 Diffractometer table. b) 3D model of the BL13 XALOC detector table.

# DEVELOPMENT AND APPLICATIONS OF THE WHITE BEAM POSITION MONITOR FOR BENDING MAGNET BEAMLINES

Chao-Yu Chang<sup>†</sup>, Chia-Feng Chang, Chien-Hung Chang, Shih-Hung Chang,  
Liang-Chih Chiang, Robert Lee, Bo-Yi Liao, Chin-Yen Liu,  
National Synchrotron Radiation Research Center (NSRRC), Hsinchu, Taiwan

## Abstract

We developed a white beam position monitor to be applied in beamlines with bending magnets. By 0.1 mm light-receiving opening, the beam is split and converted to a photocurrent intensity which can be used to detect the size and position of the beam  $\leq 50$  mm, and to align the locations of beamline components. A stop-beam measurement method is utilized, so it cannot monitor the beam in real time.

The motorized stage of the monitor has a range of motion up to  $\pm 25$  mm with position accuracy of  $\leq 1$   $\mu\text{m}$  and vacuum capability of  $\leq 5 \times 10^{-10}$  Torr, which is compatible with ultra-high vacuum environments. In addition, taking the thermal load 62.89 W of the TPS 02A beamline as an example, the thermal deformation of the analog monitor opening lead to a result that the measured value will have a maximum of 2  $\mu\text{m}$  from the center of the beam.

The monitor is equipped with other components designed by NSRRC colleagues, including a motor control system, a four-channel current amplifier, an EPICS control system, and a GDA data acquisition and analysis software. The whole system has been successfully applied in the TPS 02A beamline. All features are verified and the performance meets the requirements. Besides, the positioning tasks of Slits1 was accomplished and the position variation of the light source was detected by this beam position monitor.

## INTRODUCTION

When it comes to monitoring light source and calibration of beamline components, the size and position of the beam are extremely important information, so a beam position monitor with good performance is a necessity. The design of a white beam position monitor is more difficult than a mono beam position monitor, because the thermal load of white light will cause thermal deformation of the material such that the accuracy becomes worse. Moreover, there is more scattered stray light in the white light region than that in the mono beam region. The background value of the white light area is higher, and the scattered stray light passing through different structures may also have an asymmetric spatial distribution. Therefore, a white beam position monitor needs to be designed with an appropriate structure to accurately interpret the beam position signal while limiting the proportion of external stray light entering the detector. These are the key points that must be achieved in the design of the mechanical structure.

The white beam position monitor described in this report is based on various measurement requirements proposed by users, such as calculating the center position of the beam, obtaining the overall beam imaging distribution, analyzing the quality and stability of the beam, and calibrating the zero position of beamline components, and other functions. Because the above requirements are suitable for light-blocking measurement methods, the beam will be completely shielded during measuring. Therefore sample measurements in the experimental station and real-time feedback adjustments of beam position cannot be performed at the same time.

## MECHANICAL DESIGN

The white beam position monitor for the beamlines of deflection magnet is shown in Fig. 1. The internal mechanism and accessory design [1] is consisted of (1) cooling water inner and outer pipes (cooling water flows from the outside to the inside of the pipe), (2) fixture (fixing the temperature and electrical current measuring circuits to avoid direct radiation exposure during operation), (3) sapphire sheet (resistivity of  $1 \times 10^{11} \Omega\text{-cm}$ , excellent electrical insulation property, and good thermal conductivity and mechanical strength performance), (4) tungsten alloy plate (high melting point and good conductivity, as a metal substrate for receiving electron flow), (5) oxygen-free copper (C10100) cover (fixed on the body with a screw lock and ceramic gasket, and insulated from the ground), (6) oxygen-free copper cooling seat body, (7) composed of components such as the lower cover of the oxygen-free copper cooling seat [2].

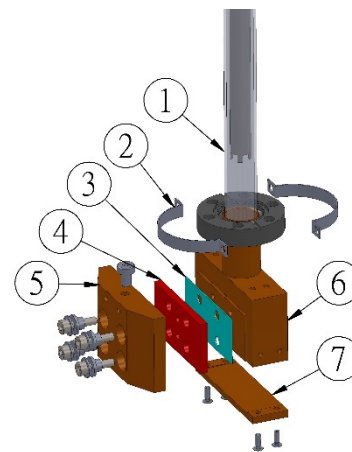


Figure 1: Internal mechanism and accessories of white beam position monitor.

<sup>†</sup>chang.cy@nsrrc.org.tw

## LINAC SECTION 3 AND 4 REPLACEMENT AT THE CANADIAN LIGHT SOURCE

E. X. Li\*, X. Shen†, R. Zwarich\*, Canadian Light Source, Saskatoon, Saskatchewan, Canada

### Abstract

The Canadian Light Source Inc. (CLSI), opened in 2004 and located in Saskatoon, Saskatchewan, Canada, is a third-generation synchrotron light source facility with a 2.9 GeV storage ring. CLSI was built based on the Saskatchewan Accelerator Laboratory (SAL) with its LINAC. The SAL LINAC was built in 1960s and refurbished to operate at 250 MeV in 2002. It was also designed at an average beam power up to 46KW. To be used by CLS, the LINAC was modified for operation at pulse power levels of 25 MW with the current 100 mA. The modified LINAC consists of an electron gun and section 0 to 6 (Fig. 1), Energy Compression System (ECS) and Section 7.

The LINAC has kept a steady performance throughout the years, along with many repairs and replacements – most of which are preventative. The original Varian type accelerating Sections are planned to be replaced gradually by SLAC type Sections. Section 3 and 4 are two of the original 3 Varian type sections left in CLS - with over 55 years of service, they were accumulating vacuum leak problems from time to time. The replacement of Section 3 and 4 was completed in 2020. The mechanical consideration of the Section 3 and 4 replacement mainly includes upgrading supporting structures, designing Waveguides, modifying LCW systems, getting solution to move the sections around in the LINAC tunnel, etc.

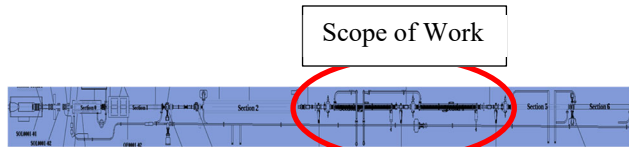


Figure 1: CLS gun and section 0-6.

### BACKGROUND

CLS has encountered gun failure in 2018, and the repairing of the device took quite a long time. The old Varian Section was discontinued and no spare could be available. We have been experiencing some vacuum leaks from the old Sections over time. It is a huge risk to run the old Varian Sections that were built at the same time as the electron gun. The old Varian Sections in CLS had been planned to be replaced gradually.

The goal this time was to replace the Section 3 and 4 and add more components together with the new Sections in between Section 2 and 5 (Fig. 2). New added components include Ion pumps, View Screens, Vacuum Valves, Steer Magnets, FCT's, CCG's, TCG's and BPM's. As well, RF Loads were replaced and Waveguides were redesigned.

\* CLS Engineering group  
 † CLS AOD group



Figure 2: Overview of the new installation.

### OLD VARIAN SECTION VS. NEW SLAC SECTION

The old Varian Section (Fig. 3a) in CLS weighs around 2 tons; its outside diameter is close to 400mm and the total length is around 5 meters. Solenoids are located surrounding outside of the Varian Section and need separate cooling.

The new SLAC Sections (Fig. 3b) are quite small compare to the old Varian ones: each one weighs around 400 kg, the contour diameter is about 145mm, and the length is around 3.1 meters. The SLAC Sections do not have solenoids.

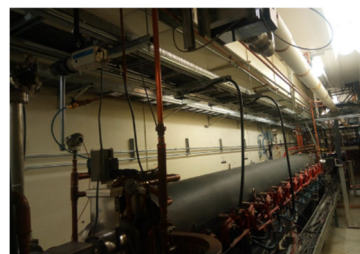


Figure 3a: An old Varian section.



Figure 3b: A new SLAC section.

# MAGNET MEASUREMENT SYSTEMS FOR THE ADVANCED PHOTON SOURCE UPGRADE\*

Scott Izzo†, Animesh Jain, Charles Doose, William Jansma  
Argonne National Laboratory, Lemont, IL 60439, USA

## Abstract

The present storage ring at the Advanced Photon Source will be replaced with a new ring based on a Multi-Bend Achromat (MBA) design as part of an upgrade currently in construction. The new ring will require about 1320 new magnets which need to be measured and fiducialized to ensure field quality and alignment requirements are met. Seven test benches were designed and built to meet these measurement requirements. Field quality in the multipole magnets is measured using four rotating coil benches, whereas the longitudinal gradient dipoles are mapped using a Hall probe system. Two rotating wire benches are used to find the magnetic centers of multipoles and relate them to magnet fiducials using laser trackers. Mechanical designs of the measurement benches are presented.

## INTRODUCTION

The Advanced Photon Source-Upgrade (APS-U) project [1] is under construction at Argonne National Laboratory. As part of this upgrade the present storage ring will be replaced with a new ring based on a Multi-Bend Achromat design. The new storage ring will require about 1320 new magnets and magnetic measurements are needed to characterize and fiducialize all these magnets to ensure field quality and alignment requirements are met.

Seven specialized test benches, as listed in Table 1, were designed and built to meet the measurement requirements for the APS-U project. Four of these benches are rotating coil benches for measuring field harmonics in multipole magnets (quadrupoles Q1-Q3, Q6 and Q7, sextupoles S1-S3, fast correctors FC, and combined dipole-quadrupole magnets Q4, Q5, Q8, M3 and M4). Two rotating wire benches were setup to fiducialize all the multipole magnets. The longitudinal gradient dipoles (M1, M2) are mapped using a Hall probe system which is also designed and built in-house. The salient mechanical features of these benches are described in the following sections.

## COMMON FEATURES

All the rotating coil and rotating wire benches employ similar design features and use standardized commercial hardware to the extent possible. All benches use a block of granite supported by a custom steel stand as the base on which the measurement equipment is mounted. The stand has six adjustable feet for levelling and to distribute the load. The magnet under test (MUT) is placed near the

center of the granite on a 1.0-inch-thick ground steel plate. All APS-U magnets have built-in side and bottom reference surfaces and the benches make use of these same surfaces to quickly align the magnets to the rotating coil axis by banking against stop blocks fixed on the magnet support plate. Magnets of different sizes are accommodated on the same bench by changing aluminum shims between the stop blocks and the magnet reference surfaces.

Table 1: Magnetic Measurement Benches for APS-U

Bench	Magnet Types	Quantity
Rotating Coil (RC1)	Q1-Q6	492
Rotating Coil (RC2)	S1-S3, FC	411
Rotating Coil (RC3)	M3, M4	123
Rotating Coil (RC4)	Q7, Q8	164
Rotating Wire (RW1)	Q1-Q5, S1-S3	656
Rotating Wire (RW2)	Q6-Q8, M3, M4	369
Hall Probe (HP1)	M1, M2	164

The rotating coil and rotating wire systems have gravity sensors on the rotary encoders and magnet support plate to allow measurement of the magnetic roll angle in a frame where the bottom reference surface of the magnets is level. The measurement resolution is  $\sim 0.010$  mrad and the absolute angle measurement is calibrated to better than 0.1 mrad.

## ROTATING COIL SYSTEMS

A total of four rotating coil measurement benches (RC1-RC4) were designed and built to accommodate the large variety and quantity of magnets needed for the APS-U project (see Table 1). A typical rotating coil bench is shown in Fig. 1.

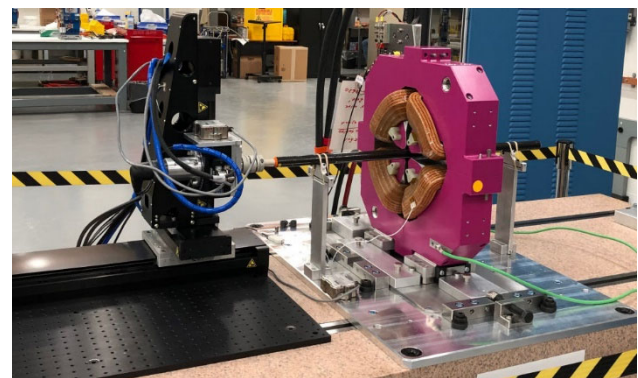


Figure 1: One of the rotating coil benches showing the granite block, XYZ- $\theta$  stages, magnet support plate, stop blocks and customized shim plates for alignment in X, Z.

\* This research used resources of the Advanced Photon Source, a U.S. Department of Energy (DOE) Office of Science User Facility at Argonne National Laboratory and is based on research supported by the U.S. DOE Office of Science-Basic Energy Sciences, under Contract No. DE-AC02-06CH11357.

† email address: sizzo@anl.gov

## DESIGN AND FABRICATION CHALLENGES OF TRANSITION SECTION FOR THE CWA MODULE\*

S. Lee†, W. Jansma, A. Siy<sup>1</sup>, S. Sorsher, K. Suthar, E. Trakhtenberg, G. Waldschmidt, A. Zholents  
Argonne National Laboratory, Lemont, IL 60439, USA  
<sup>1</sup> also at University of Wisconsin, Madison, WI 53715, USA

### Abstract

An effort to build Argonne's Sub-THz Accelerator (A-STAR) for a future multiuser x-ray free-electron laser facility proposed in [1] is underway at Argonne National Laboratory. The A-STAR machine will utilize a compact collinear wakefield accelerator (CWA) assembled in modules. To extract the wakefield and monitor beam position downstream of each module, a 45-mm-long transition section (TS) has been proposed and designed. This paper will discuss the design and fabrication challenges for production of the TS.

### INTRODUCTION

The CWA TS consists of multiple miniature components that must be brazed or TIG welded vacuum leak-tight using a multi-step brazing processes with filler material of successively lower temperature to maintain the integrity of previously brazed joints. The internal vacuum surface geometry of the TS will be fabricated by electroforming copper (Cu) on an aluminum (Al) mandrel and chemically dissolving the Al mandrel to create the structure. Micro-manufacturing processes such as high-precision milling and wire electric discharge machining (EDM) will be utilized to produce the TS Cu base. A cold drawing process will be considered to produce flexible waveguide tubes. The CWA vacuum chamber module is comprised of a corrugated tubing/strongback (CTS) unit, a bi-metal vacuum flange, and a TS unit with a bellows as shown in Fig. 1. The following sections will focus on the design and fabrication challenges of the TS unit for the CWA vacuum chamber module.

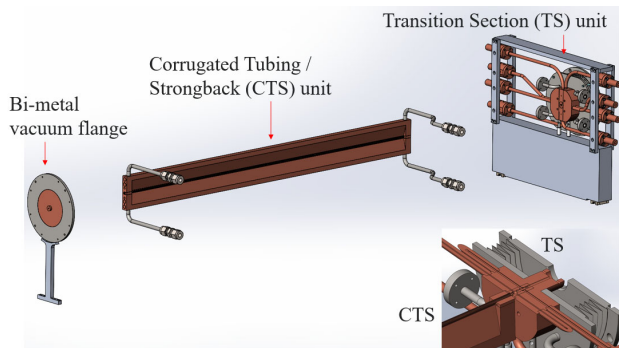


Figure 1: CWA vacuum chamber module and its components for the compact collinear wakefield accelerator.

\* This research used resources of the Advanced Photon Source, a U.S. Department of Energy (DOE) Office of Science User Facility and is based on work supported by Laboratory Directed Research and Development (LDRD) funding from Argonne National Laboratory, provided by the Director, Office of Science, of the U.S. DOE under Contract No. DE-AC02-06CH11357.

† shlee@anl.gov

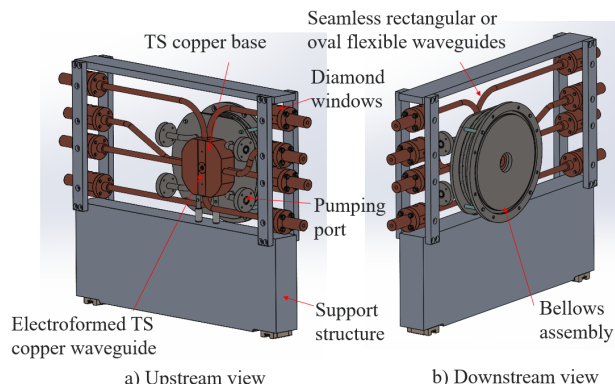


Figure 2: Transition section and its components for the compact collinear wakefield accelerator.

### DESIGN OF TRANSITION SECTION

The TS unit is comprised of an electroformed Cu waveguide, a machined Cu base, eight seamless flexible rectangular or oval waveguides, diamond windows, and a stainless-steel bellows assembly with vacuum ports (see Fig. 2). The eight waveguides are utilized to extract unused TM01 accelerating mode from the output coupler of the corrugated waveguide while allowing the TE11 transverse mode to pass through to the integrated offset monitor (IOM) for beam offset measurements [2]. As shown in Fig. 3, its design consists of a four-way rectangular waveguide cross, which interfaces to the circular waveguide via tapers and a circular cavity. Immediately following the output coupler cross is a notch filter, designed to reflect the TM01 mode. Then, the IOM is located downstream to couple the transverse TE11 modes for beam offset measurements.

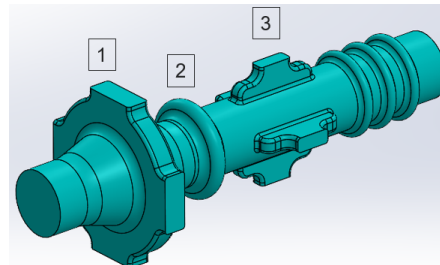


Figure 3: Geometry of the mandrel: (1) TM01 output coupler, (2) notch filter, and (3) integrated offset monitor.

Electroforming is utilized to fabricate complex features of the output coupler, notch filter and IOM in the TS. A negative form of the internal TS features is machined on an Al mandrel, and reference holes are added for alignment during future brazing and micro-machining steps. The mandrel is electroplated with Cu, and Al is then chemically dissolved, leaving behind the TS Cu structure. Finally,

# MECHANICAL DESIGN OF A COMPACT COLLINEAR WAKEFIELD ACCELERATOR\*

S. Lee<sup>†</sup>, S. Doran, W. Jansma, A. Siy<sup>1</sup>, S. Sorsher, K. Suthar, E. Trakhtenberg, G. Waldschmidt,  
 and A. Zholents, Argonne National Laboratory, Lemont, IL 60439, USA  
<sup>1</sup> also at University of Wisconsin, Madison, WI 53715, USA

## Abstract

Argonne National Laboratory is developing a Sub-THz AcceleRator (A-STAR) for a future multiuser x-ray free electron laser facility. The A-STAR machine will utilize a compact collinear wakefield accelerator (CWA) based on a miniature copper (Cu) corrugated waveguide as proposed in [1]. The accelerator is designed to operate at a 20-kHz bunch repetition rate and will utilize the 180-GHz wakefield of a 10-nC electron drive bunch with a field gradient of 100 MVm<sup>-1</sup> to accelerate a 0.3-nC electron witness bunch to 5 GeV. In this paper, we discuss specific challenges in the mechanical design of the CWA vacuum chamber module. The module consists of series of small quadrupole magnets with a high magnetic field gradient that houses a 2-mm diameter and 0.5-m-long corrugated tubing with brazed water-cooling channels and a transition section. The 45-mm-long transition section is used to extract the wakefield and to house a beam position monitor, a bellows assembly and a port to connect a vacuum pump. The CWA vacuum chamber module requires four to five brazing steps with filler metals of successively lower temperatures to maintain the integrity of previously brazed joints.

## INTRODUCTION

Development of a CWA accelerator presents significant engineering challenges due to the miniature scale of the components. The CWA vacuum chamber module is comprised of a corrugated tubing-strongback (CTS) unit, a bi-metal vacuum flange, and a transition section (TS) unit with a bellows as shown in Fig. 1. The CTS will be fabricated from cylindrical corrugated waveguide tubes with a 2-mm ID that will be electroformed from aluminum (Al) mandrels. It will generate ~100 MV/m accelerating fields during operation, and its overall length will be about 0.5 meter long. The bi-metallic flange will be brazed to the upstream end of the CTS. The TS unit consists of an electroformed TS Cu waveguide, a TS Cu base, a stainless steel welded bellows assembly, eight flexible Cu waveguides, and diamond window assemblies. The CTS, bimetal flange, and TS units will be brazed together, then machined to be embedded into the quadrupole wiggler with alternating focusing and defocusing quadrupoles. Figure 2 shows two CWA vacuum chamber modules and one quadrupole wiggler assembly to reveal the structural clarity of the

CWA vacuum chamber module. This paper will focus on the design of the CWA vacuum chamber module and its fabrication challenges.

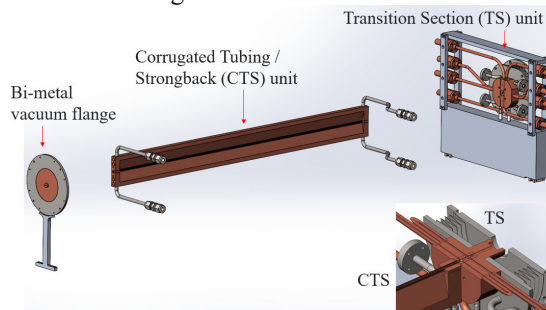


Figure 1: A vacuum chamber module and its components for the compact collinear wakefield accelerator.

## DESIGN OF A CWA VACUUM CHAMBER MODULE

Various fabrication techniques to create a corrugated waveguide structure were investigated. Based on our previous study [2, 3], electroforming was selected to produce internally corrugated tube segments for the CWA vacuum chamber module. The corrugated waveguide tubes are created by electroplating Cu on an Al mandrel [3]. The Al mandrel is then chemically dissolved, leaving behind the internally corrugated Cu structure. The internal Cu surface reflects the shape and finish of the Al mandrel surface. A micro-turning process is utilized to meet the dimensional and surface quality tolerances of the mandrels. The internal dimensions of the corrugated waveguide structure are shown in Fig. 3. The maximum length of the Al mandrel is ~100 mm; therefore, several corrugated waveguide segments must be brazed together to fabricate the 0.5-m-long vacuum chamber. The waveguide segments will be inserted into a channel-cut machined Cu strongback plate, then secured by a machined Cu bar with braze filler metal spreading adequately over the tubing surfaces or using wire rods as shown in Fig. 4. If needed, all parts will be secured by jigs and fixtures, then carefully held in position for brazing in a vacuum furnace to produce a 0.5-m-long CTS unit.

During the brazing process, compression force will be applied inwards along the length using spring sheets and spacers at both ends to maintain tight surface contact of the corrugated tubes. This will help to prevent filler metal from flowing inside the inner corrugation surface area. After the post-braze cleaning process, both end surfaces of the CTS unit are milled for vacuum leak testing (see Fig. 5). The strongback sides will be milled to produce tapered surfaces to fit within the quadrupole wiggler magnet assembly as shown in Fig. 6. The strongback end surfaces will then be

\* This research used resources of the Advanced Photon Source, a U.S. Department of Energy (DOE) Office of Science User Facility and is based on work supported by Laboratory Directed Research and Development (LDRD) funding from Argonne National Laboratory, provided by the Director, Office of Science, of the U.S. DOE under Contract No. DE-AC02-06CH11357.

<sup>†</sup> shlee@anl.gov

# MECHANICAL DESIGN OF THE BOOSTER TO STORAGE RING TRANSFER (BTS) LINE FOR APS UPGRADE\*

J. Liu<sup>†</sup>, M. Borland, T. Clute, J. Downey, M. Jaski, U. Wienands  
Argonne National Laboratory, Argonne, USA

## Abstract

The APS Upgrade selected the horizontal injection scheme which requires exchanging the x and y emittances in the BTS transport line through a series of six skew quadrupoles, as well as matching the beam parameters to the APS Upgrade storage ring through two dipoles and a conventional pulsed septum. This paper presents the layout of this BTS line section in the storage ring tunnel and key components in this section including the mechanical design of dipole magnet, quadrupole and skew quad magnets, the vacuum system, the diagnostics system, and the supports. Finally, detailed mechanical design of this BTS line section in modules and some consideration for fabrication and installation are addressed.

## INTRODUCTION

The Advanced Photon Source Upgrade Project (APS-U) is planning a storage-ring upgrade that will reduce the electron-beam emittance by a factor of  $\sim 75$  [1]. This ultra-low emittance is achieved by replacing the present storage ring lattice with a hybrid multi-bend achromat (MBA) lattice [2, 3]. The MBA lattice will increase the x-ray coherent fraction by two orders of magnitude and decrease the horizontal source size by a factor of  $\sim 20$ . The upgrade project adopts a horizontal injection scheme using a pulsed septum and fast stripline kickers for swap out injection and extraction [4]. The horizontal injection requires exchanging the x and y emittances in the BTS transport line [5]. To minimize change to the booster side of the BTS line, the section of BTS line on the SR side is redesigned and will be replaced with new a layout and components.

The scope of this paper mainly focuses on the mechanical design of the section of BTS transfer line located in the SR tunnel, including Lattice design, magnets design, vacuum system design, diagnostics design, and modular design of the whole section. Details of the designs are described in the following sections.

## DESIGNS

The mechanical design of the BTS section is based on a beam physics design. The beam physics design developed for the APS-U is a horizontal injection scheme. The scheme requires exchanging the x and y emittances using six skew quadrupoles, as well as matching the beam

parameters to the APS-U storage ring. After iterative processes of lattice and magnetic designs, the parameters were finalized for the dipole, quadrupole, and skew quadrupole magnetic designs. The mechanical design was conducted from magnetic design according to the magnetic model. All new magnet designs are consistent with the SR magnet designs to take advantage of the work and experience with the SR magnets.

## Lattice of BTS Section

Figure 1 shows the final layout of the BTS section. This section includes a total of 16 quadrupoles, 2 dipoles, 3 vertical correctors and 2 horizontal correctors. Of the 16 quadrupoles, 5 of them - BTS:BQ1 to BTS:BQ5 - are existing APS BTS magnets that will be reused. BTS:EXQs are skew quadrupoles and BTS:CQ1-3 and BTS:DQ1,2 are new quadrupole magnets. Skew and normal quadrupole magnets are of the same geometry but oriented in normal and skew orientation to reduce engineering work. All the new normal and skew quadrupoles include horizontal and vertical corrector trims. They will be operated at different parameters. BTS:BB1 and BTS:CB1 are new dipoles, but identical dipoles. BV1-3 are vertical correctors and BH1-2 are horizontal correctors. All the correctors are existing APS BTS magnets that will be reused. The locations of BPMs and Flags are also identified in Fig. 1. Between sections BTS:EXQ1B and BTS:BV3 will be the duck-under to allow passage across the BTS section.

## Magnet Design

Table 1 lists the parameters of the BB1/CB1 dipoles in the BTS section on the SR side. Table 2 lists the parameters of the new skew and normal quadrupoles.

The mechanical design of the dipole magnet is shown in Fig. 2. The dipole yoke takes a three-piece design. Four taper dowel pins holes are drilled and reamed on pilot holes after aligning and clamping the yokes to the backplate. This method gives cost effective control of pole gap tolerance with high repeatability. It has been tested successfully on our SR dipole magnets.

Dipole coils are made of water-cooled hollow copper conductor of  $SQ 6 \pm 0.1$  mm with  $3.5 \pm 0.1$  mm I.D. Each coil is made of 5 pancakes, with each pancake having two five-turn layers.

\* This research used resources of the Advanced Photon Source, a U.S. Department of Energy (DOE) Office of Science User Facility at Argonne National Laboratory and is based on research supported by the U.S. DOE Office of Science-Basic Energy Sciences, under Contract No. DE-AC02-06CH11357.

<sup>†</sup> jliu@aps.anl.gov

# MAGNET MODULE ASSEMBLY FOR THE APS UPGRADE\*

K. J. Volin<sup>†</sup>, R. R. Bechtold, A. Jain, W. G. Jansma, Z. Liu, J. J. Nudell, and Curt Preissner  
Advanced Photon Source Upgrade Project, Argonne National Laboratory (ANL), Lemont, IL, USA

## Abstract

With the Advanced Photon Source Upgrade (APSU) well into the procurement phase of the project, the APSU assembly team has completed a “DLMA Practice Assembly”, comprised of the support system and all magnets required to complete a module. The purpose of this test was to verify assembly and documentation procedures, ensure proper fit between mating components, and verify that alignment specifications can be met. The results of this exercise are presented. This test was completed on the ANL site and work continues in the APSU offsite warehouse where our first production plinths and girders have been shipped and where production modules are assembled. This space has been outfitted by ANL contractors and APSU assembly technicians with 1) five parallel DLM/FODO module assembly stations, each outfitted with a 3-ton overhead crane, retractable cleanroom, staging tables, and tools, and 2) two QMQ module assembly stations each outfitted with a 5-ton gantry crane, assembly support stands, staging tables, and tools. An overview of this production assembly space is also presented.

## INTRODUCTION

A major part of the APS Upgrade [1] is the installation of a new Multi-Bend Achromat (MBA) storage ring. The MBA storage ring is comprised of 40 sectors. Each sector is approximately 27.6 meters long (path length) with mirror symmetry about the central Q-bend (transverse-gradient dipole) magnet. There are a total of 1320 magnets comprising the new MBA storage ring. Each storage ring sector consists of three large modules with two support plates, supporting three magnets each (QMQ), bridging between them. Figure 1 shows one of the 40 sectors of the storage ring. The upstream Doublet-L-bend-Multiplet (DLM) module A supports a quadrupole doublet, an L-bend, and a multiplet array of magnets. In the center of the sector is the curved Focusing-Defocusing (FODO) module which supports five large bending/focusing magnets. The down-stream DLM module B is a mirror image of the upstream DLM module A. Each module contains a concrete plinth grouted to the floor with an alignable support girder mounted on top, which in turn supports the individual magnet strings, vacuum system, and auxiliary hardware. In addition to the 200 magnet modules comprising the storage ring, a full sector mockup

of 5 modules will be assembled and used for storage ring installation training.

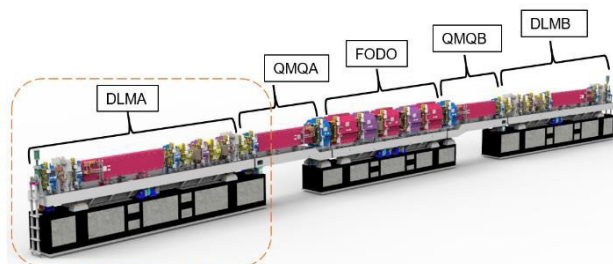


Figure 1: Typical APSU arc sector. DLMA Module (circled above) used for the first practice assembly.

## MODULE ASSEMBLY OVERVIEW

To assemble the 123 DLMA, DLMB, and FODO magnet modules, 5 assembly stations were each outfitted with a 3-ton overhead crane, steel weldment tables for staging the magnets, stainless steel (SS) tables for staging the vacuum strings, and an ISO7 (Class 10,000) retractable clean room for installing the particle-sensitive open vacuum chambers. To assemble the 82 QMQA and QMQB magnet modules, two assembly stations were each outfitted with a 5-ton gantry crane, steel weldment assembly stands for mocking up the support ends of the DLMA/B and FODO plinths, steel weldment tables for staging the magnets, and SS tables for staging the vacuum strings. The QMQ magnet modules are assembled with complete, sealed, nitrogen backfilled, vacuum chambers. There is no need for a clean room environment for the QMQ.

### DLMA Practice Assembly

With the arrival of the APSU vacuum system later than the bulk of the accelerator components, a first “practice assembly” was planned to use all magnets and support system components required to complete a DLMA assembly (see Fig. 1). The purpose of this activity was to verify assembly and documentation procedures, ensure proper fit between mating components, and verify that alignment specifications can be met.

**Magnet Installation** Extremely precise alignment of magnets within a module is necessary for achieving key performance parameters in the new machine. To achieve alignment specifications, we rely on precise machining of the girder and magnets, in conjunction with shimming.

Each magnet is fiducialized on a rotating wire bench before it is installed on a module [2]. This relates the magnet’s magnetic center to its fiducials, as well as documenting offsets from the magnetic center to its X, Y, and Z reference

\* This research used resources of the Advanced Photon Source, a U.S. Department of Energy (DOE) Office of Science User Facility, operated for the DOE Office of Science by Argonne National Laboratory under Contract No. DE-AC02-06CH11357. Extraordinary facility operations were supported in part by the DOE Office of Science through the National Virtual Biotechnology Laboratory, a consortium of DOE national laboratories focused on the response to COVID-19, with funding provided by the Coronavirus CARES Act.

<sup>†</sup> kjvolin@anl.gov

# MULTIBODY SIMULATIONS WITH REDUCED ORDER FLEXIBLE BODIES OBTAINED BY FEA

P. Brumund\*, T. Dehaeze<sup>1</sup>, ESRF, Grenoble, France

<sup>1</sup>also at Precision Mechatronics Laboratory / A&M department, Liege, Belgium

## Abstract

Tighter specifications in synchrotron instrumentation development force the design engineers more and more often to choose a mechatronics design approach. This includes actively controlled systems that need to be properly designed. The new Nano Active Stabilization System (NASS) for the ESRF beamline ID31 was designed with such an approach.

We chose a multi-body design modelling approach for the development of the NASS end-station. Significance of such models depend strongly on its input and consideration of the right stiffness of the system's components and sub-systems. For that matter, we considered sub-components in the multi-body model as *reduced order flexible bodies* representing the component's modal behaviour with reduced mass and stiffness matrices obtained from finite element analysis (FEA) models. These matrices were created from FEA models via modal reduction techniques, more specifically the component mode synthesis (CMS). This makes this design approach a combined multibody-FEA technique.

We validated the technique with a test bench that confirmed the good modelling capabilities using reduced order flexible body models obtained from FEA for an amplified piezoelectric actuator (APA).

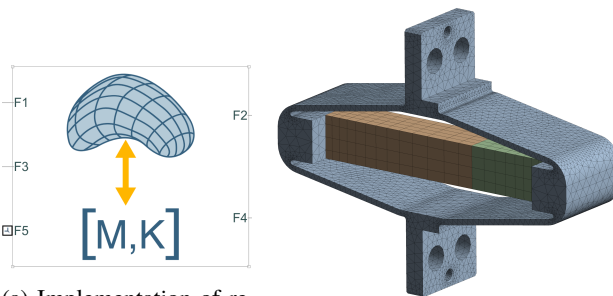
## INTRODUCTION

To meet its tight requirements in terms of precision and stability, a “model based design” approach was chosen for the development of the new ID31 end-station [1]. This type of design approach joins the need for dynamical models to test control architectures and to help specifying the requirements in the detail design stage.

We used a *MATLAB Simscape* multibody model for the detailed modular based design which is used to simulate the dynamical behaviour of the system. These models consist of *SIMULINK*-typical blocks, each representing one body or link. Such models were formerly limited to simple rigid bodies linked by “weak” links. They can be used as a first approximation. However, performances are often limited by resonances of flexible elements, i.e. the approximation by multiple solid bodies is not valid anymore.

Since recently, such *Simscape* models can be extended by a block named “Reduced Order Flexible Solid” (see Fig. 1a). This body consists of several interface points (here 5 points) and reduced FEA stiffness  $\hat{K}$  and mass matrices  $\hat{M}$  that describe its dynamical characteristics. This extends the body's represented behaviour in the simulations from pure inertial rigid-body representation to elastically deformable behaviour.

\* brumund@esrf.fr



(a) Implementation of reduced order model in *Simscape* multibody simulation block [2]. (b) Meshed FEA model of an amplified piezoelectric actuator. Number of nodes:  $\approx 130\,000$ .

Figure 1: Flexible body used in a *Simscape* model as a reduced model from a fully meshed FEA model.

## Application: Amplified Piezo Actuator

For the ID31 nano-end-station development we applied the FEA modal reduction technique to obtain reduced stiffness  $\hat{K}$  and mass matrices  $\hat{M}$  of key flexible components. This enables us to accurately model the dynamic behaviour of the end-station's nano-active-stabilization-system (NASS) hexapod. We applied the method on the hexapod struts containing amplified piezo actuators (type APA300ML, [3]) and flexible joints. We model the APAs as reduced order flexible bodies, which is explained in this paper. Figure 1b shows the fully meshed FEA model of the APA that we used for that matter. For the modal reduction of these APAs we used the commercial FEA software *ANSYS*. The resulting data was used as input in the *Simscape* multibody analysis.

## REDUCTION OF AMPLIFIED PIEZO

We applied the modal reduction technique from FEA (also called component mode synthesis) for the reduction of the high number of FEA degrees of freedom (DoF) to a smaller number of retained degrees of freedom<sup>1</sup>. For the example of the APA in Fig. 1b this results in a reduction from about  $130\,000 \times 3 = 390k$  DoF of the 3D FEA model down to only tens of DoFs, as explained in the next section. This reduced amount of DoF makes the model easy to integrate in a multibody simulation.

## FEA Modal Reduction Model

The *ANSYS* FEA model used for the modal reduction is shown with the used meshed in Fig. 2a. The points A to E mark the interfaces that were linked via a multi-point-

<sup>1</sup> Additional info on our applied procedure can be found in: <http://doi.org/10.5281/zenodo.5094419>

# ForMAX ENDSTATION – A NOVEL DESIGN COMBINING FULL-FIELD TOMOGRAPHY WITH SMALL- AND WIDE-ANGLE X-RAY SCATTERING

J. B. González<sup>†</sup>, S. A. McDonald, K. Nygård, L. Roslund, MAX IV Laboratory, Lund, Sweden

## Abstract

ForMAX is a new beamline at the MAX IV Laboratory for multi-scale structural characterization of hierarchical materials from nm to mm length scales with high temporal resolution. This is achieved by combining full-field microtomography with small- and wide-angle x-ray scattering (SWAXS) in a novel manner. The principal components of the endstation consist of two units of beam conditioning elements, a sample table, an evacuated flight tube and a detector gantry. The beam conditioning units include a diamond vacuum window, an attenuator system, a fast shutter, a slit collimation system, two sets of compound refractive lenses, three x-ray beam intensity monitors, a beam viewer and a telescopic vacuum tube. The sample table has been optimized with respect to flexibility and load capacity, while retaining sub-micron resolution of motion and high stability performance. The nine metre long and one metre diameter evacuated flight tube contains a motorised detector trolley, enabling the sample-detector position for small-angle x-ray scattering (SAXS) to be easily adjusted under vacuum conditions. Finally, a two metre high and two metre wide granite gantry permits independent and easy movement of the tomography microscope and wide-angle x-ray (WAXS) detector in and out of the x-ray beam. To facilitate propagation-based phase-contrast imaging and mounting of bulky sample environments, the gantry is mounted on motorized floor rails. All these characteristics will allow to combine multiple complementary techniques sequentially in the same experiment with fast efficient switching between setups. The ForMAX endstation is presently in the design and construction phase, with commissioning expected to commence early 2022.

## INTRODUCTION

Many natural and man-made materials are hierarchical, exhibiting important structure at several different length scales. In order to understand the structure-function relationship in such materials, one needs to characterise the structure at all these different length scales with sufficient temporal resolution to follow processes *in situ*. The versatile ForMAX instrument will address this problem by combining two complementary techniques – full-field tomographic imaging on  $\mu\text{m}$  to mm and SWAXS on nm length scales.

The main technical challenge when combining full-field tomography and SAXS stems from space constraints behind the sample; in full-field tomography one monitors the x-ray beam transmitted through the sample in forward di-

rection, while in SAXS one records the x-ray beam scattered at small angles  $\leq 3^\circ$ , i.e., in nearly forward direction. The novel approach at ForMAX is sequential tomography and SWAXS experiments, based on a motorized detector gantry that allows the tomography microscope (and WAXS detector) to be readily translated in and out of the x-ray beam, thereby allowing a fast and efficient switch of modes of operation.

In this conference paper, we outline the design of the ForMAX endstation. For an overview of the main components, see Fig. 1.

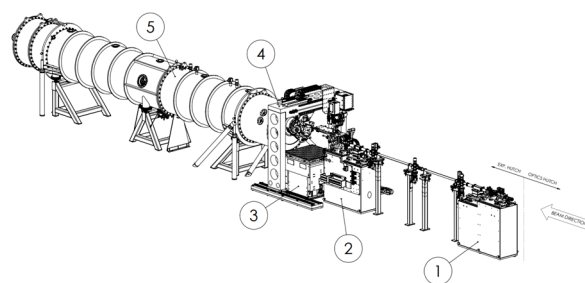


Figure 1: Main components of the endstation: (1) BCU I, (2) BCU II, (3) sample table, (4) detector gantry, and (5) flight tube.

## BEAM CONDITIONING UNITS

Two beam conditioning units (hereafter BCU I and BCU II), located upstream of the sample table, include elements and equipment needed for fine-tuning the beam characteristics (final size, microfocus, beam positioning, attenuation, etc.) for each experiment performed in the endstation. Both units consist of two independent granite blocks grouted to the floor and with the different elements mounted on the top surfaces, facilitating alignment with the beam.

BCU I is located 5 metres upstream of the sample table and includes a diamond vacuum window, an attenuator system, a fast shutter, horizontal and vertical slits and a set of beryllium compound refractive lenses (CRLs). The CRLs permit expansion of the beam during tomography experiments and their position is motorized in order to facilitate alignment in the beam.

BCU II is located directly upstream of the sample table and includes a motorized set of CRLs for microfocusing during SWAXS experiments, a beam diagnostic module, horizontal and vertical slits and a telescopic vacuum tube, permitting the users to minimize the x-ray beam path in air. The beam diagnostic module includes three x-ray beam intensity monitors and a YAG crystal screen.

<sup>†</sup> joaquin.gonzalez@maxiv.lu.se

# DESIGN AND COMMISSIONING OF THE TARUMÃ STATION AT THE CARNAÚBA BEAMLINE AT SIRIUS/LNLS

R. R. Geraldés<sup>†1</sup>, C. S. N. C. Bueno, L. G. Capovilla, F. R. Lena, D. Galante, L. C. Guedes, L. M. Kofukuda, G. N. Kontogiorgos, S. A. L. Luiz, G. B. Z. L. Moreno, I. T. Neckel, C. A. Pérez, A. C. Piccino Neto, A. C. Pinto, C. Sato, J. L. Silva, A. P. S. Sotero, V. C. Teixeira, H. C. N. Tolentino, W. H. Wilendorf, Brazilian Synchrotron Light Laboratory (LNLS), Brazilian Center for Research in Energy and Materials (CNPEM), 13083-970, Campinas, São Paulo, Brazil  
<sup>1</sup>also at the Eindhoven University of Technology (TUe), 5612AZ Eindhoven, The Netherlands

## Abstract

TARUMÃ, the sub-microprobe station at CARNAÚBA (Coherent X-Ray Nanoprobe Beamline) at Sirius at the Brazilian Synchrotron Light Laboratory (LNLS), has been designed to allow for simultaneous multi-analytical X-ray techniques both in 2D and 3D. A systemic approach, heavily based on precision engineering concepts and predictive design, has been adopted for first-time-right development, effectively achieving all-together: the alignment and stability requirements of the large KB mirrors with respect to the beam and to the sample; and the nanometer-level positioning, flyscan, tomographic and setup modularity requirements of the samples. This work presents the overall station architecture, the key aspects of its main components, and the first commissioning results.

## INTRODUCTION

CARNAÚBA (Coherent X-Ray Nanoprobe Beamline) [1] belongs to the first set of beamlines of Sirius [2], the 4th-generation synchrotron light source at the Brazilian Synchrotron Light Laboratory (LNLS). It is meant for simultaneous multi-analytical X-ray techniques in 2D and 3D, with diffraction (XRD), spectroscopy (XAS), fluorescence (XRF), luminescence (XEOL) and ptychographic coherent diffractive imaging (ptycho-CDI). It is based on an all-achromatic optical design for the energy range from 2.05 to 15 keV, granting a flux up to  $1e11$  ph/s/100mA at the probe for high-throughput experiments with flyscans.

TARUMÃ is its sub-microprobe station, located at 136 m from the undulator source, in a satellite building, and reaching fully-coherent monochromatic beam sizes from 550 to 120 nm after the achromatic KB (Kirkpatrick-Baez) focusing optics. In addition to the multiple techniques available at TARUMÃ, a large working distance of 440 mm after the ultra-high vacuum (UHV) KB system allows for another key aspect of this station, namely, a broad range of decoupled and independent sample environments. Indeed, modular setups outside vacuum allow for *in situ*, *in operando*, cryogenic and/or *in vivo* experiments, covering research areas in biology, chemistry, physics, geophysics, agriculture, environment and energy.

SAPOTI will be the in-vacuum nanoprobe station at CARNAÚBA, located at 145 m from the undulator source. With an innovative manipulator developed in collaboration with MI-Partners, operation is expected by 2022.

<sup>†</sup> renan.geraldes@lnls.br

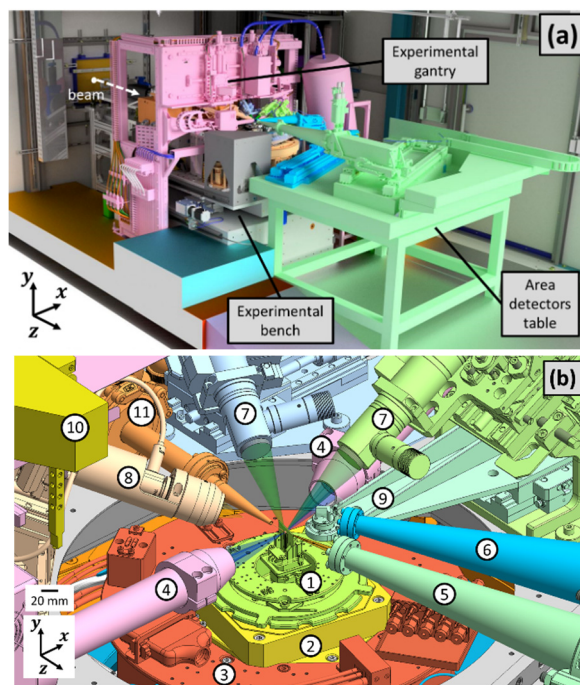


Figure 1: (a) TARUMÃ station at the experimental hutch. (b) Drawing of the region surrounding the sample, detailing: the sample setup (1), the sample stage (2 and 3), the fluorescence detectors (4), the flying paths for the transmission (5) and the diffraction (6) area detectors, the optical microscopes (7), the XEOL optics (8), a crystal analyzer spectrometer (9), the pick-and-place gripper (10), and the KB vessel exit port (11).

## OVERVIEW

Figure 1 shows an overview of the TARUMÃ station. The experimental bench hosts: the high sensitivity elements, i.e., the KB vessel and the sample stage; and essential auxiliary elements, such as a complementary metrology frame and an auxiliary rotary stage for cable management (see Fig. 3), and an auxiliary table holding two optical microscopes, the XEOL lenses and a crystal analyzer. A separate table is used for two Medipix-based area detectors with pixel size of  $55 \times 55 \mu\text{m}^2$ : a PiMEGA, with  $1536 \times 1536$  pixels at the working distance of 1.1 m, and a MobiPix, with  $512 \times 512$  pixels at 0.44 m. These detectors can be alternated between transmission and diffraction positions, and the MobiPix can still be oriented towards the crystal analyzer at the distance of 0.42 m to work as a spectrometer

# A NOVEL VACUUM CHAMBER DESIGN FOR THE APS UPGRADE OF THE 26-ID NANOPROBE

S. Bean, M. Holt<sup>1</sup>, P. Amann, M. Bartlein, Z. Cai, T. Graber<sup>†</sup>, D. Shu

Advanced Photon Source, Argonne National Laboratory, Lemont, IL 60439, USA

<sup>1</sup>also at Center for Nanoscale Materials, Argonne National Laboratory, Lemont, IL 60439, USA

<sup>†</sup>Deceased April 29, 2021

## Abstract

An enhancement design of an existing 26-ID nanoprobe [1] instrument (NPI) at APS is being completed as part of work for the APS-Upgrade (APS-U) project. As part of this enhancement design, a new vacuum chamber geometry configuration has been implemented that balances the desired simultaneous x-ray measurement methods with accessibility and serviceability of the nanoprobe. The main enabling feature on the vacuum chamber is a slanted mid-level vacuum sealing plane. The new chamber design geometrically optimizes the ability to perform simultaneous diffraction, fluorescence and optical or laser pump probe measurements on the sample. A large diffraction door geometry is strategically placed near the sample for ease of access. The newly designed chamber can be readily serviced by removal of the upper chamber section, on which most larger instrument assemblies or beamline attachments are not interfaced. The mechanical design intent and geometry of this chamber concept is described in this paper.

## INTRODUCTION

The upgrade of the 26-ID NPI will enable the observation of samples with x-ray diffraction, fluorescence, and photoluminescence while also allowing for the ability to manipulate the sample with laser or electronic stimulation and its environment with heating and cooling. This combination of measurement and sample manipulation enables world class operando studies.

The scope and breadth of the science to be performed by the upgraded 26-ID NPI are enabled by several technologies. Area and fluorescence detectors and manipulations, vacuum design, windowing, nanopositioning mechanics [2], and high resolution optics all need to be thoughtfully integrated to create an effective nanoprobe. Although trivial in technical merit compared to the other aspects and technologies of the, the vacuum chamber geometry imposes fundamental limitation on measurement capability, flexibility, and adaptability of the instrument. The limitations that can come with a vacuum chamber design may present challenges to scientific staff that could detract from their mission.

The prior nanoprobe vacuum chamber had desirable features, such as a large diffraction window, cable management that is incorporated into a lower section of the chamber, and adequate space inside the chamber for routing wiring and accessing equipment. However, this prior iteration presented challenges for adding more modalities of measurement, and also has some non-ideal

servicing steps, such as removing the x-ray fluorescence detector to take the upper portion of the chamber off.

To optimize the capabilities of the upgraded nanoprobe, the proposed vacuum chamber design incorporates a new angled sealing plane. The sealing plane is strategically positioned to enable simultaneous measurement techniques, while also balancing other serviceability and accessibility. For the upgrade door solution, inspiration was drawn from the existing NPI and the hard x-ray nanoprobe (HXN) at NSLS-II [3, 4]. An image of the entire new instrument is shown in Fig. 1.

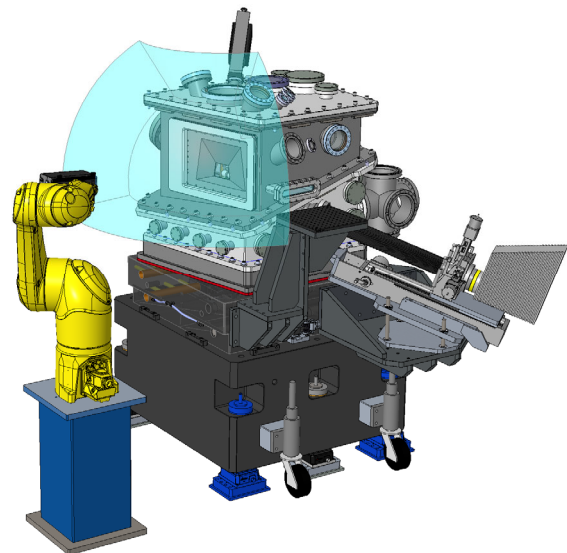


Figure 1: The new 26-ID nanoprobe enhancement as part of the advanced photon source upgrade.

## NANOPROBE CONFIGURATION METHODOLOGY

The following numbered items represent the most critical requirements of design and configuration for this instrument:

1. The design must maximize the diffraction envelope downstream of the instrument for area detection over the original design.
2. A Be window must be used for the downstream window.
3. A wide-angle range (>25deg) for optical configurations or laser pump probe measurements must be implemented on the outboard side of the chamber in the horizontal sample plane.

# CFD PREDICTIONS OF WATER FLOW THROUGH IMPELLERS OF THE ALBA CENTRIFUGAL PUMPS AND THEIR ASPIRATION ZONE. AN INVESTIGATION OF FLUID DYNAMICS EFFECTS ON CAVITATION PROBLEMS

A. González Romero\*, ESEIAAT-UPC, Terrassa, Spain

J. J. Casas, C. Colldelram, M. Quispe†, ALBA-CELLS Synchrotron, Cerdanyola del Vallès, Spain

## Abstract

Currently, the ALBA refrigeration system pumps present cavitation when operating at their nominal regime. To alleviate this phenomenon temporarily until a definitive solution was found, the water flow was reduced to 67% of its nominal value. As this flow exchanges heat with the cooling water produced in an external cogeneration plant, modifying the working point of the pumps resulted in a reduction of the Accelerator cooling capacity. However, even at such low flow conditions, the flow has an anomalous oscillatory behaviour in the distributor of the aspiration zone, implying that the cause may be in a bad dimensioning of the manifold.

This paper presents a study of Computational Fluid Dynamics (CFD) applied to the aspiration zones of the pumps, to investigate the effects of fluid dynamics on cavitation problems and understand what may be happening in the system. The need for such research arises from the urge to recover the accelerator cooling capacity and the constant pursuit for the improvement of the system. The geometries for this study include the general manifold in the aspiration zone and a simplified model of the pump impeller. The simulations have been carried out with the ANSYS-FLUENT software.

Studies performed include considering the total water flow in nominal and under current operating conditions. In addition, the cases in which the flow is distributed through the manifold tubes in uniform and non-uniform ways have been treated separately. Pressure and velocity fields are analysed for various turbulence models. Finally, conclusions and recommendations to the problem are presented.

## INTRODUCTION

During the last years, ALBA's operation has been affected by general thermal stability problems that prevent the correct performance of the system.

The cooling capacity of the facilities, which depends on the cold water supply from an external cogeneration plant (ST4), is affected by irregularities in the supplier's operation. The cogeneration plant changes its operating mode for a few hours each weekend, producing losses in the stability of the cold water supply (both in temperature and flow).

Moreover, from the ALBA side, the thermohydraulic system, described in [1], cannot move the required design flow in the heat exchange zone due to cavitation problems, which arise when the pump system (called P11) operates on design

conditions. For this reason, the operating flow was reduced by 33% to protect the pumps from such phenomenon, worsening the heat transfer efficiency between ALBA and ST4 (see detailed description in [2]).

The thermal instability promoted by these factors affects the stability of the photons generated in the synchrotron's ring and, therefore, the quality of the experiments performed by scientists.

Seeking to solve the local problem, this study focuses on investigating whether the cause of cavitation in P11 pumps is a bad configuration of the distribution panel in the suction zone or a bad dimensioning of the aspiration zone.

For this research, CFD (Computational Fluid Dynamics) systematic studies, global calculations and flow measurements are applied.

## MAIN PUMPING SYSTEM: P11 PUMPS

### Operation

P11 is the main pumping system of ALBA, composed by a couple of pumps which intersperse every 6 months their operation to avoid excessive wear or overload.

The pumps are fed by the hot water from the accelerator, after passing through filters and the three pipes connected to them (see Fig. 1). The flow is then redirected towards a group of heat exchangers before reaching the storage tank, where the water is cooled with the incoming flow from ST4.

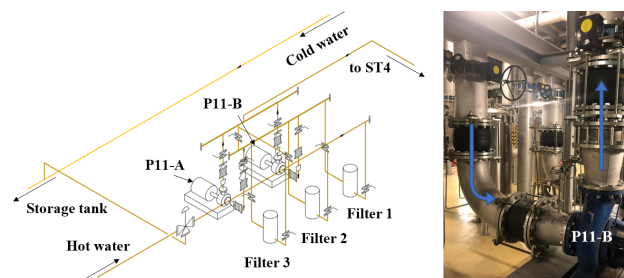


Figure 1: Schematic of the overall circuit studied (left) and photography of the P11 pumps (right).

### Encountered Problems

Different problems have been detected in the P11 system during its operation in recent years:

- Reduced flow rate to avoid cavitation problems at nominal value.

\* andreagonrom@gmail.com

† mquispe@cells.es

# A FAST SIMULATION TOOL TO CALCULATE SPECTRAL POWER DENSITY EMITTED BY WIGGLERS AND SHORT INSERTION DEVICES

J. Reyes-Herrera\* and M. Sanchez del Rio  
European Synchrotron Radiation Facility, 38000 Grenoble, France

## Abstract

The analysis of thermal stress of beamline components requires a comprehensive determination of the absorbed power profile. Consequently, accurate calculations of beam power density and its dependency on the photon energy are required. There exist precise tools to perform these calculations for undulator sources, like several methods available in the OASYS toolbox [1] considering, for example, the contribution of the different harmonics of the undulator radiation or using ray-tracing algorithms [2]. This is not the case for wiggler sources, in particular for short insertion devices that are used as source for the bending magnet beamlines in some upgraded storage rings like the ESRF-EBS. Wiggler radiation is incoherent and although it is possible the use of undulator methods for calculating it, this is very inefficient. In this work, we describe a tool that performs fast calculations of spectral power density from a wiggler source. The emission is calculated starting from a tabulated magnetic field and computes the power spatial and spectral density. It uses concepts inspired from Tanaka's work [3]. It is implemented in a user-friendly widget in OASYS and can be connected to widgets to calculate absorbed and transmitted power density along the beamline components. The accuracy of the method is verified by calculating three examples and comparing the results with ray-tracing. The three insertion devices simulated are: the EBS-ESRF-3PW (see results in Figure 1), the ESRF W150 (a high power wiggler) and the 3PW for the BEATS project [4] at the SESAME synchrotron source.

## INTRODUCTION

Currently, there are some synchrotron facilities that are implementing short insertion devices (IDs) as suitable photon sources that fits the demands of different beamlines. For example, in the new ESRF-EBS storage ring, all the 16 bending magnet beamlines have been upgraded with 3-pole wigglers, 2-pole wigglers or short bending magnets [5]. Another example is at SESAME, where a 3-pole wiggler is planned to be used at the BEAmline for Tomography at SESAME (BEATS) [4]. Therefore, in order to perform analysis of thermal stress of components of beamlines with this kind of sources, there is a demand of accurate and efficient tools to calculate the spectra power density distribution of these type of IDs. In this work, a new fast algorithm implemented as a user-friendly widget in OASYS [1] is presented.

\* juan.reyes-herrera@esrf.eu

## CALCULATION METHOD

The goal is to calculate the emitted flux by a wiggler  $F$  as a function of the horizontal and vertical coordinates  $(x, y)$  of a screen plane perpendicular to the propagation direction (optical axis) and located at a distance  $D$  from the center of the wiggler. The flux distribution is calculated for a grid of photon energies  $E$ , therefore  $F(x, y, E)$ .

We do not restrict to conventional wigglers with sinusoidal field, but use a numerical map of the magnetic field in the vertical direction  $B_y(z)$ . This allows us to simulate short IDs like the ones used at EBS-ESRF in the bending magnet photon sources, namely 3-pole wigglers (3PWs), 2-pole wigglers and 1-pole wigglers (or superbendings).

Contrary to the conventional method to calculate the differential emission at any coordinate point  $(x, y)$  for then averaging to the pixel size, we use a top-to-bottom method, first calculating the emission spectrum (integrated over an infinite size) for then distributing each integrated intensity for a given photon energy  $F(E)$  over its spatial distribution calculated ad-hoc. This method is explained in this section.

We assume (like in [3]) that i) the wiggler emission is fully incoherent (emission at every position of the electron trajectory are superimposed incoherently); ii) the electron emittances (finite size and divergence of the electron beam) are neglected, because they are usually smaller than the average sizes and divergences of the photon beam emitted by a single electron (or filament beam); and iii) the emission at a given point of the electron trajectory is the same as the Bending Magnet emission.

The calculation of the electron trajectory and emission spectrum follows the model implemented in SHADOW ([2]) and XOPPY ([1]).

### Calculation of Electron Trajectory Under a Magnetic Field

Let us start with the wiggler magnetic field, that for a conventional wiggler has only a vertical component ( $\vec{B} = (0, B_y, 0)$ ) and is given by tabulated values  $B_y(z)$ , with  $z$  the wiggler direction centered at the middle of the wiggler. An electron entering in this magnetic field will have a transversal velocity  $\beta_y$  (in  $c$  units) given by the integral of the magnetic field

$$\beta_y(z) = -\frac{c10^{-9}}{E_e[GeV]} \int_{z_1}^z B_y(s) ds. \quad (1)$$

The electron trajectory is in the horizontal plane and is given by the integral of the velocity,

$$x(z) = \int_{z_1}^z \beta_y(s) ds. \quad (2)$$

# A CRYOGENIC SAMPLE ENVIRONMENT FOR THE TARUMÃ STATION AT THE CARNAÚBA BEAMLINE AT SIRIUS/LNLS

F.R. Lena<sup>†</sup>, C.S.N.C. Bueno, F.H. Cardoso, J.C. Carvalho, M.M. Donatti, R.R. Gerales, L.M. Kofukuda, L.S. Perissinotto, E. Piragibe, C. Sato, H.C.N. Tolentino, W.H. Wilendorf, Brazilian Synchrotron Light Laboratory (LNLS), Campinas, Brazil

## Abstract

TARUMÃ is the sub-microprobe station of CARNAÚBA (Coherent X-Ray Nanoprobe Beamline) at Sirius at the Brazilian Synchrotron Light Laboratory (LNLS). Covering the tender-to-hard energy range from 2.05 to 15 keV with achromatic fixed-shape optics, the fully coherent submicron focused beam can be used for multiple simultaneous advanced micro and nanoscale X-ray techniques that include ptychography coherent diffraction imaging (ptycho-CDI), absorption spectroscopy (XAS), diffraction (XRD), fluorescence (XRF) and luminescence (XEOL). Among the broad range of materials of interest, studies of light elements present in soft tissues and other biological systems put TARUMÃ in a unique position in the Life and Environmental Sciences program at LNLS. Yet, to mitigate the detrimental effect of the high photon flux of the focused beam due to radiation damage, cryocooling may be required. Here we present the design and first results of a novel open-atmosphere cryogenic system for online sample conditioning down to 110 K. The high-stiffness and thermally-stable sample holder follows the predictive design approach based on precision engineering principles to preserve the nanometer-level positioning requirements, whereas a commercial nitrogen blower is used with a cold gas flow exhaustion system that has been developed in order to avoid unwanted cooling of surrounding parts and water condensation or icing.

## INTRODUCTION

With the advancements of low-emittance 4th-generation synchrotron light sources, small X-ray probes with higher photon flux are made possible [1]. Here we bring the case of the TARUMÃ station [2, 3] at the CARNAÚBA (Coherent X-ray Nanoprobe Beamline) [3, 4] beamline at Sirius at the Brazilian Synchrotron Light Laboratory (LNLS), where the ultra-high vacuum (UHV) KB optics is capable of delivering the submicrometric focus of 550 to 120 nm while yielding a high photon flux of up to  $1e11$  ph/s/100mA [4]. In addition, the large working distance of 440 mm after the KB set allows a broad range of sample environments outside vacuum (see [2]).

Working in the tender X-ray region, the station can be used for soft tissue and light elements multi-instrumentation probing. One of the most appealing techniques is the nano ptycho-CDI, in which the referred probe, combined with the beamline optics and the characteristics of the PiMEGA or MobiPix Medipix-based area detectors [5], can result in spatial resolution in the nanometer range [2].

Yet, this resolution limit is directly impacted not only by the relative position stability between the sample and the probe, bringing the TARUMÃ stability requirements down to the same order, but also by the characteristics of the sample itself over time. This results in two main challenges: ensuring the sample-to-probe spatial stability, that is mostly addressed by the high-stiffness and exactly-constrained optics [6]; best effort over the commercial stages composing the sample manipulator (with a complementary metrology frame) [2] and sample setups based on precision engineering principles; and mitigating the dose-induced sample degradation due to the high photon density and absorption in the tender energy range, especially in biological samples. For the latter, cryocooling the sample has been proved very effective, greatly reducing the dose damage, and improving temporal preservation during long scanning times [7]. In the following sections we present the in-house development and pre-commissioning tests of the TARUMÃ cryogenic sample environment.

## SYSTEM OVERVIEW

Aiming at implementing the needed sample cryocooling functionality for the tender X-ray TARUMÃ station and unlocking the possibility of studying soft organic and other dose-sensitive materials, a commercial liquid nitrogen (LN<sub>2</sub>) based Cryojet-5 from Oxford Cryogenics system was chosen as the cooling instrument. This choice was made because of the open-atmosphere condition of the sample stage and space constraints limiting other conductive options. Yet, despite the simplicity of the system and easily achievable gas temperatures as low as 80K, the high density of instruments around the sample (see [3]) made its integration at the station a challenging task.

Firstly, the open-atmosphere concept of the commercial cryojet might lead to thermal drift, condensation and/or icing issues in the sample or in sensitive nearby instruments, if the cold gas outflow would not be properly managed. At TARUMÃ, this is prevented with the implementation of an exhaustion system. Then, the open flow nature of this solution might be conflicting with the nanometric sample positioning requirements. This is addressed by a thermo-mechanical design that decouples the high-stiffness sample holder assembly from an auxiliary gas shield with optimized aerodynamics to minimize flow-induced disturbances. In addition to the cryojet and the sample itself, the TARUMÃ cryogenic setup (Fig. 1) is composed of three main subsystems: the *sample holder*, the *holder shield* and the *exhaustion system*.

<sup>†</sup> francesco.lena@lnls.br

# ELECTROCHEMISTRY AND MICROFLUIDIC ENVIRONMENTS FOR THE TARUMÃ STATION AT THE CARNAÚBA BEAMLINE AT SIRIUS/LNLS

W. H. Wilendorf<sup>†</sup>, R. R. Geraldes, L. M. Kofukuda, I. T. Neckel, H. C. N. Tolentino, Brazilian Synchrotron Light Laboratory (LNLS), Campinas, São Paulo, Brazil  
P. S. Fernandez, Chemistry Institute, State University of Campinas, Campinas, São Paulo, Brazil

## Abstract

TARUMÃ is a multi-technique sub-microprobe experimental station of the CARNAÚBA (Coherent X-Ray Nanoprobe Beamline) beamline at Sirius, the 4th-generation synchrotron light source at the Brazilian Synchrotron Light Laboratory (LNLS). This work describes two related setups that have been developed in-house for TARUMÃ: a small-volume electrochemical cell, and another multifunctional liquid environment that can be used both as a microfluidic device and as an electrochemistry cell that allows for fluid control over electrodes. The mechanical design of the devices, as well as the architecture for the fluid and electrical supply systems are described in detail.

## INTRODUCTION

CARNAÚBA (Coherent X-Ray Nanoprobe Beamline) [1] is a state-of-the-art multi-technique beamline of Sirius [2], the 4th-generation Light Source at the Brazilian Synchrotron Light Laboratory (LNLS) at the Brazilian Center for Research in Energy and Materials (CNPEM), with achromatic optics and fully-coherent X-ray beam in the energy range between 2.05 and 15 keV. It is equipped with two in-line experimental stations, namely: TARUMÃ [3], a sub-microprobe station in an advanced commissioning phase, for which the sample environments presented here were specially designed; and SAPOTI, a nanoprobe station still in design phase.

At the TARUMÃ station, the in-vacuum KB focusing system has been designed with a large working distance of 440 mm, allowing for a broad range of independent sample environments to be developed in open atmosphere to benefit from the spot size between 550 and 120 nm, with a flux in the order of  $1e11$  ph/s/100mA. Hence, together with a number of detectors that can be simultaneously used, as shown in Fig. 1, a wide variety of studies of organic and inorganic materials and systems are possible using cutting-edge X-ray-based techniques in the micro and nanoscale, including: coherent diffractive imaging (CDI), fluorescence (XRF), optical luminescence (XEOL), absorption spectroscopy (XAS), and diffraction (XRD). Even though samples over the centimeter range can be taken at TARUMÃ, the small beam and relatively low energies point towards optimized and small sample setups for in situ experiments. Indeed, reduced-size geometry and light materials allow lighter sample environments, helping with fast flyscan mapping and the final stability of the sample positioning system, which is composed of commercial stages for up to 6 degrees of freedom (DoF) (see [3]).

<sup>†</sup> willian.wilendorf@lnls.br

To explore the resolution and the multi-techniques available at TARUMÃ for studies in the fields of electro-chemistry (electrocatalysis) [4] and microfluidic (in situ reactions and in vivo studies) [5], two sample environments for *in situ* experiments were especially designed following the precision engineering concepts required for nanopositioning performance. The first setup is a small-volume electrochemical cell with working, counter and reference electrodes, and the machined parts made of light and non-reactive polymeric materials. The second one is a multifunctional glass-based device that can be used both as a microfluidic device only, or an electrochemical cell, by controlling fluids over embedded electrodes. This work presents the details of the mechanical designs of the two sample environments developed in-house, and the architecture for the electrical and hydraulic supply system.

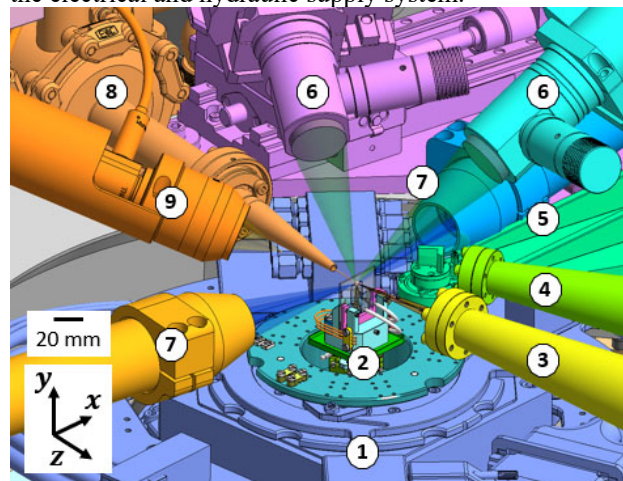


Figure 1: Sample region at TARUMÃ, with the several detectors that allow for multi-technique experiments: sample positioning stages (1), sample environment setup (2), flying paths for transmission (3) and diffraction (4) area detectors, crystal analyser spectrometer (5), optical microscopes (6), fluorescence detectors (7), exit vacuum nipple of KB chamber (8) and luminescence detector (9).

## ELECTROCHEMICAL SETUP

The setup depicted in Fig. 2 was designed for in situ experiments in electrochemistry and electrocatalysis at TARUMÃ, according to the infrastructure capabilities and interfaces at the station. It is a versatile small-volume oxidation-reduction reaction cell with external dimensions of  $45 \times 33 \times 45$  mm<sup>3</sup>. The electrolyte, with a static volume of 1 ml, as well as the working, counter and reference electrodes, may be suitably selected according to the scientific

# A COMPACT X-RAY EMISSION (mini-XES) SPECTROMETER AT CLS - DESIGN AND FABRICATION METHODS

T. W. Wysokinski<sup>†</sup>, M. Button, A. F. G. Leontowich, B. D. Moreno, CLS, Saskatoon, Canada

## Abstract

A compact X-ray emission spectrometer (mini-XES) has been designed and fabricated for use at the Brockhouse undulator beamline. The mini-XES design was developed to be as simple to fabricate and as easy to operate as possible. We tried to minimize the number of parts. From the beginning, the design was trying to achieve no tools assembly, alignment, and operation. The first tests of the spectrometer were completed and were successful.

## INTRODUCTION

A compact X-ray emission spectrometer (mini-XES) has been designed and fabricated for use at the Brockhouse undulator beamline [1]. The mini-XES uses cylindrical von Hamos geometry tuned for Fe K-edge and uses a Pilatus 100K area detector from Dectris [2]. It is based on a general design implemented at the APS [3].

The mini-XES design was developed to be as simple to fabricate and as easy to operate as possible. We tried to minimize the number of components, so there are only two main parts that create a chamber. Those two components are joined and aligned by a NW-80 flange. From the start, the design was trying to achieve no tools assembly, alignment, and operation. For lower precision alignment we decided to use the centering ring of the NW-80 flange which, together with two posts integrated with the chamber, provides an adequate method for joining the two parts of the enclosure. We use level vials for horizontal adjustment of the holder for the 10 crystals. For high precision alignment of the crystal holder, we use the Thorlab KC1/M kinematic mount, which have the adjustment screws accessible from outside of the chamber. The fabrication was done in-house using uPrint SE Plus 3D Printer [4].

The first tests of the spectrometer were completed in the Brockhouse wiggler beamline [5] and were successful. Future improvements will aim to reduce the background scatter and better position the detector, to improve the fill. Now that the relatively inexpensive design was tested and tried, there is an option to upgrade it to 3D printed tungsten or steel version that would intrinsically provide the required shielding.

## MAIN COMPONENTS

The spectrometer consists of:

- Top Chamber
- Bottom Chamber
- Crystal Holder with crystals
- Apertures

The estimates for the model material used and the print time are included in Table 1.

<sup>†</sup> wysokinski@alumni.sfu.ca

## Main Printed Components

The top chamber (Fig. 1), attaches to the detector and the design protects the sensitive part of the detector. It assures that there is no possibility of contact with the focal plane once the detector is ready to use. The other end of the chamber mates to the NW-80 flange.

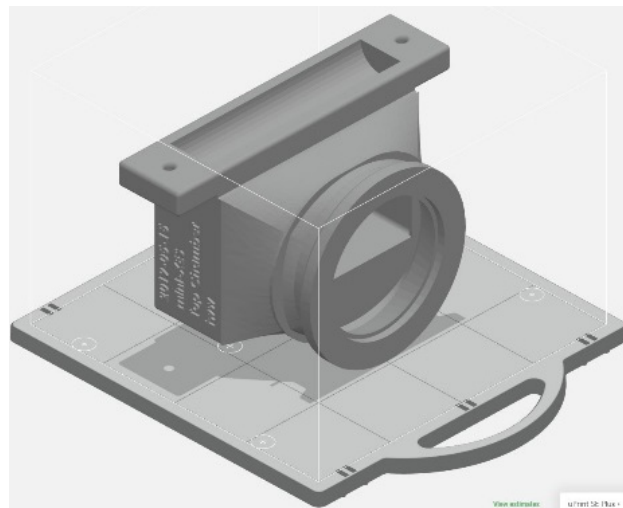


Figure 1: Top chamber model.

The bottom chamber is more complex (Fig. 2). It starts with NW-80 flange at the top that connects to the top chamber. The centering ring provides axial alignment. Two horizontal arms, that contact the backplate, provide the rotational alignment.

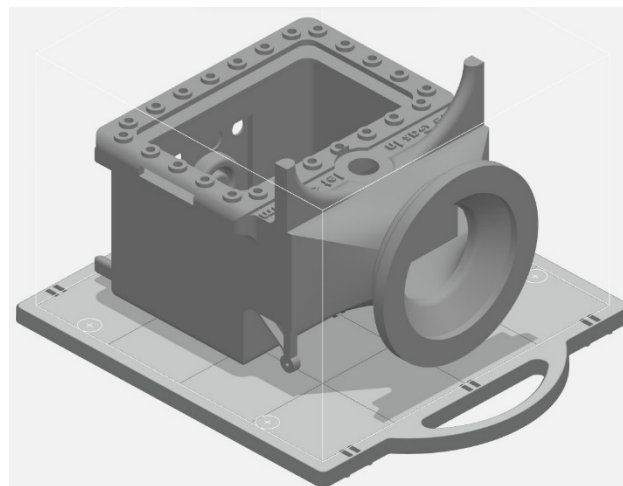


Figure 2: Bottom chamber model.

The chamber has several slots for apertures, a slot for the back door, support legs and alignment posts which combined with the alignment lines help to position the sample at the right location.

# AN IMPROVED, COMPACT HIGH TEMPERATURE SAMPLE FURNACE FOR X-RAY POWDER DIFFRACTION

E. Haas, E. Cardenas, A.P. Sirna

National Synchrotron Light Source II, Brookhaven National Laboratory,  
Upton, NY 11973-5000, USA

## Abstract

A compact sample furnace was designed to heat samples to temperatures of 2000 - 2300°C at the X-ray Powder Diffraction (XPD) beamline at NSLS-II. This furnace allows the XPD photon beam to pass through with adequate downstream opening to collect diffraction data for high-temperature materials research. Since the XPD samples did not reach the desired temperatures, engineering studies, tests, and incremental improvements were undertaken to improve performance. Several approaches were considered, and the sample holder design was improved, and high-temperature coatings were used. The engineering work undertaken to improve furnace performance is included herein.

## INTRODUCTION

The XPD Beamline at NSLS-II does materials research at temperatures ranging from cryogenic to ~1700°C, and efforts to conduct materials research at higher temperatures are ongoing. The present XPD sample furnace uses infrared lamps with ellipsoidal reflectors to focus infrared rays at a single sample. This furnace has been operating in air, and high-temperature oxidation has been destroying thermocouples. A plan therefore was developed to investigate potential areas of improvement:

- The use of IR lenses to focus forward-directed IR rays otherwise lost as halo.
- Improved sample tube holders.
- The use of inert gas shielding to prevent oxidation.
- The use of high-temperature coatings.
- The use of a custom-designed secondary reflector to redirect forward-directed IR halo.
- The use of a CO<sub>2</sub> laser as a supplementary (or primary) sample heat source
- Optimization of heat lamps and focal distance.

This paper briefly discusses each of the above options and explains why some of the above items were pursued further and others rejected. Considerations of material properties at high temperatures are also included.

## SAMPLE AND FURNACE CONDITIONS

Powder samples contained in sapphire tubes are held by ceramic holders for X-Ray Powder Diffraction research in air at atmospheric pressure. Sapphire is used for its' high-temperature and optical properties. A computer graphic (CG) image and photo of a sapphire tube in its' ceramic tube holder is shown in Fig. 1 along with an image of one infrared heat flux pattern. This heat flux for a single ellipsoidal reflector indicates loss of some flux past the sample holder tube. Infrared lamps direct 150W each of heat flux at a ceramic sample tube holder in the bandwidth

shown in Fig. 2. Six infrared lamps each have ellipsoidal reflectors and water-cooled jackets to minimize external temperatures for safety and to extend lamp life. Cooling water at 17-20°C from a chiller is circulated in parallel paths through all lamp cooling jackets and through two water-cooled outer shells.

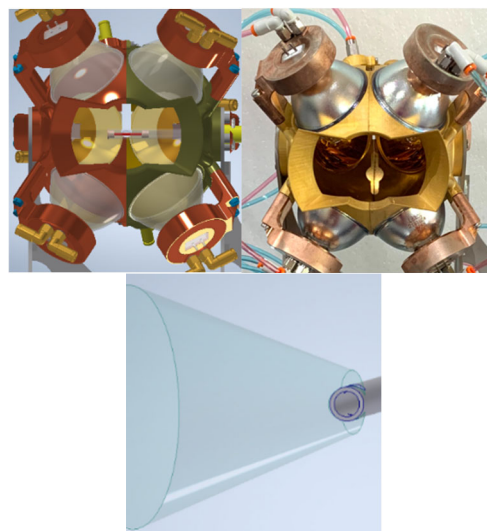


Figure 1: XPD Sample Furnace looking upstream: (a) CG image, (b) photo, and (c) heat flux pattern.

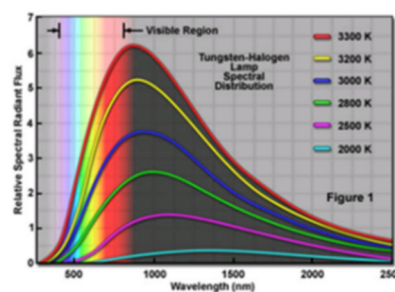


Figure 2: IR lamp flux spectrum.

## ENGINEERING INVESTIGATIONS

- The use of plano-convex infrared lenses as a primary means to focus forward-directed rays was considered, but not pursued as available infrared lens geometries and IR source distance limitations meant only a small portion of forward-directed rays were properly focused. When IR lenses were used to supplement ellipsoidal reflectors, too many reflected rays that would have been focused at the sample center were misdirected. IR lenses therefore were ruled out as a viable solution. Two IR lens configurations are shown in Fig. 3.

# THERMAL MODEL VALIDATION FOR THE CRYOGENIC MIRROR SYSTEMS FOR SIRIUS/LNLS

L.M. Volpe\*, B.A. Francisco†, J.C. Corsaletti, R.R. Gerales, M. Saveri Silva  
 Brazilian Synchrotron Light Laboratory (LNLS), Brazilian Center for Research in Energy and Materials  
 CNPEM, Campinas, São Paulo, Brazil

## Abstract

One of the challenges of fourth-generation synchrotron light sources as Sirius at the Brazilian Synchrotron Light Laboratory (LNLS) is the high power density that may affect the beamline optical elements by causing figure deformations that deteriorate the quality of the beam. Indeed, surface specifications for height errors of X-ray mirrors are often within a few nanometers. To deal with these thermal management challenges, thermo-mechanical designs based on cryogenic silicon have been developed, taking advantage of its high thermal conductance and low thermal expansion in temperatures of about 125 K. A liquid nitrogen (LN2) cryostat connected to the optics by copper braids has been used to handle moderate power loads, reducing costs when compared to closed-circuit LN2 cryocoolers and mechanically decoupling flow-induced vibrations from the optics. To guarantee the functionality of such systems, lumped mass thermal models were implemented together with auxiliary finite elements analyses. With the first systems in operation, it has been possible to compare and validate the developed models, and to carry out optimizations to improve them for future projects, by adjusting parameters such as emissivity, thermal contact resistance, and copper braid conductance. This work presents the updated models for CARNAÚBA and CATERETÊ beamlines as reference cases.

## INTRODUCTION

The analysis of thermal deformation in synchrotron mirrors is a well known research field due to the impacts in the final shape of the beam [1]. At Sirius, the 4th-generation light source at the Brazilian Synchrotron Light Laboratory (LNLS), this issue has been addressed with an innovative thermo-mechanical concept for exactly-constrained cryocooled mirrors, as detailed in [2]. Indeed, given the high conductivity and the quasi-zero-expansion properties of silicon around 125 K, detrimental thermal effects can be minimized. Here, the methodology and latest developments in thermal models for Sirius mirrors are presented, with the CARNAÚBA and CATERETÊ beamlines taken as study cases due to their demanding requirements concerning small beam sizes and high coherence [3,4]. With lower modeling effort and computational cost for the complex mirror systems, lumped mass models in MATLAB Simscape® have been preferred over finite element analyses (FEA), which are then used mainly as complementary tools as to define con-

trol parameters temperature PID, power heater and diagnosis fails in the system.

## METHODOLOGY

In lumped mass models, bodies and assemblies in complex geometries can be reduced as nodes with thermal resistances and thermal masses, which are combined according to parameters such as Biot and Fourier number [5]. The example of a node in Simscape is shown in Fig. 1.

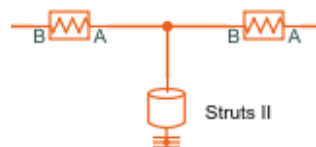


Figure 1: The center block represent the mass of the “struts II” and others are two resistances that represents the conductances between the center of the body and their extremes wich are in contact with other bodies. The central point represent the middle temperature.

### Thermal Conduction Resistance

For an 1D solid between two nodes of interest, for example, the conduction thermal resistance may be derived from Fourier’s law in Eq. (1), where:  $Q$  is the heat flow;  $\Delta T$  the temperature gradient between the ends of the body;  $A$  the cross section;  $k$  the thermal conductivity and  $\Delta x$  the solid length. Then, according to Eq. (2), the resistance  $R$  is often defined as the inverse of the conductance  $g$ , given by the ratio between  $Q$  and  $\Delta T$ . For more complex bodies, the conductances can be calculated after splitting them into simpler bodies or by FEA.

$$Q = \frac{kA\Delta T}{\Delta x} \tag{1}$$

$$g = \frac{Q}{\Delta T} = \frac{kA}{\Delta x} \longrightarrow R = \frac{1}{g} = \frac{\Delta x}{kA} \tag{2}$$

### Thermal Contact Resistance

The interfaces between bodies are also modelled as resistances and then associated with the node resistances. As shown in Eq. (3), the contact resistance  $R_c$  can be written as a function of the heat flux  $Q$  and the temperature difference between surfaces  $\Delta T$ , being typically extracted from experimental results and/or literature estimates [6, 7].

$$Q = \frac{1}{R_c} \Delta T = g_c \Delta T \tag{3}$$

\* lucas.volpe@lnls.br  
 † barbara.francisco@lnls.br

# TEMPERATURE-DEPENDENT ELASTIC CONSTANTS AND YOUNG'S MODULUS OF SILICON SINGLE CRYSTAL\*

Zunping Liu<sup>†</sup>, Advanced Photon Source, Argonne National Laboratory, Lemont, IL 60439, USA

## Abstract

Silicon crystals have been widely used for x-ray monochromators. It is an anisotropic material with temperature-dependent properties. Values of its thermal properties from cryogenic to high temperature are available in the literature for expansion, conductivity, diffusivity, heat capacity, but neither elastic constants nor Young's modulus. X-ray monochromators may be liquid-nitrogen cooled or water cooled. Finite Element Analysis (FEA) is commonly used to predict thermal performance of monochromators. The elastic constants and Young's modulus over cryogenic and high temperature are now collected and derived from literature, with the purpose of assisting in providing accurate FEA predictions.

## INTRODUCTION

Silicon single crystals have been widely used for x-ray monochromators [1], in addition to application in MEMS fabrication, both as a substrate for compatibility with semiconductor processing equipment and as a structural material for MEMS devices [2-4]. It is an anisotropic material with temperature-dependent properties, such as thermal conductivity [5, 6], thermal expansion coefficients [7-9], and elastic constants [10] or Young's modulus [11, 12]. At room temperature, Young's modulus varies from 130 GPa in the <100> directions to 190 GPa in the <111> directions.

Burenkov *et al.* [13] and Kury *et al.* [14] studied the temperature dependence of Young's modulus  $E_{\langle ijk \rangle}$  for Si and Ge. Polynomial expressions for the dependence on temperature between room temperature and 1000°C of the bi-axial Young's modulus  $E_{\langle ijk \rangle} / (1 - \nu)$ , with  $\nu$  the Poisson's ratio, were developed. Vanhellefont *et al.* reported temperature-dependent Young's modulus of silicon by means of impulse excitation technique [12]. The data  $E_{\langle ijk \rangle}$  along <100>, <110>, and <111> directions are available from room temperature to 1400°C.

McSkimin measured elastic constants  $C_{11}$ ,  $C_{12}$ ,  $C_{44}$  of silicon single crystal at low temperatures by means of ultrasonic waves [10]. The data are valid from 78 K to 300 K.

This report derives Young's modulus at low temperatures from elastic constants  $C_{11}$ ,  $C_{12}$ ,  $C_{44}$  of silicon single crystal in ref. [10], and elastic constants at high temperatures from Young's modulus in ref. [12]. Therefore, complete sets of Young's modulus and elastic constants are provided from -196°C up to 1400°C, or ~78 K to ~1673 K. Further, users may derive temperature-dependent Young's modulus or elastic constants at any arbitrary orientations.

\* This research used resources of the Advanced Photon Source, a U.S. Department of Energy (DOE) Office of Science User Facility at Argonne National Laboratory and is based on research supported by the U.S. DOE Office of Science-Basic Energy Sciences, under Contract No. DE-AC02-06CH11357.

<sup>†</sup> zpliu@anl.gov

## ELASTIC CONSTANTS

The stiffness coefficients  $C_{ijkl}$  and the compliance coefficients  $S_{ijkl}$  are defined as the proportionality constants between stress  $\sigma$  and strain  $\epsilon$  tensors in the form of generalized Hooke's law:

$$\sigma_{ij} = C_{ijkl}\epsilon_{kl}, \text{ and } \epsilon_{ij} = S_{ijkl}\sigma_{kl}. \quad (1)$$

### In the Coordinate System of a Cubic Crystal

Figure 1 shows the coordinate system with "X,Y,Z"-axes in the <100>, <010>, and <001> directions of a cubic structure. Because of its orthogonality, this coordinate system is actually a Cartesian coordinate system. An arbitrary orientation <hkl> rotating with respect to those three directions is also illustrated.

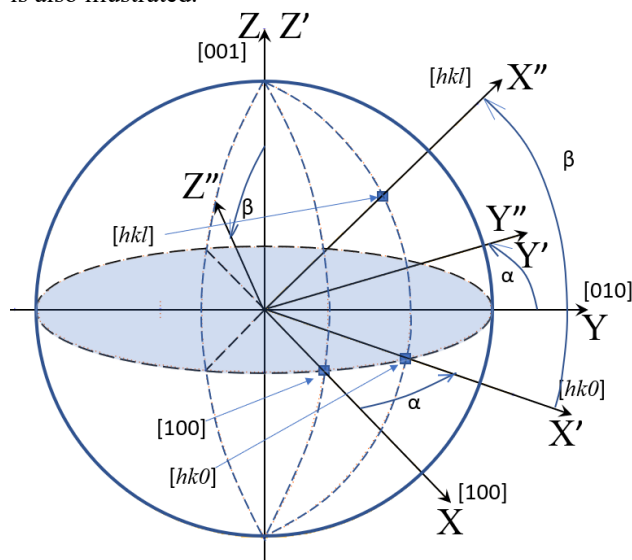


Figure 1: Illustration of coordinate system transformation with respect to the primary directions of a cubic structure.

For a cubic crystal such as silicon, the combination of cubic symmetry and the equivalence of the shear conditions enables specifying the fourth rank tensor with only three independent elastic constants. With respect to a specific basis that is commonly given for the <100> directions of the cubic structure, these tensors are given as [15, 16]:

$$\sigma_{ii} = C_{11}\epsilon_{ii} + C_{12}(\epsilon_{jj} + \epsilon_{kk}), \text{ and } \sigma_{ij} = C_{44}\epsilon_{ij}. \quad (2)$$

The stiffness matrix can be shortened as  $C_{pq}$  or:

$$C = \begin{bmatrix} C_{11} & C_{12} & C_{12} & & & \\ C_{12} & C_{11} & C_{12} & & & \\ C_{12} & C_{12} & C_{11} & & & \\ & & & C_{44} & & \\ & & & & C_{44} & \\ & & & & & C_{44} \end{bmatrix}. \quad (3)$$

The compliance matrix can be written in a similar form, which is the inverse of the stiffness matrix. The second-order elastic compliances  $S_{pq}$  can be expressed as:

# DESIGN OF VACUUM CHAMBER WITH CRYOGENIC COOLING OF SAMPLES FOR BRAGG-PLANE SLOPE ERROR MEASUREMENTS\*

J.W.J. Anton<sup>†</sup>, P. Pradhan, D. Shu, Yu. Shvyd'ko  
Advanced Photon Source, Argonne National Laboratory, Lemont, IL 60439, USA

## Abstract

Wavefront preservation is essential for numerous X-ray science applications. Research is currently underway at the Advanced Photon Source to characterize and minimize Bragg-plane slope errors in diamond crystal optics [1]. Understanding the effect of cooling the optics to cryogenic temperatures on Bragg-plane slope errors is of interest to this research. Through the use of a finite element model a custom, compact vacuum chamber with liquid nitrogen cooling of samples was designed and is being manufactured. The design process and initial results are discussed in this paper.

## INTRODUCTION

Wavefront-preserving X-ray diamond crystal optics are essential for numerous applications in X-ray science [1, 2]. Perfect crystals with flat Bragg planes are a prerequisite for wavefront preservation in Bragg diffraction. However, this condition is difficult to realize in practice because of inevitable crystal imperfections. Even for practically flawless diamond crystals, internal strain of various origins, such as mounting and low-temperature cooling, can give rise to Bragg planes slope errors and significant wavefront distortions. Research is currently underway at the Advanced Photon Source to characterize and minimize Bragg-plane slope errors in diamond crystal optics [3].

One of present major goals is to develop and test schemes for mechanically-stable strain-free diamond crystal mounting with excellent heat transport to heat sinks at room and liquid nitrogen (LN) temperatures. Use of wavefront-preserving diamond crystals in x-ray Bragg diffraction at low temperatures is essential in particular for the realization of the next generation light sources of highest brilliance such as x-ray free-electron laser oscillator (XFEL) [4].

For this purpose a low-temperature compact vibration-free diamond crystal chamber is required, which could be mounted on high-precision angular goniometers in the rocking curve imaging (RCI) [3] and wavefront imaging (WFI) setups [5]. Commercially available cryostats are too bulky for this purpose.

Through the use of a finite element model a custom, compact vacuum chamber with liquid nitrogen cooling of diamond crystal samples for RCI and WFI was designed and is being manufactured. The design process and initial results are discussed in this paper.

\* This research used resources of the Advanced Photon Source, a U.S. Department of Energy (DOE) Office of Science User Facility at Argonne National Laboratory and is based on research supported by the U.S. DOE Office of Science-Basic Energy Sciences, under Contract No. DE-AC02-06CH11357.

<sup>†</sup>anton@anl.gov

## DESIGN REQUIREMENTS

To complete the the RCI and WFI studies the following design requirements were decided on:

- Rotate crystal surface  $\pm 45^\circ$
- Keep sample temp.  $< -185^\circ\text{C}$  long enough to conduct X-ray experiment (approx. 20 min.)
- Operate in high-vacuum environment
- Size: Compact and light as possible so it can be installed on current beamline stages

Figure 1 shows a schematic view of the chamber design. Materials with low thermal conductivity are used to mount the crystal holder and the N2 reservoir. Oxygen-free copper is used to conduct heat away from the crystal and cooled by the liquid nitrogen. Mylar sheeting was used to shield the N2 Reservoir from radiation heat loads.

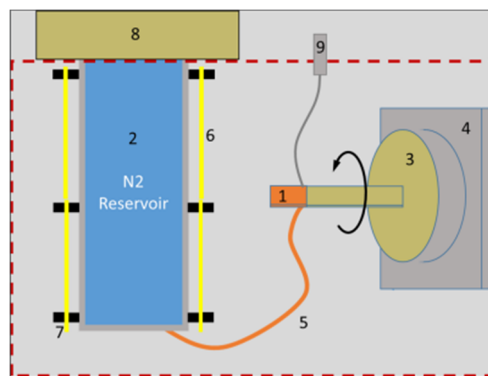


Figure 1: Schematic diagram of the sample cryogenic cooling: 1. Crystal sample (diamond), 2. N2 reservoir, 3. crystal mount (PEEK), 4. rotation stage, 4. thermal conductor (OFHC), 5. rad. shielding (Mylar), 6. Spacer/clamps (PEEK), 7. reservoir flange (PEEK), 8. temp. sensor (RT100).

## VACUUM SEAL AT CRYOGENIC TEMPERATURES

Vacuum seal at cryogenic temperatures: Relatively large thermal contraction will happen between the N2 Reservoir (AL-6061) and the Reservoir Flange (PEEK). A vacuum seal using an indium wire allows the seal to hold even at very low temperatures. Figure 2 shows the flange mating with the N2 reservoir.

# A NEW EXPERIMENTAL STATION FOR LIQUID INTERFACE X-RAY SCATTERING AT NSLS-II BEAMLINE 12-ID

D. M. Bacescu<sup>†</sup>, L. E. Berman, S. L. Hulbert, B. M. Ocko, Z. Yin, National Synchrotron Light Source II (NSLS-II), Brookhaven National Laboratory, Upton, New York 11973, USA

## Abstract

Open Platform and Liquids Scattering (OPLS) is a new experimental station recently built and currently being commissioned at the Soft Matter Interfaces (SMI) beamline 12-ID at NSLS-II. The new instrument expands SMI's beamline scientific capabilities via the addition of X-ray scattering techniques from liquid surfaces and for measurements that require an open platform.

The design of this new instrument, located inside the 12-ID-B beamline shielding enclosure, uses a single Ge (111) crystal deflector to bounce the incident x-ray beam by a variable angle  $\alpha$  downwards away from the horizontal by rotating the large Huber Eulerian cradle  $\chi$  stage. Tilting the beam is essential for liquid samples where gravity dictates the sample normal.

The OPLS instrument has a variable deflector-to-sample distance ranging from 0.6 m to 1.5 m where the larger distances are preferred for large processing chambers. Up to three X-ray detectors are mounted on a 2-theta scattering arm located downstream of the sample location. These detectors support a variety of X-ray techniques including X-ray reflectivity (XR), Grazing Incidence (GI) Small-Angle X-ray Scattering (SAXS) and Wide-Angle X-ray Scattering (WAXS), and grazing-incidence angle X-ray fluorescence.

Currently, the OPLS experimental station intercepts the 12-ID beam that otherwise propagates to the SMI experimental station located in hutch 12-ID-C and can be retracted to a "parking" position laterally out of this beam to allow installation of a removable shielded beam pipe that is needed to support operations in hutch 12-ID-C.

The design of OPLS is flexible enough to adapt to a planned future configuration of the SMI beamline in which OPLS is illuminated independently of SMI via a second, canted undulator source and a separate photon delivery system. In this future configuration, both branches will be able to operate independently and simultaneously.

## INTRODUCTION

SMI beamline is one of the five beamlines of the Complex Scattering Program at NSLS-II. The beamline is served by a 2.8m long, 23mm period length, in-vacuum undulator (IVU23) generating x-rays with energy ranging from 2.05 – 24 keV. OPLS, one of the two experimental stations of the 12-ID (SMI) beamline, is located at approx. 51m from the source, inside shielded hutch enclosure, 12-ID-B (see Fig. 1). The OPLS uses the same photon delivery system as the SMI branch. The bimorph optical mirrors of

the SMI beamline can focus the beam at one of the two end station or at a secondary source aperture.

The OPLS experimental station is a liquid surface spectrometer designed with an open sample platform, which is a unique feature which offers high versatility, and allows X-ray scattering studies from liquid surfaces and interfaces, as well from different processing environments (e.g., roll-to-roll processing). The OPLS experimental station is designed to operate from 8 – 24 keV, with a beam spot size of approx. 20  $\mu\text{m}$  vertically and 400  $\mu\text{m}$  horizontally, and a photon flux of approx.  $10^{12}$  ph./sec. [1].

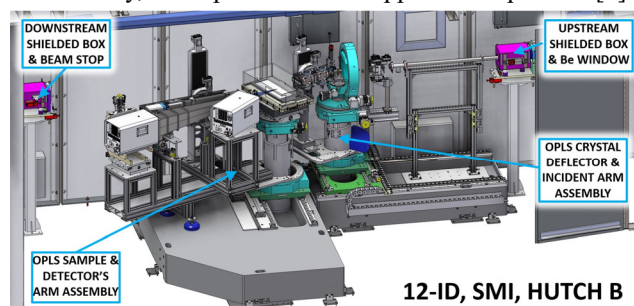


Figure 1: OPLS instrument (shown in operation mode).

## THE OPLS DESIGN OVERVIEW

To illuminate the rear hutch (12-ID-C) the SMI X-ray beam propagates through a removable and interlocked shielded beam transport pipe (approx. 4.5 m long), located in hutch 12-ID-B. For OPLS operation, this beam pipe is removed, the upstream vacuum section is terminated by a Beryllium (Be) window and a removable lead beam stop is mounted at the downstream end, thereby defining the space available for OPLS experimental station.

### The Crystal Deflector Assembly

The crystal deflector assembly (see Fig. 2) has a granite base (0.89m×1.85m×0.30m) with sufficient length to allow the motion along Z-axis, to accommodate a variable deflector-to-sample distance ranging from 0.6 m to 1.5 m.

The Z-axis translation stage ( $\pm 650\text{mm}$ ) is actuated by a stepper motor and rack and pinion mechanism. To overcome the pinion backlash, the motion control system uses feedback from an incremental encoder. To lock the stage into position, an air-actuated clutch-brake module is used on the inboard guide rail. The brake module uses spring energy to clamp onto the guide rail and air pressure to overcome the spring force and release it [2].

The X-axis translation stage ( $\pm 150\text{mm}$ ), actuated by a stepper motor and a preloaded ball screw assembly (NSK PSS25-05-N1-D-0499), is used to center the crystal deflector into the beam using the cross-hair alignment

<sup>†</sup> dbacescu@bnl.gov

# SAMPLE AND DETECTOR POSITIONING INSTRUMENTS FOR THE WIDE ANGLE XPCS END STATION AT 8-ID-E, A FEATURE BEAMLINE FOR THE APS UPGRADE\*

K. Wakefield†, S. Bean, D. Capatina, E. M. Dufresne, M. Fisher,  
M. J. Highland, S. Narayanan, A. Sandy, R. Ziegler  
Advanced Photon Source, Argonne National Laboratory, Lemont, Illinois, USA

## Abstract

The X-ray Photon Correlation Spectroscopy (XPCS) beamline at the Advanced Photon Source (APS) has been selected as one of the nine feature beamlines being designed to take advantage of the increase in coherent flux provided by the APS Upgrade. The 8-ID-E enclosure at the beamline will have a dedicated instrument for performing Wide Angle XPCS (WA-XPCS) measurements across a range of length and time scales. The instrument will feature a high-stability 6-circle diffractometer, a moveable Long Distance Detector Positioner (LDDP) for positioning a large pixel array detector, and a removable flight path assembly. For intermediate sample to detector distances of 1.5 to 2 meters, a large pixel array detector will be positioned on the diffractometer detector arm. For longer sample to detector distances up to 4 meters, an horizontal scattering geometry will be utilized based on the LDDP to position a second large pixel array detector. The LDDP will consist of a large granite base on which sits a combination of motorized stages. The base will sit on air casters that allow the LDDP to be coarsely positioned manually within the enclosure. Final positioning of the detector will be achieved with the mounted stages. The spatial relationship between the sample and the free moving LDDP will be monitored using a laser tracking system. A moveable flight path will be supported by the diffractometer arm and a mobile floor support to minimize air scattering while using the LDDP. The WA-XPCS instrument has been designed with users and beamline staff in mind and will allow them to efficiently utilize the highly enhanced coherent beam provided by the APS Upgrade.

## INTRODUCTION

The Advanced Photon Source Upgrade Project (APS-U) is planning a storage-ring upgrade that will reduce the electron-beam emittance by a factor of  $\sim 75$ . This ultra-low emittance is achieved by replacing the present storage ring lattice with a multi-bend achromat (MBA) lattice. The MBA lattice will increase the x-ray coherent fraction by two orders of magnitude and decrease the horizontal source size by a factor of  $\sim 20$ . In addition, the APS-U is planning to build nine new featured beamlines and make optics upgrades to many others.

\* This research used resources of the Advanced Photon Source, a U.S. Department of Energy (DOE) Office of Science User Facility at Argonne National Laboratory and is based on research supported by the U.S. DOE Office of Science-Basic Energy Sciences, under Contract No. DE-AC02-06CH11357.

† kwakefield@anl.gov

One of the feature beamlines built as part of the APS-U will be dedicated to X-ray Photon Correlation Spectroscopy (XPCS) studies at sector 8ID of the APS. The 8-ID-E enclosure of the XPCS beamline will primarily perform Wide Angle XPCS (WA-XPCS) measurements and occasionally be used for positioning samples during Ultra-Small Angle XPCS measurements. Two key elements to the instrumentation required to perform these measurements are a large 6-circle diffractometer for precise positioning of samples in 3 spatial and 3 angular co-ordinates, detectors, and a Long Distance Detector Positioner (LDDP) that will allow x-ray detectors to be positioned up to 4 m away from the sample location and will span an angular range of 3-55 degrees. These instruments are shown in Fig. 1 below.

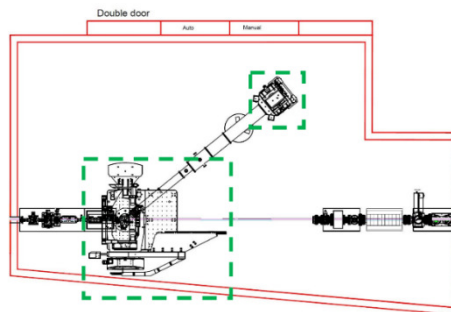


Figure 1: 8-ID-E enclosure layout with WA-XPCS instruments, diffractometer and LDDP outlined in green.

## SCIENCE DRIVER

Photon correlation spectroscopy (PCS) provides information about dynamic heterogeneity in complex systems by characterizing fluctuations in condensed matter across a broad range of length and time scales while x-ray scattering provides sensitivity to order and motion at scales spanning the mesoscale to the atomic scale. A general subset of the areas of scientific investigation that will be pursued at the beamline include the role of fluctuations and dynamic heterogeneity in the properties of phase-change materials, understanding structural relaxations in supercooled liquids and their connection to glass formation, the effect of interfaces and confinement on nanoparticle dynamics, and the connection between dynamics and relaxation of shearthinned and shear thickened states. To perform successful WA-XPCS measurements requires, the formation of a small coherent x-ray spot, accurate and stable positioning of a sample, and the ability to resolve coherent x-ray speckles with an area detector. These requirements have driven the overall design of the WA-XPCS instrument.

# DETERMINATION OF MAXIMUM REPETITION RATE OF A CORRUGATED-WAVEGUIDE-BASED WAKEFIELD ACCELERATOR

K. Suthar\*, A. Siy<sup>1</sup>, G. J. Waldschmidt, S. Lee, S. Sorsher,  
 E. Trakhtenberg, and A. Zholents,  
 Advanced Photon Source, Argonne National Laboratory, Lemont, USA  
<sup>1</sup>also at University of Wisconsin, Madison, USA

## Abstract

Beam-driven wakefield accelerators hold great promise toward reducing the size of contemporary accelerators. One possibility under study at Argonne National Laboratory is the use of a miniature corrugated waveguide for generation of the wakefield. The effect of electromagnetic heating by the electron beam traveling on its centerline is investigated applying the steady-state thermal analysis coupled with computational fluid dynamics, and structural mechanics. A design of the accelerator module suitable for acceleration of electrons with an energy gain up to  $100 \text{ MeV m}^{-1}$  is considered. A heat load on the waveguide inner surface with corrugations is calculated using a conservative assumption for the copper electrical conductivity at a high frequency of the electromagnetic field. It is shown that the von Mises stress caused by thermal expansion grows with the increased bunch repetition rate and reaches a yield level in a most stressed location at the bunch repetition rate of  $16.5 \text{ kHz}$ . Other effects associated with the waveguide heating, such as waveguide expansion and contraction, are quantified.

## INTRODUCTION

A miniature accelerator employing a copper cylindrical corrugated waveguide is being designed at Argonne National Laboratory to produce Čerenkov radiation at  $180 \text{ GHz}$  using a high charge electron bunch traveling longitudinally on the centerline of the waveguide. The radiation field accelerates a low-charge electron bunch traveling behind with an energy gain of  $\sim 100 \text{ MeV m}^{-1}$  [1]. The electromagnetic (EM) wave of Čerenkov radiation propagates downstream of the waveguide with a slower group velocity than the beam velocity. Interacting with corrugations, it excites surface currents responsible for the waveguide heating. As shown in Fig. 1, the waveguide is embedded into a "bow-tie"-shaped copper structure with four water cooling channels, although the optimal location of these channels and thermal conductivity from the corrugated surface to water is severely limited by external constraints. The heat load deposition gradually increases along the  $0.5 \text{ m}$  length of the waveguide and produces a temperature gradient that leads to progressively higher thermal expansion in the downstream direction. The stress from the differential expansion can lead to material tensile-yield failure, surface cracking, arcing, and beam loss. Therefore, determination of the acceptable bunch repetition rate and the ultimate performance of the accelerator are directly related to

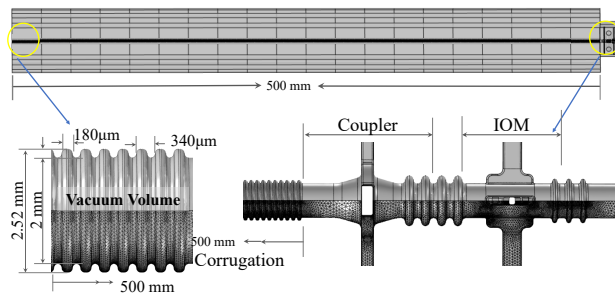


Figure 1: The corrugated waveguide and transition section showing surface mesh.

the thermal management of the average heat load deposited by the electron beam on the corrugations in a steady state operation. Quantitative analysis of the differential dimensional changes is critical for understanding of the operating conditions, and we are investigating the limits based on heat transfer, cooling, and mechanical integrity of the structure applying fully coupled multiphysics finite element analysis while the EM design [2] and prototype fabrication efforts [3] are still developing.

## MULTIPHYSICS FORMULATION

Multiphysics calculations were performed with CST Microwave Studio<sup>®</sup> [4] and COMSOL Multiphysics<sup>®</sup> software [5]. Modeling electromagnetic heating with computational fluid dynamics (CFD) and solid mechanics in the corrugated waveguide follow the scheme shown in Fig. 2a, and are summarized in the following steps:

- Solve the electromagnetic problem in CST studio<sup>®</sup> to find the electromagnetic fields and calculate the electromagnetic surface losses on the wall.
- Apply thermal loads induced by the electromagnetic fields in the heat transfer module to perform the calculation for the temperature rise.
- Apply the flow condition in the CFD, then define the temperature field as a coupling parameter to couple both physics.
- Define the boundary conditions for the Structural Mechanics module, then create a coupling parameter that couples the temperature field of Structure Mechanics for thermal expansion.
- Have the coupled solution compute the temperature field as a fully coupled equation between the heat transfer and the CFD modules, and use it as input for the

\* suthar@anl.gov

# A FAMILY OF HIGH-STABILITY GRANITE STAGES FOR SYNCHROTRON APPLICATIONS\*

C.A. Preissner<sup>†</sup>, S.J. Bean, M. Erdmann

Advanced Photon Source, Argonne National Laboratory, Lemont, IL 60439, USA

M. Bergeret, J.R. Nasiatka

Advanced Light Source, Lawrence Berkeley National Laboratory, Berkeley, CA 94720, USA

## Abstract

Engineers at the APS have developed a granite, air-bearing stage concept that provides many millimeters of motion range and nanometer-level vibrational stability. This technique was first conceptualized and used on the Velociprobe x-ray microscope [1, 2]. The success of that design spurred adaption of the approach to over 90 devices, including many new instruments at the APS [3] and high performing instruments at other synchrotrons [4]. This paper details the design concept, some performance measurements, and new developments allowing for a six-degree-of-freedom device.

## BACKGROUND

The stability needs of multi-bend achromat (MBA) synchrotrons [5] mean that both the accelerator and beam line equipment require more stable platforms as compared to those of the previous generation of synchrotrons. At facilities like the APS-U, new and more precise x-ray beam position monitors are required for the front ends and numerous fine-focusing (tens of nm or better) instruments are being deployed. Each of these requires multiple axes to align the equipment to the beam.

Many of these axes are simply to position or align the instrument and are not moved during a measurement or moved only for alignment. Conventional rolling element bearings are readily available in many forms and easily integrated into designs and make these motions easy to implement. However, there is a price to pay when using these rolling-element bearings: compliance.

Engineers at the APS were frustrated that the bearings necessary to allow for a practical and easy to use instrument also amplified floor vibration and reduced performance potential. Granite air bearing staging systems can offer advantages over conventional rolling-element bearing staging systems, including a) higher stiffness, b) lower thermal expansion, c) slow thermal changes/drift, and d) low angular position errors. While planar air bearings were in common usage, air bearing vertical stages required a novel wedge design [2] to realize a design in which there is no cantilevered load. This paper provides insight into basic aspects of the granite stage design, some measured performance, illustration of some examples, and new developments.

\* This research used resources of the Advanced Photon Source, a U.S. Department of Energy (DOE) Office of Science User Facility at Argonne National Laboratory and is based on research supported by the U.S. DOE Office of Science-Basic Energy Sciences, under Contract No. DE-AC02-06CH11357.

<sup>†</sup> preissner@anl.gov

## DESIGN CONSIDERATIONS

The basic principles of the Velociprobe-style air bearing stages are to integrate orifice-balanced air bearings [6] into granite blocks (Fig. 1), flow air to create a stiff film for movement, and vent the bearings when not moving to provide a stiff structure. All current systems are designed as positioning systems, meaning they are moved into position and then the air bearings are vented. Figure 1 shows the geometry of a typical granite block with integrated air bearings.

The integration of the bearing into the granite takes advantage of both the favorable granite thermal properties ( $\sim 4 \times 10^{-6}$  m/m/ $^{\circ}$ C thermal expansion coefficient) and the high level of flatness that can be achieved [7]. Normally “flat-on-flat” contacts should be avoided, as surfaces are not exactly flat. However, the high level of flatness achievable with granite enables a stiff “flat-on-flat” type of contact when the bearings are vented. The “fly height” (air film thickness) is controlled by the size of the orifice located upstream of the bearing surface. The target film thickness is between seven and ten microns, and the APS has developed a spreadsheet to estimate the orifice size necessary to achieve this fly height. Alternatively, fly height can be determined during assembly by measuring the fly height and changing orifice size to achieve the desired fly height.

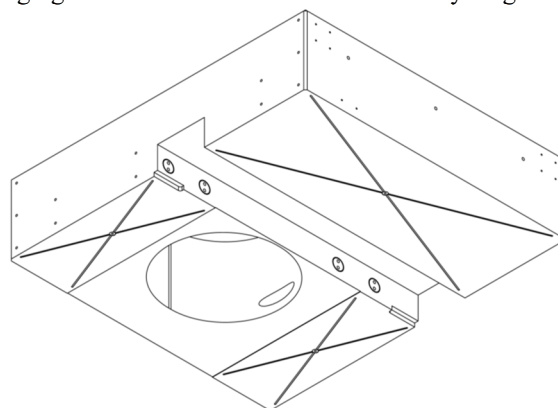


Figure 1: Picture of a typical granite block with three integrated, orifice balanced, air bearings. The orifices are located at the center of the “Xs”.

Stiffness of a vented granite air bearing is over 20 times that of the stiffest configuration of rolling-element bearings. Figure 2 shows a comparison of various rolling element bearings to a flat-on-flat contact typical of granite. Hertzian contact stiffness as described in Puttock [8] is compared to the AE/L stiffness of granite, with reference

# A NEW TRAVELING INTERFEROMETRIC SCHEME FOR THE APS UPGRADE OF THE 2-ID BIONANOPROBE\*

S. Bean, S. Chen, T. Graber<sup>†</sup>, C. Jacobsen, B. Lai, E. Maxey,  
T. Mooney, C. Preissner, X. Shi, D. Shu, J. Tan, M. Wojcik

Advanced Photon Source, Argonne National Laboratory, Lemont, IL 60439, USA

<sup>†</sup> Deceased April 29, 2021

## Abstract

The Advanced Photon Source (APS) at Argonne National Laboratory (ANL) is being upgraded to a multi-bend achromat (MBA) lattice storage ring which will increase brightness and coherent flux by several orders of magnitude. As part of this upgrade a total of 15 beamlines were selected to be enhanced to take advantage of the new source – these are designated as “Enhanced Beamlines”. Among these is the enhancement to 2-ID, which includes an upgrade and move of the existing Bionanoprobe (BNP) from 9-ID [1]. This instrument will become the second generation Bionanoprobe II (BNP-II) with intent of studying cryogenic samples with sub-10 nm resolution. This upgrade requires a high performing metrology configuration and design to achieve the desired spatial resolution while adapting to the various constraints of the instrument. The cryogenic sample environment and detection constraints offer significant challenges for implementing a metrology scheme. In this paper we report on the new traveling interferometer configuration proposed for BNP-II.

## INTRODUCTION

The unique challenge for implementing metrology for BNP-II is the cryogenic sample environment. The desired instrument resolution lends to a design that measures positions as close to the actual cryogenic sample as is feasible. This must be accomplished for a sample that translates in X/Y/Z directions and rotates around a vertical (Y) axis.

Recent developments at Swiss Light Source have resulted robust metrology solutions for rotating samples such as passive anti rotation and tracking interferometer designs [2-4]. These schemes were considered for BNP-II. Implementation would come with a unique set of challenges for BNP-II give the space limitations in the XZ plane, and the desire to measure a reference object which is at cryogenic temperatures.

Our design incorporates a new traveling interferometer concept for the sample as shown in Figure 1. A traveling interferometer platform tracks a cryogenic cylindrical reference in the horizontal plane and is decoupled from the other degrees of freedom (DOF) of the sample stage stack. A set of stationary global interferometers measure

information both from the reference and from the traveling platform.

It is worth note that the desired instrument resolution is pushing the limits on off-the-shelf interferometer hardware. Periodic error is considered for the design but is not discussed further [5].

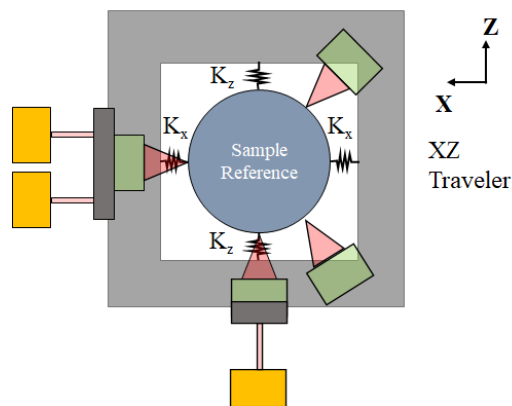


Figure 1: The coupled traveling interferometer concept. The traveling XZ traveler support is coupled to the sample reference on the X and Z degrees of freedom, while decoupled in the other degrees of freedom. Focused traveling interferometers (green) and global stationary interferometers (gold) are depicted.

## SCANNING & METROLOGY METHODOLOGY

The following numbered items represent the most critical and complex set of requirements of the metrology strategies for BNP-II:

1. The metrology system must provide position information below 2 nm in order to achieve a 10 nm fluorescence resolution for the instrument.
2. The cryogenic sample will be continuously scanned while the optics are stationary during measurement.
3. The metrology scheme must be able to measure re-positioning of the sample through translations and one main vertical rotation axis.
4. The sample metrology reference optic and the sample should be intimately coupled.
5. The metrology must incorporate relative measurements between the optic and sample positions for both positioning and scanning.
6. The metrology should be non-intrusive to the nearby XZ (horizontal) plane of the sample to allow for signal collection, beam-conditioning optics, and thermal shielding.

\* This research used resources of the Advanced Photon Source, a U.S. Department of Energy (DOE) Office of Science User Facility at Argonne National Laboratory and is based on research supported by the U.S. DOE Office of Science-Basic Energy Sciences, under Contract No. DE-AC02-06CH11357.

# ALIGNMENT STRATEGIES AND FIRST RESULTS ON SIRIUS BEAMLINES

G. Rovigatti<sup>†</sup>, H. Geraissate, R. Leão, CNPEM, Campinas, Brazil

## Abstract

The new Brazilian Synchrotron Light Source had its first friendly users late in 2019. During 2020, the first experimental stations were aligned and had the first beam successfully at the sample. The reference network of points used for the storage ring alignment was connected to an external network located in the experimental hall. Following this step, it was possible to extend these references to the hutches environment, where the beamlines components are installed. During the alignment of the first beamlines, a sequence of common tasks was performed, from the bluelining of the hutches footprints, to the components fine alignment. The position and orientation deviation of the main components will be presented for the Manacá, Catteretê, Ema, and Carnaúba beamlines. Two specific measurement strategies used for aligning special components will also be presented: (1) an indirect fiducialization procedure developed for most of the mirrors and their mechanisms using a mix of coordinate measuring machine and articulated measuring arm measurements, and (2) a multi-station setup arranged for the alignment of a 30 meters long detector carriage, using a mix of laser tracker, physical artifacts, and a rotary laser alignment system used as a straightness reference.

## INTRODUCTION

Sirius, the 4<sup>th</sup> generation Brazilian synchrotron light source is designed to accommodate 38 beamlines. The initial phase comprises 14 beamlines to be delivered until 2022 [1]. By the end of 2020, Manacá, Catteretê, Ema and Carnaúba concluded their installation and alignment phase and started their commissioning with friendly users.

All beamlines of Sirius have many critical requirements to work properly, such as stability and temperature. Alignment is one of these requirements, and its importance begins at the installation phase, guiding the positioning of big components (e.g. hutches and girders); continues at the commissioning, supporting the scientists in making the beam reach the sample position and remains essential over time, when installing new components, verifying deformations, etc.

This work describes how the beamlines alignment was managed and details particular cases where metrological methodologies were developed.

## REFERENCE NETWORK

Alignment is a critical requirement to the well-being of a synchrotron accelerator. To reach the designed tolerances, not only a reliable equipment is necessary but also a metrological reference network needs to be created.

The main reference was created inside the radiation shielding (RS) of the storage ring (SR). Approximately 1220 SMR nests were distributed on the floor, walls and ceiling. Outside the tunnel, a secondary network was created for the Experimental Hall (EH). This one is referenced to the primary network and has approximately 730 points, at walls, floor, and columns. Also, tertiary networks were created for the hutches and long beamlines.

The strategy used to create the networks was a classical laser tracker (LT) survey, with several stations along the volume measuring the points of the network with redundancy. The stations followed a “zig zag” pattern and different heights were used for the instruments [2]. All LTs used were from the Leica AT400 family. Also, levelling campaigns were done inside the accelerators tunnel, at the EH and long beamlines. The equipment used was the optical level Leica NA2. Radius measurements were done from the central pillar of the Sirius building to inside the RS, to bring more robustness to the network [3].

A normal connection between networks would be done by a simple overlapping of common points between the environments. But, as the RS is fully enclosed, there is no way to do this between the Sirius primary and secondary networks. The only free lines of sight from inside to outside the RS are holes with  $\varnothing 150$  mm and 1 m length. So, the link was done using a reciprocal connection technique, using two LTs measuring each other and fitting spheres that constructs the rotation center of the instrument. With mathematical manipulations of the centers created, the located LT from inside the RS will reference the second instrument at the EH [3-5].

After each network is calculated, they are adjusted in space by means of least square transformations. The SR network is adjusted with respect to the last epoch and become the reference for the subsequent ones. The Hall network is then adjusted to the SR, preserving its level and using the common points for the other degrees of freedom; and the tertiary networks are adjusted to the Hall's following the same strategy, except for the hutches networks, which inherits the same level as their parent network.

Through the adjustment steps, the network uncertainty propagation is done with a Python based script, developed in-house, using Monte Carlo simulations of the possible transformation matrix between two networks, which considers the individual uncertainty value for each point on the networks [6]. It creates point-clouds for each network, calculates the different transformations possibilities and apply these transformations to the network being adjusted. As expected, the uncertainty results are influenced by which coordinate system is being used. A study was made to evaluate how it propagates from a source point within the

<sup>†</sup> gustavo.rovigatti@cnpem.br

# THERMAL CONTACT CONDUCTANCE IN A TYPICAL SILICON CRYSTAL ASSEMBLY FOUND IN PARTICLE ACCELERATORS

P. Navarro, Diamond Light Source Ltd., Didcot, England

## Abstract

Every mirror at Diamond Light Source (the UK's Particle Accelerator) has been installed with the premise of clamping the cooling copper manifolds as lightly as possible to minimize distortion. The problem with this approach is that the Thermal Contact Conductance (TCC) depends on the applied pressure among other factors. The assembly is usually a symmetric stack of Copper - Indium Foil - Silicon Crystal - Indium Foil - Copper. Variables that interest the most are those that are easily adjustable in the set-up assembly (number of clamps, pressure applied and cooling water flow rate) PT100 temperature sensors have been used along the surface of the crystal and along the surface of the copper manifolds. Custom PCB units have been created for this project to act as a mean of collecting data and Matlab has been used to plot the temperature measurements vs. time. Another challenge is the creation of an accurate model in Ansys that matches reality up to a good compromise where the data that is being recorded from the sensors matches Ansys results within reason.

## INTRODUCTION

The set-up (Fig. 1) of a typical Silicon Crystal assembly is comprised of a symmetric stack of Copper - Indium Foil - Silicon Crystal - Indium Foil - Copper.

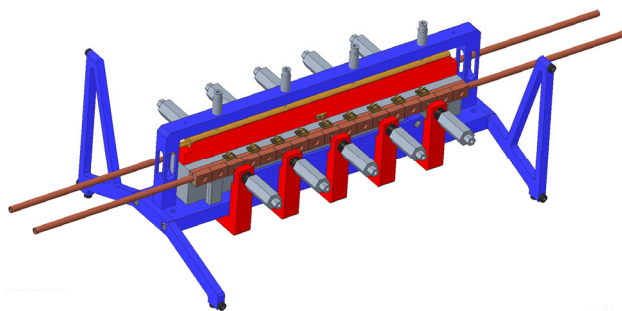


Figure 1: 3D model for the experimental assembly.

A cartridge heater embedded in an aluminium block and located at the top surface of the crystal mimics the input power of the beam that bounces off the silicon mirrors in a particle accelerator. An industrial chiller is used for cooling down the water flowing through the copper manifolds. Temperature is read by PT100 sensors along the surface of the Crystal and at the other side of the interface (along the surface of the copper manifolds) so the drop in temperature across the interface is known. The PT100 sensors have been glued on both surfaces. Custom adjustable spring clamps with a fine thread (0.75mm pitch) along the crystal control the amount of force applied to the interface. Strips of Indium Foil (100µm thick) have been used between the silicon crystal and copper manifolds to cope with surface's irregularities like roughness, waviness and flatness. Spring

pushers at the top, screwed into an arch and exerting a force on to the heater to make sure that a good contact among the parts is achieved. A thin layer of oil has been added at the interface between the aluminium block and the silicon crystal to improve the TCC at that interface. The silicon crystal is sat on three sprung stainless-steel balls at the bottom and up against two more at the back. A 4mm insulating layer of Calcium-Magnesium Silicate covers the cartridge heater and aluminium block make sure that most of the power goes into the crystal (Fig. 2).

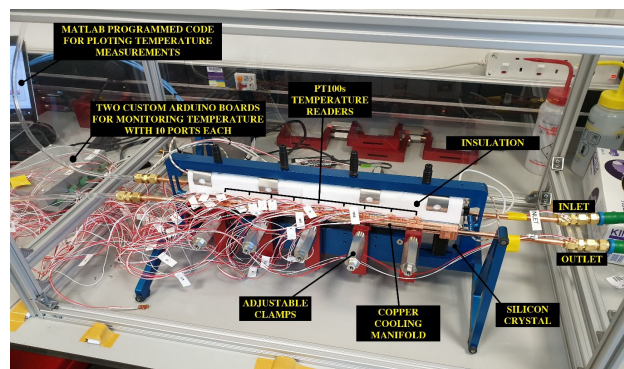


Figure 2: Experimental assembly set-up.

The TCC between two components defines how much heat energy flows through the interface per unit of area and unit of time. The bigger the TCC, the better thermal contact among the parts and thus, more heat flows through the interface. At the microscopic level, only a few discrete points are actually in contact [1]. The TCC depends on many factors [2] (Fig. 3).

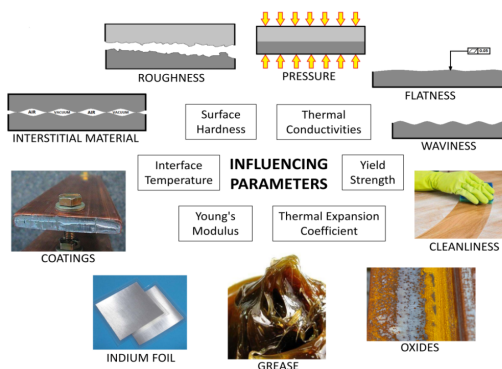


Figure 3: Variables of thermal contact conductance.

## ANALYSIS

The following studies have been performed in this project:

- Comparison between a perfect TCC vs actual value (Fig. 4 and Fig. 5).
- Temperature comparison using different Power Inputs (100W, 150W & 200W).

# HEAT LOAD SIMULATION OF OPTIC MATERIALS AT EUROPEAN XFEL

F. Yang\*, D. La Civita†, M. Vannoni, H. Sinn  
European XFEL GmbH, Schenefeld, Germany

## Abstract

In the beam transport system at European XFEL, the optic components which have direct contact with the beam, e. g. mirror, absorber and beam shutter, etc., could get up to 10kW heat load on a sub-mm spot in 0.6 ms. Therefore, the thermo-mechanical performance of these optic components is playing an important role in the safety operation of the facility, restricting the maximum allowed beam power delivered to each experiment station. In this contribution, using finite element simulation tools, a parametric study about coupled thermo-mechanical behavior of some general used materials, e. g. CVD diamond and B<sub>4</sub>C. is presented. Based on the design of several devices which are already in operation at European XFEL [1], a generalized model for setting up the damage threshold of these materials is established, with respect to the corresponding beam parameters. These simulation results can be referred as design and operation benchmark for the optic elements in the beamlines.

## INTRODUCTION

Heat load simulation has been a main subject during the design and operation phases for the beamline instruments [2]. In this contribution, only the components that have the function of power absorbing are briefly presented, the heat load on the reflecting elements like mirrors have been discussed in detail in other publications, e.g. [3,4]. Considering the X-Ray laser beam as equivalent heat load, the numerical model to simulate the interaction of the beam with matters using the numerical tools (including FEM and FVM codes based on continuum mechanics formulations) could be complex. In Fig. 1, some of the multiphysical phenomena involved in the simulation models are listed. The corresponding numerical methods, e.g. the level set, elastoplastic model [5] and deformed geometry or moving mesh are required for the multiphysics simulations, to study the damage process after the damage threshold are reached.

But to set up a damage threshold in the scope of engineering design, the multiphysics model is not essential. A standard patch test model will be presented in the following sections.

## GENERALIZED MODELS FOR SETTING UP DAMAGE THRESHOLD

According to the material tests for the current used optic materials at European XFEL, e.g. beam stop and upgraded frontends (see Fig. 2 and 3), CVD diamond and B<sub>4</sub>C

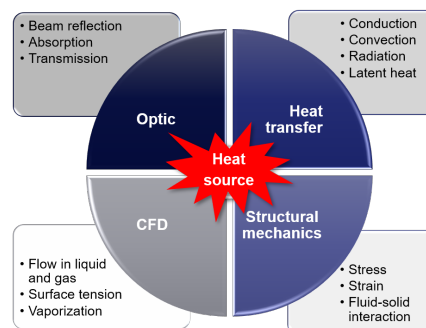


Figure 1: Physical phenomena involved.

are chosen with priority as optic components to absorb the beam power. A generalized simulation model is defined in Fig. 4. Only a quarter of the model is simulated due to symmetry of the boundary conditions in ANSYS and COMSOL, and the results with single pulse/train has been compared consistently with the analytical solutions, see [6, 7]. In ANSYS, nonlinear coupled-field elements, PLANE223 and SOLID226 are used by implement APDL code in workbench to simulate the coupled thermo-mechanical behaviors directly.

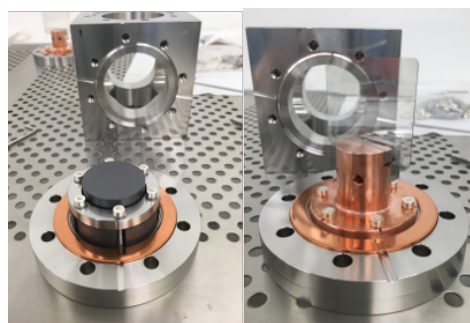


Figure 2: Beam stop.

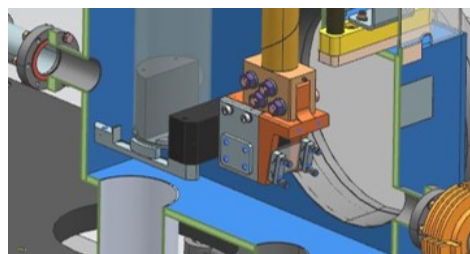


Figure 3: Upgraded frontend.

To improve the precision and reliability of the simulation results, With the support of IKTS Fraunhofer Institute, the temperature dependent diffusivity was measured for various B<sub>4</sub>C samples, see Fig. 5. For the material param-

\* fan.yang@xfel.eu

† daniele.lacivita@xfel.eu

# INNOVATIVE AND BIOLOGICALLY INSPIRED PETRA IV GIRDER DESIGN\*

S. Andresen<sup>†</sup>, Alfred Wegener Institute Helmholtz Center for Polar and Marine  
 Research (AWI), Bremerhaven, Germany

N. Meyners, D. Thoden, Deutsches Elektronen-Synchrotron (DESY), Hamburg, Germany

## Abstract

DESY (Deutsches Elektronen Synchrotron) is currently expanding the PETRA III storage ring X-ray radiation source to a high-resolution 3D X-ray microscope providing all length scales from the atom to millimeters. This PETRA IV project involves an optimization of the girder magnet assemblies to reduce the impact of ambient vibrations on the particle beam. For this purpose, an innovative and biologically inspired girder structure has been developed. Beforehand, a large parametric study analyzed the impact of different loading and boundary conditions on the eigenfrequencies of a magnet-girder assembly. Subsequently, the girder design process was generated, which combined topology optimizations with biologically inspired structures (e.g., complex Voronoi combs, hierarchical structures, and smooth connections) and cross section optimizations using genetic algorithms to obtain a girder magnet assembly with high eigenfrequencies, a high stiffness, and reduced weight. The girder was successfully manufactured from gray cast iron and first vibration experiments have been conducted to validate the simulations.

## INTRODUCTION

Biomimetics is a scientific discipline that deals systematically with the technical implementation and application of constructions, processes, and development principles of biological systems. Biological models are not copied, but investigated, understood, and applied to technical problems [1,2].

Natural structures are often complex and show good mechanical properties. They are highly optimized during the process of evolution and usually fulfil different functions.

In particular, aquatic plankton organisms with silicate cell covers (such as diatoms and radiolaria) have developed an extremely high diversity of irregular structures that show efficient lightweight design principles. Aside from the high stiffness and strength observed in these lightweight structures [3,4], diatom shells are expected to also protect the inner cell against vibrational load cases.

In different studies, irregular biologically inspired structures were analyzed regarding their natural vibrations. Irregular honeycomb and lattice structures show significantly higher eigenfrequencies compared to regular structures [5,6]. In addition, pre-deforming structures according to mode shapes, which can be observed in diatom shells [7], strongly raises the eigenfrequencies [8].

\* Work financed by the Alfred Wegener Institute and the Deutsches Elektronen-Synchrotron.

<sup>†</sup> simone.andresen@awi.de

In a case study, biologically inspired structures and optimization techniques were applied to a PETRA IV girder. The PETRA IV project at DESY aims at upgrading the currently running synchrotron radiation facility PETRA III. For more information about this project it is referred to [9,10]. Generally, a high particle beam stability is essential to obtain a low-emittance and diffraction limited storage ring [11]. Magnet-girder assemblies play an important role, because they have to prevent that amplified ground vibrations reach the particle beam.

The objective of the here presented study was to design an innovative, bio-inspired PETRA IV girder.

## MATERIAL AND METHOD

The applied girder design process was based on seven steps:

### *Definition of the Boundary Conditions*

Figure 1 shows the considered boundary conditions. The girder was equipped with eight magnets and connected at three locations to three pedestals.

The overall design objectives were the maximization of the 1<sup>st</sup> magnet-girder eigenfrequency, the minimization of the static deformation due to gravity, and the minimization of the girder mass.

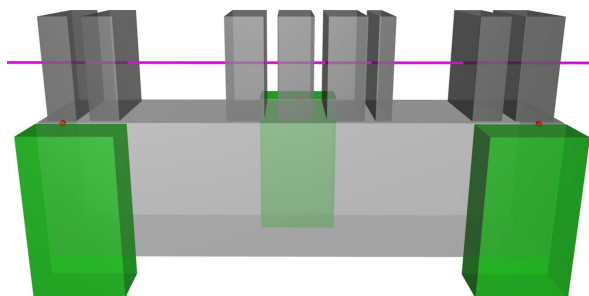


Figure 1: Model assembly including the girder design space (light gray), the magnets (dark gray), the pedestals (green), and the connection of the design space to the pedestals using beams (red). The position of the vacuum chamber is demonstrated in magenta.

### *Topology Optimization*

A topology optimization was conducted to reveal an optimum material distribution. Thus, during the optimization process, material was removed from the design space shown in Fig. 1.